Charles University in Prague

Faculty of Sciences

Program: Molecular and Cell Biology, Genetics and Virology

Václav Urban

The role of human RECQ5 helicase in the maintenance of genomic stability

PhD Thesis

Academy of Sciences of the Czech Republic

Institute of Molecular Genetics

Department of Genome Integrity

Supervisor: Dr. Pavel Janščák, Ph.D.

Prague, 2016

The author of thesis, Václav Urban, declares that the entire content of this thesis or its major part was not previously utilized for obtaining of the same or other academic degree.

Prague

Signature

Abstract

DNA replication is the most vulnerable process of DNA metabolism in proliferating cells and therefore it is tightly controlled and coordinated with processes that maintain genomic stability. Human RecQ helicases are among the most important factors involved in the maintenance of replication fork integrity, especially under conditions of replication stress. Collisions between replication and transcription machineries represent a significant source of genomic instability. RECQ5 DNA helicase binds to RNA-polymerase (RNAP) II during transcription elongation and suppresses transcription-associated genomic instability. Here we show that RECQ5 also associates with RNAPI and enforces the stability of ribosomal DNA arrays in cells exposed to replication stress. We demonstrate that RECQ5 associates with transcription complexes in DNA replication foci and counteracts replication fork stalling in RNAPI- and RNAPII-transcribed genes, suggesting that RECQ5 exerts its genome stabilizing effect by acting at sites of concomitant replication and transcription. Moreover, RECQ5-deficient cells accumulate RAD51 foci that are formed in a BRCA1-dependent manner at sites of interference between replication and transcription and likely represent unresolved replication intermediates. Importantly, BRCA1-dependent formation of RAD51 foci at these sites requires active transcription. Further, we provide evidence that RECQ5 promotes RAD18-dependent PCNA ubiquitination at sites of replication-transcription interference by its interaction with PCNA. This is also manifested by the accumulation of RAD18 foci in the absence of RECQ5 or the presence of a RECQ5 mutant defective in PCNA binding. The helicase activity of RECQ5 promotes unloading of ubiquitinated PCNA from chromatin and counteracts the accumulation of RAD51 foci in S-phase cells. These findings suggest that RECQ5 promotes PCNA remodeling at replication forks stalled due to the collision with transcription complex and in coordination with BRCA1-mediated replication fork stabilization promotes the resolution of replication-transcription collisions.

Abstrakt

V průběhu replikace často dochází k zastavení postupu replikačních vidlic v důsledku poškození DNA templátu, přítomnosti transkripčních komplexů nebo tvorby sekundárních struktur DNA. RecQ helikázy patří v buňce k nejdůležitějším faktorům, které zajišťují stabilitu genomu za podmínek replikačního stresu. Přestože jsou transkripce i replikace esenciálními buněčnými mechanismy, jejich vzájemná interference může vést k poškození DNA a následné genomové nestabilitě. RECQ5 helikáza interaguje s RNA polymerázou II během elongační fáze transkripce a zabraňuje vzniku transkripcí indukovaného poškození DNA. V této studii ukazujeme, že RECQ5 interaguje také s RNA polymerázou I a zabraňuje ztrátě či znásobení úseků ribozomální DNA, na kterých dochází k přepisu ribozomální RNA. Prokázali jsme, že během S-fáze buněčného cyklu RECQ5 asociuje s transkripcí v místech právě probíhající replikace. Odstranění RECQ5 pomocí RNA interference vede k zastavení replikačních vidlic v oblastech transkribovaných RNA polymerázou I nebo II, což naznačuje, že RECQ5 udržuje stabilitu genomu v místech kolize mezi replikací a transkripcí. Snížením exprese RECQ5 pomocí RNA interference dochází v jádrech replikujících buněk k akumulaci RAD51 a RAD18 fokusů, které pravděpodobně představují nerozřešené replikační intermediáty, které jsme v buňkách po odstranění RECQ5 také detekovali. Vznik RAD51 fokusů v místech kolize mezi replikací a transkripcí je závislý na přítomnosti BRCA1 a aktivní transkripci. Také jsme prokázali, že aktivní transkripce zabraňuje kolapsu replikačních vidlic a je potřeba pro jejich restart. V místech kolize mezi replikací a transkripcí indukuje helikázová aktivita RECQ5 částečné odstranění PCNA z replikační vidlice, přičemž zbylé PCNA je díky interakci s RECQ5 posttranslačně modifikováno ubikvitinací. RECQ5 pomocí své helikázové aktivity umožňuje také rozřešení replikačních intermediátů stabilizovaných pomocí RAD51. Přítomnost RECQ5 v místech kolize mezi replikací a transkripcí tedy indukuje změny na zastavené replikační vidlici, která je současně chráněna pomocí BRCA1 před kolapsem. Oba tyto procesy vedou k rozřešení kolize a restartu replikace. Tato práce identifikuje RECQ5 jako jeden z klíčových faktorů při řešení kolize mezi replikací a transkripcí.

Abbreviations

ActD	actinomycin D
ALT	Alternative lengthening of telomeres
Aph	aphidicolin
ATR	ataxia telangiectasia and Rad3 related
CFS	common fragile site
CMG	CDC45-MCM-GINS
CPT	camptothecin
CTD	C-terminal domain
dNTPs	deoxynucleotide triphosphates
ERFS	early replicating fragile site
FRAP	fluorescence recovery after photobleaching
GFP	green fluorescence protein
HJ	Holliday junction
HR	homologous recombination
HU	hydroxyurea
ChIP	chromatin immunoprecipitation
CHK1	checkpoint kinase 1
IRI	internal RNAPII-interacting
kb	kilo base pairs
KIX	kinase-inducible interaction
Mb	mega base pairs

MCM2-7	minichromosome maintenance proteins 2–7
nt	nucleotides
PCNA	proliferating cell nuclear antigen
PIP	PCNA-interacting peptide
qPCR	quantitative real-time polymerase chain reaction
rDNA	ribosomal DNA
RNAP	RNA polymerase
rRNA	ribosomal RNA
SCE	sister chromatide exchange
SRI	Set2-Rpb1-interacting
UV	ultraviolet

Contents

Abstract 1

Abstrakt 2

Abbreviations 3

1. Introduction 6

1.1. DNA replication – a brief overview 6

1.2. Cellular response to replication fork stalling 8

1.2.1. S-phase checkpoint 8

1.2.2. Replication fork remodeling 9

1.3. Sources of replication stress 10

1.4. Replication-transcription collisions 11

1.5. RecQ helicases 14

1.5.1. RecQ helicases associate with replisome components 15

1.5.2. Role of RECQ4 in the initiation of DNA replication 16

1.5.4. WRN promotes restart of stalled replication forks 19

1.5.5. RECQ1 unwinds reversed replication forks 21

1.5.6. RECQ5 suppresses transcription associated DNA breakage during replication 22

2. Aims of the study 24

3. List of used methods 25

4. List of publications 26

5. Participation of Václav Urban on presented publications 27

6. Linking of publications 28

7. Discussion 29

8. Conclusions 35

9. References 36

10. Publications 50

1. Introduction

Faithful replication of the genome is essential for cell survival. The fidelity of DNA replication is ensured by the high accuracy of replicative DNA polymerases and by a number of associated factors involved in checkpoint signaling pathways, DNA repair, chromatin remodeling, sister chromatid cohesion and cell cycle control. Defects in any of these activities can cause replication fork slowing or stalling, a condition referred to as replication stress, which leads to genomic instability manifested by birth defects, developmental abnormalities, neurodegeneration, premature aging and cancer predisposition (Boyer et al., 2016; Losada, 2014; Macheret and Halazonetis, 2015; Zeman and Cimprich, 2014; Zhang et al., 2016). DNA replication is the most vulnerable process of DNA metabolism in proliferating cells and therefore it is tightly controlled and coordinated with processes that maintain genomic stability. RecQ helicases promote recovery of replication forks being stalled due to different replication roadblocks of either exogenous or endogenous source. They prevent generation of aberrant replication fork structures and replication fork collapse, and are involved in proper checkpoint signaling. The essential role of human RecQ helicases in the genome maintenance during DNA replication is underlined by association of defects in their function with cancer predisposition.

1.1. DNA replication – a brief overview

The initial step of DNA replication is the assembly of origin recognition complex (ORC1 to ORC6 subunits) in late mitosis or early G1 phase (Fragkos et al., 2015). Next, CDC6 (cell-division cycle 6) and CDT1 (cdc10-dependent transcript 1) assist to load an inactive double hexamer of minichromosome maintenance proteins 2–7 (MCM2-7) to complete the formation of pre-replication complex required for the establishment of bidirectional replication forks (Fragkos et al., 2015). At the G1/S boundary, S-phase specific DDK (DBF4-dependent kinase) and CDK (CDK2/cyclin A/E) kinases activate MCM2-7, which requires the recruitment of CDC45 and the GINS complex to form the so-called CMG complex (CDC45-MCM-GINS) (Fragkos et al., 2015). Activation of the CMG complex at origins of replication is achieved by recruitment of additional initiation factors including TOBP1, Treslin/TICRR, RECQ4 and MCM10, and the loading of DNA polymerase α/ε permit DNA synthesis (Fragkos et al., 2015). MCM2-7 complex serves as a catalytic core of the replicative DNA helicase that uses ATP binding and hydrolysis to unwind double-stranded DNA at the replication fork. However, only

a subset of pre-replication complexes is activated during S-phase. Mammalian cells replicate their genome by firing 20,000-50,000 origins, which is likely less than 10 percent of the total licensed origins (Rivera-Mulia and Gilbert, 2016). The large excess of licensed origins ensures the completion of genome duplication under conditions of perturbed replication that leads to activation of the dormant origins (Rivera-Mulia and Gilbert, 2016). The firing of origins over the course of S-phase is regulated at the level of replication domains (400 kb to 1 Mb in mammalian cells) that each contains a cluster of synchronously activated origins (Fragkos et al., 2015). Replication of genome in a domain fashion has a distinctive temporal order that is developmentally regulated and coordinated with specific changes in transcriptional activity and genome organization (Rivera-Mulia and Gilbert, 2016). Replication domains can be visualized as replication foci by either labeling replisome components or by detecting sites of nucleotide incorporation upon pulse labeling using nucleotide analogs (Fragkos et al., 2015). The number of replication foci detected per nucleus range from 800 to 5000 (each containing 4 to 6 origins on average) depending on the stage of S-phase (Chagin et al., 2016; Fragkos et al., 2015).

Genome duplication is performed by a multiprotein complex called replisome that simultaneously replicates both strands of the parental duplex. DNA duplication is initiated at both the leading and lagging strands with synthesis of short RNA primers by DNA polymerase α/primase complex. Binding of PCNA to the 3′ end of the primer enables the exchange of DNA polymerase α for replicative polymerases with higher processivity (Maga and Hubscher, 2003). The leading and lagging strands use two different DNA polymerases, DNA polymerase ε and DNA polymerase δ, respectively. PCNA functions as a processivity factor for DNA polymerases δ/ε and a platform that mediates interactions with other replisome components (Maga and Hubscher, 2003). DNA polymerases extend DNA only in the 5′–3′ direction. On the lagging strand, which is copied in the opposite direction than MCM2-7 helicase unwinding, this is solved by synthesis of multiple Okazaki fragments (Johnson and O'Donnell, 2005). Each Okazaki fragment is initiated by DNA polymerase α/primase complex, which generates a ∼10-nt RNA primer followed by a limited primer extension with deoxynucleotides. DNA polymerase δ completes the synthesis of Okazaki fragment (∼200 nt in length), which requires reloading of PCNA (Burgers, 2009). Connection between the leading and lagging strand polymerases leads to the accumulation of discontinuous stretches of single-stranded DNA at the lagging strand template, which is tightly bound by single-stranded DNA binding protein complex, replication protein A (RPA). Maturation of the Okazaki fragments is achieved by the removal of initiating

primers from the 5′-end of each fragment and the generation of a covalently linked daughter strand. This process requires coordinated activities of DNA polymerase δ, flap endonuclease FEN1, DNA2 nuclease/helicase and DNA ligase I (Zheng and Shen, 2011). The velocity of replication fork progression differs during S-phase. Replication forks move at a rate of 1.2 kb/min during early S-phase and slow down in mid S-phase to 0.74 kb/min. In contrast, during late S-phase, fork rates steadily increased to a maximum of 2.3 kb/min (Herrick and Bensimon, 2008).

1.2. Cellular response to replication fork stalling

Progression of replication forks is challenged by various types of obstacles that results in replication fork slowing or stalling, a condition generally referred to as replication stress. Replication fork stalling causes physical changes of the fork and the replisome. Cells respond to replication stress by activating a complex network of pathways that lead to replication fork stabilization followed by replication resumption. Under conditions of prolonged replication stress, the cell may not be able to rescue the stalled forks, which can result in DNA double-stranded break formation and a concomitant replication fork collapse. DNA double-stranded breaks need to be processed by any of DNA repair pathway with predominance of homologous recombination (Zeman and Cimprich, 2014).

1.2.1. S-phase checkpoint

The stalling of replication fork results in the formation of single-stranded DNA stretches that are coated by RPA. This structure is essential to activate S-phase checkpoint. RPA-coated single-stranded DNA recruits ATR (ataxia telangiectasia and Rad3-related protein) through an ATRIP-RPA interaction. ATR is a serine/threonine-specific protein kinase that phosphorylates a variety of proteins to induce replication stress checkpoint (Zeman and Cimprich, 2014). Activation of ATR is a multistep process that includes recruitment of RAD17 again by RPA followed by loading of RAD9/RAD1/HUS1 complex (called checkpoint clamp complex). This complex recruits TOPBP1 to activate ATR (Allen et al., 2011). The most important downstream effector of ATR is CHK1 kinase (Checkpoint kinase 1). ATR phosphorylates CHK1 on Ser317 and Ser345, which is mediated by the interaction between RPA, Tipin, Timeless and Claspin (Kemp et al., 2010). Phosphorylated CHK1 dissociates from chromatin and targets downstream effector molecules. CHK1 phosphorylates particularly CDC25A phosphatase to promote its proteasome-dependent degradation, which is followed by CDK2 inactivation, inhibition of

origin firing and cell cycle arrest (Sorensen and Syljuasen, 2012). The effect of CHK1 activation is suppression of late origin firing and simultaneously activation of dormant origins at the local replication domain (Rivera-Mulia and Gilbert, 2016). The global effect of ATR/CHK1 pathway activation protects cell from exhaustion of RPA at stalled forks and their subsequent collapse by conversion to DNA double-stranded breaks (Toledo et al., 2013). CHK1 also targets factors that promote replication fork stabilization and repair like RAD51, BRCA2 and BLM (Gonzalez Besteiro and Gottifredi, 2015). Apart from CHK1, ATR directly regulates the activity or localization of fork repair proteins including WRN, BRCA1, RPA and others. Phosphorylation of RPA32 subunit at Ser33 and CHK1 at Ser345 are the most specific indications of replication stress.

1.2.2. Replication fork remodeling

During replication stalling, several changes at protein and DNA level have been observed at replication fork. Uncoupling of MCM2-7 helicase from DNA polymerase leads to generation single-stranded DNA stretches coated by RPA, which leads to activation of S-phase checkpoint. In yeast, it was shown that PCNA and DNA polymerase ε retain their association with the leading strand during replication fork stalling (Cobb et al., 2003; Yu et al., 2014). However, PCNA is unloaded from the lagging strand of stalled forks. PCNA unloading depends on the presence of Elg1, on the PCNA ubiquitination at Lys164 performed by RAD6-RAD18, and on the activation of S-phase checkpoint (Yu et al., 2014).

Stalled replication forks can undergo fork reversal by rewinding the parental DNA and annealing of the two nascent strands behind the fork to generate regressed arm (also called "chicken foot") that resembles Holliday junction (HJ) structure (Neelsen and Lopes, 2015). The formation and/or stabilization of regressed arm are dependent on RAD51, a central homologous recombination factor (Zellweger et al., 2015). Other homologous recombination factors BRCA1/2 protect nascent strands of stalled forks from unscheduled DNA-end resection by stabilizing RAD51 filament (Schlacher et al., 2011; Schlacher et al., 2012). The conversion of stalled forks to the HJ structure by fork reversal may be a global response to replication stress (Zellweger et al., 2015). The formation of regressed arm may stabilize stalled fork for repair or removal of the roadblock, and the regressed arm also represents a suitable substrate for replication fork recovery by homology-driven invasion of the re-annealed template strands, avoiding DNA double-stranded break formation (Neelsen and Lopes, 2015).

A specific response to replication fork stalling at lesions in DNA (such as pyrimidine dimmers) is an exchange of replicative DNA polymerase for translesion polymerases. These polymerases are capable of DNA synthesis over the damaged DNA (Guo et al., 2009).

1.3. Sources of replication stress

There are various inhibitors used under experimental conditions that directly or indirectly block replication fork progression. The most common inhibitors used are the following. Hydroxyurea (HU) inhibits the enzyme ribonucleotide reductase, resulting in decreased pools of dNTPs and thus inhibition of DNA synthesis. Aphidicolin (Aph) is a selective inhibitor of DNA polymerase α. Camptothecin (CPT) inhibits topoisomerase I by stabilizing the DNA-topoisomerase I covalent complex. Mitomycin C and cisplatinum generate DNA inter-strand cross-links. Inhibitors of ATR or CHK1 cause uncontrolled origin activation. Last but not least UV irradiation induces helix-distorting DNA lesions, such as cyclobutane pyrimidine dimmers.

However, replisomes also encounter a substantial number of natural impediments during fork progression (Figure 1). Genomic regions containing repetitive DNA sequences represent such hard-to-replicate loci. Trinucleotide repeats can form secondary DNA structures like hairpins that cause replication fork stalling. As a result of this, repetitive sequences are prone to expansions or contractions of the repeat sequence, and subsequent gene dysfunction (Kim and Mirkin, 2013). Another obstacle is DNA structure called G-quadruplex that forms at guanine-rich sequences. In mammals, telomeres consisting of long TTAGGG tandem repeats are regions with the highest concentration of G-quadruplexes (Lipps and Rhodes, 2009). Chemical stabilization of G-quadruplexes by pyridostatin or PhenDC3 results in slower replication fork progression, increased DNA breakage and telomere fragility (Zimmer et al., 2016).

The physiological status of the cells also determines the level of replication stress. Embryonic stem cells represent a transient biological state, where pluripotency is coupled with fast proliferation. Embryonic stem cells display a constitutively active ATR pathway. They display accumulation of single-stranded DNA gaps, reduced fork speed and frequent fork reversal. All these features are lost upon onset of differentiation. Replication stress appears to be linked with contracted cell cycle structure in embryonic stem cells, consisting of a short G1- and G2-phase and a high proportion of cells in S-phase (Ahuja et al., 2016).

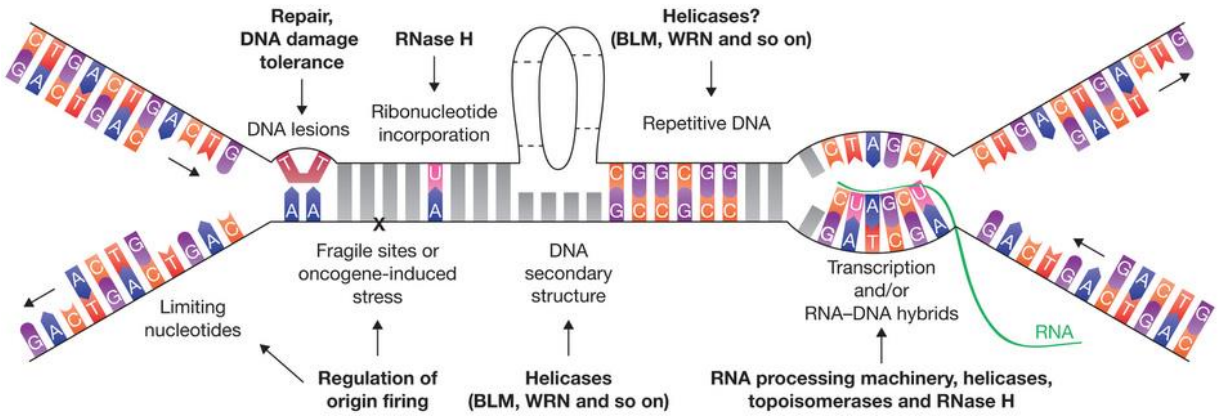

Figure 1. Sources of replication stress. There are a number of conditions or obstacles that can slow or stall DNA replication, including limiting nucleotides, DNA lesions, ribonucleotide incorporation, repetitive DNA elements, transcription complexes and/or RNA–DNA hybrids, DNA secondary structure, fragile sites, and oncogene-induced stress. Some of the key resolution pathways that are known for each source of stress are indicated in bold (Zeman and Cimprich, 2014).

Constitutive activation or overexpression of oncogenes is a frequent feature of precancerous cells and leads to perturbation of replication (Halazonetis et al., 2008). Oncogene activation results in unscheduled replication initiation that cause re-replication and/or premature origin activation as seen upon expression of cyclin E, cyclin D2, CDC25 and MYC oncogenes. The increased origin firing is a condition that can lead to depletion of nucleotide pools or interference between replication and transcription (Zeman and Cimprich, 2014).

1.4. Replication-transcription collisions

Studies in bacterial, yeast and mammalian cells have shown that replication-transcription encounters are unavoidable and represent one of the major sources of replication stress. Replication-transcription encounters cause spontaneous DNA breakage and chromosomal rearrangements, particularly if cells are subjected to other source of replication stress (Helmrich et al., 2013). Replication fork encounters the transcription machinery head-on on the lagging strand template and co-directionally on the leading strand. Although both types of collisions are associated with replication fork stalling *in vivo*, several lines of evidence indicate that the head-on clashes between replication and transcription mainly affect genome stability (Azvolinsky et al., 2009; Brambati et al., 2015; Merrikh et al., 2011). In bacteria, head-on encounters are clearly more severe since insertion of an inducible ColE1 replication origin upstream or downstream of

a ribosomal RNA (rRNA) operon in *E. coli* demonstrated that head-on transcription significantly impairs replication progression (French, 1992). The organization of bacterial genomes probably reflects the unfavourable effects of head-on collisions between replication and transcription. All sequenced bacterial genomes are biased for the majority of genes to be encoded on the leading strand. In *B. subtilis*, ~95% of essential genes and 75% of the other genes are on the leading strand independently of the level of expression (Rocha, 2008).

In yeast, highly expressed chromosomal regions are potential hot spots for replication-transcription conflicts irrespective of the orientation of collisions (Azvolinsky et al., 2009). By genome-wide mapping of replicative DNA polymerase binding to yeast chromatin, it has been demonstrated that highly transcribed RNA polymerase (RNAP) II genes are sites of replication fork pausing (Azvolinsky et al., 2009). In yeast, specific reporter assays have shown that RNAPII transcription concomitant to head-on oncoming, but not co-directional, replication causes a replication fork pause that is linked to a significant increase in DNA recombination (Prado and Aguilera, 2005). However, it remains unclear why head-on collisions are more challenging to preserve genomic stability. DNA instability can arise from tethering of highly transcribed genes to the nuclear envelope, which may lead to generation of topological tension as replication fork approaches (Bermejo et al., 2011). Phosphorylation of nucloeporins by S-phase checkpoint kinases detach transcribed genes from nuclear pores to prevent DNA breakage (Bermejo et al., 2011). Importantly, transcription machinery itself has a direct role in defects of replication fork progression. Yeast cells harbouring mutation of RNAPII (*rpb1-1, rpb1-S751F* and *rpb9Δ)* that display transcription elongation defects are sensitive to HU and accumulate replication-born DNA breaks. Moreover, replication defect observed in *rpb1-1* leads to the accumulation of Rad51-dependent HJ-intermediates and activation of dormant origins. *rpb1-1* mutant showed an increased retention of RNAPII on genes, suggesting that active transcription suppresses replication fork slowing (Felipe-Abrio et al., 2015).

In human cells, replication fork slowing is caused by perturbed transcription due to the lack or CPT-induced inhibition of DNA topoisomerase I (Ribeyre et al., 2016; Tuduri et al., 2009). Cells treated with CPT also display increased level of CHK1 phosphorylation at Ser345 and accumulate reversed forks. All the above mentioned phenotypes are rescued by premature termination of transcription using cordycepin, suggesting that transcription is the major determinant of replication hindrance by CPT or topoisomerase I deficiency (Ribeyre et al., 2016; Tuduri et al., 2009). Interference between replication and transcription also underlies replication

fork slowing and DNA breakage in cells with an oncogene-induced hyperactivation of replication origins (Jones et al., 2013). Cyclin E over-expression significantly increases the number of early S-phase replication foci, which can escalate the number of replication-transcription encounters leading to multiple replication fork stalling. As a result of that, cells accumulate RAD51 foci. However, the inhibition of transcription rescues the rate of replication fork progression and decreases DNA breakage without affecting the replication fork itself (Jones et al., 2013).

A correlation between replication stress–provoked genomic instability and active transcription is particularly apparent in case of common fragile sites (CFSs) and recently identified early replicating fragile sites (ERFSs) (Barlow et al., 2013; Helmrich et al., 2011). CFSs are specific genomic regions that exhibit increased frequency of gaps or breaks on metaphase chromosomes if DNA replication is partially inhibited (Durkin and Glover, 2007). Interestingly, CFSs are frequently located within the coding regions of very long genes (>650 kb), whose transcription is completed even within more than one complete cell cycle that is a prerequisite for inevitable replication-transcription collisions (Helmrich et al., 2011; Helmrich et al., 2006). Further, collisions between replication and transcription complexes at CFSs are accompanied by the formation of RNA:DNA hybrids, structures referred to as R-loops, which can cause chromosomal breakage. There is also evidence that the chromosomal breakage at CFSs is an outcome of replication paucity and subsequent incompletion due to a low density of replication origins within these loci (Debatisse et al., 2012). In contrast to late replicating CFSs, ERFSs are located within early replicating regions that contain clusters of highly transcribed genes (Barlow et al., 2013). ERFSs break spontaneously during replication, but their fragility is significantly increased by early S-phase replication stress induced by HU, oncogene activation or ATR inhibition. ERFSs are characterized by the instability of early replication forks whose stalling occurs at intragenic sequences and promoters of highly transcribed genes (Barlow et al., 2013). Importantly, the chromosomal breakage at selected ERFS near *SWAP70* gene is greatly dependent on the level of transcription, suggesting that it is driven by replication-transcription encounters (Barlow et al., 2013). An accumulation of BRCA1 accompanied the replication fork stalling at these sites, indicating involvement of homologous recombination process in replication fork protection and restart (Barlow et al., 2013; Schlacher et al., 2012).

Despite accumulating evidence that conflicts between replication and transcription are frequent events in proliferating cells and have detrimental effects on genome integrity, little is known about the molecular mechanisms underlying their resolution.

1.5. RecQ helicases

Evidence suggests that members of the RecQ helicase family are among the most important factors that maintain genomic stability during DNA replication, especially under conditions of replication stress. The importance of RecQ helicases is underlined by the presence of at least one RecQ family member in all organisms with some exceptions for bacteria and archaea that mostly possess small genomes (Nakayama, 2002). Bacteria and yeasts usually contain a single representative of the RecQ family, namely RecQ in *E. coli*, Sgs1p in *S. cerevisiae* and Rqh1p in *S. pombe*. Intriguingly, the number of RecQ family members expressed in particular organism increases with the size of its genome (Nakayama, 2002). Non-redundant functions of multiple RecQ homologues in an organism are apparent from their structure. Eukaryotic RecQ helicases share an evolutionary conserved helicase domain flanked by unique N- and C-terminal regions containing interaction sites for other proteins that determine specific functions (Figure 2) (Croteau et al., 2014). In humans, five RecQ homologues have been identified thus far and named RECQ1, BLM, WRN, RECQ4 and RECQ5 (encoded by *RECQL*, *BLM*, *WRN*, *RECQL4* and *RECQL5* genes, respectively). The significance of these RecQ helicases is highlighted by the association of mutations in the genes encoding for BLM, WRN and RECQ4 with severe hereditary disorders named Bloom, Werner and Rothmund-Thompson syndrome, respectively (Croteau et al., 2014). These rare recessive disorders are characterized by genomic instability and predisposition to cancer (Oshima et al., 1993; Oshima et al., 2016; Sanz et al., 1993; Wang and Plon, 1993). Recently, defects in RECQ1 and RECQ5 have been also connected to cancer development (Cybulski et al., 2015; He et al., 2014; Qi and Zhou, 2014; Sun et al., 2015; Zhi et al., 2014). Moreover, the *RECQL* gene has been added on the list of breast cancer susceptibility genes that mostly contains genes involved in the maintenance of the integrity of replication forks like *BRCA1/2* (Banerjee and Brosh, 2015; Venkitaraman, 2014).

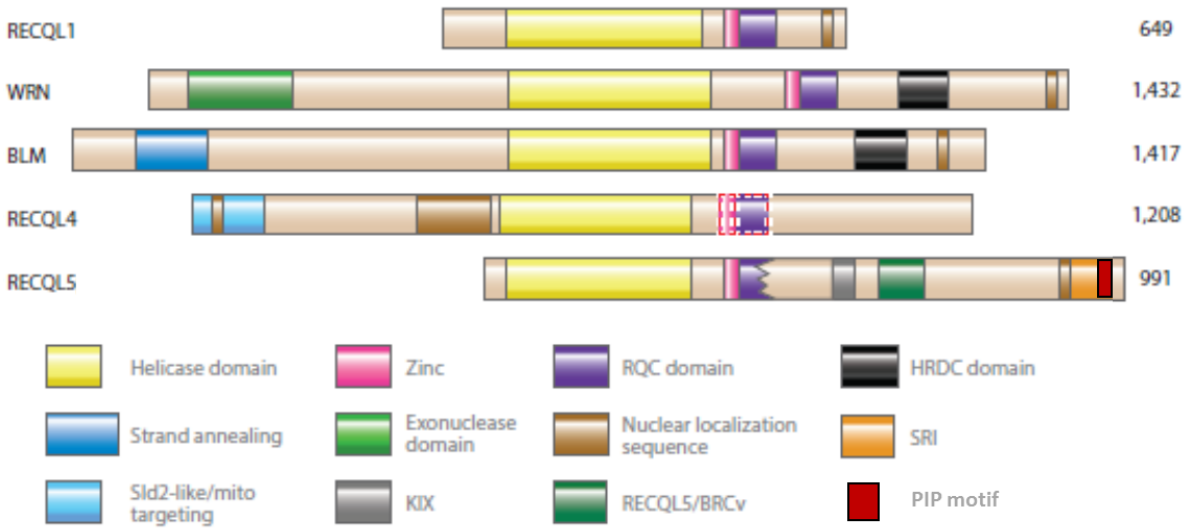

Figure 2. The domain structure of human RecQ helicases (adapted from Croteau et al., 2014).

Despite the accumulating evidence for the role of human RecQ helicases in the maintenance of genome stability, the underlying molecular mechanisms remain elusive. Human RecQ helicases have been associated with DNA repair by homologous recombination, base excision repair and non-homologous end joining (Croteau et al., 2014). However, recent studies have particularly demonstrated the involvement of human RecQ helicases in different aspects of DNA replication.

1.5.1. RecQ helicases associate with replisome components

Slow replication fork movement has been observed in cells depleted for BLM, WRN, RECQ1, but not for RECQ4 and RECQ5 (Hand and German, 1975; Kim et al., 2015; Park et al., 2006; Sidorova et al., 2013; Sidorova et al., 2008; Thangavel et al., 2010). However, a decreased proliferation of mouse embryonic fibroblasts lacking RECQ4 was observed (Sangrithi et al., 2005). Interaction partners of RecQ helicases indicate their participation in processes associated with replication fork progression. RECQ5 and WRN possess the so-called PIP (PCNA-interacting peptide) motif that mediates interaction with PCNA, one of the key replisome components, and both helicases localize to replication factories in unperturbed cells (Kanagaraj et al., 2010; Rodriguez-Lopez et al., 2003). WRN, RECQ5, BLM and RECQ1 interact with FEN1 flap endonuclease that participates in Okazaki fragment maturation, and all stimulate 5'-flap DNA cleavage by FEN1 *in vitro*, in a manner independent of their helicase

activity (Bachrati and Hickson, 2008; Sami et al., 2015). Moreover, RECQ1 was shown to facilitate efficient binding of FEN1 to telomeres (Sami et al., 2015). WRN interacts with DNA polymerase δ and facilitates copying tetraplex and hairpin structures (Kamath-Loeb et al., 2001). Moreover, WRN exonuclease is involved in proofreading during DNA synthesis by DNA polymerase δ (Kamath-Loeb et al., 2012). WRN can also help overcome DNA lesions during replication by interacting with translesion polymerases and stimulating their action (Kamath-Loeb et al., 2007; Phillips and Sale, 2010) and by serving as their proofreader (Maddukuri et al., 2012). However, recent studies have shown that rather than forming a stable part of replisome, human RecQ helicases remove replication roadblocks and act to promote replication resumption.

1.5.2. Role of RECQ4 in the initiation of DNA replication

RECQ4 seems to be involved in the DNA replication process *per se*, specifically in replication origin activation (Collart et al., 2013; Matsuno et al., 2006; Thangavel et al., 2010). The N-terminus of RECQ4 shares a weak but significant homology to the yeast Sld2 that assists in the recruitment of GINS to replication origins during S phase in a manner dependent on CDK activity (Matsuno et al., 2006; Sangrithi et al., 2005; Tanaka et al., 2007; Zegerman and Diffley, 2007). Indeed, the N-terminal region of RECQ4 was shown to be essential for cell viability (Abe et al., 2011; Ichikawa et al., 2002; Matsuno et al., 2006). RECQ4 associates with several proteins involved in replication initiation like the MCM2-7 complex, MCM10, GINS, CDC45 (Im et al., 2009; Xu et al., 2009). The absence of RECQ4 was shown to significantly affect the formation of CMG complex (Im et al., 2009; Xu et al., 2009). Moreover, other replication factors including RPA, PCNA and particularly DNA polymerase α display reduced binding to chromatin in the absence of RECQ4 (Sangrithi et al., 2005; Thangavel et al., 2010). RECQ4 is recruited to replication origins at G1/S boundary upon ORC and MCM complex assembly, and forms a complex with CTF4 and MCM10 in a process dependent on the CDK and DDK kinase activities (Im et al., 2015; Thangavel et al., 2010; Xu et al., 2009). The efficient binding of RECQ4 to replication origins followed by their firing may be controlled by the interaction between RECQ4 and MCM10 (Im et al., 2009; Im et al., 2015; Kliszczak et al., 2015; Thangavel et al., 2010). However, the interaction between RECQ4 and MCM10 is not required for cell viability (Kliszczak et al., 2015). Moreover, MCM10, the prominent interactor of RECQ4, was recently shown to promote replication fork progression under conditions of replication stress (Chadha et al., 2016). Depletion of both, MCM10 and RECQ4, results in reduced binding of DNA

polymerase α and PCNA on chromatin (Chadha et al., 2016; Sangrithi et al., 2005; Thangavel et al., 2010). Thus, MCM10 and RECQ4 may act together to keep or recover DNA polymerase α, PCNA, CDC45 and GINS at lagging strand during replication fork stalling. Consistently, the essential role of both proteins in initiation of replication is in conflict with proficient bulk DNA synthesis after their depletion (Park et al., 2008; Thangavel et al., 2010). Interestingly, studies in budding yeast revealed that PCNA is unloaded only from the lagging strand arm of forks stalled by HU treatment (Yu et al., 2014). Thus, RECQ4 and MCM10 may be involved in the recovery of replisome at stalled forks.

1.5.3. BLM promotes resolution of aberrant DNA structures at stalled replication forks

Common feature of cells deficient in BLM is increased frequency of sister chromatid exchanges (SCEs) that are thought to arise from aberrant repair of damaged replication forks (Hickson, 2003). To suppress excessive homologous recombination, BLM is recruited to sites of replication fork stalling in a manner dependent on RNF8/RNF168-mediated ubiquitination of the N-terminal region of BLM and subsequent BLM binding to the ubiquitin-interacting motifs of RAP80 (Tikoo et al., 2013). BLM is required for efficient replication fork restart and suppression of dormant origin firing after replication blockage, which is dependent on its helicase activity and phosphorylation (at Thr99) via the ATR/Chk1 pathway (Davies et al., 2007; Sidorova et al., 2013). Cells derived from Bloom syndrome patients accumulate abnormal replication intermediates and display increased levels of single-stranded DNA and RAD51-containing foci, which is pronounced after replication blockage by HU or Aph (Lonn et al., 1990; Rassool et al., 2003). RAD51 is a central homologous recombination factor that plays an important role in the resumption of stalled and collapsed replication forks (Petermann et al., 2010). BLM and RAD51 act together during fork recovery (Sidorova et al., 2013). Sumoylation of BLM increases the *in vitro* interaction between RAD51 and BLM, and may regulate the recovery of stalled forks by facilitating RAD51 recruitment or stabilization of its binding to stalled forks, and preventing the accumulation of single-stranded DNA coated by RPA. Accordingly, impaired BLM sumoylation (at lysine K317 and K331) increases fork collapse and cell death (Ouyang et al., 2009; Ouyang et al., 2013).

Four-way DNA structures called Holliday junctions (HJs) can arise during the recovery of stalled replication forks (Petermann and Helleday, 2010). BLM forms a complex with topoisomerase IIIα (TOPOIIIα) and RMI1/2 to dissolve double-HJs, which arise during homologous recombination, via a strand passage mechanism preventing crossover outcomes

(Wu and Hickson, 2003). The TOPOIIIα-interacting domain of BLM is required for the suppression of SCEs in BS cells (Hu et al., 2001). RMI1 also suppress SCEs and the interaction between BLM and RMI1 promotes proper fork progression and recovery from replication stress (Yang et al., 2012; Yin et al., 2005). The BLM-TOPOIIIα-RMI1/2 complex localizes to subnuclear foci, which is pronounced after replication blockage by HU or Aph (Yang et al., 2012). Thus, the excess of nuclear foci containing single-stranded DNA in the absence of BLM can arise due to the impaired localization of TOPOIIIα (Yang et al., 2010). Recently, FANCD2 was shown to be involved in the efficient assembly of the BLM-TOPOIIIα-RMI1/2 complex at sites of stalled replication forks and to act with BLM in a common pathway to promote replication fork restart and suppression of new origin firing (Chaudhury et al., 2013). The dissolution reaction catalyzed by the BLM-TOPOIIIα-RMI1/2 complex appears to be a unique function of BLM among human RecQ helicases (Wu et al., 2005). This activity is also important at sites of termination of DNA replication, because BLM accumulates on late replication intermediates to assist in duplex separation so that DNA replication can be efficiently completed (Barefield and Karlseder, 2012; Chan et al., 2007; Chen and Brill, 2010; Lukas et al., 2011).

In addition to double-HJs dissolution, BLM is able to unwind G-quadruplexes formed at guanine rich sequences (Sun et al., 1998). In mammals, telomeres are regions with the highest concentration of G-quadruplexes (Lipps and Rhodes, 2009). Indeed, BLM was shown to maintain stability of telomeres (Barefield and Karlseder, 2012; Lillard-Wetherell et al., 2004). BLM can suppress G-quadruplex formation both genome-wide and, specifically, at telomeres (Drosopoulos et al., 2015). BLM binds to the telomere-specific shelterin proteins TRF1, TRF2 and POT1, which are essential for telomere capping and repression of DNA damage signaling (Lillard-Wetherell et al., 2004; Opresko et al., 2005; Opresko et al., 2002). BLM-deficient mouse cells show a high frequency of spontaneous telomere fragility visible as a separation of telomeric signals from chromatid ends (Sfeir et al., 2009; Zimmermann et al., 2014). Moreover, it was shown that TRF1 binding to BLM prevented telomere fragility, with most of the fragile telomeres resulting from lagging strand DNA synthesis (Zimmermann et al., 2014). The majority of telomeres are replicated by forks moving toward the telomere end using the TTAGGG repeat strand as the template for lagging strand DNA synthesis (Sfeir et al., 2009). However, compared to BLM-proficient cells, BLM-deficient cells also show a slower rate of leading strand synthesis that initiates within the telomere and higher frequency of replication initiation originating closer to the telomere (Drosopoulos et al., 2015). Further, slowdown of

telomeric replication fork movement was observed upon treatment of BLM-deficient cells with G-quadruplex stabilizer PhenDC3, suggesting that BLM facilitates telomere replication by resolving G-quadrulexes (Drosopoulos et al., 2015). However, the G-quadruplex-stabilizing compound pyridostatin increases telomeric-SCEs in cells lacking homologous recombination factors such as BRCA1, BRCA2 or RAD51 and reduces the viability of these cells (Zimmer et al., 2016). Thus, the above mention activities of BLM (in homologous recombination or double-HJs dissolution) may be utilized to promote restart of stalled forks at G-quadruplexes.

BLM is also implicated in recombination-mediated mechanism of telomere maintenance, referred to as alternative lengthening of telomeres (ALT) (Rezazadeh, 2013). Overexpression of BLM in cells using ALT increases telomeric signals, suggesting that BLM promotes ALT (Stavropoulos et al., 2002). Depletion of BLM in cells using ALT leads to increased levels of telomere length attrition and telomeric SCEs (Bhattacharyya et al., 2009; Hagelstrom et al., 2010; Sarkar et al., 2015). In the absence of functional BLM, the SLX4-nuclease complex resolves persistent HR intermediates to yield crossover products, resulting in increased SCEs (Sarkar et al., 2015; Wechsler et al., 2011). Recently, it has been shown that BLM function is modulated by BRCA1 and FANCD2 during ALT (Acharya et al., 2014; Root et al., 2016).

1.5.4. WRN promotes restart of stalled replication forks

Cells derived from Werner syndrome patients display a high frequency of chromosomal translocations, deletions and telomere loss, but not SCEs (Fukuchi et al., 1989; Gebhart et al., 1988; Schulz et al., 1996). Further, fibroblasts isolated from Werner syndrome patients show chromosome and chromatid fusions that result from repair attempts of dysfunctional telomeres (Crabbe et al., 2007). Werner syndrome cells are also highly sensitive to replication-perturbing agents (Pichierri et al., 2001; Poot et al., 2002; Poot et al., 1999; Poot et al., 2001). Similarly, WRN-deficient cells exposed to various types of replication stress accumulate DNA double-stranded breaks and show increased expression of CFSs as compared to WRN-proficient cells (Basile et al., 2014; Franchitto et al., 2008; Murfuni et al., 2012; Murfuni et al., 2013; Pirzio et al., 2008). Replication stress triggers extensive co-localization of WRN with RPA at nuclear foci in a manner dependent on WRN phosphorylation by ATR (Ammazzalorso et al., 2010; Constantinou et al., 2000; Franchitto and Pichierri, 2004). Consistently, WRN possesses two RPA binding sites (Doherty et al., 2005). Moreover, WRN was shown to promote ATR-dependent checkpoint activation upon replication fork stalling (Basile et al., 2014; Hyun et al.,

2016; Patro et al., 2011). The effect of WRN on the ATR-signaling pathway as well as WRN phosphorylation by ATR may result from its interaction with the checkpoint sliding clamp RAD9-RAD1-HUS1 that upon fork arrest recruits the ATR activator TOPBP1 (Pichierri et al., 2012). The significance of WRN phosphorylation is underlined by the fact that stalled forks undergo collapse followed by DNA double-stranded break formation in cells expressing ATR-unphosphorylable mutant of WRN, like in WRN-deficient cells (Ammazzalorso et al., 2010; Franchitto et al., 2008; Murfuni et al., 2013). The accumulation of DNA double-stranded breaks in WRN-deficient cells is dependent on MUS81 nuclease activity (Franchitto et al., 2008; Murfuni et al., 2013). However, a co-depletion of MUS81 and WRN has more severe effect on cell viability than depletion of either protein, even without induction of replication stress, suggesting existence of alternative mechanisms for response to replication fork stalling (Franchitto et al., 2008; Murfuni et al., 2013).

Decreased rate of replication fork progression in the absence of functional WRN is accompanied by a significant asymmetry of bidirectional forks (Rodriguez-Lopez et al., 2002). The recovery of stalled forks is impaired in WRN-deficient cells, which is consistent with proposed function of WRN in sustaining replication (Ammazzalorso et al., 2010; Franchitto et al., 2008; Sidorova et al., 2008; Thangavel et al., 2015). Importantly, WRN-depleted cells accumulate reversed forks, which is more prominent after HU treatment (Thangavel et al., 2015). Moreover, the human DNA2 and WRN form complex to promote replication restart that is dependent on degradation of nascent DNA by nuclease activity of DNA2 and helicase activity of WRN (Thangavel et al., 2015).

While the processing of replication intermediates by WRN/DNA2 is independent of other nucleases that are typically involved in DNA resection like EXO1, MRE11 or CTIP, recent evidence implicated exonuclease activity of WRN in protection of nascent DNA strands against unscheduled degradation by combined action of MRE11 and EXO1 after low dose of CPT (Iannascoli et al., 2015). Moreover, WRN protein independently of its enzymatic activities is required to prevent degradation of nascent DNA at replication-dependent double-stranded breaks induced by high doses of CPT (Su et al., 2014). In this case, NBS1 recruits WRN to replication-associated DNA breaks to stabilize RAD51 binding and limit activity of MRE11 (Su et al., 2014).

The characteristic features of cells derived from Werner syndrome patients is premature senescence and accelerated telomere shortening, suggesting that WRN has a critical function in

telomere maintenance (Crabbe et al., 2004; Opresko et al., 2003; Schulz et al., 1996). Similar to BLM, WRN associates with telomeres during S-phase and binds to the telomere-specific shelterin proteins TRF2 and POT1, which are essential for telomere capping and repression of DNA damage signaling (Crabbe et al., 2004; Opresko et al., 2005; Opresko et al., 2002). WRN has been shown to suppress defects in telomere lagging strand synthesis (Crabbe et al., 2004). Mutational inactivation of WRN helicase domain results in loss of telomeric signal only from the chromatid that uses G-rich strand as template for lagging strand synthesis, while leading strand telomere is not lost (Crabbe et al., 2004). Consistently, WRN deficiency results in increased frequency of G-quadruplex formation genome-wide and at telomeres (Drosopoulos et al., 2015). Although BLM helicase is also contributing to chromosome-end maintenance, WRN has distinct role in this process. This is supported by observation that simultaneous loss of both helicases substantially exacerbates the telomere dysfunction in comparison to loss of individual helicase (Barefield and Karlseder, 2012; Drosopoulos et al., 2015; Sfeir et al., 2009).

1.5.5. RECQ1 unwinds reversed replication forks

Cells lacking RECQ1 display an elevated number of genomic and telomeric SCEs (Popuri et al., 2014; Sharma and Brosh, 2007; Sharma et al., 2007). RECQ1 deficiency results in sensitivity to various DNA damaging agents that directly or indirectly block replication fork progression (Popuri et al., 2012). RECQ1 associates with replication origins in unperturbed cells and shows an increased binding to the lamin B2 origin and CFSs under conditions of replication stress (Thangavel et al., 2010). RECQ1-depleted cells or cells expressing RECQ1 mutants that lack helicase or branch migration activity display reduced replication fork rates and defects in checkpoint activation under conditions of replication stress (Banerjee et al., 2015; Thangavel et al., 2010). RECQ1-defficiency also leads to nascent strand degradation at stalled replication forks, which is dependent on DNA2 and WRN (Thangavel et al., 2015). A recent study revealed a role for RECQ1 in restarting stalled replication forks caused by DNA topoisomerase I inhibition with CPT (Berti et al., 2013). The ATPase activity of RECQ1 is essential for replication fork progression in cells exposed to CPT (Berti et al., 2013). In the presence of CPT, replication forks stall and undergo fork reversal, which prevents replication fork run-off and formation of DNA double-stranded breaks (Ray Chaudhuri et al., 2012). The poly(ADP-ribosyl)ation activity of PARP1 is necessary for stabilization of regressed forks upon CPT treatment until the lesion is repaired (Ray Chaudhuri et al., 2012). PARP1 was shown to interact with RECQ1 and to regulate the restart of stabilized forks in the regressed state by RECQ1-

mediated unwinding of the regressed arm (Berti et al., 2013; Sharma et al., 2012). *In vitro* experiments indicated that PARylated PARP1 inhibits fork restoration activity of RECQ1 (Berti et al., 2013). Reversed forks accumulate in RECQ1-depleted cells (Berti et al., 2013). Inhibition of PARP1 activity causes an untimely restart of reversed forks in a manner dependent on RECQ1, which results in DSB formation (Berti et al., 2013). Moreover, the restart of reversed forks by RECQ1-mediated mechanism can be a more general response to a wide variety of replication blocking agents (Zellweger et al., 2015).

1.5.6. RECQ5 suppresses transcription associated DNA breakage during replication

Subunits of RNA polymerase (RNAP) II are the most prominent proteins that co-immunoprecipitate with RECQ5 from human cell extracts (Aygun et al., 2008; Izumikawa et al., 2008). RECQ5 was shown to interact with the largest catalytic subunit of RNAPII, termed RPB1 (Aygun et al., 2008), and this interaction is enhanced during S-phase (Li et al., 2011). Two regions of RECQ5 polypeptide were identified to mediate the interaction with RPB1: (i) the internal RNAPII-interacting (IRI) domain including KIX motif, which binds to RPB1 jaw domain; and (ii) the Set2-Rpb1-interacting (SRI) domain, which binds to the hyperphosphorylated C-terminal repeat domain (CTD) of RPB1 (Islam et al., 2010; Kanagaraj et al., 2010; Kassube et al., 2013). Intriguingly, the tertiary structure of the KIX domain resembles the domain II of TFIIS that resolves the paused state of backtracked RNAPII (Kassube et al., 2013; Wind and Reines, 2000). RECQ5 associates with chromatin particularly at RNAPII-transcribed regions (Izumikawa et al., 2008; Kanagaraj et al., 2010; Saponaro et al., 2014). Moreover, RECQ5 controls the movement of RNAPII across genes to prevent it from pausing or arrest, a condition referred to as transcription stress (Saponaro et al., 2014). Importantly, RECQ5 also localizes to DNA replication foci throughout S phase and interacts physically with the proliferating cell nuclear antigen (PCNA), a key component of the replisome (Kanagaraj et al., 2006). A slight increase in the nuclear level of RECQ5 helps to deal with thymidine-induced replication stress (Blundred et al., 2010). It has been shown that replication stress results in the accumulation of RPA at stalled forks, which can lead to RPA exhaustion and subsequent fork collapse (Toledo et al., 2013). Consistently, the slight increase of RECQ5 cellular concentration suppresses the increased level of RPA foci observed under conditions of replication stress (Blundred et al., 2010). RECQ5-deficient cells display an increased level of RAD51 foci and elevated SCEs (Hu et al., 2007). Depletion of RECQ5 results in transcription-dependent chromosome fragmentation during S phase and accumulation of chromosomal

rearrangements with the breakpoints located in the genes and common fragile sites (CFSs) (Li et al., 2011; Saponaro et al., 2014). Interestingly, the incidents of genome instability in RECQ5-depleted cells colocalize with the areas of elevated transcription stress (Saponaro et al., 2014). Finally, inactivation of the *Recql5* gene in mice results in cancer susceptibility which supports the role of RECQ5 as a tumor suppressor (Hu et al., 2007). Together, these finding suggest that RECQ5 prevents genomic instability at sites of concomitant replication and transcription. However, it is unclear whether RECQ5 operates directly at sites of replication-transcription interference.

2. Aims of the study

The main aim of the study was to elucidate the role of RECQ5 helicase in the maintenance of genomic stability.

The specific aims of this study were:

- To characterize the association of RECQ5 with RNA polymerase I and II
- To explore the role of RECQ5 at the interface of replication and transcription
- To study the molecular mechanism underlying the resolution of replication-transcription encounters

3. List of used methods

Standard molecular biology techniques (nucleic acid isolation, DNA cloning, reverse transcription, qPCR, SDS-PAGE, immunoblotting, immunoprecipitation, immunofluorescence)

Cell culture, RNA interference, DNA transfection

Flow cytometry

Cell fractionation

Chromatin Immunoprecipitation (ChIP)

Comet assay

Protein purification, antibody production

Fluorescence recovery after photobleaching (FRAP)

4. List of publications

1# RECQ5 helicase promotes resolution of conflicts between replication and transcription in human cells.

Urban V, Dobrovolna J, Hühn D, Fryzelkova J, Bartek J, Janscak P.

J Cell Biol. 2016 Aug 15;214(4):401-15

2# RecQ-core of BLM unfolds telomeric G-quadruplex in the absence of ATP.

Budhathoki JB, Ray S, Urban V, Janscak P, Yodh JG, Balci H.

Nucleic Acids Res. 2014 Oct;42(18):11528-45

3# RECQ5 helicase associates with the C-terminal repeat domain of RNA polymerase II during productive elongation phase of transcription.

Kanagaraj R, Huehn D, MacKellar A, Menigatti M, Zheng L, Urban V, Shevelev I, Greenleaf AL, Janscak P.

Nucleic Acids Res. 2010 Dec;38(22):8131-40.

4# Distinct functions of human RecQ helicases during DNA replication.

Urban V, Dobrovolna J, Janscak P.

Submitted in Biophysical Chemistry.

5. Participation of Václav Urban on presented publications

Research paper #1 – Václav Urban as a first author performed all of the experiments, participated on manuscript preparation and submission

Research paper #2 – Václav Urban as co-author performed purification of some proteins used for biochemical assays

Research paper #3 – Václav Urban as a co-author participated on cloning of RECQ5 variants for mapping of the interaction between RECQ5 and RPB1

Review paper #4 – Václav Urban as a first author participated on manuscript preparation and submission

6. Linking of publications

Publications #1 and #3 characterize the interaction of RECQ5 with RNAPI and RNAPII, respectively. We describe the interaction domains of RECQ5 with both RNAPs and association of RECQ5 with coding regions devoted to RNAPI and II transcription. Publication #1 further investigates the role of RECQ5 at the interface of replication and transcription. We show that RECQ5 promotes resolution of replication-transcription conflicts in human cells. We characterize distinct roles of helicase and PCNA-interacting domains of RECQ5 in the resolution of replication intermediates that arise at sites of replication-transcription encounters.

Publication #2 suggests a possible biochemical mechanism how BLM helicase may disrupt G-quadruplex structures that represent a significant impediment for replication fork progression.

In publication #4, distinct roles of human RecQ helicases are reviewed with emphasis on the role of human RecQ helicases in the processing of stalled replication forks. The major outcomes of publication #1 are presented there.

7. Discussion

The roles of human RecQ helicases during DNA replication are unwavering. Their common feature is to promote recovery of forks being stalled due to different replication roadblocks of either exogenous or endogenous source. Human RecQ helicases participate particularly in replication fork progression through genomic loci that represent natural impediment for replication such as CFSs, repetitive sequences, telomeres and actively transcribed regions. The overview of their proposed functions during DNA replication was reviewed in publication #4 and is depicted in Figure 3.

RECQ5 DNA helicase is essential for maintenance of genomic stability, but its exact molecular functions remain unclear. Recent studies (including publication #3) have shown that human RECQ5 binds to RNAPII during transcription elongation and maintains genomic stability at RNAPII-transcribed genes by acting as a factor that prevents transcription pausing

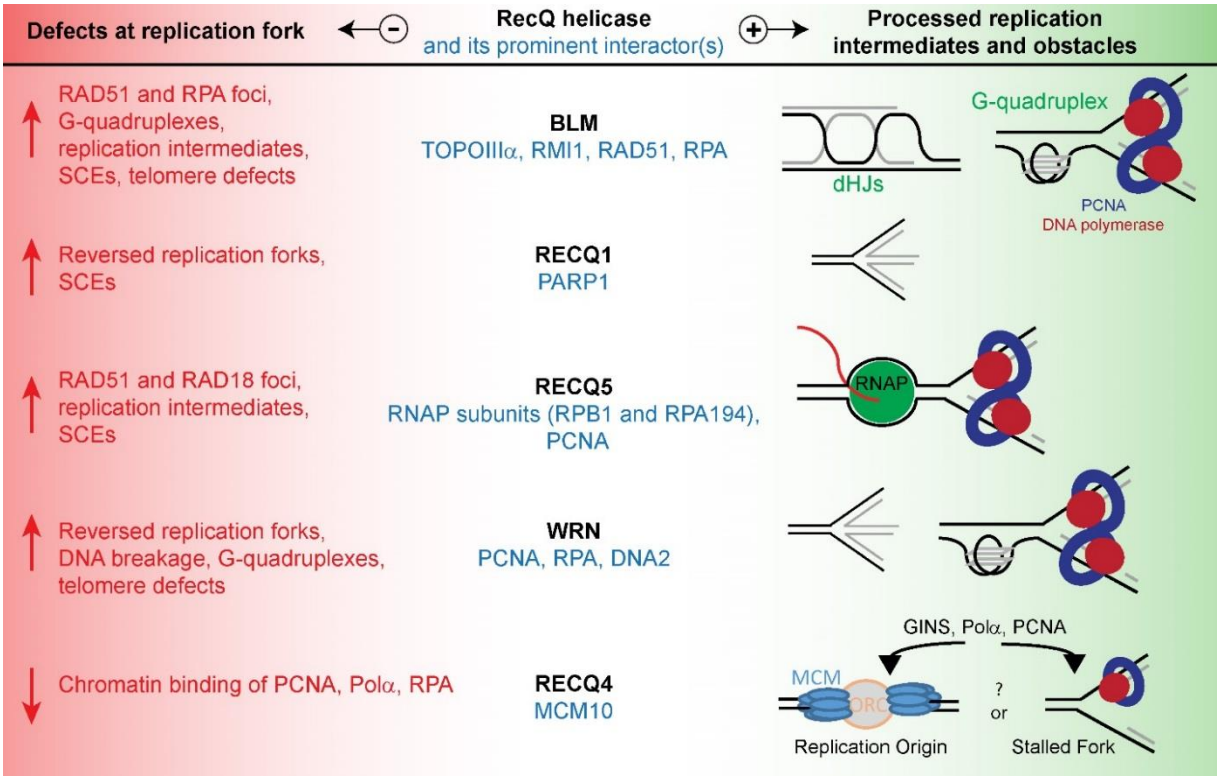

Figure 3. Overview of the functions of human RecQ helicases in genome maintenance during DNA replication. Replication intermediates or obstacles proposed to be resolved by the individual RecQ helicases are shown (right). Interaction partners of human RecQ helicases involved in their actions at replication forks are also listed along with phenotypic consequences of deficiency in individual RecQ helicases (left). Upwards arrows indicate increase; downwards arrows indicate decrease (Urban et al., unpublished)

or arrest, a condition termed transcription stress (Kanagaraj et al., 2010; Li et al., 2011; Saponaro et al., 2014). In our study (publication #1), we show that RECQ5 also forms a complex with RNAPI, namely with its the largest catalytic subunit, RPA194. RECQ5 was significantly enriched on the pre-rRNA coding region, showing a distribution pattern similar to that of RPA194. Interestingly, we observed a significant enrichment of RNAPI in the pre-rRNA coding region, but not on the promoter, in cells lacking RECQ5. These data suggest that RECQ5 associates with RNAPI and might counteract RNAPI transcription stalling. Our data describing association between RNAPI and RECQ5 are consistent with the proposal that RECQ5 acts as a general transcription elongation factor that is important for preserving genome stability during transcription (Kanagaraj et al., 2010; Li et al., 2011; Saponaro et al., 2014).

However, we also demonstrate that RECQ5 depletion caused DNA copy number variations, particularly within the pre-rRNA coding region of the rDNA repeat unit. Importantly, upon replication stress induced by HU treatment, RECQ5 depletion caused a significant amplification of DNA sequences only within the transcribed part of rDNA. Further, we also demonstrate that RECQ5 depletion causes the persistence of unresolved replication intermediates with replisomes stalled in both RNAPI- and RNAPII-transcribed genes. These findings suggest that the genome stabilization effect of RECQ5 at sites of transcription might reflect a role for RECQ5 in resolving collisions between the replication and transcription machineries. In support of this hypothesis, we have found that inhibition of transcription by ActD dramatically impaired the mobility of GFP-RECQ5 in replication foci, whereas no change in the mobility of GFP-RECQ5 outside the replication foci was observed. Thus, RECQ5 associates with active transcription complexes in DNA replication foci, suggesting that it acts at sites of concomitant transcription and replication.

Mechanisms that cells evolved to resolve conflicts between replication and transcription remain elusive. Studies in bacteria and yeast have shown that specific helicases act in conjunction with the replisome to remove transcription complexes and other obstacles that impair replication fork progression (Azvolinsky et al., 2009; Boubakri et al., 2010; Sabouri et al., 2012). However, on very long genes in mammalian cells, collisions between transcription and replication complexes occur within each round of transcription, because the synthesis of the full-length transcript of these genes takes more than one cell cycle (Helmrich et al., 2013). Therefore, to ensure proper gene expression, cells must have mechanisms that permit RNA chain elongation after the collision with replication fork. In our study, we provide evidence that

RECQ5, BRCA1, and RAD18 are recruited independently of each other to sites of replication-transcription collisions. Based on the counts of BRCA1 and RAD18 foci detected in S-phase nuclei, we can speculate that collision between replication and transcription is a quite frequent event in dividing cells. We have concluded that coordinated action of RECQ5 and BRCA1 at sites of replication-transcription interference promotes resolution of the conflict. BRCA1-dependent loading of RAD51 on stalled replication forks, which depends on active transcription, leads to fork stabilization. RECQ5 promotes RAD18-dependent PCNA ubiquitination and unloading at sites of replication-transcription interference that might allow the passage of oncoming transcription complexes across the fork to complete RNA synthesis (Figure 4). Failure of either of these activities would lead to persistence of stalled replication forks, resulting in genomic instability. In the absence of BRCA1, RECQ5 can mediate PCNA ubiquitination and unloading, but the replication fork fails to restart because of the impaired RAD51 loading. In the absence of RECQ5 or RAD18, BRCA1 can promote assembly of RAD51 filaments to protect stalled replication forks, but RNA polymerase cannot translocate across the replication fork, and hence replication restart is prevented (Figure 4).

RECQ5 deficiency leads to accumulation of RAD18 and RAD51 foci in S-phase cells. Recently, RAD51 has been shown to form and/or stabilize the regressed arm of replication fork converted to HJ-structure in response to replication fork stalling (Zellweger et al., 2015). Thus, RAD51 foci in RECQ5-deficient cells likely represent unresolved replication intermediates. Consistently, they display a long-term stability in the presence of RAD51 inhibitor B02, which prevents the formation of RAD51 foci in normal cells. We have shown that the helicase activity of RECQ5 is crucial to resolve these replication intermediates. RECQ5 also promotes RAD18-dependent ubiquitination of PCNA at sites of replication-transcription interference by directly interacting with PCNA via its PIP motif. The absence of RECQ5 or inactivation of its PIP motif increased both chromatin binding of RAD18 and frequency of RAD18 foci in S-phase nuclei, suggesting that it is a consequence of a defect in PCNA ubiquitination. Moreover, the helicase activity of RECQ5 is required for PCNA unloading from chromatin. Both activities, ubiquitination and unloading of PCNA, are intensified under brute overexpression of RECQ5 in cells, which results in the inhibition of replication and arrest of cells at G1/S boundary of the cell cycle. In contrast to the finding that RECQ5 inhibits RNAPII-transcription *in vitro* in a manner dependent on the IRI domain (Aygun et al., 2009), we have not observed any negative effect of RECQ5 overexpression on the rate of transcription *in vivo*, suggesting that RECQ5

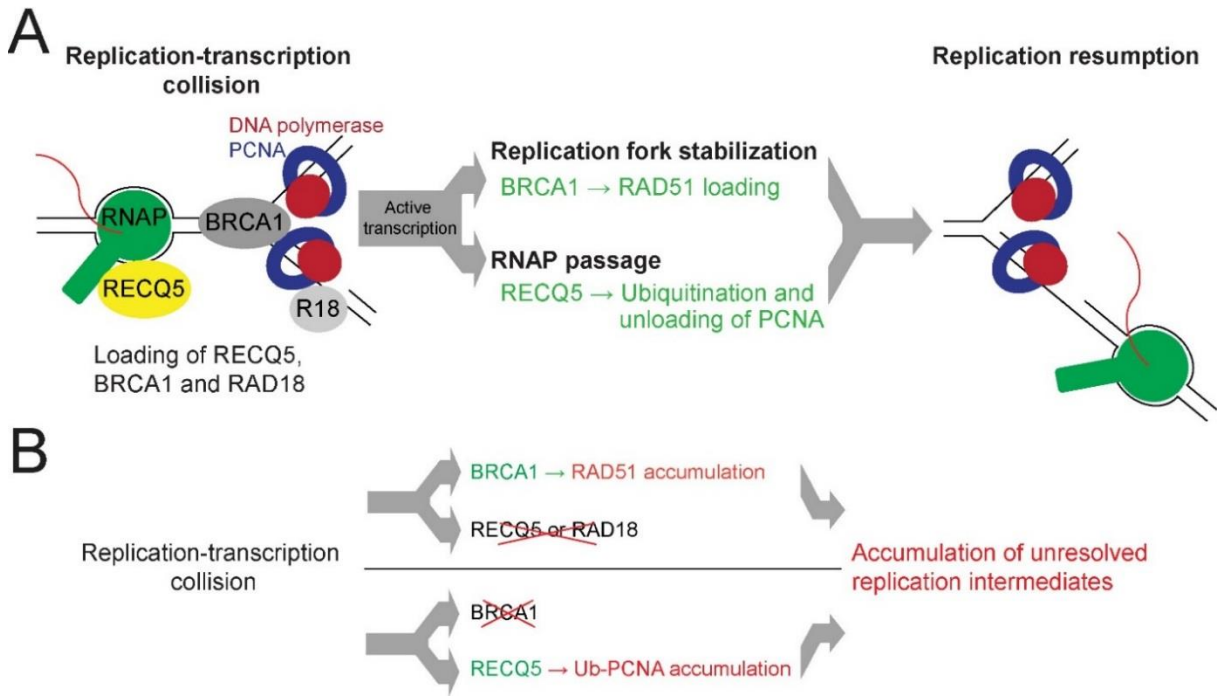

Figure 4. Model for resolution of conflicts between replication and transcription. (A) Scheme of the model. RECQ5, BRCA1, and RAD18 (R18) are recruited independently of each other to sites of replication-transcription collisions. BRCA1-dependent loading of RAD51 on stalled replication forks, which depends on active transcription, leads to fork stabilization. RECQ5 promotes RAD18-dependent PCNA ubiquitination and unloading at sites of replication-transcription interference that might allow the passage of oncoming transcription complexes across the fork to complete RNA synthesis. (B) Consequences of BRCA1 and RECQ5/RAD18 deficiencies. In the absence of BRCA1, RECQ5 can mediate PCNA ubiquitination and unloading, but the replication fork fails to restart because of the defect in RAD51 loading. In the absence of RECQ5 or RAD18, BRCA1 can promote assembly of RAD51 filaments to protect stalled replication forks, but RNA polymerase cannot translocate across the replication fork, and hence replication restart is prevented. Failure of either of these activities would lead to persistence of stalled replication forks, resulting in genomic instability. (Urban et al., 2016)

influences the replisome to favour transcription. Studies in budding yeast have shown that strains defective in PCNA unloading (e.g., Δelg1 or PCNA-K164R mutants) exhibit uncontrolled DNA replication and accumulate Rad52 foci, an indication of genomic instability (Yu et al., 2014). Interestingly, these studies have revealed that PCNA is unloaded only from the lagging strand arm of forks stalled by HU treatment (Yu et al., 2014). Thus, one can speculate that RECQ5-driven PCNA unloading and ubiquitination might allow the passage of oncoming transcription complexes across the fork to complete RNA synthesis.

BRCA1 acts to form RAD51 filaments at arrested replication forks to protect them from nucleolytic degradation (Schlacher et al., 2012). Similarly to RECQ5, BRCA1 mobility in S-phase foci was dramatically reduced in cells treated with ActD to arrest transcription. In

agreement with the immobilization of BRCA1 upon ActD treatment, the formation of RAD51 foci in S-phase cells was strongly attenuated by ActD, which further confirmed that BRCA1 activity is dependent on active transcription. In support of this notion, previous studies have shown that BRCA1 binds to hyperphosphorylated RNAPII that is present in the transcription elongation complex (Krum et al., 2003). Thus, it is possible that, in the process of resolution of replication-transcription collisions, BRCA1 acts in association with the transcription machinery.

There is accumulating evidence suggesting a role for active transcription in the resolution of replication-transcription collisions. It was shown that RNA polymerase translocation is required for the resolution of head-on collisions between the transcription machinery and bacteriophage Φ29 DNA polymerase in *Bacillus subtilis* (Elias-Arnanz and Salas, 1999). Similarly, studies in budding yeast have shown that RNAPII mutants with a defect in transcription elongation impair replication fork progression and cause genomic instability (Felipe-Abrio et al., 2015). In our study, we have shown that halted RNAPI transcription complexes prevented the movement of the replisome through rDNA in human cells. Interestingly, the data from our ChIP experiments showed that ActD-induced arrest of transcription complex at transcription start site of rDNA results in the increased binding of DNA polymerase ε within the transcription unit peaking at the site located approximately 8 kb from the transcription start site. This suggests the presence of a topological barrier between colliding transcription and replication complexes, which was recently linked with genomic instability of highly transcribed genes in yeast (Bermejo et al., 2011). Moreover, we provide evidence that replication forks stalled by halted transcription complexes could be elongated once the RNA polymerase is allowed to resume transcription. Thus, RNA polymerase might actively participate in the resolution of replication-transcription encounters.

In conclusion, the process of replication fork stalling and recovery may be a very tangled mechanism that includes complex remodeling of both DNA and protein moieties of replication fork. The study of RecQ helicases can uncover individual steps of this process that prevents genomic instability. In our study, we provide evidence that RECQ5 exerts its genome maintenance function through its involvement in the resolution of collisions between replication and transcription complexes. Interference between replication and transcription represents a significant source of genome instability and contributes to oncogene-induced tumorigenesis (Poveda et al., 2010). Because RECQ5 deficiency is associated with cancer susceptibility in mice (Hu et al., 2007), our study provides further evidence for the role of replication-

transcription interference in cancer development. Understanding the mechanisms that maintain replication fork stability may be crucial for diagnosis and therapy of human diseases caused by defects in response to replication stress.

8. Conclusions

In this work, we have provided evidence that RECQ5 prevents genomic instability resulting from replication-transcription collisions. We have proposed a mechanism for the resolution of replication-transcription encounters, which involves the coordinated action of RECQ5, BRCA1/RAD51 and RAD18. The major outcomes of this study can be summarized as follows:

- RECQ5 interacts with both RNAPI and II.
- RECQ5 is enriched at the coding regions of RNAPI- and II-transcribed genes.
- RECQ5 prevents RNAPI-transcription stress, and enforces the stability of the pre-rRNA coding regions of rDNA arrays.
- Depletion of RECQ5 leads to accumulation of unresolved replication intermediates with replisomes stalled in both RNAPI- and RNAPII-transcribed genes.
- RECQ5 associates with transcription complexes in replication foci.
- BRCA1, RAD18, RAD51 are recruited to sites of replication-transcription collisions.
- BRCA1 promotes transcription-dependent formation of RAD51 filaments in unperturbed cells.
- RECQ5 promotes RAD18-dependent ubiquitination of PCNA at sites of replication-transcription interference by directly interacting with PCNA.
- The helicase activity of RECQ5 is required for the resolution of replication intermediates stabilized by RAD51 filaments upon replication-transcription encounters.
- Transcription forms a barrier for replication fork progression and active transcription promotes resolution of replication-transcription collisions.

9. References

Abe, T., Yoshimura, A., Hosono, Y., Tada, S., Seki, M., and Enomoto, T. (2011). The N-terminal region of RECQL4 lacking the helicase domain is both essential and sufficient for the viability of vertebrate cells Role of the N-terminal region of RECQL4 in cells. Bba-Mol Cell Res *1813*, 473-479.

Acharya, S., Kaul, Z., Gocha, A.S., Martinez, A.R., Harris, J., Parvin, J.D., and Groden, J. (2014). Association of BLM and BRCA1 during Telomere Maintenance in ALT Cells. PloS one *9*, e103819.

Ahuja, A.K., Jodkowska, K., Teloni, F., Bizard, A.H., Zellweger, R., Herrador, R., Ortega, S., Hickson, I.D., Altmeyer, M., Mendez, J., *et al.* (2016). A short G1 phase imposes constitutive replication stress and fork remodelling in mouse embryonic stem cells. Nature communications *7*, 10660.

Allen, C., Ashley, A.K., Hromas, R., and Nickoloff, J.A. (2011). More forks on the road to replication stress recovery. Journal of molecular cell biology *3*, 4-12.

Ammazzalorso, F., Pirzio, L.M., Bignami, M., Franchitto, A., and Pichierri, P. (2010). ATR and ATM differently regulate WRN to prevent DSBs at stalled replication forks and promote replication fork recovery. The EMBO journal *29*, 3156-3169.

Aygun, O., Svejstrup, J., and Liu, Y. (2008). A RECQ5-RNA polymerase II association identified by targeted proteomic analysis of human chromatin. Proceedings of the National Academy of Sciences of the United States of America *105*, 8580-8584.

Aygun, O., Xu, X., Liu, Y., Takahashi, H., Kong, S.E., Conaway, R.C., Conaway, J.W., and Svejstrup, J.Q. (2009). Direct inhibition of RNA polymerase II transcription by RECQL5. The Journal of biological chemistry *284*, 23197-23203.

Azvolinsky, A., Giresi, P.G., Lieb, J.D., and Zakian, V.A. (2009). Highly transcribed RNA polymerase II genes are impediments to replication fork progression in Saccharomyces cerevisiae. Molecular cell *34*, 722-734.

Bachrati, C.Z., and Hickson, I.D. (2008). RecQ helicases: guardian angels of the DNA replication fork. Chromosoma *117*, 219-233.

Banerjee, T., and Brosh, R.M., Jr. (2015). RECQL: a new breast cancer susceptibility gene. Cell cycle *14*, 3540-3543.

Banerjee, T., Sommers, J.A., Huang, J., Seidman, M.M., and Brosh, R.M., Jr. (2015). Catalytic strand separation by RECQ1 is required for RPA-mediated response to replication stress. Current biology : CB *25*, 2830-2838.

Barefield, C., and Karlseder, J. (2012). The BLM helicase contributes to telomere maintenance through processing of late-replicating intermediate structures. Nucleic acids research *40*, 7358-7367.

Barlow, J.H., Faryabi, R.B., Callen, E., Wong, N., Malhowski, A., Chen, H.T., Gutierrez-Cruz, G., Sun, H.W., McKinnon, P., Wright, G., *et al.* (2013). Identification of early replicating fragile sites that contribute to genome instability. Cell *152*, 620-632.

Basile, G., Leuzzi, G., Pichierri, P., and Franchitto, A. (2014). Checkpoint-dependent and independent roles of the Werner syndrome protein in preserving genome integrity in response to mild replication stress. Nucleic acids research *42*, 12628-12639.

Bermejo, R., Capra, T., Jossen, R., Colosio, A., Frattini, C., Carotenuto, W., Cocito, A., Doksani, Y., Klein, H., Gomez-Gonzalez, B., *et al.* (2011). The replication checkpoint protects fork stability by releasing transcribed genes from nuclear pores. Cell *146*, 233-246.

Berti, M., Ray Chaudhuri, A., Thangavel, S., Gomathinayagam, S., Kenig, S., Vujanovic, M., Odreman, F., Glatter, T., Graziano, S., Mendoza-Maldonado, R., *et al.* (2013). Human RECQ1 promotes restart of replication forks reversed by DNA topoisomerase I inhibition. Nature structural & molecular biology *20*, 347-354.

Bhattacharyya, S., Keirsey, J., Russell, B., Kavecansky, J., Lillard-Wetherell, K., Tahmaseb, K., Turchi, J.J., and Groden, J. (2009). Telomerase-associated protein 1, HSP90, and topoisomerase IIalpha associate directly with the BLM helicase in immortalized cells using ALT and modulate its helicase activity using telomeric DNA substrates. The Journal of biological chemistry *284*, 14966-14977.

Blundred, R., Myers, K., Helleday, T., Goldman, A.S., and Bryant, H.E. (2010). Human RECQL5 overcomes thymidine-induced replication stress. DNA Repair (Amst) *9*, 964-975.

Boubakri, H., de Septenville, A.L., Viguera, E., and Michel, B. (2010). The helicases DinG, Rep and UvrD cooperate to promote replication across transcription units in vivo. The EMBO journal *29*, 145-157.

Boyer, A.S., Walter, D., and Sorensen, C.S. (2016). DNA replication and cancer: From dysfunctional replication origin activities to therapeutic opportunities. Seminars in cancer biology *37-38*, 16-25.

Brambati, A., Colosio, A., Zardoni, L., Galanti, L., and Liberi, G. (2015). Replication and transcription on a collision course: eukaryotic regulation mechanisms and implications for DNA stability. Frontiers in genetics *6*, 166.

Burgers, P.M. (2009). Polymerase dynamics at the eukaryotic DNA replication fork. The Journal of biological chemistry *284*, 4041-4045.

Chadha, G.S., Gambus, A., Gillespie, P.J., and Blow, J.J. (2016). Xenopus Mcm10 is a CDK-substrate required for replication fork stability. Cell cycle, 1-13.

Chagin, V.O., Casas-Delucchi, C.S., Reinhart, M., Schermelleh, L., Markaki, Y., Maiser, A., Bolius, J.J., Bensimon, A., Fillies, M., Domaing, P., *et al.* (2016). 4D Visualization of replication foci in mammalian cells corresponding to individual replicons. Nature communications *7*, 11231.

Chan, K.L., North, P.S., and Hickson, I.D. (2007). BLM is required for faithful chromosome segregation and its localization defines a class of ultrafine anaphase bridges. The EMBO journal *26*, 3397-3409.

Chaudhury, I., Sareen, A., Raghunandan, M., and Sobeck, A. (2013). FANCD2 regulates BLM complex functions independently of FANCI to promote replication fork recovery. Nucleic acids research *41*, 6444-6459.

Chen, C.F., and Brill, S.J. (2010). An essential DNA strand-exchange activity is conserved in the divergent N-termini of BLM orthologs. The EMBO journal *29*, 1713-1725.

Cobb, J.A., Bjergbaek, L., Shimada, K., Frei, C., and Gasser, S.M. (2003). DNA polymerase stabilization at stalled replication forks requires Mec1 and the RecQ helicase Sgs1. The EMBO journal *22*, 4325-4336.

Collart, C., Allen, G.E., Bradshaw, C.R., Smith, J.C., and Zegerman, P. (2013). Titration of four replication factors is essential for the Xenopus laevis midblastula transition. Science *341*, 893-896.

Constantinou, A., Tarsounas, M., Karow, J.K., Brosh, R.M., Bohr, V.A., Hickson, I.D., and West, S.C. (2000). Werner's syndrome protein (WRN) migrates Holliday junctions and co-localizes with RPA upon replication arrest. EMBO reports *1*, 80-84.

Crabbe, L., Jauch, A., Naeger, C.M., Holtgreve-Grez, H., and Karlseder, J. (2007). Telomere dysfunction as a cause of genomic instability in Werner syndrome. Proceedings of the National Academy of Sciences of the United States of America *104*, 2205-2210.

Crabbe, L., Verdun, R.E., Haggblom, C.I., and Karlseder, J. (2004). Defective telomere lagging strand synthesis in cells lacking WRN helicase activity. Science *306*, 1951-1953.

Croteau, D.L., Popuri, V., Opresko, P.L., and Bohr, V.A. (2014). Human RecQ helicases in DNA repair, recombination, and replication. Annual review of biochemistry *83*, 519-552.

Cybulski, C., Carrot-Zhang, J., Kluzniak, W., Rivera, B., Kashyap, A., Wokolorczyk, D., Giroux, S., Nadaf, J., Hamel, N., Zhang, S., *et al.* (2015). Germline RECQL mutations are associated with breast cancer susceptibility. Nature genetics *47*, 643-646.

Davies, S.L., North, P.S., and Hickson, I.D. (2007). Role for BLM in replication-fork restart and suppression of origin firing after replicative stress. Nature structural & molecular biology *14*, 677-679.

Debatisse, M., Le Tallec, B., Letessier, A., Dutrillaux, B., and Brison, O. (2012). Common fragile sites: mechanisms of instability revisited. Trends in genetics : TIG *28*, 22-32.

Doherty, K.M., Sommers, J.A., Gray, M.D., Lee, J.W., von Kobbe, C., Thoma, N.H., Kureekattil, R.P., Kenny, M.K., and Brosh, R.M., Jr. (2005). Physical and functional mapping of the replication protein a interaction domain of the werner and bloom syndrome helicases. The Journal of biological chemistry *280*, 29494-29505.

Drosopoulos, W.C., Kosiyatrakul, S.T., and Schildkraut, C.L. (2015). BLM helicase facilitates telomere replication during leading strand synthesis of telomeres. The Journal of cell biology *210*, 191-208.

Durkin, S.G., and Glover, T.W. (2007). Chromosome fragile sites. Annual review of genetics *41*, 169-192.

Elias-Arnanz, M., and Salas, M. (1999). Resolution of head-on collisions between the transcription machinery and bacteriophage phi29 DNA polymerase is dependent on RNA polymerase translocation. The EMBO journal *18*, 5675-5682.

Felipe-Abrio, I., Lafuente-Barquero, J., Garcia-Rubio, M.L., and Aguilera, A. (2015). RNA polymerase II contributes to preventing transcription-mediated replication fork stalls. The EMBO journal *34*, 236-250.

Fragkos, M., Ganier, O., Coulombe, P., and Mechali, M. (2015). DNA replication origin activation in space and time. Nature reviews. Molecular cell biology *16*, 360-374.

Franchitto, A., and Pichierri, P. (2004). Werner syndrome protein and the MRE11 complex are involved in a common pathway of replication fork recovery. Cell cycle *3*, 1331-1339.

Franchitto, A., Pirzio, L.M., Prosperi, E., Sapora, O., Bignami, M., and Pichierri, P. (2008). Replication fork stalling in WRN-deficient cells is overcome by prompt activation of a MUS81-dependent pathway. The Journal of cell biology *183*, 241-252.

French, S. (1992). Consequences of replication fork movement through transcription units in vivo. Science *258*, 1362-1365.

Fukuchi, K., Martin, G.M., and Monnat, R.J., Jr. (1989). Mutator phenotype of Werner syndrome is characterized by extensive deletions. Proceedings of the National Academy of Sciences of the United States of America *86*, 5893-5897.

Gebhart, E., Bauer, R., Raub, U., Schinzel, M., Ruprecht, K.W., and Jonas, J.B. (1988). Spontaneous and induced chromosomal instability in Werner syndrome. Human genetics *80*, 135-139.

Gonzalez Besteiro, M.A., and Gottifredi, V. (2015). The fork and the kinase: a DNA replication tale from a CHK1 perspective. Mutation research. Reviews in mutation research *763*, 168-180.

Guo, C., Kosarek-Stancel, J.N., Tang, T.S., and Friedberg, E.C. (2009). Y-family DNA polymerases in mammalian cells. Cellular and molecular life sciences : CMLS *66*, 2363-2381.

Hagelstrom, R.T., Blagoev, K.B., Niedernhofer, L.J., Goodwin, E.H., and Bailey, S.M. (2010). Hyper telomere recombination accelerates replicative senescence and may promote premature aging. Proceedings of the National Academy of Sciences of the United States of America *107*, 15768-15773.

Halazonetis, T.D., Gorgoulis, V.G., and Bartek, J. (2008). An oncogene-induced DNA damage model for cancer development. Science *319*, 1352-1355.

Hand, R., and German, J. (1975). A retarded rate of DNA chain growth in Bloom's syndrome. Proceedings of the National Academy of Sciences of the United States of America *72*, 758-762.

He, Y.J., Qiao, Z.Y., Gao, B., Zhang, X.H., and Wen, Y.Y. (2014). Association between RECQL5 genetic polymorphisms and susceptibility to breast cancer. Tumor Biol *35*, 12201-12204.

Helmrich, A., Ballarino, M., Nudler, E., and Tora, L. (2013). Transcription-replication encounters, consequences and genomic instability. Nature structural & molecular biology *20*, 412-418.

Helmrich, A., Ballarino, M., and Tora, L. (2011). Collisions between replication and transcription complexes cause common fragile site instability at the longest human genes. Molecular cell *44*, 966-977.

Helmrich, A., Stout-Weider, K., Hermann, K., Schrock, E., and Heiden, T. (2006). Common fragile sites are conserved features of human and mouse chromosomes and relate to large active genes. Genome research *16*, 1222-1230.

Herrick, J., and Bensimon, A. (2008). Global regulation of genome duplication in eukaryotes: an overview from the epifluorescence microscope. Chromosoma *117*, 243-260.

Hickson, I.D. (2003). RecQ helicases: caretakers of the genome. Nature reviews. Cancer *3*, 169-178.

Hu, P., Beresten, S.F., van Brabant, A.J., Ye, T.Z., Pandolfi, P.P., Johnson, F.B., Guarente, L., and Ellis, N.A. (2001). Evidence for BLM and Topoisomerase IIIalpha interaction in genomic stability. Human molecular genetics *10*, 1287-1298.

Hu, Y., Raynard, S., Sehorn, M.G., Lu, X., Bussen, W., Zheng, L., Stark, J.M., Barnes, E.L., Chi, P., Janscak, P., *et al.* (2007). RECQL5/Recql5 helicase regulates homologous recombination and suppresses tumor formation via disruption of Rad51 presynaptic filaments. Genes & development *21*, 3073-3084.

Hyun, M., Choi, S., Stevnsner, T., and Ahn, B. (2016). The Caenorhabditis elegans Werner syndrome protein participates in DNA damage checkpoint and DNA repair in response to CPT-induced double-strand breaks. Cellular signalling *28*, 214-223.

Iannascoli, C., Palermo, V., Murfuni, I., Franchitto, A., and Pichierri, P. (2015). The WRN exonuclease domain protects nascent strands from pathological MRE11/EXO1-dependent degradation. Nucleic acids research *43*, 9788-9803.

Ichikawa, K., Noda, T., and Furuichi, Y. (2002). [Preparation of the gene targeted knockout mice for human premature aging diseases, Werner syndrome, and Rothmund-Thomson syndrome caused by the mutation of DNA helicases]. Nihon yakurigaku zasshi. Folia pharmacologica Japonica *119*, 219-226.

Im, J.S., Ki, S.H., Farina, A., Jung, D.S., Hurwitz, J., and Lee, J.K. (2009). Assembly of the Cdc45-Mcm2-7-GINS complex in human cells requires the Ctf4/And-1, RecQL4, and Mcm10

proteins. Proceedings of the National Academy of Sciences of the United States of America *106*, 15628-15632.

Im, J.S., Park, S.Y., Cho, W.H., Bae, S.H., Hurwitz, J., and Lee, J.K. (2015). RecQL4 is required for the association of Mcm10 and Ctf4 with replication origins in human cells. Cell cycle *14*, 1001-1009.

Islam, M.N., Fox, D., 3rd, Guo, R., Enomoto, T., and Wang, W. (2010). RecQL5 promotes genome stabilization through two parallel mechanisms--interacting with RNA polymerase II and acting as a helicase. Molecular and cellular biology *30*, 2460-2472.

Izumikawa, K., Yanagida, M., Hayano, T., Tachikawa, H., Komatsu, W., Shimamoto, A., Futami, K., Furuichi, Y., Shinkawa, T., Yamauchi, Y., *et al.* (2008). Association of human DNA helicase RecQ5beta with RNA polymerase II and its possible role in transcription. The Biochemical journal *413*, 505-516.

Johnson, A., and O'Donnell, M. (2005). Cellular DNA replicases: components and dynamics at the replication fork. Annual review of biochemistry *74*, 283-315.

Jones, R.M., Mortusewicz, O., Afzal, I., Lorvellec, M., Garcia, P., Helleday, T., and Petermann, E. (2013). Increased replication initiation and conflicts with transcription underlie Cyclin E-induced replication stress. Oncogene *32*, 3744-3753.

Kamath-Loeb, A.S., Lan, L., Nakajima, S., Yasui, A., and Loeb, L.A. (2007). Werner syndrome protein interacts functionally with translesion DNA polymerases. Proceedings of the National Academy of Sciences of the United States of America *104*, 10394-10399.

Kamath-Loeb, A.S., Loeb, L.A., Johansson, E., Burgers, P.M., and Fry, M. (2001). Interactions between the Werner syndrome helicase and DNA polymerase delta specifically facilitate copying of tetraplex and hairpin structures of the d(CGG)n trinucleotide repeat sequence. The Journal of biological chemistry *276*, 16439-16446.

Kamath-Loeb, A.S., Shen, J.C., Schmitt, M.W., and Loeb, L.A. (2012). The Werner syndrome exonuclease facilitates DNA degradation and high fidelity DNA polymerization by human DNA polymerase delta. The Journal of biological chemistry *287*, 12480-12490.

Kanagaraj, R., Huehn, D., MacKellar, A., Menigatti, M., Zheng, L., Urban, V., Shevelev, I., Greenleaf, A.L., and Janscak, P. (2010). RECQ5 helicase associates with the C-terminal repeat domain of RNA polymerase II during productive elongation phase of transcription. Nucleic acids research *38*, 8131-8140.

Kanagaraj, R., Saydam, N., Garcia, P.L., Zheng, L., and Janscak, P. (2006). Human RECQ5beta helicase promotes strand exchange on synthetic DNA structures resembling a stalled replication fork. Nucleic acids research *34*, 5217-5231.

Kassube, S.A., Jinek, M., Fang, J., Tsutakawa, S., and Nogales, E. (2013). Structural mimicry in transcription regulation of human RNA polymerase II by the DNA helicase RECQL5. Nature structural & molecular biology *20*, 892-899.

Kemp, M.G., Akan, Z., Yilmaz, S., Grillo, M., Smith-Roe, S.L., Kang, T.H., Cordeiro-Stone, M., Kaufmann, W.K., Abraham, R.T., Sancar, A., *et al.* (2010). Tipin-replication protein A interaction mediates Chk1 phosphorylation by ATR in response to genotoxic stress. The Journal of biological chemistry *285*, 16562-16571.

Kim, J.C., and Mirkin, S.M. (2013). The balancing act of DNA repeat expansions. Current opinion in genetics & development *23*, 280-288.

Kim, T.M., Son, M.Y., Dodds, S., Hu, L., Luo, G., and Hasty, P. (2015). RECQL5 and BLM exhibit divergent functions in cells defective for the Fanconi anemia pathway. Nucleic acids research *43*, 893-903.

Kliszczak, M., Sedlackova, H., Pitchai, G.P., Streicher, W.W., Krejci, L., and Hickson, I.D. (2015). Interaction of RECQ4 and MCM10 is important for efficient DNA replication origin firing in human cells. Oncotarget *6*, 40464-40479.

Krum, S.A., Miranda, G.A., Lin, C., and Lane, T.F. (2003). BRCA1 associates with processive RNA polymerase II. The Journal of biological chemistry *278*, 52012-52020.

Li, M., Xu, X., and Liu, Y. (2011). The SET2-RPB1 interaction domain of human RECQ5 is important for transcription-associated genome stability. Molecular and cellular biology *31*, 2090-2099.

Lillard-Wetherell, K., Machwe, A., Langland, G.T., Combs, K.A., Behbehani, G.K., Schonberg, S.A., German, J., Turchi, J.J., Orren, D.K., and Groden, J. (2004). Association and regulation of the BLM helicase by the telomere proteins TRF1 and TRF2. Human molecular genetics *13*, 1919-1932.

Lipps, H.J., and Rhodes, D. (2009). G-quadruplex structures: in vivo evidence and function. Trends in cell biology *19*, 414-422.

Lonn, U., Lonn, S., Nylen, U., Winblad, G., and German, J. (1990). An Abnormal Profile of DNA-Replication Intermediates in Blooms Syndrome. Cancer Res *50*, 3141-3145.

Losada, A. (2014). Cohesin in cancer: chromosome segregation and beyond. Nature reviews. Cancer *14*, 389-393.

Lukas, C., Savic, V., Bekker-Jensen, S., Doil, C., Neumann, B., Pedersen, R.S., Grofte, M., Chan, K.L., Hickson, I.D., Bartek, J., *et al.* (2011). 53BP1 nuclear bodies form around DNA lesions generated by mitotic transmission of chromosomes under replication stress. Nature cell biology *13*, 243-253.

Macheret, M., and Halazonetis, T.D. (2015). DNA replication stress as a hallmark of cancer. Annual review of pathology *10*, 425-448.

Maddukuri, L., Ketkar, A., Eddy, S., Zafar, M.K., Griffin, W.C., and Eoff, R.L. (2012). Enhancement of human DNA polymerase eta activity and fidelity is dependent upon a bipartite interaction with the Werner syndrome protein. The Journal of biological chemistry *287*, 42312-42323.

Maga, G., and Hubscher, U. (2003). Proliferating cell nuclear antigen (PCNA): a dancer with many partners. Journal of cell science *116*, 3051-3060.

Matsuno, K., Kumano, M., Kubota, Y., Hashimoto, Y., and Takisawa, H. (2006). The N-terminal noncatalytic region of Xenopus RecQ4 is required for chromatin binding of DNA polymerase alpha in the initiation of DNA replication. Molecular and cellular biology *26*, 4843-4852.

Merrikh, H., Machon, C., Grainger, W.H., Grossman, A.D., and Soultanas, P. (2011). Co-directional replication-transcription conflicts lead to replication restart. Nature *470*, 554-557.

Murfuni, I., De Santis, A., Federico, M., Bignami, M., Pichierri, P., and Franchitto, A. (2012). Perturbed replication induced genome wide or at common fragile sites is differently managed in the absence of WRN. Carcinogenesis *33*, 1655-1663.

Murfuni, I., Nicolai, S., Baldari, S., Crescenzi, M., Bignami, M., Franchitto, A., and Pichierri, P. (2013). The WRN and MUS81 proteins limit cell death and genome instability following oncogene activation. Oncogene *32*, 610-620.

Nakayama, H. (2002). RecQ family helicases: roles as tumor suppressor proteins. Oncogene *21*, 9008-9021.

Neelsen, K.J., and Lopes, M. (2015). Replication fork reversal in eukaryotes: from dead end to dynamic response. Nature reviews. Molecular cell biology *16*, 207-220.

Opresko, P.L., Cheng, W.H., von Kobbe, C., Harrigan, J.A., and Bohr, V.A. (2003). Werner syndrome and the function of the Werner protein; what they can teach us about the molecular aging process. Carcinogenesis *24*, 791-802.

Opresko, P.L., Mason, P.A., Podell, E.R., Lei, M., Hickson, I.D., Cech, T.R., and Bohr, V.A. (2005). POT1 stimulates RecQ helicases WRN and BLM to unwind telomeric DNA substrates. The Journal of biological chemistry *280*, 32069-32080.

Opresko, P.L., von Kobbe, C., Laine, J.P., Harrigan, J., Hickson, I.D., and Bohr, V.A. (2002). Telomere-binding protein TRF2 binds to and stimulates the Werner and Bloom syndrome helicases. The Journal of biological chemistry *277*, 41110-41119.

Oshima, J., Martin, G.M., and Hisama, F.M. (1993). Werner Syndrome. In GeneReviews(R), R.A. Pagon, M.P. Adam, H.H. Ardinger, S.E. Wallace, A. Amemiya, L.J.H. Bean, T.D. Bird, C.T. Fong, H.C. Mefford, R.J.H. Smith, and K. Stephens, eds. (Seattle (WA)).

Oshima, J., Sidorova, J.M., and Monnat, R.J., Jr. (2016). Werner syndrome: Clinical features, pathogenesis and potential therapeutic interventions. Ageing research reviews.

Ouyang, K.J., Woo, L.L., Zhu, J., Huo, D., Matunis, M.J., and Ellis, N.A. (2009). SUMO modification regulates BLM and RAD51 interaction at damaged replication forks. PLoS biology *7*, e1000252.

Ouyang, K.J., Yagle, M.K., Matunis, M.J., and Ellis, N.A. (2013). BLM SUMOylation regulates ssDNA accumulation at stalled replication forks. Frontiers in genetics *4*, 167.

Park, J.H., Bang, S.W., Jeon, Y., Kang, S., and Hwang, D.S. (2008). Knockdown of human MCM10 exhibits delayed and incomplete chromosome replication. Biochemical and biophysical research communications *365*, 575-582.

Park, S.J., Lee, Y.J., Beck, B.D., and Lee, S.H. (2006). A positive involvement of RecQL4 in UV-induced S-phase arrest. DNA and cell biology *25*, 696-703.

Patro, B.S., Frohlich, R., Bohr, V.A., and Stevnsner, T. (2011). WRN helicase regulates the ATR-CHK1-induced S-phase checkpoint pathway in response to topoisomerase-I-DNA covalent complexes. Journal of cell science *124*, 3967-3979.

Petermann, E., and Helleday, T. (2010). Pathways of mammalian replication fork restart. Nature reviews. Molecular cell biology *11*, 683-687.

Petermann, E., Orta, M.L., Issaeva, N., Schultz, N., and Helleday, T. (2010). Hydroxyurea-stalled replication forks become progressively inactivated and require two different RAD51-mediated pathways for restart and repair. Molecular cell *37*, 492-502.

Phillips, L.G., and Sale, J.E. (2010). The Werner's Syndrome protein collaborates with REV1 to promote replication fork progression on damaged DNA. DNA Repair (Amst) *9*, 1064-1072.

Pichierri, P., Franchitto, A., Mosesso, P., and Palitti, F. (2001). Werner's syndrome protein is required for correct recovery after replication arrest and DNA damage induced in S-phase of cell cycle. Molecular biology of the cell *12*, 2412-2421.

Pichierri, P., Nicolai, S., Cignolo, L., Bignami, M., and Franchitto, A. (2012). The RAD9-RAD1-HUS1 (9.1.1) complex interacts with WRN and is crucial to regulate its response to replication fork stalling. Oncogene *31*, 2809-2823.

Pirzio, L.M., Pichierri, P., Bignami, M., and Franchitto, A. (2008). Werner syndrome helicase activity is essential in maintaining fragile site stability. The Journal of cell biology *180*, 305-314.

Poot, M., Gollahon, K.A., Emond, M.J., Silber, J.R., and Rabinovitch, P.S. (2002). Werner syndrome diploid fibroblasts are sensitive to 4-nitroquinoline-N-oxide and 8-methoxypsoralen: implications for the disease phenotype. FASEB journal : official publication of the Federation of American Societies for Experimental Biology *16*, 757-758.

Poot, M., Gollahon, K.A., and Rabinovitch, P.S. (1999). Werner syndrome lymphoblastoid cells are sensitive to camptothecin-induced apoptosis in S-phase. Human genetics *104*, 10-14.

Poot, M., Yom, J.S., Whang, S.H., Kato, J.T., Gollahon, K.A., and Rabinovitch, P.S. (2001). Werner syndrome cells are sensitive to DNA cross-linking drugs. FASEB journal : official publication of the Federation of American Societies for Experimental Biology *15*, 1224-1226.

Popuri, V., Croteau, D.L., Brosh, R.M., Jr., and Bohr, V.A. (2012). RECQ1 is required for cellular resistance to replication stress and catalyzes strand exchange on stalled replication fork structures. Cell cycle *11*, 4252-4265.

Popuri, V., Hsu, J., Khadka, P., Horvath, K., Liu, Y., Croteau, D.L., and Bohr, V.A. (2014). Human RECQL1 participates in telomere maintenance. Nucleic acids research *42*, 5671-5688.

Poveda, A.M., Le Clech, M., and Pasero, P. (2010). Transcription and replication: breaking the rules of the road causes genomic instability. Transcription *1*, 99-102.

Prado, F., and Aguilera, A. (2005). Impairment of replication fork progression mediates RNA polII transcription-associated recombination. The EMBO journal *24*, 1267-1276.

Qi, Y., and Zhou, X. (2014). Haplotype analysis of RECQL5 gene and laryngeal cancer. Tumour biology : the journal of the International Society for Oncodevelopmental Biology and Medicine *35*, 2669-2673.

Rassool, F.V., North, P.S., Mufti, G.J., and Hickson, I.D. (2003). Constitutive DNA damage is linked to DNA replication abnormalities in Bloom's syndrome cells. Oncogene *22*, 8749-8757.

Ray Chaudhuri, A., Hashimoto, Y., Herrador, R., Neelsen, K.J., Fachinetti, D., Bermejo, R., Cocito, A., Costanzo, V., and Lopes, M. (2012). Topoisomerase I poisoning results in PARP-mediated replication fork reversal. Nature structural & molecular biology *19*, 417-423.

Rezazadeh, S. (2013). On BLM helicase in recombination-mediated telomere maintenance. Molecular biology reports *40*, 3049-3064.

Ribeyre, C., Zellweger, R., Chauvin, M., Bec, N., Larroque, C., Lopes, M., and Constantinou, A. (2016). Nascent DNA Proteomics Reveals a Chromatin Remodeler Required for Topoisomerase I Loading at Replication Forks. Cell reports *15*, 300-309.

Rivera-Mulia, J.C., and Gilbert, D.M. (2016). Replicating Large Genomes: Divide and Conquer. Molecular cell *62*, 756-765.

Rocha, E.P. (2008). The organization of the bacterial genome. Annual review of genetics *42*, 211-233.

Rodriguez-Lopez, A.M., Jackson, D.A., Iborra, F., and Cox, L.S. (2002). Asymmetry of DNA replication fork progression in Werner's syndrome. Aging cell *1*, 30-39.

Rodriguez-Lopez, A.M., Jackson, D.A., Nehlin, J.O., Iborra, F., Warren, A.V., and Cox, L.S. (2003). Characterisation of the interaction between WRN, the helicase/exonuclease defective in progeroid Werner's syndrome, and an essential replication factor, PCNA. Mechanisms of ageing and development *124*, 167-174.

Root, H., Larsen, A., Komosa, M., Al-Azri, F., Li, R., Bazett-Jones, D.P., and Stephen Meyn, M. (2016). FANCD2 limits BLM-dependent telomere instability in the alternative lengthening of telomeres pathway. Human molecular genetics.

Sabouri, N., McDonald, K.R., Webb, C.J., Cristea, I.M., and Zakian, V.A. (2012). DNA replication through hard-to-replicate sites, including both highly transcribed RNA Pol II and Pol III genes, requires the S. pombe Pfh1 helicase. Genes & development *26*, 581-593.

Sami, F., Lu, X., Parvathaneni, S., Roy, R., Gary, R.K., and Sharma, S. (2015). RECQ1 interacts with FEN-1 and promotes binding of FEN-1 to telomeric chromatin. The Biochemical journal *468*, 227-244.

Sangrithi, M.N., Bernal, J.A., Madine, M., Philpott, A., Lee, J., Dunphy, W.G., and Venkitaraman, A.R. (2005). Initiation of DNA replication requires the RECQL4 protein mutated in Rothmund-Thomson syndrome. Cell *121*, 887-898.

Sanz, M.M., German, J., and Cunniff, C. (1993). Bloom's Syndrome. In GeneReviews(R), R.A. Pagon, M.P. Adam, H.H. Ardinger, S.E. Wallace, A. Amemiya, L.J.H. Bean, T.D. Bird, C.T. Fong, H.C. Mefford, R.J.H. Smith, and K. Stephens, eds. (Seattle (WA)).

Saponaro, M., Kantidakis, T., Mitter, R., Kelly, G.P., Heron, M., Williams, H., Soding, J., Stewart, A., and Svejstrup, J.Q. (2014). RECQL5 Controls Transcript Elongation and Suppresses Genome Instability Associated with Transcription Stress. Cell *157*, 1037-1049.

Sarkar, J., Wan, B., Yin, J., Vallabhaneni, H., Horvath, K., Kulikowicz, T., Bohr, V.A., Zhang, Y., Lei, M., and Liu, Y. (2015). SLX4 contributes to telomere preservation and regulated processing of telomeric joint molecule intermediates. Nucleic acids research *43*, 5912-5923.

Schlacher, K., Christ, N., Siaud, N., Egashira, A., Wu, H., and Jasin, M. (2011). Double-strand break repair-independent role for BRCA2 in blocking stalled replication fork degradation by MRE11. Cell *145*, 529-542.

Schlacher, K., Wu, H., and Jasin, M. (2012). A distinct replication fork protection pathway connects Fanconi anemia tumor suppressors to RAD51-BRCA1/2. Cancer cell *22*, 106-116.

Schulz, V.P., Zakian, V.A., Ogburn, C.E., McKay, J., Jarzebowicz, A.A., Edland, S.D., and Martin, G.M. (1996). Accelerated loss of telomeric repeats may not explain accelerated replicative decline of Werner syndrome cells. Human genetics *97*, 750-754.

Sfeir, A., Kosiyatrakul, S.T., Hockemeyer, D., MacRae, S.L., Karlseder, J., Schildkraut, C.L., and de Lange, T. (2009). Mammalian telomeres resemble fragile sites and require TRF1 for efficient replication. Cell *138*, 90-103.

Sharma, S., and Brosh, R.M., Jr. (2007). Human RECQ1 is a DNA damage responsive protein required for genotoxic stress resistance and suppression of sister chromatid exchanges. PloS one *2*, e1297.

Sharma, S., Phatak, P., Stortchevoi, A., Jasin, M., and Larocque, J.R. (2012). RECQ1 plays a distinct role in cellular response to oxidative DNA damage. DNA Repair (Amst) *11*, 537-549.

Sharma, S., Stumpo, D.J., Balajee, A.S., Bock, C.B., Lansdorp, P.M., Brosh, R.M., Jr., and Blackshear, P.J. (2007). RECQL, a member of the RecQ family of DNA helicases, suppresses chromosomal instability. Molecular and cellular biology *27*, 1784-1794.

Sidorova, J.M., Kehrli, K., Mao, F., and Monnat, R., Jr. (2013). Distinct functions of human RECQ helicases WRN and BLM in replication fork recovery and progression after hydroxyurea-induced stalling. DNA Repair (Amst) *12*, 128-139.

Sidorova, J.M., Li, N., Folch, A., and Monnat, R.J., Jr. (2008). The RecQ helicase WRN is required for normal replication fork progression after DNA damage or replication fork arrest. Cell cycle *7*, 796-807.

Sorensen, C.S., and Syljuasen, R.G. (2012). Safeguarding genome integrity: the checkpoint kinases ATR, CHK1 and WEE1 restrain CDK activity during normal DNA replication. Nucleic acids research *40*, 477-486.

Stavropoulos, D.J., Bradshaw, P.S., Li, X., Pasic, I., Truong, K., Ikura, M., Ungrin, M., and Meyn, M.S. (2002). The Bloom syndrome helicase BLM interacts with TRF2 in ALT cells and promotes telomeric DNA synthesis. Human molecular genetics *11*, 3135-3144.

Su, F., Mukherjee, S., Yang, Y., Mori, E., Bhattacharya, S., Kobayashi, J., Yannone, S.M., Chen, D.J., and Asaithamby, A. (2014). Nonenzymatic role for WRN in preserving nascent DNA strands after replication stress. Cell reports *9*, 1387-1401.

Sun, H., Karow, J.K., Hickson, I.D., and Maizels, N. (1998). The Bloom's syndrome helicase unwinds G4 DNA. The Journal of biological chemistry *273*, 27587-27592.

Sun, J., Wang, Y., Xia, Y., Xu, Y., Ouyang, T., Li, J., Wang, T., Fan, Z., Fan, T., Lin, B., *et al.* (2015). Mutations in RECQL Gene Are Associated with Predisposition to Breast Cancer. PLoS genetics *11*, e1005228.

Tanaka, S., Umemori, T., Hirai, K., Muramatsu, S., Kamimura, Y., and Araki, H. (2007). CDK-dependent phosphorylation of Sld2 and Sld3 initiates DNA replication in budding yeast. Nature *445*, 328-332.

Thangavel, S., Berti, M., Levikova, M., Pinto, C., Gomathinayagam, S., Vujanovic, M., Zellweger, R., Moore, H., Lee, E.H., Hendrickson, E.A., *et al.* (2015). DNA2 drives processing and restart of reversed replication forks in human cells. The Journal of cell biology *208*, 545-562.

Thangavel, S., Mendoza-Maldonado, R., Tissino, E., Sidorova, J.M., Yin, J., Wang, W., Monnat, R.J., Jr., Falaschi, A., and Vindigni, A. (2010). Human RECQ1 and RECQ4 helicases play distinct roles in DNA replication initiation. Molecular and cellular biology *30*, 1382-1396.

Tikoo, S., Madhavan, V., Hussain, M., Miller, E.S., Arora, P., Zlatanou, A., Modi, P., Townsend, K., Stewart, G.S., and Sengupta, S. (2013). Ubiquitin-dependent recruitment of the Bloom syndrome helicase upon replication stress is required to suppress homologous recombination. The EMBO journal *32*, 1778-1792.

Toledo, L.I., Altmeyer, M., Rask, M.B., Lukas, C., Larsen, D.H., Povlsen, L.K., Bekker-Jensen, S., Mailand, N., Bartek, J., and Lukas, J. (2013). ATR prohibits replication catastrophe by preventing global exhaustion of RPA. Cell *155*, 1088-1103.

Tuduri, S., Crabbe, L., Conti, C., Tourriere, H., Holtgreve-Grez, H., Jauch, A., Pantesco, V., De Vos, J., Thomas, A., Theillet, C., *et al.* (2009). Topoisomerase I suppresses genomic instability by preventing interference between replication and transcription. Nature cell biology *11*, 1315-1324.

Urban, V., Dobrovolna, J., Huhn, D., Fryzelkova, J., Bartek, J., and Janscak, P. (2016). RECQ5 helicase promotes resolution of conflicts between replication and transcription in human cells. The Journal of cell biology *214*, 401-415.

Venkitaraman, A.R. (2014). Cancer suppression by the chromosome custodians, BRCA1 and BRCA2. Science *343*, 1470-1475.

Wang, L.L., and Plon, S.E. (1993). Rothmund-Thomson Syndrome. In GeneReviews(R), R.A. Pagon, M.P. Adam, H.H. Ardinger, S.E. Wallace, A. Amemiya, L.J.H. Bean, T.D. Bird, C.T. Fong, H.C. Mefford, R.J.H. Smith, and K. Stephens, eds. (Seattle (WA)).

Wechsler, T., Newman, S., and West, S.C. (2011). Aberrant chromosome morphology in human cells defective for Holliday junction resolution. Nature *471*, 642-646.

Wind, M., and Reines, D. (2000). Transcription elongation factor SII. BioEssays : news and reviews in molecular, cellular and developmental biology *22*, 327-336.

Wu, L., Chan, K.L., Ralf, C., Bernstein, D.A., Garcia, P.L., Bohr, V.A., Vindigni, A., Janscak, P., Keck, J.L., and Hickson, I.D. (2005). The HRDC domain of BLM is required for the dissolution of double Holliday junctions. The EMBO journal *24*, 2679-2687.

Wu, L., and Hickson, I.D. (2003). The Bloom's syndrome helicase suppresses crossing over during homologous recombination. Nature *426*, 870-874.

Xu, X., Rochette, P.J., Feyissa, E.A., Su, T.V., and Liu, Y. (2009). MCM10 mediates RECQ4 association with MCM2-7 helicase complex during DNA replication. The EMBO journal *28*, 3005-3014.

Yang, J., Bachrati, C.Z., Ou, J., Hickson, I.D., and Brown, G.W. (2010). Human topoisomerase IIIalpha is a single-stranded DNA decatenase that is stimulated by BLM and RMI1. The Journal of biological chemistry *285*, 21426-21436.

Yang, J., O'Donnell, L., Durocher, D., and Brown, G.W. (2012). RMI1 promotes DNA replication fork progression and recovery from replication fork stress. Molecular and cellular biology *32*, 3054-3064.

Yin, J., Sobeck, A., Xu, C., Meetei, A.R., Hoatlin, M., Li, L., and Wang, W. (2005). BLAP75, an essential component of Bloom's syndrome protein complexes that maintain genome integrity. The EMBO journal *24*, 1465-1476.

Yu, C., Gan, H., Han, J., Zhou, Z.X., Jia, S., Chabes, A., Farrugia, G., Ordog, T., and Zhang, Z. (2014). Strand-specific analysis shows protein binding at replication forks and PCNA unloading from lagging strands when forks stall. Molecular cell *56*, 551-563.

Zegerman, P., and Diffley, J.F. (2007). Phosphorylation of Sld2 and Sld3 by cyclin-dependent kinases promotes DNA replication in budding yeast. Nature *445*, 281-285.

Zellweger, R., Dalcher, D., Mutreja, K., Berti, M., Schmid, J.A., Herrador, R., Vindigni, A., and Lopes, M. (2015). Rad51-mediated replication fork reversal is a global response to genotoxic treatments in human cells. The Journal of cell biology *208*, 563-579.

Zeman, M.K., and Cimprich, K.A. (2014). Causes and consequences of replication stress. Nature cell biology *16*, 2-9.

Zhang, C., Lu, J., and Zhang, P. (2016). The Roles of Chromatin Remodeling Proteins in Cancer. Current protein & peptide science *17*, 446-454.

Zheng, L., and Shen, B. (2011). Okazaki fragment maturation: nucleases take centre stage. Journal of molecular cell biology *3*, 23-30.

Zhi, L.Q., Ma, W., Zhang, H., Zeng, S.X., and Chen, B. (2014). Association of RECQL5 gene polymorphisms and osteosarcoma in a Chinese Han population. Tumour biology : the journal of the International Society for Oncodevelopmental Biology and Medicine *35*, 3255-3259.

Zimmer, J., Tacconi, E.M., Folio, C., Badie, S., Porru, M., Klare, K., Tumiati, M., Markkanen, E., Halder, S., Ryan, A., *et al.* (2016). Targeting BRCA1 and BRCA2 Deficiencies with G-Quadruplex-Interacting Compounds. Molecular cell *61*, 449-460.

Zimmermann, M., Kibe, T., Kabir, S., and de Lange, T. (2014). TRF1 negotiates TTAGGG repeat-associated replication problems by recruiting the BLM helicase and the TPP1/POT1 repressor of ATR signaling. Genes & development *28*, 2477-2491.

10. Publications

Published August 8, 2016

RECQ5 helicase promotes resolution of conflicts between replication and transcription in human cells

Vaclav Urban,[1] Jana Dobrovolna,[1] Daniela Hühn,[2] Jana Fryzelkova,[1] Jiri Bartek,[1,3,4] and Pavel Janscak[1,2]

[1]Institute of Molecular Genetics, Academy of Sciences of the Czech Republic, 142 20 Prague, Czech Republic
[2]Institute of Molecular Cancer Research, University of Zurich, 8057 Zurich, Switzerland
[3]Genome Integrity Unit, Danish Cancer Society Research Center, 2100 Copenhagen, Denmark
[4]Department of Medical Biochemistry and Biophysics, Karolinska Institute, 17177 Stockholm, Sweden

Collisions between replication and transcription machineries represent a significant source of genomic instability. RECQ5 DNA helicase binds to RNA-polymerase (RNAP) II during transcription elongation and suppresses transcription-associated genomic instability. Here, we show that RECQ5 also associates with RNAPI and enforces the stability of ribosomal DNA arrays. We demonstrate that RECQ5 associates with transcription complexes in DNA replication foci and counteracts replication fork stalling in RNAPI- and RNAPII-transcribed genes, suggesting that RECQ5 exerts its genome-stabilizing effect by acting at sites of replication-transcription collisions. Moreover, RECQ5-deficient cells accumulate RAD18 foci and BRCA1-dependent RAD51 foci that are both formed at sites of interference between replication and transcription and likely represent unresolved replication intermediates. Finally, we provide evidence for a novel mechanism of resolution of replication-transcription collisions wherein the interaction between RECQ5 and proliferating cell nuclear antigen (PCNA) promotes RAD18-dependent PCNA ubiquitination and the helicase activity of RECQ5 promotes the processing of replication intermediates.

Introduction

DNA replication and transcription are mediated by robust machineries that compete for the same regions of the genome during S phase of the cell cycle. Studies in yeast and mammalian cells have shown that replication-transcription encounters are unavoidable and represent one of the major sources of DNA breakage and chromosomal rearrangements, particularly in cells subjected to replication stress (Azvolinsky et al., 2009; Barlow et al., 2013; Helmrich et al., 2013; Jones et al., 2013; Wilson et al., 2015). A correlation between replication stress–provoked genomic instability and active transcription is particularly apparent in case of common fragile sites (CFSs) and recently identified early replicating fragile sites (ERFSs; Helmrich et al., 2011; Barlow et al., 2013). CFSs are specific genomic regions that manifest as gaps or breaks on metaphase chromosomes, particularly when DNA replication is partially inhibited (Durkin and Glover, 2007). Interestingly, CFSs are frequently located within the coding region of very long genes whose transcription takes even more than one cell cycle, making replication-transcription collisions inevitable (Helmrich et al., 2011). In contrast to late replicating CFSs, ERFSs are located within early replicating regions that contain clusters of highly transcribed genes (Barlow et al., 2013). ERFSs break spontaneously during replication, but their fragility is significantly increased by exogenously induced replication arrest in early S phase (Barlow et al., 2013). ERFS fragility is also dependent on the level of transcription activity at these loci, suggesting that it is driven by replication-transcription encounters (Barlow et al., 2013).

Despite accumulating evidence that conflicts between replication and transcription are frequent events in proliferating cells and have detrimental effects on genome integrity, little is known about the molecular mechanisms underlying their resolution. In fission yeast, the progression of replication forks through actively transcribed genes depends on DNA helicase Pfh1, suggesting a general role for accessory helicases in the displacement of transcription complexes at sites of replication-transcription collisions (Sabouri et al., 2012). However, studies in budding yeast have shown that RNA-polymerase (RNAP) II mutants defective in transcription elongation impair replication fork progression and cause genomic instability, suggesting that RNAPII transcription complex might actively participate in the resolution of replication-transcription conflicts (Felipe-Abrio et al., 2015).

Correspondence to Pavel Janscak: pjanscak@imcr.uzh.ch

Abbreviations used: ActD, actinomycin D; CFS, common fragile site; ChIP, chromatin immunoprecipitation; CTD, C-terminal repeat domain; ERFS, early replicating fragile site; HU, hydroxyurea; IF, immunofluorescence staining; IP, immunoprecipitation; IRI, internal RNAPII–interacting; NC, nocodazole; PCNA, proliferating cell nuclear antigen; PI, propidium iodide; Pol ε, polymerase ε; qPCR, quantitative real-time PCR; RNAP, RNA-polymerase; SRI, Set2-Rpb1-interacting; TSS, transcription start site; WB, Western blotting.

The Rockefeller University Press $30.00
J. Cell Biol.
www.jcb.org/cgi/doi/10.1083/jcb.201507099

Published August 8, 2016

Human RECQ5 belongs to the RecQ family of DNA helicases (Croteau et al., 2014). RECQ5 is known to associate with RNAPII during transcription elongation (Izumikawa et al., 2008; Kanagaraj et al., 2010). It also localizes to DNA replication foci throughout S phase and interacts physically with the proliferating cell nuclear antigen (PCNA), a key component of the replisome (Kanagaraj et al., 2006). A recent study shows that RECQ5 controls the movement of RNAPII across genes to prevent it from pausing or arrest, a condition referred to as transcription stress (Saponaro et al., 2014). RECQ5 depletion results in transcription-dependent chromosome fragmentation during S phase and accumulation of chromosomal rearrangements with the breakpoints located in genes and CFSs (Li et al., 2011; Saponaro et al., 2014). Although the incidents of genome instability in RECQ5-depleted cells colocalize with the areas of elevated transcription stress (Saponaro et al., 2014), it is unclear whether RECQ5 operates directly at sites of interference between replication and transcription.

Here, we demonstrate that RECQ5 associates with transcription complexes in DNA replication foci and counteracts replication fork stalling in RNAPI- and RNAPII-transcribed genes. We present evidence for a novel molecular mechanism involved in the resolution of replication-transcription collisions wherein RECQ5 promotes RAD18-dependent PCNA ubiquitination by directly interacting with PCNA, and the helicase activity of RECQ5 promotes the processing of replication intermediates protected by BRCA1-dependent RAD51 filaments.

Results

RECQ5 associates with RNAPI transcription complexes

Previous studies have suggested that RECQ5 acts as an elongation factor of the RNAPII transcription machinery (Saponaro et al., 2014). To assess whether RECQ5 is also involved in RNAPI transcription, we tested by chromatin immunoprecipitation (ChIP) whether RECQ5 associates with rDNA. Chromatin prepared from asynchronously growing HEK293 cells was precipitated with antibodies against RECQ5 or the largest catalytic subunit of RNAPI, RPA194. Immunoprecipitated DNA was subjected to quantitative real-time PCR (qPCR) analysis using primer pairs covering the entire rDNA repeat unit: (a) the promoter region (amplicon H42); (b) the transcription start site (TSS); (c) the pre-rRNA coding region (H0.4-H13); and (d) the intergenic spacer (IGS; H18 and H27; Fig. 1 A). We found that RECQ5 was significantly enriched on the pre-rRNA coding region, showing a distribution pattern similar to that of RPA194 (Fig. 1 B). Moreover, inhibition of transcription by actinomycin D (ActD) resulted in the accumulation of RPA194 and RECQ5 at the pre-rRNA TSS (Fig. 1 B).

To determine whether RECQ5 interacts with the components of RNAPI transcription complex, a HEK293 cell extract was subjected to immunoprecipitation (IP) with anti-RECQ5 antibody, and the immunoprecipitated material was tested for the presence of RPA194. To exclude RNA- or DNA-mediated interactions, the extract was treated with benzonase nuclease. We found that RPA194 coprecipitated with anti-RECQ5 antibody but not with control IgG, suggesting that RECQ5 forms a complex with RNAPI (Fig. 1 C). RECQ5-RNAPI interaction was confirmed by coimmunoprecipitation of RECQ5 with ectopically expressed RPA43-GFP (Fig. S1 A).

To determine which region of RECQ5 is required for its interaction with RNAPI, different C-terminally truncated variants of GFP-tagged RECQ5 were overexpressed in HEK293 cells and tested for RPA194 binding by IP (Fig. S1, B and C). The results showed that the interaction between RECQ5 and RPA194 was abolished by deletion of the last 61 C-terminal amino acids of the RECQ5 polypeptide (Fig. 1 D and Fig. S1, B and C). It should be noted that this RECQ5 variant (RECQ5ΔCt) also lacks a part of the Set2-Rpb1-interacting (SRI) domain, which binds to the hyperphosphorylated C-terminal repeat domain (CTD) of RNAPII and mediates the association of RECQ5 with RNAPII-transcribed genes (Kanagaraj et al., 2010). Accordingly, RECQ5ΔCt showed reduced binding to the hyperphosphorylated form of RNAPII (IIo), whereas its binding to the hypophosphorylated form of RNAPII (IIa), mediated by the internal RNAPII–interacting (IRI) domain, was similar to that of wild-type RECQ5 (Kanagaraj et al., 2010; Fig. 1 D). Importantly, a RECQ5 variant lacking the IRI and SRI domains (GFP-RECQ5ΔIRIΔSRI), which failed to bind RNAPII, still retained RPA194 binding activity (Fig. 1 D), suggesting that the RNAPI-interacting domain of RECQ5 is located adjacent to the SRI domain.

Finally, by ChIP assay using anti-GFP antibody, we compared the binding of ectopically expressed GFP-RECQ5 and GFP-RECQ5ΔCt to rDNA in HEK293 cells. The results showed that the C-terminal region of RECQ5 is required for the efficient binding of RECQ5 to the pre-rRNA coding region of the rDNA repeat unit (Fig. 1 E). Collectively, these results provide evidence that RECQ5 binds to RNAPI during rDNA transcription.

RECQ5 depletion increases RNAPI density in the pre-rRNA coding region

To explore the possible involvement of RECQ5 in processes associated with RNAPI-directed transcription, we analyzed the effect of RECQ5 depletion on RPA194 density along rDNA repeat units in HEK293 cells. Interestingly, we observed a significant enrichment of RNAPI in the pre-rRNA coding region, but not on the promoter, in cells lacking RECQ5 (Fig. 1 F). These cells did not show any alteration in the cell cycle profile compared with mock-depleted cells (Fig. S1 D), excluding the possibility that the observed increase in RNAPI occupancy on rDNA was caused by an increase in the proportion of S/G2 cells, where RNAPI-directed transcription reaches its highest level (Grummt, 2003). These data suggest that RECQ5 might counteract RNAPI transcription stalling.

RECQ5 depletion leads to amplification of DNA segments within the pre-rRNA coding region in cells exposed to replication stress

To determine whether RECQ5 is required for the stability of rDNA arrays, it was kept knocked down in HEK293 cells for 12 d by successive siRNA transfections (Fig. 2 A). Subsequently, genomic DNA was isolated, and rDNA copy numbers at selected amplicons were measured by qPCR relative to *Oct-4* gene, which is not transcribed in HEK293 cells (Nejepinska et al., 2012). To assess whether RECQ5 prevents rDNA recombination arising as a consequence of interference between transcription and replication, cells were also exposed to mild replication stress generated by 0.2 mM hydroxyurea (HU; Fig. 2 A). We found that RECQ5 depletion caused DNA copy number variations, particularly within the pre-rRNA coding region of the rDNA repeat unit (Fig. 2 B). Importantly, upon HU

Published August 8, 2016

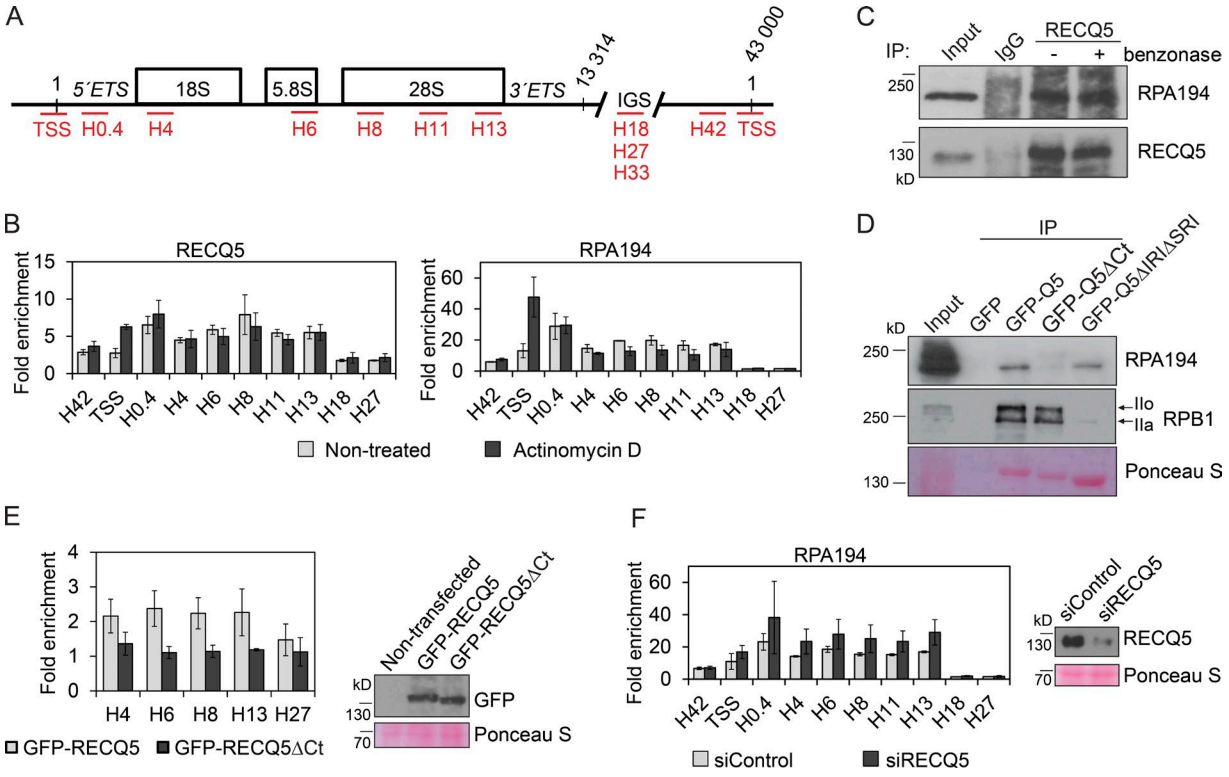

Figure 1. **RECQ5 associates with RNAPI during transcription elongation.** (A) Scheme of the human rDNA repeat unit showing location of the amplicons (in red) used in this study. ETS, external transcribed spacer; IGS, intergenic spacer. (B) Distribution of RECQ5 and RNA polymerase I (RPA194 subunit) along the rDNA repeat unit in nontreated or ActD-treated (1 µg/ml, 1 h) HEK293 cells determined by ChIP assay. (C) Coimmunoprecipitation of RPA194 with RECQ5 from extracts of HEK293 cells. Where indicated, cell extract was treated with benzonase nuclease to degrade nucleic acids. (D) Interaction of RPA194 or RPB1 (the largest catalytic subunit of RNAPII) with wild-type and mutant forms of GFP-RECQ5 expressed ectopically in HEK293 cells. Cell extracts were subjected to IP with GFP-Trap_A beads. Bound proteins were analyzed by WB. The RECQ5 variants were visualized by Ponceau S staining. IIo, hyperphosphorylated form of RPB1; IIa, hypophosphorylated form of RPB1. (E) Binding of GFP-RECQ5 and GFP-RECQ5ΔCt to rDNA in HEK293 cells determined by ChIP assay using anti-GFP antibody. Expression of GFP-RECQ5 and GFP-RECQ5ΔCt was confirmed by WB (right). (F) RPA194 density along rDNA repeat unit in mock- or RECQ5-depleted HEK293 cells determined by ChIP assay. RECQ5 down-regulation (using siRECQ5 #1) was confirmed by WB (right). For B, E, and F, data are represented as mean ± SD.

treatment, a significant amplification of DNA sequences within the pre-rRNA coding region was observed in RECQ5-depleted cells, but not in mock-depleted cells (Fig. 2 C). Such structural changes of rDNA likely arose as the consequence of DNA double-strand breaks generated within the pre-rRNA coding region by clashes between transcription and replication complexes, suggesting an important role for RECQ5 in preventing rDNA instability arising from interference between replication and transcription.

Depletion of RECQ5 causes replisome stalling in actively transcribed genes

To explore the hypothesis that RECQ5 is involved in the resolution of collisions between replication and transcription machineries, we investigated whether RECQ5 depletion leads to replication fork stalling at rDNA arrays. To this end, we measured DNA polymerase ε (Pol ε) occupancy along the rDNA repeat unit in mock- and RECQ5-depleted HEK293 cells released synchronously from a nocodazole (NC) block. The characteristic feature of rDNA arrays is that the actively transcribed rDNA repeats are replicated in early S phase, whereas the silent repeats are replicated in late S phase (Li et al., 2005). Therefore, we first determined rDNA replication timing in our experimental setup. By IP of BrdU pulse-labeled DNA followed by PCR analysis, we found that the first wave of rDNA replication occurred 6–9 h after NC block release, whereas the late-replicating rDNA was detected 12–16 h after release (Fig. 3 A). Hence, mock- and RECQ5-depleted cells were cross-linked at 8 or 14 h after NC block release and subjected to ChIP assay using antibody against the catalytic subunit of Pol ε. We found that RECQ5 depletion was associated with a significant enrichment of Pol ε on rDNA 8 h after NC block release (Fig. 3, B–D), when the replication of actively transcribed repeats occurred (Fig. 3 A). In contrast, the Pol ε occupancy profile at the late-replicating portion of rDNA (14 h after NC block release) was not affected by RECQ5 knockdown (Fig. 3 D). This suggests that RECQ5 counteracts replication fork stalling in transcriptionally active rDNA repeats during early S phase.

We also examined the effect of RECQ5 depletion on replication fork progression through rDNA in cells exposed to mild replication stress. Mock- and RECQ5-depleted HEK293 cells were released from NC block in medium containing 0.2 mM HU, and the level of Pol ε binding to rDNA was analyzed 8 or 14 h after NC block release. As expected, HU treatment slowed down cell cycle progression, with cells being in early S phase at 14 h after release from the NC block (Fig. 3 B). Importantly, we observed that RECQ5 knockdown caused a gradual accumulation of Pol ε on the rDNA repeat unit over the analyzed time period (Fig. 3 E).

Finally, we investigated whether RECQ5 depletion led to replication fork stalling in RNAPII-transcribed genes. We used

Published August 8, 2016

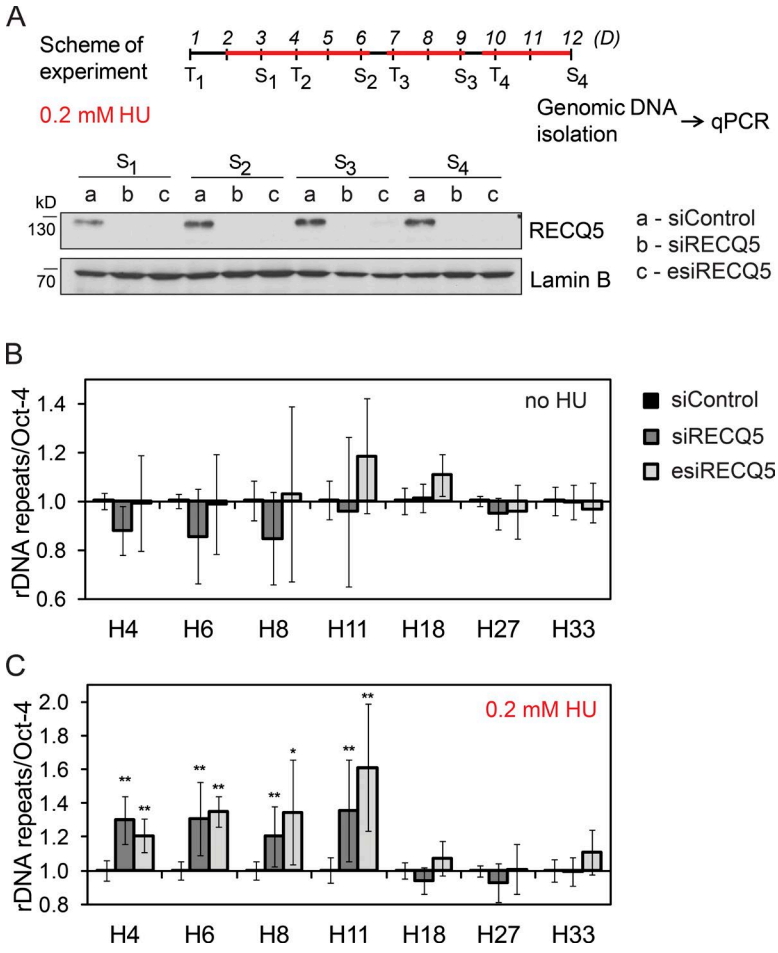

Figure 2. **Ribosomal DNA instability in RECQ5-depleted cells.** (A) Experimental scheme. RECQ5 was kept down-regulated in HEK293 cells for 12 d by successive transfections (T) of either siRECQ5#1 or esiRECQ5. Samples of cells were collected after each splitting (S) and analyzed by WB (bottom). Lamin B was used as loading control. Cells were treated with 0.2 mM HU at indicated time intervals (red lines) or left untreated. (B and C) Effect of RECQ5 depletion on rDNA stability in the absence or presence of 0.2 mM HU. The rDNA copy number at indicated amplicons (see Fig. 1 A) was measured by qPCR of genomic DNA (~2 ng) relative to the *Oct-4* gene. Data are represented as mean ± SD. *, $P < 0.0005$; **, $P < 0.00005$ (two-tailed unpaired *t* test).

chromatin prepared from HEK293 cells exposed to 0.2 mM HU to analyze Pol ε occupancy on the coding regions of several constitutively transcribed genes. We chose the *ACTG1* gene, which was previously shown to be occupied by RECQ5 in a RNAPII-dependent manner (Kanagaraj et al., 2010), and the genes encoding the ribosomal proteins RPS19 and RPL22. We found that RECQ5 depletion resulted in a significant enrichment of Pol ε on the coding regions of all three genes at 14 h after NC block release (Fig. 3 F). Importantly, no significant enrichment of Pol ε was observed at amplicon ACTG1-I, which represents an intergenic region located ~2 kb downstream of the *ACTG1* transcription termination site (Fig. 3 F). Collectively, these results suggest that RECQ5 counteracts replication fork stalling in actively transcribed genes, particularly under conditions of replication stress.

RECQ5 associates with transcription machinery in replication foci

RECQ5 was previously shown to accumulate in DNA replication foci (Kanagaraj et al., 2006). To identify the core complex bound by RECQ5 in these foci, we used the FRAP technique to measure the intranuclear mobility of GFP-tagged RECQ5 before and after the blockage of transcription or replication. HEK293 cells were transfected with vectors expressing GFP-tagged RECQ5 and RFP-tagged PCNA and brought to early S phase by the release from NC block. Live cell imaging revealed that GFP-RECQ5 formed discrete nuclear foci that largely colocalized with RFP-PCNA foci (Fig. 4 A, left). FRAP measurements of GFP-RECQ5 in circular regions containing one to three replication foci showed a very high mobility of RECQ5, in both the replication foci and the surrounding area (Fig. 4, right). In contrast, PCNA is characterized by a very slow fluorescence recovery, on the order of minutes, indicating a stable association with replication forks (Sporbert et al., 2002; unpublished data). Thus, the observed fast fluorescence recovery of GFP-RECQ5 in replication foci suggests that RECQ5 is not stably bound to the replication machinery. This was also supported by our observation that GFP-RECQ5 mobility in replication foci was not affected by aphidicolin (Aph), which inhibits DNA replication (Fig. 4). In contrast, inhibition of transcription by ActD dramatically impaired the mobility of GFP-RECQ5 in replication foci (Fig. 4), whereas no change in the mobility of GFP-RECQ5 outside the replication foci was observed (Fig. 4, magnified sections). These findings suggest that RECQ5 associates with transcription machinery in replication foci.

BRCA1 and RAD51 function at sites of replication-transcription interference

To gain insight into the role of RECQ5 in the resolution of conflicts between replication and transcription, we explored its functional relationship with proteins that are involved in the repair of damaged replication forks. BRCA1, an important tumor suppressor, has been implicated in the stabilization and processing of stalled replication forks, and it is known to be recruited to ERFSs both after HU-induced replication arrest and during normal replication (Schlacher et al., 2012; Barlow et al., 2013; Willis et al., 2014). BRCA1 forms discrete nuclear foci in unperturbed S-phase cells (Scully et al., 1997). Interestingly, we

Published August 8, 2016

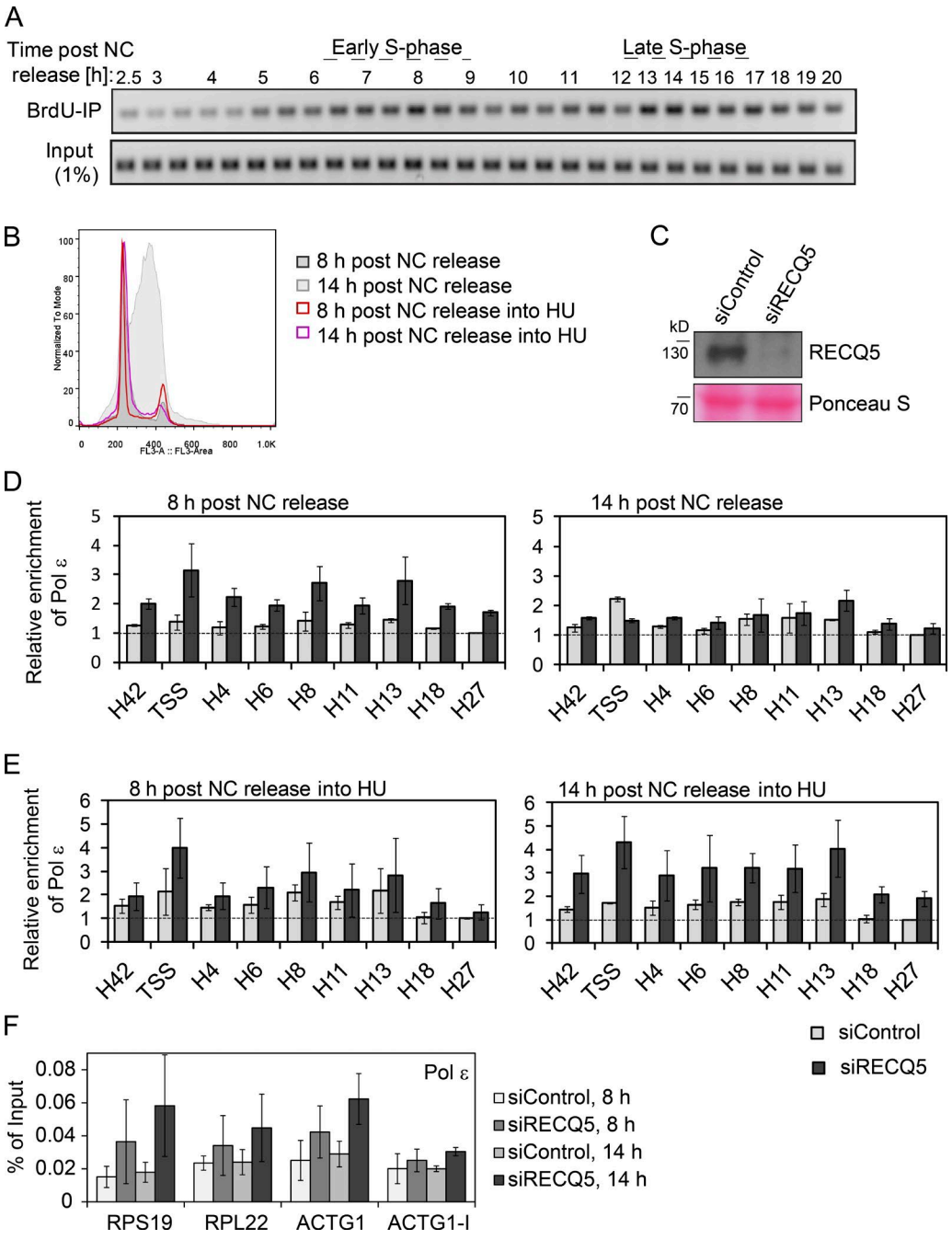

Figure 3. **RECQ5 depletion leads to replication fork stalling in actively transcribed genes.** (A) rDNA replication timing in HEK293 cells. Cells were released from NC block and pulse labeled with BrdU for 30 min before harvesting at the indicated time points. BrdU-labeled DNA was immunoprecipitated and analyzed by PCR using primer pair for amplicon H6. (B) Cell cycle distribution of HEK293 cells released from NC block for indicated periods of time in the presence or absence of 0.2 mM HU. (C) Western blot analysis of RECQ5 protein levels in chromatin (10 µg) used for ChIP assays. (D) DNA Pol ε occupancy on rDNA repeat unit in HEK293 cells transfected with either control siRNA (siControl) or RECQ5 siRNA (siRECQ5#1). Chromatin was isolated at indicated time points after the release from NC block and subjected to ChIP assay. (E) As in D, but cells were released from NC block into medium containing 0.2 mM HU. (F) Effect of RECQ5 knockdown on Pol ε occupancy on the indicated RNAPII-transcribed genes (*RPS19*, *RPL22*, and *ACTG1*). Chromatin for ChIP assay was prepared as in E. ATCG1-I represents a nontranscribed intergenic region located ~2 kb downstream of *ACTG1* stop codon. For D, E, and F, data are represented as mean ± SD.

found that the formation of BRCA1 foci in U2OS cells was impaired by cordycepin, which causes premature termination of transcription (Fig. 5, A and B; and Fig. S2 A), thus lowering the probability of replication-transcription clashes (Jones et al., 2013). In contrast, the number of BRCA1 foci increased if cells were exposed to ActD, which is capable of arresting transcription complexes on DNA, thereby creating a barrier to replication fork movement (Fig. 5, A–C; and Fig. S2 A). In agreement with this notion, RNAPI transcription complexes arrested on DNA by ActD treatment (Fig. 1 B) caused a significant increase in Pol ε occupancy on the rDNA repeat unit (Fig. S3 A). Neither of the transcription inhibitors used altered the percentage of S-phase cells (Fig. S2 B). Importantly, inhibition of DNA replication by Aph or HU significantly decreased the number of BRCA1 foci

Published August 8, 2016

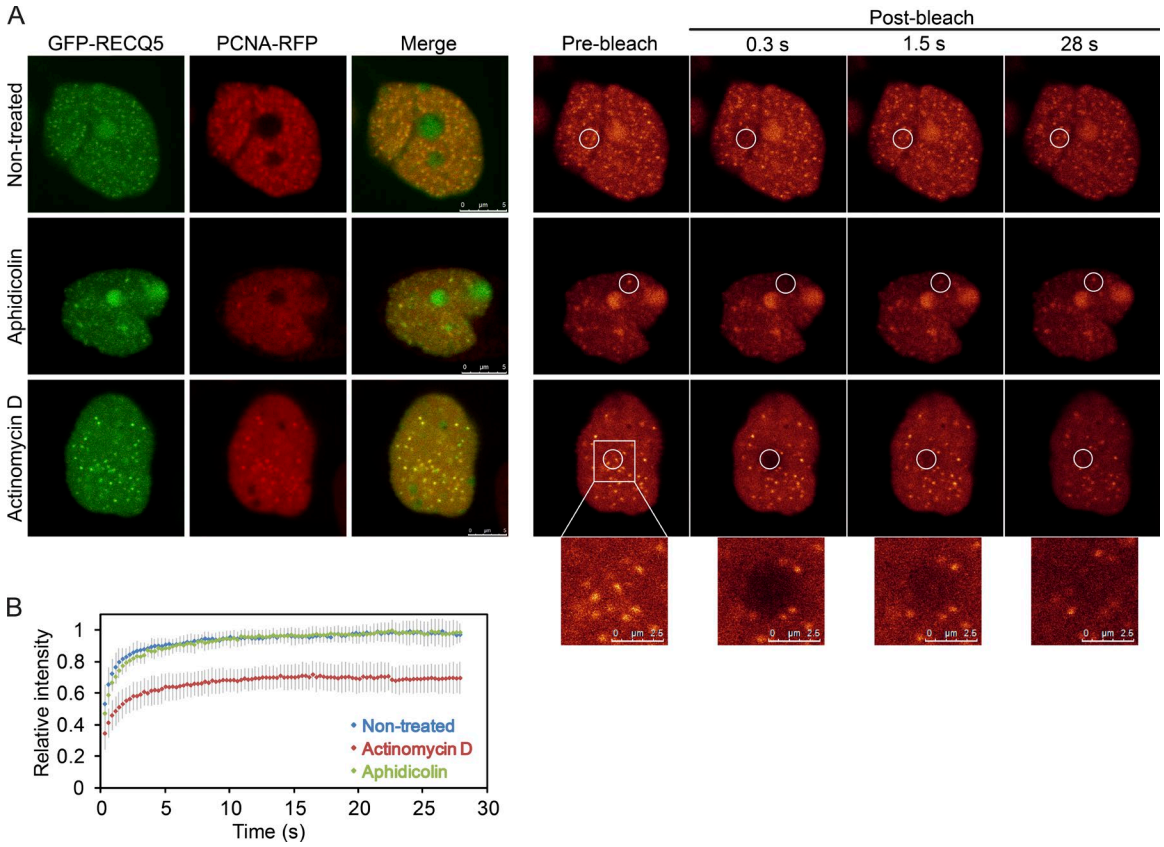

Figure 4. **RECQ5 associates with transcription complexes in replication foci.** (A, left) GFP-RECQ5 foci selected for FRAP analysis colocalize with PCNA-RFP foci in mock-, aphidicolin-, and ActD-treated HEK293 cells. (right) Representative images from a FRAP sequence showing the fluorescence recovery of GFP-RECQ5 in replication foci under indicated conditions. Bleached regions are depicted in white circles and also separately magnified for ActD-treated cells. FRAP measurements of GFP-RECQ5 were performed 6–9 h after release of cells from NC block. (B) Graph showing mean ± SD (n = 8–12) of relative fluorescence recovery in the bleached regions as a function of time.

in both mock- and ActD-treated cells (Fig. 5 C and Fig. S2, C and D), suggesting that the formation of these foci is driven by interference between replication and transcription. To further characterize the nature of BRCA1 foci, we performed FRAP experiments to measure GFP-BRCA1 mobility in these sites before and after replication or transcription arrest. We found that BRCA1 mobility in cells treated with Aph (replication arrest) was similar to that measured in mock-treated cells (Figs. 5 D and S2 E). In contrast, BRCA1 mobility was dramatically reduced in cells treated with ActD (transcription arrest; Figs. 5 D and S2 E). These data suggest that BRCA1 localized in S-phase foci associates with the transcription machinery at sites of replication-transcription interference.

BRCA1 acts to form RAD51 filaments at arrested replication forks to protect them from nucleolytic degradation (Schlacher et al., 2012). Like BRCA1, RAD51 forms discrete nuclear foci in unperturbed S-phase cells, and the formation of these foci is strictly dependent on the presence of BRCA1 (Scully et al., 1997; Fig. 5 E). Of note, RAD51 foci colocalize with BRCA1 foci only partially, suggesting that BRCA1 dissociates from these sites upon RAD51 recruitment (Scully et al., 1997; Fig. S2 F). In agreement with the immobilization of BRCA1 upon ActD treatment, the formation of RAD51 foci in S-phase cells was strongly attenuated by ActD (Fig. 5 F and Fig. S2, C and G), which further confirmed that BRCA1 activity is dependent on active transcription. RAD51 foci formation was also impaired in cells treated with the transcription terminator cordycepin or replication inhibitors HU and Aph (Fig. 5 F and Fig. S2, C and G). Combined treatment of cells with ActD and either HU or Aph further decreased the number of RAD51 foci per cell (Fig. 5 F and Fig. S2, C and G), suggesting that the formation of these foci is driven by replication-transcription interference.

Depletion of RECQ5 causes accumulation of unresolved replication intermediates

Next, we analyzed the frequency of BRCA1 foci in cells depleted of RECQ5. Interestingly, RECQ5 depletion led to a reduction in the frequency of BRCA1 foci in unperturbed cells but not in ActD-treated cells (Fig. 5, A and B; and Fig. S2 A). These results suggest that RECQ5 is not required for BRCA1 foci formation, but rather affects late steps of the process initiated by BRCA1 at sites of replication-transcription interference. Thus, we investigated the effect of RECQ5 depletion on the frequency of RAD51 foci in S-phase cells. We found that in RECQ5-deficient cells, the number of RAD51 foci that did not colocalize with a BRCA1 focus was increased compared with RECQ5-proficient cells, whereas the number of colocalizing foci was not affected (Fig. 5 G). Interestingly, the RAD51 inhibitor B02, which strongly inhibited RAD51 foci formation in mock-depleted cells, did not significantly reduce RAD51 foci in RECQ5-depleted cells (Fig. 5 H). This suggests that in the absence of RECQ5, cells accumulate replication intermediates stabilized by RAD51.

Published August 8, 2016

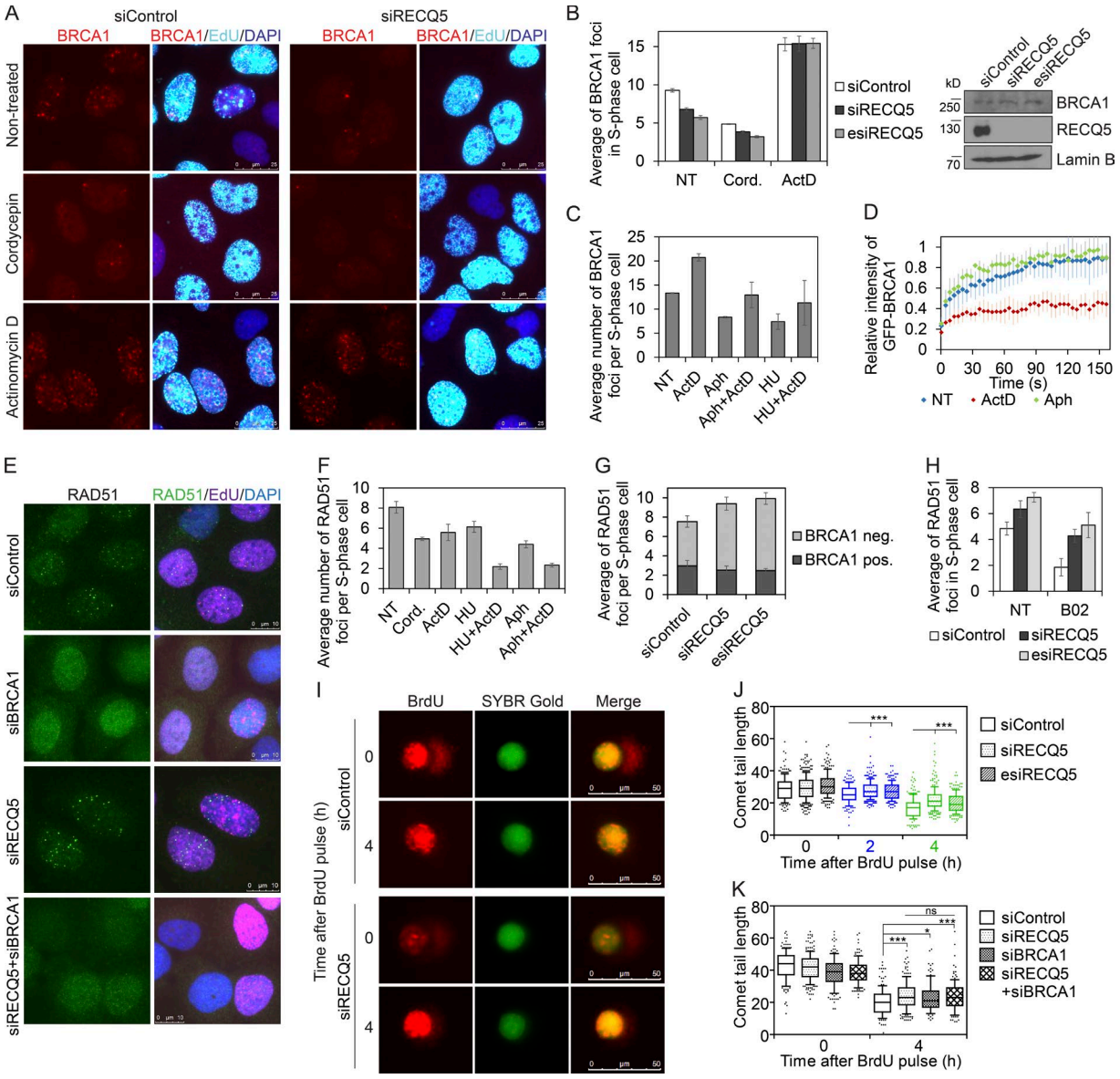

Figure 5. **RECQ5 depletion leads to accumulation of unresolved replication intermediates at sites of replication-transcription interference.** (A) Representative images of mock- and RECQ5-depleted (siRECQ5#2) U2OS cells stained for BRCA1 and EdU. Nuclei were stained with DAPI. EdU (20 µM) was added to cell cultures 1 h before fixation. Where indicated, cells were treated with cordycepin (50 µM) for 2 h or ActD (1 µg/ml) for 1 h before fixation. (B, left) Quantification of BRCA1 foci counts in EdU-positive nuclei of mock- or RECQ5-depleted U2OS cells represented in A. (right) Western blot analysis of U2OS cells transfected with indicated siRNAs. (C) Analysis of BRCA1 foci counts in EdU-positive nuclei of U2OS cells exposed to inhibitors of replication (5 µM Aph or 2 mM HU) for 90 min and/or transcription inhibitor (1 µg/ml ActD) for 1 h before fixation. Note that EdU was added 1 h before addition of Aph or HU. (D) Graph showing time dependency of relative fluorescence recovery for bleached nuclear regions containing GFP-BRCA1 foci in mock-, Aph-, and ActD-treated HEK293 cells. HEK293 cells were transfected with GFP-BRCA1 and PCNA-RFP (to identify cells in S phase) constructs, and FRAP measurements were performed 6–9 h after the release of cells from NC block. (E) Representative images of mock-, BRCA1-, RECQ5-, and BRCA1/RECQ5-depleted U2OS cells stained for RAD51 and EdU. Nuclei were stained with DAPI. (F) Analysis of RAD51 foci counts in EdU-positive nuclei of cells treated with 50 µM cordycepin for 2 h, or as in C. (G) Effect of RECQ5 depletion on the frequency of BRCA1-positive and BRCA1-negative RAD51 foci in U2OS cells. (H) Analysis of RAD51 foci counts in EdU-positive nuclei of RECQ5-proficient and RECQ5-deficient cells treated or not with the Rad51 inhibitor B02 (20 µM) for 6 h. (I) Representative images of mock- or RECQ5-depleted U2OS cells analyzed by alkaline BrdU comet assay. U2OS cells were pulse labeled with 20 µM BrdU for 20 min and harvested at the indicated time points after the BrdU wash-off to perform alkaline comet assay followed by immunostaining of BrdU-labeled DNA and staining with SYBR Gold. (J and K) Statistical analysis of BrdU-positive comet tail lengths measured for mock-, RECQ5-, and BRCA1-depleted U2OS cells. Whiskers indicate 10th to 90th percentile. ns, not significant; *, $P < 0.01$; ***, $P < 0.0001$ (two-tailed unpaired *t* test). Data in B–D and F–H are represented as mean ± SD.

To further explore this hypothesis, we monitored replication fork elongation in RECQ5-proficient and RECQ5-deficient cells by alkaline BrdU comet assay (Mórocz et al., 2013). In this assay, the stretches of newly synthesized DNA pulse labeled with BrdU are separated from the parental strand by alkaline denaturation and electrophoresis and are visualized as a comet tail by immunostaining with anti-BrdU antibody (Fig. 5 I). If DNA replication continues after BrdU pulse labeling, the nascent DNA strands become continuous and remain in the comet head (Fig. 5 I). In our experiments, we measured comet tail lengths at time points of 0, 2, and 4 h after the BrdU pulse. We found that at 4 h after BrdU labeling, RECQ5-depleted cells showed

Published August 8, 2016

substantially longer comet tails than mock-depleted cells, confirming that RECQ5 deficiency is associated with accumulation of unresolved replication intermediates (Fig. 5, I and J). Similarly, BRCA1-depleted cells also displayed longer comet tail lengths compared with mock-depleted cells (Fig. 5 K). Importantly, cells depleted for both RECQ5 and BRCA1 did not show a further increase in comet tail length as compared with cells depleted for either protein (Fig. 5 K). Collectively, the data described point to a coordinated action of RECQ5 and BRCA1/RAD51 at sites of replication-transcription interference to promote replication fork recovery.

RECQ5 is required for RAD18-dependent PCNA ubiquitination at sites of replication-transcription interference

Studies in budding yeast have shown that PCNA sliding clamp is unloaded from the lagging strand arm of stalled replication forks in a manner dependent on its ubiquitination at lysine 164 (Yu et al., 2014). To explore the possible involvement of RECQ5 and BRCA1 in replisome remodeling during the resolution of conflicts between replication and transcription machineries, we examined effects of their depletion on the level of ubiquitinated PCNA (Ub-PCNA) in chromatin fraction of unperturbed HEK293 cells. Ub-PCNA was monitored by Western blotting (WB) as a form of PCNA with reduced electrophoretic mobility that is readily detected in chromatin fraction of cells exposed to HU (Fig. 6, A and B). Depletion of BRCA1, but not that of RECQ5, substantially increased the level of Ub-PCNA in chromatin (Fig. 6, A and B). This PCNA ubiquitination was largely alleviated by cordycepin, suggesting that it arises as a consequence of interference between replication and transcription (Fig. 6, A and B). Importantly, almost no Ub-PCNA was detected in chromatin of cells depleted for both BRCA1 and RECQ5, suggesting that Ub-PCNA formation in the absence of BRCA1 depends on RECQ5 (Fig. 6, A and B). Moreover, depletion of RECQ5 alone increased the level of unmodified PCNA in chromatin, suggesting that RECQ5 might promote PCNA unloading (Fig. 6, A [low exposure] and C).

To explore this further, we measured the levels of Ub-PCNA and unmodified PCNA in the chromatin fraction of HEK293 cells overexpressing GFP-RECQ5. We found that GFP-RECQ5 overexpression stimulated PCNA ubiquitination and reduced the levels of unmodified PCNA on chromatin in both mock-depleted and BRCA1-depleted cells (Fig. 6 D). A similar phenotype was seen upon replication arrest induced by HU (Fig. 6 A). Consistently, DNA synthesis in GFP-RECQ5–overexpressing cells was strongly attenuated as revealed by measurement of EdU incorporation (Fig. 6 E). In contrast, overexpression of GFP-RECQ5 did not significantly affect transcription as measured by incorporation of 5-fluorouridine (Fig. 6 F). Interestingly, BRCA1-depleted cells overexpressing GFP-RECQ5 contained significantly higher levels of chromatin-bound Ub-PCNA compared with BRCA1-proficient cells overexpressing GFP-RECQ5 or BRCA1-deficient cells expressing only GFP (Fig. 6 D). This suggests that in the absence of BRCA1, Ub-PCNA generated by a RECQ5-mediated mechanism accumulates on chromatin.

To confirm that RECQ5 promotes PCNA ubiquitination and unloading, we examined the effect of GFP-RECQ5 overexpression on chromatin binding of a His-tagged version of a nonubiquitinable PCNA mutant, PCNA-K164R. We found that overexpression of GFP-RECQ5 did not affect the binding of PCNA-K164R to chromatin, whereas it significantly reduced chromatin binding of wild-type PCNA (Fig. 6 G, low exposure). As expected, binding of PCNA-K164R to chromatin was also not affected upon HU treatment (Fig. 6 G). Interestingly, overexpression of a helicase/ATPase-dead mutant of RECQ5, GFP-RECQ5-K58R (Garcia et al., 2004), dramatically increased the level of Ub-PCNA in chromatin without reducing the level of unmodified PCNA (Fig. 6 G), suggesting a role for the helicase activity of RECQ5 in PCNA unloading.

We also tested the effect of GFP-RECQ5 overexpression on the level of Ub-PCNA in chromatin of cells lacking RAD18, an E3 ubiquitin ligase, which is recruited to stalled replication forks to monoubiquitinate PCNA (Tsuji et al., 2008). We found that depletion of RAD18 impaired PCNA ubiquitination induced by the overexpression of wild-type GFP-RECQ5 or GFP-RECQ5-K58R, suggesting that RECQ5 promotes RAD18-dependent PCNA ubiquitination (Fig. 6 H).

Next, we investigated a relationship between RECQ5 and RAD18 at the interface of replication and transcription. First, we characterized the nature of RAD18 foci in cells exposed to different transcription or replication inhibitors (Fig. S4). The formation of RAD18 foci in S-phase cells was decreased upon cordycepin treatment (Fig. 6 I), which prematurely terminates transcription. Cells exposed to HU or ActD treatment, conditions leading to replication fork blockage, showed an increased number of RAD18 foci compared with untreated cells (Fig. 6 I). Importantly, combined treatment of cells with ActD and HU significantly decreased the number of RAD18 foci per cell (Fig. 6 I), suggesting that RAD18 foci formation is dependent on replication fork stalling caused by collisions with transcription complexes. As in the case of RECQ5, RAD18 depletion increased the number of RAD51 foci in S-phase cells, and these foci also persisted after exposure of cells to B02 (Fig. 6 J). Moreover, codepletion of RAD18 and RECQ5 did not cause a further increase in the number of RAD51 foci in comparison with depletion of either protein (Fig. 6 J), suggesting that RAD18 and RECQ5 act in the same pathway to resolve replication intermediates. Importantly, RECQ5 depletion caused accumulation of RAD18 foci in S-phase cells, implying that RECQ5 is not involved in the recruitment of RAD18 to stalled forks (Fig. 6 K). Moreover, BRCA1 depletion, which causes replication stalling, did not significantly change the number of RAD18 foci in S-phase cells (Fig. 6 K), suggesting that the increased frequency of RAD18 foci in RECQ5-deficient cells is a consequence of a defect in PCNA ubiquitination, leading to persistence of RAD18 at sites of stalled replication forks.

Helicase and PCNA-interacting domains of RECQ5 have distinct roles in the resolution of replication intermediates

Next, we wanted to identify the domains of RECQ5 involved in PCNA ubiquitination. For this, we prepared GFP-RECQ5 variants containing the K58R mutation in the helicase domain (its overexpression caused accumulation of Ub-PCNA on chromatin; Fig. 6, G and H) in combination with either a R943A mutation in the SRI domain (abolishment of RECQ5 binding to RNAPII CTD) or mutations in the PCNA-interacting peptide (PIP4A, abolishment of RECQ5–PCNA interaction). We tested the effect of overexpression of these RECQ5 variants on the level of chromatin-bound PCNA in HEK293 cells. We found that the K58R/PIP4A variant largely failed to induce PCNA ubiquitination, whereas K58R/R943A stimulated PCNA

Published August 8, 2016

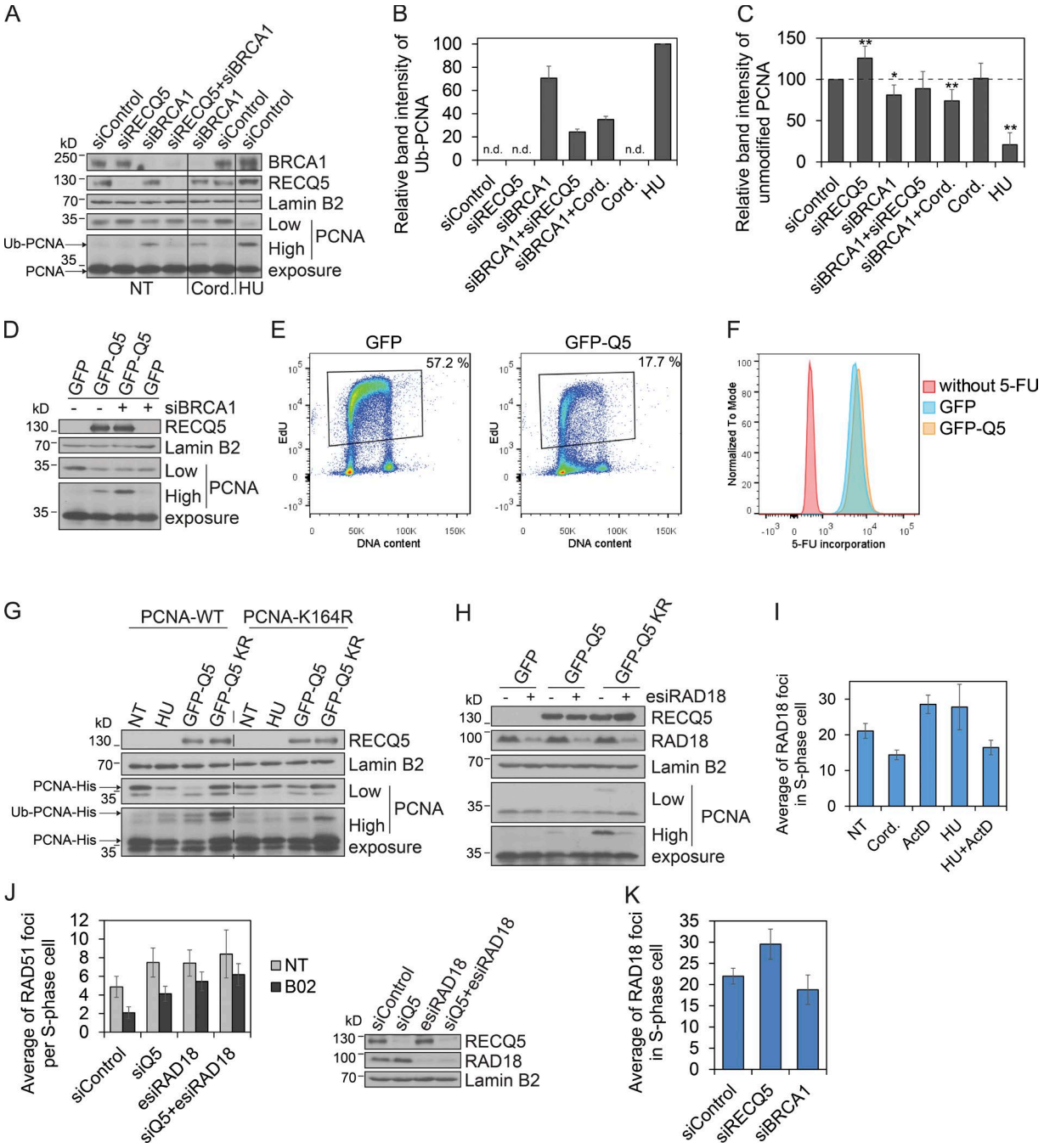

Figure 6. **RECQ5 promotes RAD18-dependent PCNA ubiquitination at sites of replication-transcription interference.** (A) Western blot analysis of PCNA, RECQ5, BRCA1, and Lamin B2 (loading control) levels in chromatin fractions isolated from HEK293 cells transfected with indicated siRNAs. Where indicated, cells were treated with 2 mM HU for 14 h or 50 µM cordycepin (Cord.) for the last 2 h. NT, nontreated. For unmodified PCNA, high and low exposures are shown. (B and C) Quantitative analysis of band intensity of ubiquitinated PCNA (Ub-PCNA) and unmodified PCNA, respectively, on Western blots represented in A. PCNA intensity was normalized to Lamin B2 intensity. Data are expressed as percentage of Ub-PCNA levels in chromatin of HU-treated cells or as percentage of unmodified PCNA levels in chromatin of mock-depleted cells, respectively. n.d., signal was not detected. *, $P < 0.01$; **, $P < 0.005$ (two-tailed unpaired *t* test). (D) Western blot analysis of PCNA levels in chromatin fractions of mock- or BRCA1-depleted HEK293 cells transiently overexpressing either GFP or GFP-RECQ5. Lamin B2 was used as loading control. (E) Flow cytometry analysis of EdU incorporation (*y* axis) and DNA content (propidium iodide, *x* axis) in HEK293 cells performed 48 h after transfection of vectors expressing either GFP or GFP-RECQ5. Only GFP-positive cells were analyzed. (F) Flow cytometry analysis of 5-FU incorporation into nascent RNA in HEK293 cells expressing either GFP or GFP-RECQ5. Mock-treated HEK293 cells (without 5-FU) served as noise-signal control. (G) Western blot analysis of PCNA levels in chromatin fractions isolated from HEK293 cells transiently expressing wild-type (WT) or mutant (K164R) forms of His-tagged PCNA. Cells were treated with 2 mM HU for 14 h or transfected with vectors expressing either wild-type (GFP-Q5) or helicase/ATPase-dead mutant (GFP-Q5 K58R) of RECQ5. (H) Western blot analysis of PCNA levels in chromatin of HEK293 cells transiently overexpressing GFP, GFP-Q5, or GFP-Q5 K58R that were either mock- or RAD18-depleted. (I) Analysis of RAD18 foci counts in EdU-positive nuclei of U2OS cells exposed to transcription inhibitors cordycepin (Cord.; 50 µM for 2 h) and ActD (1 µg/ml for 1 h) and/or replication inhibitor (2 mM HU) for 90 min before fixation. Note that EdU was added 1 h before addition of HU or fixation. (J, left) Analysis of RAD51 foci counts in EdU-positive nuclei of mock-, RECQ5-, and/or RAD18-depleted cells treated or not with the Rad51 inhibitor B02 (20 µM) for 6 h. (right) Western blot analysis of U2OS cells transfected with indicated siRNAs. (K) Analysis of RAD18 foci counts in EdU-positive nuclei of U2OS cells transfected with indicated siRNAs. Data in B, C, and I–K are represented as mean ± SD.

Published August 8, 2016

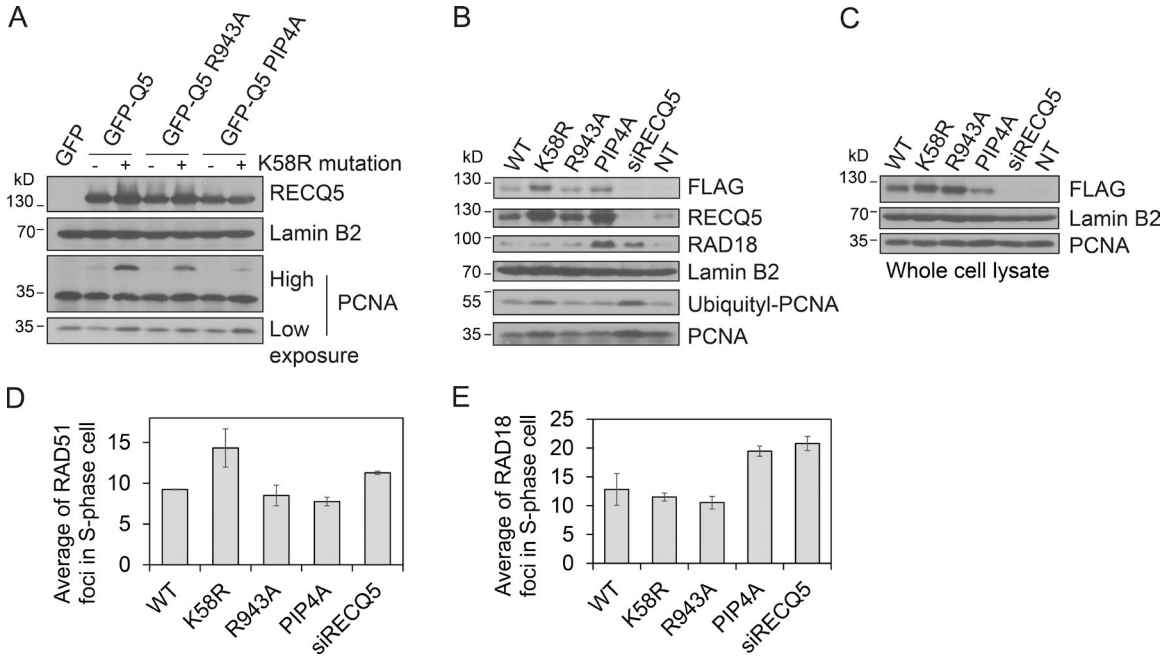

Figure 7. **Distinct roles of the helicase and PCNA-interacting domains of RECQ5 in resolution of replication intermediates.** (A) Western blot analysis of PCNA levels in chromatin of HEK293 cells transiently overexpressing various mutants of GFP-RECQ5 with defects in the helicase activity (K58R), RNA PIIo binding (R943A), and PCNA-interacting motif (PIP4A). (B) Western blot analysis of chromatin fraction of U2OS T-REx cells with doxycycline-regulated expression of Flag-tagged (shRNA-resistant) wild-type RECQ5 (WT), RECQ5-K58R (K58R), RECQ5-R934A (R934A), or RECQ5-PIP4A (PIP4A). Endogenous RECQ5 in these cells is down-regulated by shRNA. Parental U2OS T-REx cells were transfected with siControl or siRECQ5. (C) Western blot analysis of whole cell extracts of U2OS T-REx cells in B. (D and E) Analysis of RAD51 or RAD18 foci counts in EdU-positive nuclei of U2OS T-REx cells as in B. Data in D and E are represented as mean ± SD.

ubiquitination, although to a lesser extent compared with the K58R mutant (Fig. 7 A). These data suggest that RECQ5 promotes PCNA ubiquitination by directly interacting with PCNA via the PIP motif.

To investigate the phenotypes of RECQ5 mutants if expressed at levels comparable to that of endogenous RECQ5 protein, we established a cellular system that uses a pAIO-based vector (Ghodgaonkar et al., 2014) for inducible replacement of the endogenous RECQ5 with an shRNA-resistant mutant of interest. We prepared stable U2OS T-REx cell lines inducibly expressing Flag-tagged versions of wild-type RECQ5, RECQ5-K58R, RECQ5-R943A, and RECQ5-PIP4A, along with an shRNA targeting endogenous RECQ5. Thus, cells exposed to doxycycline (0.4 ng/ml) expressed a RECQ5 variant of interest with concomitant down-regulation of endogenous RECQ5 (Fig. S5). To detect Ub-PCNA in unchallenged cells, we used an antibody specifically recognizing ubiquityl-PCNA (Lys 164). We found that the substitution of endogenous RECQ5 with RECQ5-K58R caused accumulation of both Ub-PCNA and unmodified PCNA on chromatin (Fig. 7 B). Moreover, the lack of RECQ5 helicase activity increased the number of RAD51 foci in S-phase cells (Fig. 7 D). These results suggest that the helicase activity of RECQ5 prevents the accumulation of unresolved replication intermediates. On the contrary, the substitution of endogenous RECQ5 with RECQ5-PIP4A did not cause accumulation of unmodified PCNA nor Ub-PCNA on chromatin (Fig. 7 B). Instead, it increased the level of RAD18 in chromatin fraction and the number of RAD18 foci in S-phase cells (Fig. 7, B and E), which is consistent with our earlier finding of the requirement of RECQ5–PCNA interaction for PCNA ubiquitination. Interestingly, although the expression levels of all RECQ5 variants were comparable (Fig. 7 C), the levels of RECQ5-K58R and RECQ5-PIP4A in chromatin were significantly increased compared with that of wild-type RECQ5 (Fig. 7 B), providing a further evidence for a defect in their function. Together, these results suggest that a coordinated action of the helicase and PCNA-interacting domains of RECQ5 promotes the resolution of replication-transcription encounters.

Discussion

RECQ5 DNA helicase is essential for maintenance of genomic stability, but its exact molecular functions remain unclear. Recent studies have shown that human RECQ5 binds to RNAPII during transcription elongation and maintains genomic stability at RNAPII-transcribed genes by acting as a factor that prevents transcription pausing or arrest, a condition termed transcription stress (Kanagaraj et al., 2010; Li et al., 2011; Saponaro et al., 2014). Here, we show that RECQ5 also forms a complex with RNAPI during rDNA transcription, prevents RNAPI-transcription stress, and enforces the stability of the pre-rRNA coding regions of rDNA arrays. These results are consistent with the proposal of RECQ5 acting as a general transcription elongation factor that is important for preserving genome stability during transcription (Kanagaraj et al., 2010; Li et al., 2011; Saponaro et al., 2014). However, we also demonstrate that RECQ5 depletion causes the persistence of unresolved replication intermediates with replisomes stalled in both RNAPI- and RNA PII-transcribed genes. These findings suggest that the genome stabilization effect of RECQ5 at sites of transcription might reflect a role for RECQ5 in resolving collisions between the replication and transcription machineries. In support of this hypothesis, we have found that RECQ5 associates with active

Published August 8, 2016

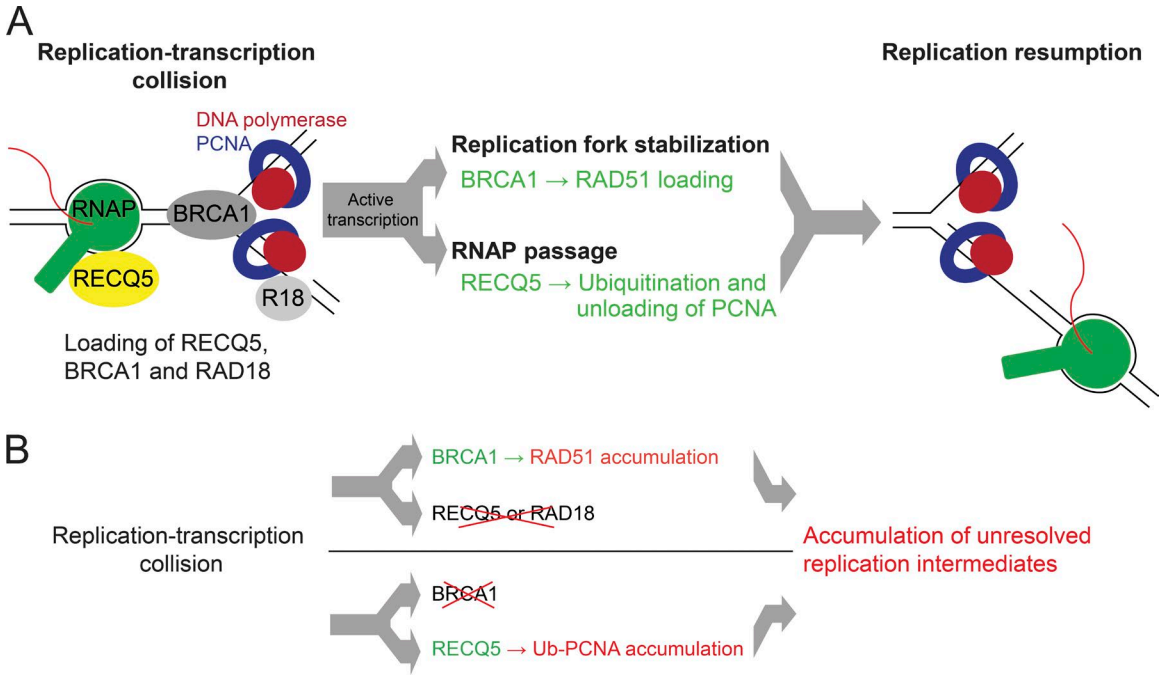

Figure 8. **Model for resolution of conflicts between replication and transcription.** (A) Scheme of the model. RECQ5, BRCA1, and RAD18 (R18) are recruited independently of each other to sites of replication-transcription collisions. BRCA1-dependent loading of RAD51 on stalled replication forks, which depends on active transcription, leads to fork stabilization. RECQ5 promotes RAD18-dependent PCNA ubiquitination and unloading at sites of replication-transcription interference that might allow the passage of oncoming transcription complexes across the fork to complete RNA synthesis. (B) Consequences of BRCA1 and RECQ5/RAD18 deficiencies. In the absence of BRCA1, RECQ5 can mediate PCNA ubiquitination and unloading, but the replication fork fails to restart because of the defect in RAD51 loading. In the absence of RECQ5 or RAD18, BRCA1 can promote assembly of RAD51 filaments to protect stalled replication forks, but RNA polymerase cannot translocate across the replication fork, and hence replication restart is prevented. Failure of either of these activities would lead to persistence of stalled replication forks, resulting in genomic instability.

transcription complexes in DNA replication foci, suggesting that it acts at sites of concomitant replication and transcription. Moreover, our data show that BRCA1, RAD51, and RAD18, proteins involved in the stabilization and restart of stalled forks, form foci at sites of replication-transcription interference, where they cooperate with RECQ5 to resume replication. Finally, we provide evidence that RECQ5 promotes RAD18-dependent ubiquitination of PCNA by directly interacting with PCNA and that the helicase activity of RECQ5 promotes the resolution of replication intermediates stabilized by RAD51 filaments upon replication-transcription encounters.

Mechanisms that cells evolved to resolve conflicts between replication and transcription remain elusive. Studies in bacteria and yeast have shown that specific helicases act in conjunction with the replisome to disrupt transcription complexes and other obstacles that impair replication fork progression (Azvolinsky et al., 2009; Boubakri et al., 2010; Sabouri et al., 2012). However, on very long genes in mammalian cells, collisions between transcription and replication complexes occur within each round of transcription, because the synthesis of the full-length transcript of these genes takes more than one cell cycle (Helmrich et al., 2013). Therefore, to ensure proper gene expression, cells must have mechanisms that permit RNA chain elongation after the collision with replication fork. Here, we provide evidence that RECQ5, BRCA1, and RAD18 are recruited independently of each other to sites of replication-transcription collisions. BRCA1-dependent loading of RAD51 stabilizes the stalled replication forks for replication resumption (Schlacher et al., 2012). RECQ5 promotes RAD18-dependent PCNA ubiquitination and unloading from replication forks upon their collision with active transcription. It is therefore likely that RECQ5-mediated replisome remodeling at stalled forks might allow the passage of oncoming transcription complexes across the fork to complete RNA synthesis (Fig. 8 A). There is accumulating evidence suggesting a role for active transcription in the resolution of replication-transcription collisions. It was shown that RNA polymerase translocation is required for the resolution of head-on collisions between the transcription machinery and bacteriophage Φ29 DNA polymerase in *Bacillus subtilis* (Elías-Arnanz and Salas, 1999). Similarly, studies in budding yeast have shown that RNAPII mutants with a defect in transcription elongation impair replication fork progression and cause genomic instability (Felipe-Abrio et al., 2015). In addition, we have shown in human cells that halted RNAPI transcription complexes prevented the movement of the replisome through rDNA (Fig. S3 A). Moreover, we provide evidence that replication forks stalled by halted transcription complexes could be elongated once the RNA polymerase is allowed to resume transcription (Fig. S3 B). Thus, RNA polymerase might actively participate in the resolution of replication-transcription collisions.

Studies in budding yeast revealed the presence of a Fob1-dependent replication fork barrier at the 3′-end of the rDNA transcription unit that prevents head on clashes of the replisome with RNAPI transcription complexes (Takeuchi et al., 2003). However, termination of DNA replication throughout the rDNA transcription units has been observed in human cells, suggesting that replication fork barriers at the 3′ end of rDNA transcription units may not be absolute and that some leftward-moving forks pass through the barriers and enter the transcribed

Published August 8, 2016

region (Little et al., 1993). Such events would require a resolution mechanism like the one suggested by our study.

Our study provides evidence for a coordinated action of RECQ5 and BRCA1 at sites of replication-transcription collisions, which leads to their resolution. We have found that cells lacking BRCA1 show increased levels of Ub-PCNA in chromatin, which is dependent on RECQ5 and transcription. On the other hand, cells lacking RECQ5 (as well as cells lacking RAD18) accumulate RAD51 nuclear foci that are formed in a BRCA1-dependent manner at sites of concomitant replication and transcription. These RAD51 foci in RECQ5-deficient cells likely represent unresolved replication intermediates because they display a long-term stability in the presence of RAD51 inhibitor B02, which prevents the formation of RAD51 foci in normal cells. Our findings imply that in the absence of BRCA1, RECQ5 can mediate PCNA ubiquitination and unloading followed by RNA polymerase bypass, but the replication fork fails to restart because of the defect in RAD51 loading (Schlacher et al., 2012; Fig. 8 B). In the absence of RECQ5, BRCA1 can promote assembly of RAD51 filaments to protect stalled replication forks, but RNA polymerase cannot translocate across the replication fork; hence replication restart is prevented (Fig. 8 B). Thus, both the RECQ5-RAD18-PCNA and the BRCA1-RAD51 "arms" of this mechanism are required to properly resolve replication-transcription collisions. Failure of either of these activities would lead to the persistence of stalled replication forks, resulting in genomic instability (Fig. 8 B).

Studies in budding yeast have shown that strains defective in PCNA unloading (e.g., Δ*elg1* or PCNA-K164R mutants) exhibit uncontrolled DNA replication and accumulate Rad52 foci, an indication of genomic instability (Yu et al., 2014). Interestingly, these studies have revealed that PCNA is unloaded only from the lagging strand arm of forks stalled by HU treatment (Yu et al., 2014). In human cells, the process of replisome remodeling at stalled forks is not understood. We have shown that the PIP motif of RECQ5 induces RAD18-dependent ubiquitination of PCNA, which accumulated on chromatin of cells expressing a helicase-dead mutant of RECQ5. Mutational inactivation of the PIP motif of RECQ5 resulted in accumulation of RAD18 on chromatin in S-phase cells, indicating a failure in PCNA ubiquitination. However, PIP motif mutations did not apparently affect PCNA unloading induced by overexpression of GFP-RECQ5, which is also dependent on the modification of PCNA Lys-164 (Fig. 7 A, compare lanes 3 and 6). Of note, overexpression of GFP-RECQ5 led to the accumulation of Ub-PCNA on chromatin, whereas unmodified PCNA was largely absent in chromatin under these conditions. A similar scenario can be observed for PCNA in HU-treated cells. Therefore, it is possible that the PIP motif of RECQ5 is involved in ubiquitination of PCNA trimers that remain at stalled forks during the resolution of replication-transcription encounters. The unloaded PCNA is likely to be ubiquitinated independently of RECQ5's PIP motif, but the unloading process depends on the helicase activity of RECQ5. This would explain our observation of increased Ub-PCNA levels in chromatin of RECQ5-depleted U2OS cells (Fig. 7 B, lane 5).

Interestingly, we have obtained evidence that BRCA1 associates with the transcription machinery at sites of replication-transcription interference. Moreover, we have found that active transcription is required for the formation of BRCA1-dependent RAD51 foci in S-phase cells. Thus, BRCA1 might act in association with the transcription machinery during the process of resolution of replication-transcription collisions. Consistently, previous studies have shown that BRCA1 binds to hyperphosphorylated RNAPII present in the transcription elongation complex (Krum et al., 2003).

Interference between replication and transcription represents a significant source of genome instability and contributes to oncogene-induced tumorigenesis (Poveda et al., 2010). Here, we provide evidence that RECQ5 exerts its genome maintenance function through its involvement in the resolution of collisions between replication and transcription complexes. Because RECQ5 deficiency is associated with cancer susceptibility in mice (Hu et al., 2007), our study provides further evidence for the role of replication-transcription interference in cancer development.

Materials and methods

Antibodies, siRNAs, and plasmids

The following antibodies were used for WB, IP, ChIP, or immunofluorescence staining (IF): rabbit polyclonal anti-RPA194 (WB, IP, and ChIP; sc-28714; Santa Cruz Biotechnology, Inc.), rabbit polyclonal anti-RECQ5 (WB, IP, ChIP, and IF; made in the laboratory), mouse monoclonal anti-GFP (WB and ChIP; ab290; Abcam), mouse monoclonal anti-Pol ε (ChIP; ab3163; Abcam), bridging antibody for mouse IgG (ChIP; 53017; Active Motif), mouse monoclonal anti–lamin B (WB; NA12; EMD Millipore), mouse monoclonal anti–lamin B2 (WB; gtx628803; GeneTex), rabbit polyclonal anti-TFIIH (WB; sc-293; Santa Cruz Biotechnology, Inc.), mouse monoclonal anti-PCNA (WB; sc-56; Santa Cruz Biotechnology, Inc.), mouse monoclonal anti-RNA PII (clone 7C2; WB; gift from J.-M. Egly, Institute of Genetics and Molecular and Cellular Biology, Illkirch, France), mouse monoclonal anti-BrdU (IF and IP; B2531; Sigma-Aldrich), mouse monoclonal anti-BRCA1 (WB; GTX70111; GeneTex), mouse monoclonal anti-BRCA1 (IF; sc-6954; Santa Cruz Biotechnology, Inc.), rabbit monoclonal anti-RAD18 (IF and WB; #9040; Cell Signaling Technology), rabbit monoclonal anti-ubiquityl-PCNA Lys164 (WB; #13439; Cell Signaling Technology), and mouse monoclonal anti-Flag (WB; F1804; Sigma-Aldrich). The siRNA oligonucleotides used in this study were purchased from Microsynth AG. The sequences of the sense strand of siRNA duplexes are 5′-CGUACGCGGAAUACUUCGA-3′ (siControl); 5′-GGAGAGUGCGACCAUGGCU-3′ (siRECQ5#1); 5′-CAGGUUUGUCGCCCAUUGGAA-3′ (siRECQ5#2); and 5′-CAGGAAAUGGCUGAACUAGAA-3′ (siBRCA1). The esiRECQ5 (MISSION esiRNA human RECQL5; Sigma-Aldrich) and esiRAD18 (MISSION esiRNA human RAD18; Sigma-Aldrich) are an siRNA pool. Transfections of siRNAs (10–40 nM) were done using Lipofectamine RNAiMax (Invitrogen) according to the manufacturer's instructions. Cells were harvested 48–72 h after siRNA transfection. The EcoRV–KpnI fragment of the plasmid pJP136 containing human RECQ5 ORF was subcloned into the plasmid pAIO digested with EcoRV and KpnI (Schwendener et al., 2010; Ghodgaonkar et al., 2014). The resulting construct was further modified as follows: (a) a DNA oligoduplex encoding for an shRNA corresponding to siRECQ5#1 (top strand: 5′-GATCCCCGGAGAGTGCGACCATGGCTTTCAAGAGAAGCCATGGTCGCACTCTCCTTTTTGGAAA-3′; bottom strand: 5′-AGCTTTTCCAAAAAGGAGAGTGCGACCATGGCTTCTCTTGAAAGCCATGGTCGCACTCTCCGGG-3′) was introduced between the HindIII and BglII sites; (b) silent mutations were introduced into the RECQ5 cDNA between nucleotides 102 and 120 to render the resulting RECQ5 transcript resistant to the shRNA; (c) the STOP codon in the RECQ5 cDNA was removed by site-directed mutagenesis to put the RECQ5 ORF in frame with the

Published August 8, 2016

3xFLAG tag present in the pAIO vector; (d) mutations were introduced into the RECQ5 ORF to generate K58R, R943A, PIP4A substitutions, respectively. Mutagenesis was performed using a QuickChange Site-Directed Mutagenesis kit (Agilent Technologies). The pEGFP-C1 derivatives expressing GFP-tagged wild-type RECQ5, RECQ5ΔIRIΔSRI, or BRCA1 were described previously (Mailand et al., 2007; Kanagaraj et al., 2010). The previously mentioned point mutations were subcloned into GFP-RECQ5 construct. The truncated forms of GFP-RECQ5 coding for amino acids 1–930 (RECQ5ΔCt), 1–651, and 1–502 were cloned by PCR using *Pfu* DNA polymerase (Fermentas) and reverse primers 5′-TCCTCGAGGCCCTCCTTGTAGAAAGGGGTG-3′, 5′-TCCTCGAGTTTGAGCGAGTACACATGGG-3′, and 5′-GCAGGATCCGCTTGTGGGCCTCATCTCTG-3′, respectively. The resulting amplicons were digested with ScaI–XhoI (for 1–930 and 1–651) or ScaI–BamHI (for 1–502) and inserted between the ScaI–SalI or ScaI–BamHI sites in the GFP-RECQ5 plasmid. The PCNA-RFP and RPA43-GFP expression constructs were gifts from D. Stanek (Institute of Molecular Genetics, Prague, Czech Republic) and M. Dundr (Rosalind Franklin University of Medicine and Science, Chicago, IL), respectively. pcDNA3.1 derivatives encoding for His-tagged wild-type PCNA or PCNA-K164R were described previously (Niimi et al., 2008). Plasmid transfections were performed using TransIT-2020 Reagent (Mirus Bio) according to the manufacturer's instructions.

Cell culture

HEK293 and U2OS cells were cultured in DMEM (Sigma-Aldrich) supplemented with 10% FBS (Thermo Fisher Scientific) and streptomycin/penicillin (100 U/ml). DMEM for cultivation of U2OS T-REx cells (Invitrogen) was supplemented with 10% Tet-system approved FBS (Biochrom). U2OS T-REx cells stably transfected with pAIO derivatives were selected in the presence of 1 µg/ml puromycin (InvivoGen). Doxycyclin (0.4 ng/ml) was added for 48 h to induce expression of recombinant RECQ5 proteins and down-regulate endogenous RECQ5. HEK293 cells were synchronized in mitosis by treatment with NC (0.1 µg/ml) for 14 h. Mitotic cells were shaken off, collected, washed twice with complete DMEM, and replated with fresh media. Where required, EdU was added to cell culture medium to a final concentration of 20 µM.

Flow cytometry

For analysis of cell cycle distribution by flow cytometry, cells were fixed with ethanol and stained with propidium iodide (PI; 10 µg/ml). EdU (20 µM, 1 h) or 5-FU (1 mM, 30 min) was added to medium before fixation with 4% paraformaldehyde in PBS, followed by permeabilization with 0.25% Triton X-100 in PBS for 5 min, EdU click reaction, or immunostaining with anti-BrdU antibody, respectively, and PI staining. Flow cytometry was performed using LSRII (BD) and FlowJo software (Tree Star).

Immunoprecipitation

For IP experiments, harvested cells were resuspended in lysis buffer (50 mM Tris-HCl, pH 7.5, 120 mM NaCl, and 0.5% Nonidet P-40) supplemented with protease inhibitor cocktail (Roche) and incubated for 5 min on ice. After sonication and subsequent centrifugation (16,000 *g* for 10 min at 4°C), the supernatants (500 µg protein) were incubated at 4°C either for 1 h with 10 µl GFP-Trap_A beads (for GFP-tagged proteins; ChromoTek) or overnight with 2 µg primary antibody and ChIP-IT Protein G Magnetic Beads (Active Motif). Where indicated, mixtures were supplemented with 25 U Benzonase nuclease (EMD Millipore) and 5 mM $MgCl_2$. Beads were washed three times in lysis buffer, and bound proteins were eluted by boiling with 2× Laemmli sample buffer.

Analysis of rDNA copy number

HEK293 cells were cultured on 6-cm dishes. The final concentration of siRNAs/esiRNA used for RECQ5 down-regulation was 40 nM at 0.4 ng/µl for the first transfection and 20 nM at 0.2 ng/µl for subsequent transfections. HU (0.2 mM) was added after cell passage or at indicated time points (Fig. 3 A). Samples for WB were collected during each passage. Genomic DNA was isolated using GenElute Mammalian Genomic DNA Miniprep kit (Sigma-Aldrich) according to the manufacturer's instructions. Extracted DNA was diluted to a concentration of 2 ng/µl and subjected to qPCR performed on a LightCycler 480 PCR System using LightCycler 480 SYBR Green I Master Mix (Roche). The changes in rDNA copy number were calculated by the comparative ΔCp method ($2^{-\Delta\Delta Cp}$) using *Oct-4* gene for DNA amount normalization. The sequences of primers used for qPCR are shown in Table S1.

ChIP assays

ChIP assays were performed using the ChIP-IT Express kit (Active Motif) according to the manufacturer's instructions. HEK293 cells were fixed with 1% formaldehyde for 10 min. Mock- or RECQ5-knockdown cells (asynchronous) were fixed 40 h after siRNA transfection. Cells released from NC block were fixed at indicated time points. NC was added 24 h after siRNA transfection to synchronize cells in mitosis, and treatment with 0.2 mM HU was started immediately after NC block release. HEK293 cells transfected with GFP-RECQ5 plasmids were fixed 24 h after transfection. Cross-linked chromatin was sheared by sonication (Diagenode Bioruptor, water-bath sonicator) to achieve DNA fragments of ∼300 bp. Fragmented chromatin containing ∼15 µg DNA was immunoprecipitated with 2 µg of specific antibody or control IgG (or bridging antibody) overnight at 4°C. In the case of ChIP with anti-GFP antibody, reactions contained only ∼7 µg chromatin. After elution, cross-link reversal, and proteinase K digestion of the immunoprecipitated chromatin, DNA was recovered using QIAquick PCR Purification kit (QIAGEN) and analyzed by qPCR. The sequences of primers used are shown in Table S1. The input chromatin was processed in the same way. DNA amounts were determined from a standard curve generated using input chromatin. Fold enrichment was calculated as a ratio of DNA amount precipitated by specific antibody versus DNA amount obtained with control IgG (or bridging antibody). Relative enrichment was calculated as the amount of precipitated DNA relative to the amount of DNA present in input chromatin (% of input), and normalized to the amplicon H27 of control sample.

Replication timing analysis

HEK293 cells were released from NC-induced mitotic arrest at indicated time points and incubated with 30 µM BrdU for 30 min before harvesting. Genomic DNA was isolated by phenol/chloroform extraction. 1 µg heat-denatured DNA was mixed with 5 µg anti-BrdU antibody and 15 µl ChIP-IT Protein G Magnetic Beads in 100 µl DNA binding buffer (50 mM Tris-HCl, pH 8, 120 mM NaCl, and 0.05% Triton X-100). After 1-h incubation, beads were washed with DNA binding buffer, and immunoprecipitated DNA was eluted by proteinase K treatment in the presence of 0.5% SDS. DNA was isolated using a QIAquick PCR Purification kit and subjected to PCR with primers amplifying the amplicon H6 (Fig. 1 B and Table S1). PCR products were analyzed by agarose electrophoresis.

Immunofluorescence microscopy and ScanR analysis

Cells grown on coverslips were fixed with 4% paraformaldehyde in PBS for 15 min and permeabilized with 0.25% Triton X-100 in PBS for 5 min. Coverslips were blocked with 1% BSA in PBS before incubation with primary antibodies for 90 min. After washing in PBS, coverslips were incubated with appropriate Alexa Fluor–conjugated

Published August 8, 2016

secondary antibodies (Thermo Fisher Scientific) and mounted using Vectashield reagent (Vector Laboratories). Cell images were captured on a DM 6000 fluorescence microscope (Leica Biosystems) using an oil-immersion objective, 63×/1.4 NA. For RAD18 immunostaining, cells were preextracted with 25 mM Hepes-NaOH. pH 7.5, buffer containing 50 mM NaCl, 1 mM EDTA, 3 mM $MgCl_2$, 0.3 M sucrose, and 0.5% Triton X-100 for 4 min at 4°C before fixation. In the case of BRCA1 and RAD51 immunostaining, methanol was used for permeabilization of cells (20 min at −20°C). EdU click reactions were performed in buffer containing 100 mM Tris-HCl, pH 8.5, 2 mM $CuSO_4$, 100 mM ascorbate, and 5 µM Alexa Fluor 647 azide (Thermo Fisher Scientific) for 30 min in the dark followed by two washes with 1% BSA in PBS and immunostaining. DNA was counterstained with DAPI. For BRCA1, RAD51, and RAD18 foci counting and analysis, automated image acquisition was performed on an IX70 microscope (Olympus) equipped with ScanR imaging platform and 40×/1.3 NA oil-immersion objective. Nuclei were identified based on DAPI signal, and foci counts for each nuclear object were analyzed using a spot detection module of the Analysis ScanR software. At least 144 images were acquired and analyzed per sample (2,000 nuclei on average).

FRAP assays

FRAP measurements of GFP-RECQ5 and GFP-BRCA1 mobility in HEK293 cells were performed 6–9 h after the release from NC block. NC was added simultaneously with plasmid transfection (GFP-RECQ5/GFP-BRCA1 and PCNA-RFP), and cells were plated on glass-bottomed Petri dishes after NC removal. ActD (1 µg/ml) or Aph (10 µM) was added 30 min before the start of imaging. The cells were imaged with a SP5 confocal microscope equipped with an oil immersion objective (HCX Plan-Apochromat 63×/1.4 NA) and an environmental chamber controlling temperature (37°C) and CO_2 level (5%). For GFP-RECQ5, data acquisition was performed using a 512 × 512-pixel format at a 1,000-Hz scan speed and 1.6-Airy pinhole in 8-bit resolution. After acquisition of eight prebleach images, a region of interest (circular spot 1.7 µm in diameter, covering one to three foci) was bleached with 100% laser power (488-nm line from an argon laser), and fluorescence recovery was monitored at low laser intensity in 110 iterations at 0.29-s intervals. For GFP-BRCA1, data acquisition was performed with modification in pixel format (1,024 × 1,024), and fluorescence recovery was monitored in 40 iterations at 4-s intervals. Fluorescence intensities of the bleached region and a proportionally equal distal unbleached area of the nucleus were measured at each time point using Fiji software. Values were corrected for extracellular background intensity and normalized to prebleach intensity to obtain relative fluorescence intensity.

Alkaline BrdU comet assay

Alkaline BrdU comet assay was performed as described previously (Mórocz et al., 2013). In brief, U2OS cells were pulse labeled with 20 µM BrdU for 20 min and chased in fresh medium for indicated periods of time. After washing in ice-cold PBS, 2×10^4 cells were resuspended in 40 µl of 0.95% low-melting agarose (37°C; SeaPlaque GTG agarose; Lonza) dissolved in PBS, and the suspension was spread onto an agarose-coated slide by covering with a coverslip. Agarose-embedded cells were lysed in ice-cold solution containing 10 mM Tris-HCl, pH 10, 2.5 M NaCl, 100 mM EDTA, 1% Triton X-100, and 0.5% *N*-lauroylsarcosine sodium salt for 90 min, with detergents added freshly before use, and washed three times for 5 min in PBS. The slides were placed in ice-cold alkaline electrophoresis solution (0.3 M NaOH and 1 mM EDTA, pH >13) for 40 min. Electrophoresis was subsequently conducted at 1 V/cm for 20 min in the same buffer. The slides were washed three times for 5 min in neutralization buffer (0.4 mM Tris-HCl, pH 7.4) and twice for 5 min in PBS and blocked with PBS-BT (PBS containing 0.1% Tween 20 and 0.1% BSA) for 30 min before immunostaining. The slides were incubated with mouse monoclonal anti-BrdU antibody (B2531; Sigma-Aldrich) for 1 h and washed three times with PBS and once with PBS-BT. Then the slides were incubated with secondary antibody Alexa Fluor 647 and SYBR Gold (both Thermo Fisher Scientific) for 45 min. After three washes in PBS, slides were covered with coverslips and kept in a humidified box until microscopy. Comet images were captured on a DM 6000 fluorescence microscope using a 20× objective, and the comet tail length was evaluated using OpenComet software (http://www.cometbio.org). At least 50 cells were analyzed for each of at least three independent experiments. Statistical analysis was done using GraphPad Prism5.

Cell fractionation

To obtain chromatin fractions, cells were resuspended in buffer A (10 mM Hepes-NaOH, pH 7.9, 10 mM KCl, 1.5 mM $MgCl_2$, 0.34 M sucrose, 10% glycerol, and 1 mM DTT) supplemented with 1 mg/ml digitonin and incubated on ice for 5 min. Nuclei were collected by centrifugation at 1,500 *g* for 4 min, washed once with buffer A, resuspended in buffer B (3 mM EDTA, 0.2 mM EGTA, and 1 mM DTT), and incubated on ice for 15 min. Chromatin was separated from nucleoplasmic fraction by centrifugation at 2,000 *g* for 5 min and sheared by sonication in buffer B.

Online supplemental material

Fig. S1 shows interaction of ectopically expressed RECQ5 variants with RPA194. Fig. S2 shows frequencies of BRCA1 and RAD51 foci in nuclei of cells exposed to different replication and transcription inhibitors, and images from a FRAP sequence showing fluorescence recovery of GFP-BRCA1 foci in mock-, Aph-, and ActD-treated HEK293 cells. Fig. S3 shows occupancy of Pol ε on rDNA repeat units and analysis of BrdU comet tail lengths in nontreated and ActD-treated cells. Fig. S4 shows representative images of RAD18 foci in nuclei of cells exposed to different replication and transcription inhibitors. Fig. S5 shows relative mRNA abundance of endogenous and total RECQ5 in U2OS T-REx cells expressing RECQ5 variants. Table S1 lists the sequences of primers used for qPCR. Online supplemental material is available at http://www.jcb.org/cgi/content/full/jcb.201507099/DC1.

Acknowledgments

We thank Radek Malik and Jana Urbanova for comments on the manuscript and help with real-time PCR, and Miroslav Dundr, David Stanek, and Alan R. Lehmann for providing plasmid constructs.

This work was supported by the Czech Science Foundation (14-05743S), the Swiss National Science Foundation (31003A-146206), the Danish Council for Independent Research (DFF-1331-00262), the Swedish Research Council, the Ministry of Education, Youth and Sports of the Czech Republic (KONTAKT II LH14037), and the Neuron Fund for Support of Science.

The authors declare no competing financial interests.

Submitted: 27 July 2015
Accepted: 11 July 2016

References

Azvolinsky, A., P.G. Giresi, J.D. Lieb, and V.A. Zakian. 2009. Highly transcribed RNA polymerase II genes are impediments to replication fork progression in *Saccharomyces cerevisiae*. *Mol. Cell.* 34:722–734. http://dx.doi.org/10.1016/j.molcel.2009.05.022

Barlow, J.H., R.B. Faryabi, E. Callén, N. Wong, A. Malhowski, H.T. Chen, G. Gutierrez-Cruz, H.W. Sun, P. McKinnon, G. Wright, et al. 2013. Identification of early replicating fragile sites that contribute to genome instability. *Cell.* 152:620–632. http://dx.doi.org/10.1016/j.cell.2013.01.006

Boubakri, H., A.L. de Septenville, E. Viguera, and B. Michel. 2010. The helicases DinG, Rep and UvrD cooperate to promote replication across transcription units in vivo. *EMBO J.* 29:145–157. http://dx.doi.org/10.1038/emboj.2009.308

Croteau, D.L., V. Popuri, P.L. Opresko, and V.A. Bohr. 2014. Human RecQ helicases in DNA repair, recombination, and replication. *Annu. Rev. Biochem.* 83:519–552. http://dx.doi.org/10.1146/annurev-biochem-060713-035428

Durkin, S.G., and T.W. Glover. 2007. Chromosome fragile sites. *Annu. Rev. Genet.* 41:169–192. http://dx.doi.org/10.1146/annurev.genet.41.042007.165900

Elías-Arnanz, M., and M. Salas. 1999. Resolution of head-on collisions between the transcription machinery and bacteriophage phi29 DNA polymerase is dependent on RNA polymerase translocation. *EMBO J.* 18:5675–5682. http://dx.doi.org/10.1093/emboj/18.20.5675

Felipe-Abrio, I., J. Lafuente-Barquero, M.L. García-Rubio, and A. Aguilera. 2015. RNA polymerase II contributes to preventing transcription-mediated replication fork stalls. *EMBO J.* 34:236–250. http://dx.doi.org/10.15252/embj.201488544

Garcia, P.L., Y. Liu, J. Jiricny, S.C. West, and P. Janscak. 2004. Human RECQ5beta, a protein with DNA helicase and strand-annealing activities in a single polypeptide. *EMBO J.* 23:2882–2891. http://dx.doi.org/10.1038/sj.emboj.7600301

Ghodgaonkar, M.M., P. Kehl, I. Ventura, L. Hu, M. Bignami, and J. Jiricny. 2014. Phenotypic characterization of missense polymerase-δ mutations using an inducible protein-replacement system. *Nat. Commun.* 5:4990. http://dx.doi.org/10.1038/ncomms5990

Grummt, I. 2003. Life on a planet of its own: Regulation of RNA polymerase I transcription in the nucleolus. *Genes Dev.* 17:1691–1702. http://dx.doi.org/10.1101/gad.1098503R

Helmrich, A., M. Ballarino, and L. Tora. 2011. Collisions between replication and transcription complexes cause common fragile site instability at the longest human genes. *Mol. Cell.* 44:966–977. http://dx.doi.org/10.1016/j.molcel.2011.10.013

Helmrich, A., M. Ballarino, E. Nudler, and L. Tora. 2013. Transcription-replication encounters, consequences and genomic instability. *Nat. Struct. Mol. Biol.* 20:412–418. http://dx.doi.org/10.1038/nsmb.2543

Hu, Y., S. Raynard, M.G. Sehorn, X. Lu, W. Bussen, L. Zheng, J.M. Stark, E.L. Barnes, P. Chi, P. Janscak, et al. 2007. RECQL5/Recql5 helicase regulates homologous recombination and suppresses tumor formation via disruption of Rad51 presynaptic filaments. *Genes Dev.* 21:3073–3084. http://dx.doi.org/10.1101/gad.1609107

Izumikawa, K., M. Yanagida, T. Hayano, H. Tachikawa, W. Komatsu, A. Shimamoto, K. Futami, Y. Furuichi, T. Shinkawa, Y. Yamauchi, et al. 2008. Association of human DNA helicase RecQ5beta with RNA polymerase II and its possible role in transcription. *Biochem. J.* 413:505–516. http://dx.doi.org/10.1042/BJ20071392

Jones, R.M., O. Mortusewicz, I. Afzal, M. Lorvellec, P. García, T. Helleday, and E. Petermann. 2013. Increased replication initiation and conflicts with transcription underlie Cyclin E-induced replication stress. *Oncogene.* 32:3744–3753. http://dx.doi.org/10.1038/onc.2012.387

Kanagaraj, R., N. Saydam, P.L. Garcia, L. Zheng, and P. Janscak. 2006. Human RECQ5beta helicase promotes strand exchange on synthetic DNA structures resembling a stalled replication fork. *Nucleic Acids Res.* 34:5217–5231. http://dx.doi.org/10.1093/nar/gkl677

Kanagaraj, R., D. Huehn, A. MacKellar, M. Menigatti, L. Zheng, V. Urban, I. Shevelev, A.L. Greenleaf, and P. Janscak. 2010. RECQ5 helicase associates with the C-terminal repeat domain of RNA polymerase II during productive elongation phase of transcription. *Nucleic Acids Res.* 38:8131–8140. http://dx.doi.org/10.1093/nar/gkq697

Krum, S.A., G.A. Miranda, C. Lin, and T.F. Lane. 2003. BRCA1 associates with processive RNA polymerase II. *J. Biol. Chem.* 278:52012–52020. http://dx.doi.org/10.1074/jbc.M308418200

Li, J., R. Santoro, K. Koberna, and I. Grummt. 2005. The chromatin remodeling complex NoRC controls replication timing of rRNA genes. *EMBO J.* 24:120–127. http://dx.doi.org/10.1038/sj.emboj.7600492

Li, M., X. Xu, and Y. Liu. 2011. The SET2-RPB1 interaction domain of human RECQ5 is important for transcription-associated genome stability. *Mol. Cell. Biol.* 31:2090–2099. http://dx.doi.org/10.1128/MCB.01137-10

Little, R.D., T.H. Platt, and C.L. Schildkraut. 1993. Initiation and termination of DNA replication in human rRNA genes. *Mol. Cell. Biol.* 13:6600–6613. http://dx.doi.org/10.1128/MCB.13.10.6600

Mailand, N., S. Bekker-Jensen, H. Faustrup, F. Melander, J. Bartek, C. Lukas, and J. Lukas. 2007. RNF8 ubiquitylates histones at DNA double-strand breaks and promotes assembly of repair proteins. *Cell.* 131:887–900. http://dx.doi.org/10.1016/j.cell.2007.09.040

Mórocz, M., H. Gali, I. Raskó, C.S. Downes, and L. Haracska. 2013. Single cell analysis of human RAD18-dependent DNA post-replication repair by alkaline bromodeoxyuridine comet assay. *PLoS One.* 8:e70391. http://dx.doi.org/10.1371/journal.pone.0070391

Nejepinska, J., R. Malik, J. Filkowski, M. Flemr, W. Filipowicz, and P. Svoboda. 2012. dsRNA expression in the mouse elicits RNAi in oocytes and low adenosine deamination in somatic cells. *Nucleic Acids Res.* 40:399–413. http://dx.doi.org/10.1093/nar/gkr702

Niimi, A., S. Brown, S. Sabbioneda, P.L. Kannouche, A. Scott, A. Yasui, C.M. Green, and A.R. Lehmann. 2008. Regulation of proliferating cell nuclear antigen ubiquitination in mammalian cells. *Proc. Natl. Acad. Sci. USA.* 105:16125–16130. http://dx.doi.org/10.1073/pnas.0802727105

Poveda, A.M., M. Le Clech, and P. Pasero. 2010. Transcription and replication: breaking the rules of the road causes genomic instability. *Transcription.* 1:99–102. http://dx.doi.org/10.4161/trns.1.2.12665

Sabouri, N., K.R. McDonald, C.J. Webb, I.M. Cristea, and V.A. Zakian. 2012. DNA replication through hard-to-replicate sites, including both highly transcribed RNA Pol II and Pol III genes, requires the *S. pombe* Pfh1 helicase. *Genes Dev.* 26:581–593. http://dx.doi.org/10.1101/gad.184697.111

Saponaro, M., T. Kantidakis, R. Mitter, G.P. Kelly, M. Heron, H. Williams, J. Söding, A. Stewart, and J.Q. Svejstrup. 2014. RECQL5 controls transcript elongation and suppresses genome instability associated with transcription stress. *Cell.* 157:1037–1049. http://dx.doi.org/10.1016/j.cell.2014.03.048

Schlacher, K., H. Wu, and M. Jasin. 2012. A distinct replication fork protection pathway connects Fanconi anemia tumor suppressors to RAD51-BRCA1/2. *Cancer Cell.* 22:106–116. http://dx.doi.org/10.1016/j.ccr.2012.05.015

Schwendener, S., S. Raynard, S. Paliwal, A. Cheng, R. Kanagaraj, I. Shevelev, J.M. Stark, P. Sung, and P. Janscak. 2010. Physical interaction of RECQ5 helicase with RAD51 facilitates its anti-recombinase activity. *J. Biol. Chem.* 285:15739–15745. http://dx.doi.org/10.1074/jbc.M110.110478

Scully, R., J. Chen, A. Plug, Y. Xiao, D. Weaver, J. Feunteun, T. Ashley, and D.M. Livingston. 1997. Association of BRCA1 with Rad51 in mitotic and meiotic cells. *Cell.* 88:265–275. http://dx.doi.org/10.1016/S0092-8674(00)81847-4

Sporbert, A., A. Gahl, R. Ankerhold, H. Leonhardt, and M.C. Cardoso. 2002. DNA polymerase clamp shows little turnover at established replication sites but sequential de novo assembly at adjacent origin clusters. *Mol. Cell.* 10:1355–1365. http://dx.doi.org/10.1016/S1097-2765(02)00729-3

Takeuchi, Y., T. Horiuchi, and T. Kobayashi. 2003. Transcription-dependent recombination and the role of fork collision in yeast rDNA. *Genes Dev.* 17:1497–1506. http://dx.doi.org/10.1101/gad.1085403

Tsuji, Y., K. Watanabe, K. Araki, M. Shinohara, Y. Yamagata, T. Tsurimoto, F. Hanaoka, K. Yamamura, M. Yamaizumi, and S. Tateishi. 2008. Recognition of forked and single-stranded DNA structures by human RAD18 complexed with RAD6B protein triggers its recruitment to stalled replication forks. *Genes Cells.* 13:343–354. http://dx.doi.org/10.1111/j.1365-2443.2008.01176.x

Willis, N.A., G. Chandramouly, B. Huang, A. Kwok, C. Follonier, C. Deng, and R. Scully. 2014. BRCA1 controls homologous recombination at Tus/Ter-stalled mammalian replication forks. *Nature.* 510:556–559. http://dx.doi.org/10.1038/nature13295

Wilson, T.E., M.F. Arlt, S.H. Park, S. Rajendran, M. Paulsen, M. Ljungman, and T.W. Glover. 2015. Large transcription units unify copy number variants and common fragile sites arising under replication stress. *Genome Res.* 25:189–200. http://dx.doi.org/10.1101/gr.177121.114

Yu, C., H. Gan, J. Han, Z.X. Zhou, S. Jia, A. Chabes, G. Farrugia, T. Ordog, and Z. Zhang. 2014. Strand-specific analysis shows protein binding at replication forks and PCNA unloading from lagging strands when forks stall. *Mol. Cell.* 56:551–563. http://dx.doi.org/10.1016/j.molcel.2014.09.017

Urban et al., http://www.jcb.org/cgi/content/full/jcb.201507099/DC1

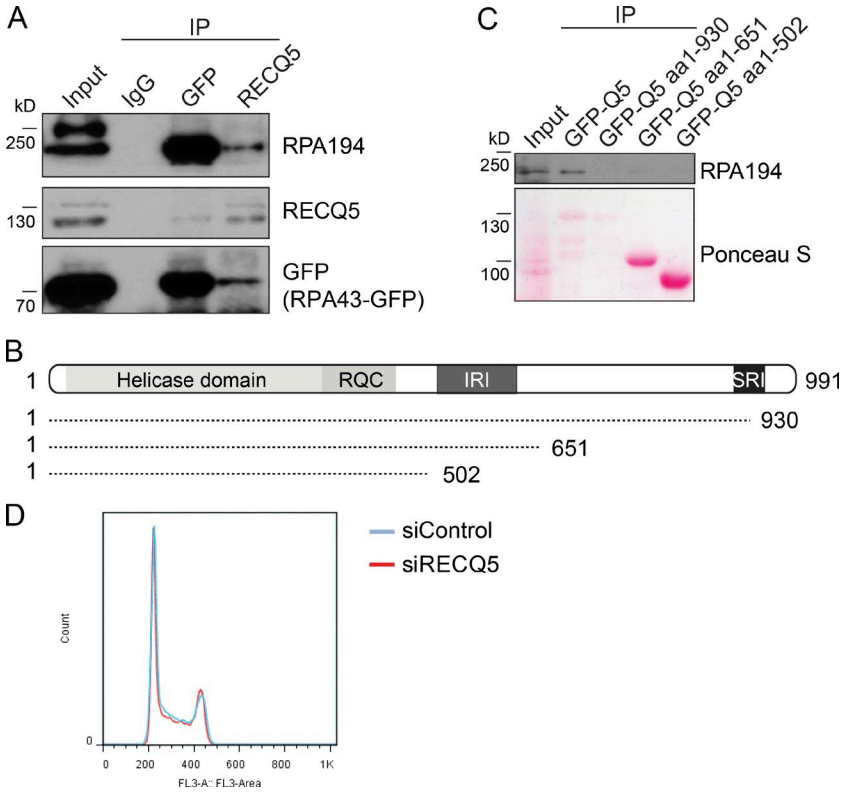

Figure S1. **Interaction between RECQ5 and RNAPI.** (A) Reciprocal coimmunoprecipitation of RECQ5 and RNAPI. Ectopically expressed subunit of RNAPI, RPA43-GFP, was pulled down from HEK293 cell extract using GFP-Trap_A beads. RPA194, the catalytic subunit of RNAPI. (B) Scheme of truncated variants of RECQ5 used for mapping of its RNAPI-interacting domain. Helicase domain, RecQ-C terminal (RQC) domain, IRI domain and SRI domain are depicted. (C) Coimmunoprecipitation of RPA194 with indicated RECQ5-GFP variants expressed in HEK293 cells. GFP-RECQ5 variants are visualized by Ponceau S staining. Note that GFP-RECQ5 aa 1–930 is referred to as GFP-RECQ5ΔCt. (D) Cell cycle distribution of mock- and RECQ5-depleted (siRECQ5 #1) HEK293 cells.

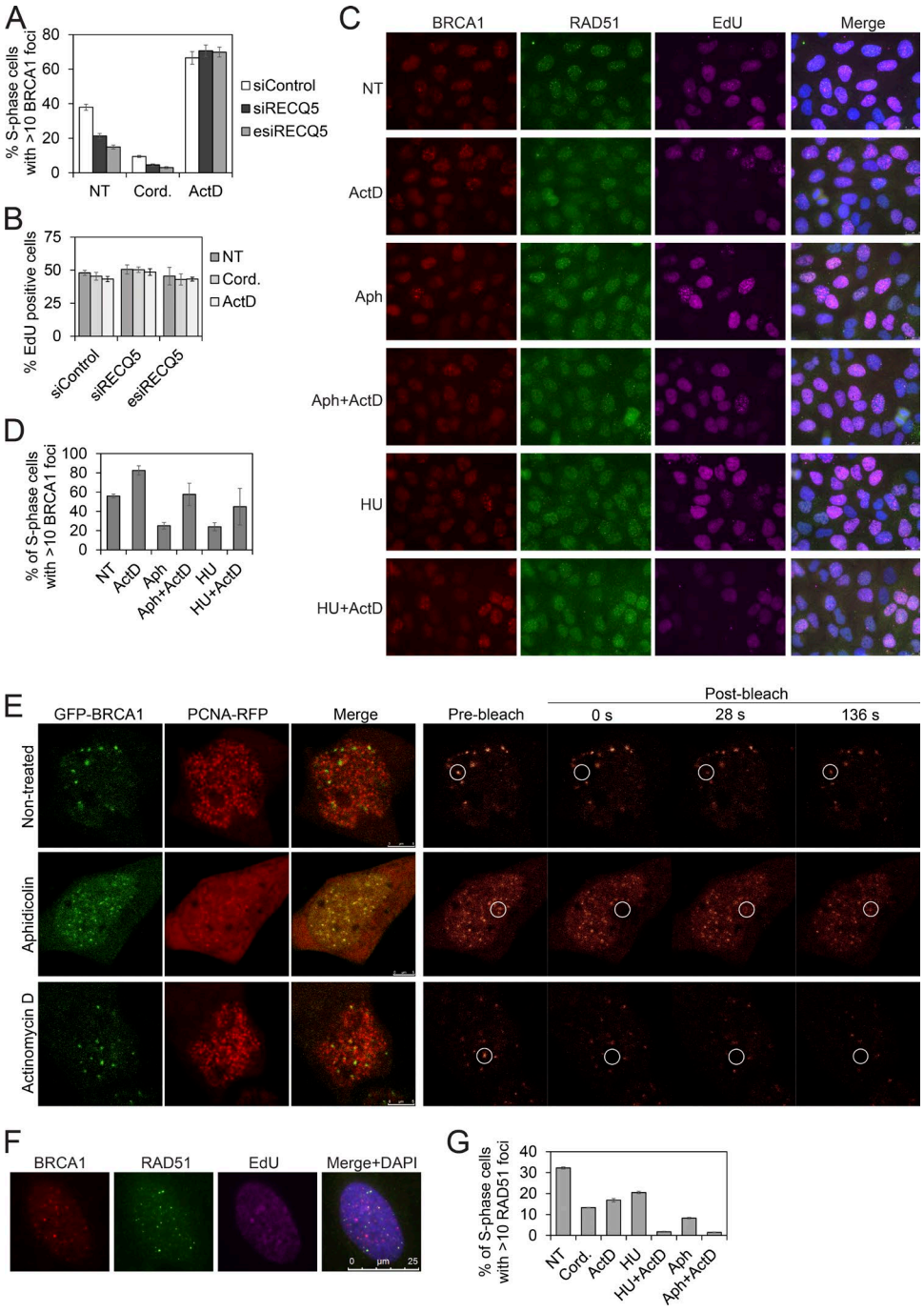

Figure S2. **BRCA1 and RAD51 form foci at sites of interference between replication and transcription.** (A) Quantitative analysis of BRCA1 foci in mock- and RECQ5-depleted U2OS cells represented in Fig. 5 A. Where indicated, cells were treated with cordycepin (Cord.; 50 µM) for 2 h or ActD (1 µg/ml) for 1 h before fixation. EdU-positive cells containing more than 10 BRCA1 foci were scored as positive. (B) Effect of ActD (1 µg/ml) and cordycepin (50 µM) on EdU incorporation in mock- and RECQ5-depleted cells. Percentage of EdU-positive cells is plotted. (C) Representative images of U2OS cells stained for BRCA1, RAD51, and EdU upon treatment with replication and/or transcription inhibitors as indicated. Aphidicolin (Aph; 5 µM) and hydroxyurea (HU; 2 mM) were added 90 min before fixation, whereas ActD (1 µg/ml) was added 1 h before fixation. EdU was added 1 h before addition of replication inhibitors. For ActD-treated cells, EdU was added 1 h before fixation. Nuclei were stained with DAPI. NT, nontreated. (D) Quantitative analysis of BRCA1 foci in EdU-positive nuclei represented in C. Cells containing more than 10 foci were scored as positive. (E) Representative images from a FRAP sequence showing fluorescence recovery of GFP-BRCA1 foci in mock-, Aph-, and ActD-treated HEK293 cells. Cells were transfected with GFP-BRCA1 and PCNA-RFP constructs, and measurements were performed 6–9 h after release of cells from NC block. (F) Partial colocalization of BRCA1 and RAD51 foci in EdU-positive U2OS cells. Nuclei were stained with DAPI. (G) Quantitative analysis of RAD51 foci in EdU-positive nuclei represented in C. Cells containing more than 10 foci were scored as positive. For A, B, D, and G, data are represented as mean ± SD.

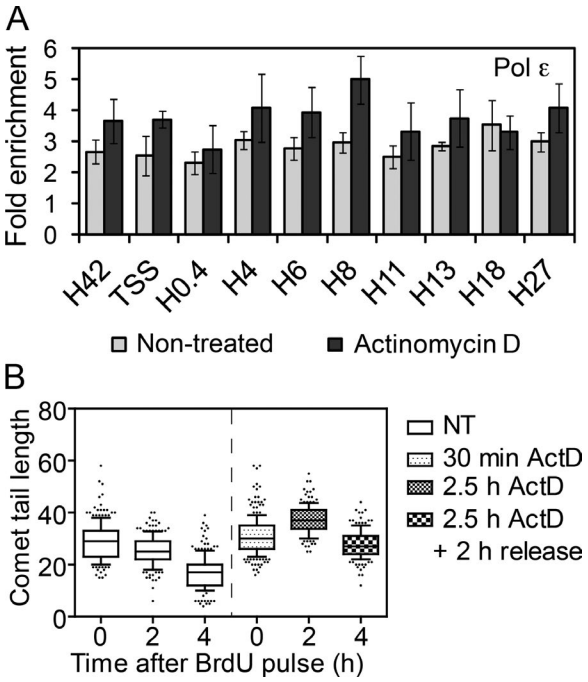

Figure S3. **Halted transcription complexes form a barrier for replication fork progression.** (A) Occupancy of Pol ε on rDNA repeat unit in nontreated and ActD-treated (1 µg/ml) cells. ChIP assay was performed on chromatin used in Fig. 1 B. Data are represented as mean ± SD. (B) Statistical analysis of BrdU-positive comet tail lengths measured for mock- or ActD-treated U2OS cells. ActD (1 µg/ml) was added 10 min before the BrdU pulse labeling (20 min) and readded after the BrdU wash-off. Whiskers indicate 10th to 90th percentile.

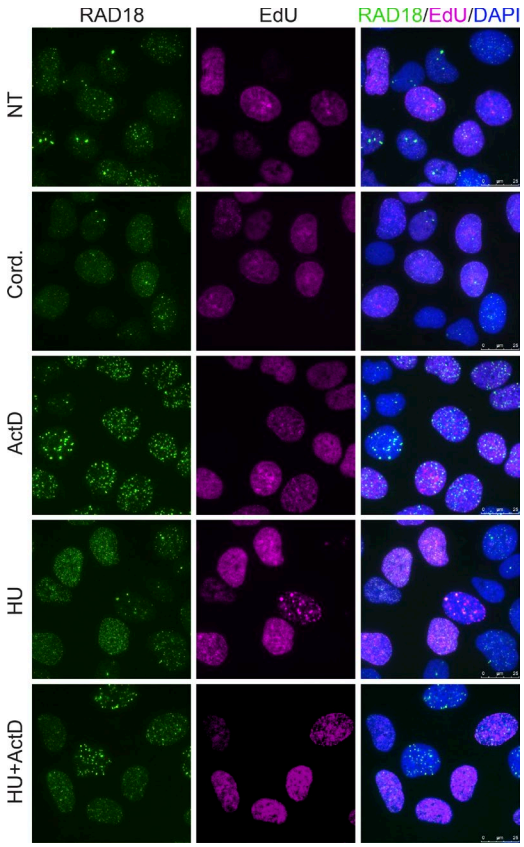

Figure S4. **RAD18 forms foci at sites of interference between replication and transcription.** Representative images of U2OS cells stained for RAD18 and EdU upon treatment with replication and/or transcription inhibitors as indicated. HU (2 mM) was added for 90 min, ActD (1 µg/ml) was added for 1 h, cordycepin (Cord.; 50 µM) was added for 2 h. EdU was added 1 h before addition of HU or fixation. Nuclei were stained with DAPI. NT, nontreated.

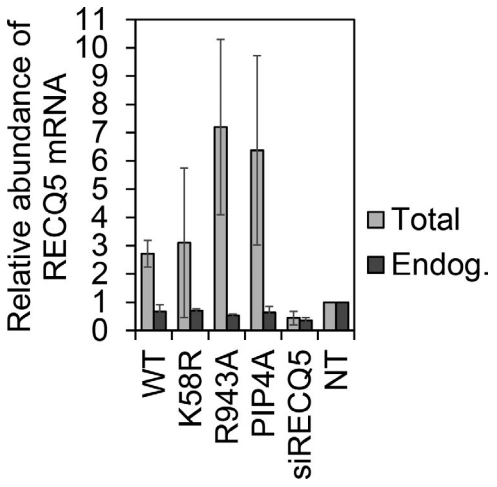

Figure S5. **Relative expression of Flag-tagged RECQ5 variants and endogenous RECQ5 in U2OS T-REx cells.** Relative mRNA abundance of endogenous or total RECQ5 (endogenous plus Flag-tagged wild-type RECQ5, RECQ5-K58R, RECQ5-R934A, or RECQ5-PIP4A) normalized to ALAS1 (5′-aminolevulinate synthase 1). Cells were cultured in the presence of doxycycline (0.4 ng/ml) for 48 h. Parental U2OS T-REx cells were transfected with siControl or siRECQ5. RNA was isolated using TRI reagent (Sigma-Aldrich). cDNA was prepared using the Superscript III reverse transcription (Invitrogen) with 1 µg total RNA in the reaction. cDNA was analyzed by qPCR using primers to distinguish endogenous RECQ5 (forward primer match to shRNA silent mutations in Flag-tagged variants) from total RECQ5 (Table S1). Data are represented as mean ± SD.

Table S1. **Sequences of primers used for quantitative real-time PCR**

Amplicon	Forward (5′ to 3′)	Reverse (5′ to 3′)
H42	AGAGGGGCTGCGTTTTCGGCC	CGAGACAGATCCGGCTGGCAG
TSS	CCCGGGGGAGGTATATCTTT	CCAACCTCTCCGACGACA
H0.4	CAGGCGTTCTCGTCTCCG	CACCACATCGATCGAAGAGC
H4	CGACGACCCATTCGAACGTCT	CTCTCCGGAATCGAACCCTGA
H6	CAGCTAGCTGCGAGAATTAATG	CGATTGATCGGCAAGCGAC
H8	AGTCGGGTTGCTTGGGAATGC	CCCTTACGGTACTTGTTGACT
H11	GGACCAGGGGAATCCGAC	CGCTTCATTGAATTTCTTCAC
H13	ACCTGGCGCTAAACCATTCGT	GGACAAACCCTTGTGTCGAGG
H18	GTTGACGTACAGGGTGGACTG	GGAAGTTGTCTTCACGCCTGA
H27	CCTTCCACGAGAGTGAGAAGCG	CTCGACCTCCCGAAATCGTACA
H33	ATCTCTTGACCTCGTGACCCG	TTGCGTTTCTCTGGACTGACTTC
Oct-4	GTATTCAGCCAAACGACCATC	CCCACCCTTACCTCCTGAAG
RSP19	GAGGCAGAGGTTGCAGTGAGTC	CTGGTAGAGAACAAGCTCCCAT
RPL22	GTGAACGGAAAAGCTGGGAAC	CTGGGCACTGGGTGCACGCA
ACTG1	GGTGACACAGCATCACTAAGGG	GACAGCACCGTGTTGGCGTA
ACTG1-I	GGTGACACAGTGAGACCCTATCT	GGCGTTCTTTACATATTGTGGAT
RECQL5, total	GTGAACAGCTGGCCATAGAGC	GGACCTTCTCCTCCATCCAGTC
RECQL5, endogenous	CCTTTACAGGAGAGTGCGACC	GGAGAGACTACAATGGTGATGC
ALAS1	CCACTGGAAGAGCTGTGTGATGTG	GCGATGTACCCTCCAACACAACC

11528–11545 *Nucleic Acids Research, 2014, Vol. 42, No. 18* *Published online 22 September 2014*
doi: 10.1093/nar/gku856

RecQ-core of BLM unfolds telomeric G-quadruplex in the absence of ATP

Jagat B. Budhathoki[1], Sujay Ray[1], Vaclav Urban[2], Pavel Janscak[2,3], Jaya G. Yodh[4,*] and Hamza Balci[1,*]

[1]Department of Physics, Kent State University, Kent, OH 44242, USA, [2]Institute of Molecular Genetics AS CR, Prague, Czech Republic, [3]Institute of Molecular Cancer Research, University of Zurich, Zurich, Switzerland and [4]Department of Physics and Center for the Physics of Living Cells, University of Illinois at Urbana-Champaign, Urbana, IL 61801, USA

Received January 27, 2014; Revised September 03, 2014; Accepted September 9, 2014

ABSTRACT

Various helicases and single-stranded DNA (ssDNA) binding proteins are known to destabilize G-quadruplex (GQ) structures, which otherwise result in genomic instability. Bulk biochemical studies have shown that Bloom helicase (BLM) unfolds both intermolecular and intramolecular GQ in the presence of ATP. Using single molecule FRET, we show that binding of RecQ-core of BLM (will be referred to as BLM) to ssDNA in the vicinity of an intramolecular GQ leads to destabilization and unfolding of the GQ in the absence of ATP. We show that the efficiency of BLM-mediated GQ unfolding correlates with the binding stability of BLM to ssDNA overhang, as modulated by the nucleotide state, ionic conditions, overhang length and overhang directionality. In particular, we observed enhanced GQ unfolding by BLM in the presence of non-hydrolysable ATP analogs, which has implications for the underlying mechanism. We also show that increasing GQ stability, via shorter loops or higher ionic strength, reduces BLM-mediated GQ unfolding. Finally, we show that while WRN has similar activity as BLM, RecQ and RECQ5 helicases do not unfold GQ in the absence of ATP at physiological ionic strength. In summary, our study points to a novel and potentially very common mechanism of GQ destabilization mediated by proteins binding to the vicinity of these structures.

INTRODUCTION

Human Bloom helicase (BLM) is a member of RecQ family (1,2), which includes *Escherichia coli* RecQ, *Saccharomyces cerevisiae* Sgs1p, *Schizosaccharomyces pombe* Rqh1 and human WRN, RECQL1, RECQL4 and RECQL5 helicases (3–7). RecQ helicases share a central domain that includes Walker A and B box which bind and hydrolyze adenosine triphosphate (ATP). Deficiencies in BLM cause Bloom syndrome, which is marked by genomic instability and increased predisposition to cancer, infertility and dwarfism (8,9). BLM is particularly important in suppressing reciprocal exchanges between sister chromatids. BLM has been shown to form a hexameric ring (10) and other multimeric structures (11). However, BLM mutants lacking the oligomerization domain can unwind dsDNA, in the 3′ to 5′ direction (12). BLM works as part of a larger multiprotein complex called the 'dissolvasome' or BTR complex (a complex of BLM, topoisomerase IIIα, RMI1 and RMI2) to remove non-canonical DNA structures as part of homologous recombination-dependent repair during DNA replication and telomere maintenance (13,14). Even though BLM is capable of forming multimeric structures, recent studies suggest that such structures dissociate upon ATP hydrolysis and it is the BLM monomer that unwinds dsDNA and resolves non-canonical DNA structures, such as Holliday junctions and D-loops (11).

G-quadruplex structures (GQs) are non-canonical DNA structures that form in guanine-rich regions of the genome. GQs are stabilized by Hoogsteen hydrogen bonding between guanosines, stacking of G-tetrad layers, coordination of Hoogsteen bonds by monovalent cations that intercalate between the tetrad layers and by hydration (15–18). Telomeric DNA is capable of folding into GQs in eukaryotes (19–21) and GQs are considered to take part in maintenance and elongation of telomeres (22,23). In addition, potentially intramolecular GQ forming sequences (PQS) have been computationally identified in several hundred thousand sites in the human genome (19,24–26). PQS are particularly concentrated in promoter sites (27–31), suggesting a potential role in transcription level gene expression regulation (32,33). Therefore, GQs have been targeted by specific drugs to modulate gene expression (34). Similarly, RNA GQs in

*To whom correspondence should be addressed. Tel: +1 330 672 2577; Fax: +1 330 672 2959; Email: hbalci@kent.edu
Correspondence may also be addressed to Jaya G. Yodh. Tel: +1 217 244 1155; Fax: +1 217 333 4778; Email: jyodh@illinois.edu

the 5′-UTR region (30) have been demonstrated to regulate translation level gene expression (35–38). GQs were recently shown to exist in human cells being modulated during the cell cycle (39), further highlighting the physiological relevance of studying the interactions between these structures and relevant proteins. GQs are typically thermally very stable and require protein activity to be unfolded (40–43). Genome-wide studies have shown that eliminating helicases that have GQ unfolding activity, such as *S. cerevisiae* Pif1 or human BLM, resulted in increased DNA breaks in PQS and severe retardation of DNA replication (41,44–48). It was recently shown that Pif1 suppresses genome instability at GQ motifs (48). In addition, in Sgs1 deficient cells, mRNA levels from regions of the genome rich in PQS were repressed at significantly higher levels relative to other regions, including G-rich regions unable to form GQ (49). These measurements suggested that Sgs1 targets GQ and destabilizes it, enabling transcription machinery to proceed. Similar results were obtained in BLM deficient human cells as well (47). In addition, BLM was proposed to have a genome-wide activity of resolving regions that are difficult to replicate, including telomeres, which could form GQs (13).

In vitro studies have demonstrated that both Sgs1 and BLM bind GQ with high affinity ($K_D \approx 5$ nM) and can efficiently unfold intermolecular GQs (50–53). Electron microscopy studies showed that BLM preferentially interacts with GQ located within a much longer dsDNA, which is a better representative of genomic DNA compared to isolated short GQ constructs (54). A consensus exists among various studies on the requirement of a 3′ overhang for successful unfolding of GQ by BLM (55). However, the majority of the previous studies probing BLM-GQ interactions were performed on intermolecular GQs. Interactions with intramolecular GQs, which are more likely to form in the PQS regions of the genome, were only recently studied using bulk fluorescence quenching and polarization methods (56). This study concluded that BLM unfolds intramolecular GQs with much lower efficiency compared to unwinding dsDNA, which is in contrast to the intermolecular GQ case. Other conclusions of this study were that BLM unfolding of intramolecular GQ requires ATP and is inversely proportional to the stability of the GQ structure.

In this study, we present findings that challenge the current understanding of the mechanism of BLM-mediated GQ unfolding, and helicase-GQ interactions in general. We used single molecule Förster Resonance Energy Transfer (smFRET) to measure unfolding of intramolecular GQ by RecQ-core of BLM in the nucleotide-free (nt-free), ATPγS and ADP states under physiological salt concentrations. This truncated BLM construct, lacking the oligomerization region, was used to study the activity of BLM monomers (12) and will simply be referred to as BLM in the rest of the manuscript. We used DNA constructs of human telomeric repeat that form a single intramolecular GQ and terminate with a 3′ overhang of 2–15 nt. We have found that BLM-mediated GQ unfolding activity is most efficient in the ATPγS-bound state (will be referred to as ATPγS state), followed by the nt-free state and then the ADP-bound state (will be referred to as ADP state). This order correlates with the binding stability of BLM to the overhang ssDNA for these nucleotide states. In addition, we observed BLM-mediated GQ unfolding for overhang lengths as short as 6 nt, but not for shorter overhangs. Enhancing GQ stability by shortening the loops resulted in a decrease in BLM-mediated GQ unfolding, and reducing GQ stability by using lower ion concentration increased GQ unfolding. We observed significantly less BLM-mediated GQ unfolding with a 5′ overhang compared to a 3′ overhang. Finally, RecQ and RECQ5 showed much weaker GQ unfolding activity compared to BLM. In contrast, WRN had a similar GQ unfolding activity as BLM.

MATERIALS AND METHODS

DNA and proteins

The GQ forming DNA constructs used in our study, with one exception, contained the human telomeric sequence, $(GGGTTA)_3GGG$, as well as a 3′ overhang of 2–15 nt. For the exception, we used a sequence that forms a three layer GQ with 1 nt loops: $(GGGT)_3GGG$. The sequences of these constructs (purchased from and high pressure liquid chromatography purified by Integrated DNA Technologies, Coralville, IA, USA) are given in Table 1. The underlined segment of sequences in Table 1 folds into GQ upon addition of K^+ ions. In order to minimize the interaction of the GQ and BLM with the surface, partial duplex DNA (pdDNA) constructs with an 18 base pair long RNA/DNA heteroduplex stem and a flanking 3′ ssDNA were used. The flanking 3′-ssDNA contains the GQ forming segment and the overhang of 2, 4, 6, 8, 10, 12 or 15 nt (hGQxT or hGQ4nt in Table 1). With the exception of 4 nt overhang, which has a TTAG sequence, all other overhangs are polythymine. The pdDNA constructs were formed by annealing the GQ containing ssDNA with the RNA-Stem (Table 1), and are called pd-hGQxT with $x = 2$, 6, 8, 10, 12 or 15. The construct with 4 nt overhang is called pd-hGQ4nt. In pdDNA constructs, Cy5 and biotin are on the RNA-Stem and Cy3 is at the flanking 3′-end. The exception to this is pd-hGQ12T-5′, the construct with a free 5′ end, which has a Cy5 at the 5′-end and a Cy3 and biotin on the DNA-Stem. See Figure 1A for schematics of the constructs. In addition to these GQ forming constructs, three DNA constructs that did not form GQ or any other secondary structure, polyT15, polyT15–5′ and polyT35, were annealed with the RNA-Stem to form pd-polyT15, pd-polyT15–5′ and pd-polyT35, respectively. These constructs were used for measurements in which binding of BLM to the ssDNA in the absence of GQ were probed.

A truncated core BLM ($BLM^{642–1290}$) was purified and characterized as described (57). In addition, mutant form of core BLM, BLM^{K695M}, carrying a K695M substitution in helicase motif I was generated using QuikChange Site-Directed Mutagenesis Kit (Stratagene), and purified using a similar protocol to core BLM. Core BLM lacks the oligomerization domain, and therefore all experiments in this report are performed with monomeric BLM. BLM protein was stored in storage buffer that contains 50 mM Tris-HCl (pH = 7.5), 200 mM NaCl, 50% (v/v) glycerol and 1 mM dithiothreitol (DTT), and diluted in imaging solution, described in the smFRET Assay section below, to the desired concentration before being added to the microfluidic

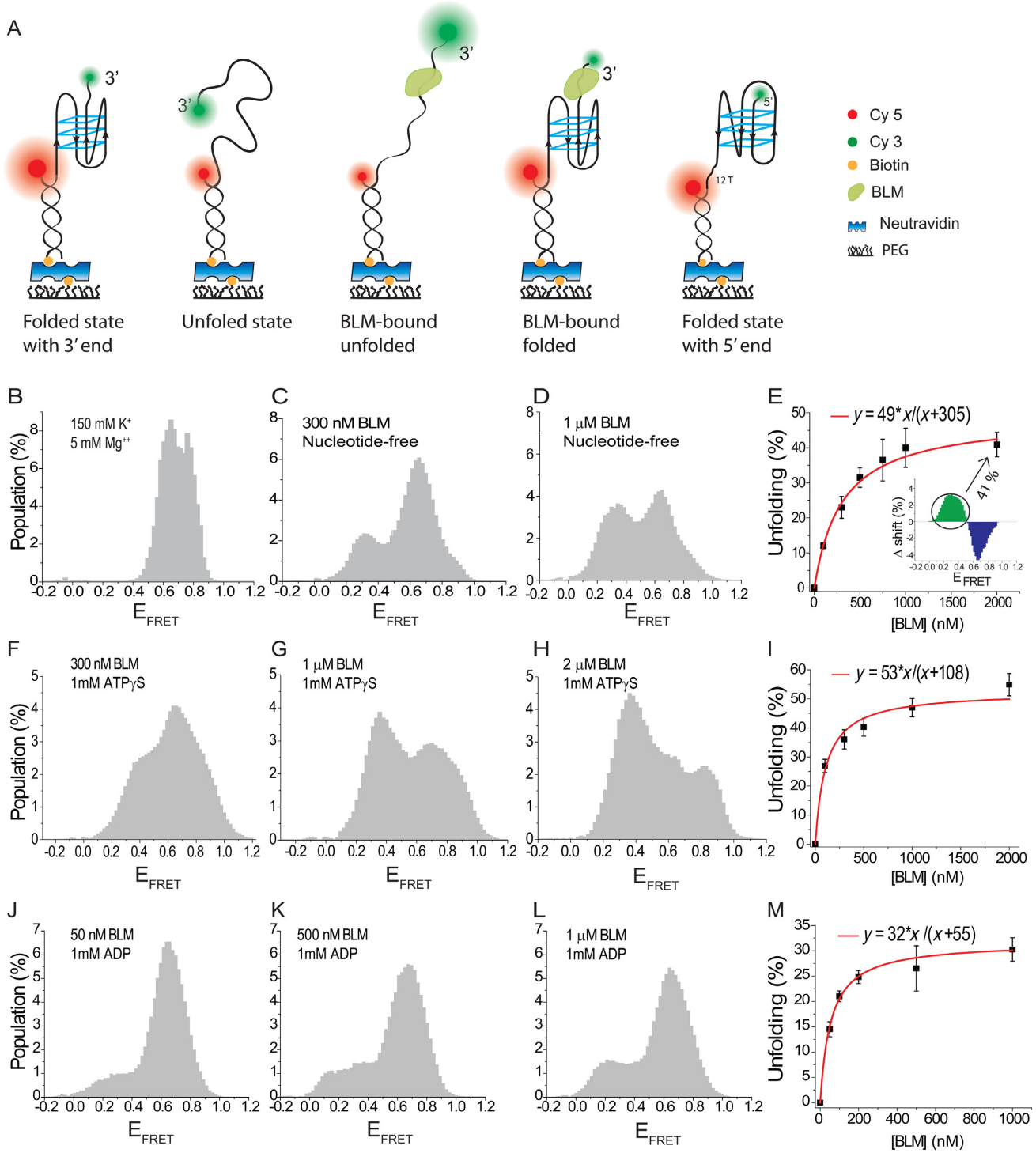

Figure 1. BLM-mediated unfolding for pd-hGQ12T (the GQ construct with 12 nt long 3′ overhang) in which BLM concentration is titrated in nt-free, 1 mM ATPγS, or 1 mM ADP states. All measurements were performed at 150 mM K^+. (A) Cartoons depicting different DNA and BLM-DNA complex conformations that are referred to in the manuscript. The size of circles representing the donor (green) and acceptor (red) fluorophores are drawn to reflect their relative brightness in the relevant conformation. The folded GQ state has the highest E_{FRET} and the BLM-bound unfolded state has the lowest E_{FRET}. (B)–(E) BLM titration in the nt-free state. (B) The folded GQ state before BLM is introduced. (C) Adding 300 nM BLM results in emergence of a low FRET peak. (D) Adding 1 μM BLM further increases the low FRET peak population. (E) BLM-mediated GQ unfolding is quantified by subtracting the FRET distribution of folded GQ, shown in (B), from the FRET distribution at various BLM concentrations. The inset shows a representative histogram that results from this subtraction. The cumulative positive area is plotted as a function of BLM concentration. The redline is a Langmuir isotherm fit to the data. (F)–(I) BLM-mediated GQ unfolding at 1 mM ATPγS for different BLM concentrations. (F) 300 nM BLM; (G) 1 μM BLM; (H) 2 μM BLM. (I) Similar analysis as in (D) is performed for the ATPγS data. The redline is a Langmuir isotherm fit to the data. (J)–(M) BLM-mediated GQ unfolding at 1 mM ADP for different BLM concentrations. (J) 100 nM BLM; (K) 500 nM BLM; (L) 1 μM BLM. (M) A summary of the data at 1 mM ADP and a Langmuir binding isotherm fit to these data.

Table 1. The DNA constructs used in these studies

Name	Sequence
hGQxT	5′- TGG CGA CGG CAG CGA GGC TAG GGT TAG GGT TAG GGT TAG GG (xT) Cy3 $x = 2, 6, 8, 10, 12,$ or 15
hGQ4nt	5′- TGG CGA CGG CAG CGA GGC TAG GGT TAG GGT TAG GGT TAG GG TTAG Cy3
3Ly1Lp12T	5′- TGG CGA CGG CAG CGA GGC TTG GGT GGG TGG GTG GG(12T) Cy3
hGQ12T-5′	5′-Cy5-(12T) GGG TTA GGG TTA GGG TTA GGG TT TGG CGA CGG CAG CGA GGC
12ThGQ-5′	5′-Cy3-TT GGG TTA GGG TTA GGG TTA GGG(12T) TGG CGA CGG CAG CGA GGC
polyT15	5′- TGG CGA CGG CAG CGA GGC (15T) Cy3
polyT15–5′	5′-Cy5-(15T) TGG CGA CGG CAG CGA GGC
polyT35	5′-TGG CGA CGG CAG CGA GGC (35T) Cy3
RNA-Stem	5′- Cy5 GCC UCG CUG CCG UCG CCA Biotin
DNA-Stem	5′- Biotin GCC TCG CTG CCG TCG CCA Cy3

The constructs whose names are in bold letters are hybridized with the RNA-Stem to form a pdDNA. polyT15–5′ and DNA-Stem are hybridized to form pd-polyT15–5′. The underlined nucleotides form the GQ structure. The number of consecutive thymines are written in parenthesis, e.g. (12T) means 12 consecutive thymines.

channel. Purification of *E. coli* RecQ (58), human full length RECQ5 (59) and full length WRN (60) helicases was performed according to protocols in the cited references.

Sample preparation

To create the sample chamber, double-sided tape was sandwiched between a quartz slide and a glass cover slip. The quartz slide was first drilled, cleaned and coated with polyethylene-glycol (PEG) and biotin-PEG in the ratio of ∼100:1 (m-PEG-5000:biotin-PEG-5000 from Laysan Bio Inc.). Nucleic acid immobilization on the surface was achieved via a neutravidin-biotin linker. DNA and RNA-stems were hybridized by annealing them at 95°C for 5 min., followed by cooling to room temperature over 2–3 h. A stock concentration of 1 μM was prepared for this annealing step, which was diluted to 15 pM in multiple steps before injection into chamber. After 1–2 min of incubation, the chamber was washed to remove excess DNA. A density of roughly 250 molecules/imaging area ($\sim 5 \times 10^3$ μm^2) is obtained as a result of this protocol. Note that all experiments were carried out with samples that had undergone annealing the same day.

smFRET assay

A prism-type total internal reflection microscope built around an Olympus IX-71 microscope was used for all the measurements. Data were acquired at 40 ms time resolution using Andor Ixon EMCCD camera (iXon DV 887-BI EMCCD, Andor Technology, CT, USA). The imaging solution used in all measurements contained Tris base (50 mM, pH 7.5), 2 mM trolox, 0.8 mg/ml glucose, 0.1 mg/ml bovine serum albumin, 1 mM DTT, 0.1 mg/ml glucose oxidase, 0.02 mg/ml catalase, 5 mM $MgCl_2$ and 150 or 50 mM KCl. The few cases in which NaCl was used instead of KCl, to reduce the stability of GQ structure, are explicitly stated. As the cation concentration (K^+) is significant for GQ stability, we henceforth refer to KCl as K^+. In all assays performed in this study, the Mg^{++} was kept at 5 mM, regardless of monovalent cation type or concentration. Therefore, only the cation concentration will be mentioned where relevant, but it should be assumed that 5 mM Mg^{++} is also present in all assays. BLM as well as ATP, ADP and ATPγS were mixed in imaging solution at the desired concentration. The imaging solution was incubated with the DNA sample for 15 min to allow the system to reach steady state. Longer incubation times up to 1 h did not have a significant effect on the smFRET distributions. Long (1000–4000 frames) and short movies (30 frames) were recorded for two different types of analysis.

Data analysis and quantification of BLM-mediated GQ unfolding

Long movies were analyzed using custom software to generate intensity and FRET efficiency (E_{FRET}) time traces for each molecule. Such traces were filtered to ensure that only single molecules were selected and the background was subtracted from each of these selected molecules using a custom Matlab code. These traces were used to build population histograms of E_{FRET}. Folded GQ constructs show high $E_{FRET} \approx 0.60$–0.80, whereas unfolded and protein-bound unfolded constructs show significantly lower E_{FRET}, which depend on the construct used but is typically <0.40. The histograms were normalized to a percentage scale such that the total number of molecules in the histogram represents 100%. This normalization is necessary for the subtraction analysis which is employed to quantify the effect of BLM or nucleotides (effectors) on the E_{FRET} distribution. In this analysis, a normalized reference histogram, i.e. the histogram representing the state that does not contain the titrated effector, is subtracted from normalized histograms representing various effector concentrations. The relevant reference histogram used for each subtraction analysis is specifically mentioned in the related section describing the data. In general, if BLM is titrated (at a constant nucleotide concentration), the histogram at zero BLM concentration is used as the reference. On the other hand, if a nucleotide is titrated (at constant BLM concentration) then the histogram at zero nucleotide concentration (in the presence of relevant BLM concentration) is used as the reference. For example, for BLM titration experiments in Figure 1B–E, the reference histogram is the folded GQ histogram (at 150 mM K^+) before BLM is introduced to the chamber (Figure 1B). This reference is subtracted from the normalized histograms of BLM-titrations (Figure 1C and D in this case). On the other hand, to quantify the influence of 20 μM

ATPγS on BLM-mediated GQ unfolding, the FRET distribution at 1 μM BLM and zero ATPγS concentration (Figure 1D) was subtracted from the distribution at 1 μM BLM and 20 μM ATPγS (Figure 2B). The subtraction results in a distribution with equal positive and negative populations since both the minuend and subtrahend histograms are normalized to 100% (see inset of Figure 1E). The negative population at the higher E_{FRET} represents the decrease in the folded GQ population, which results upon adding BLM in a particular nucleotide concentration to the chamber. The total positive population at the lower E_{FRET} region represents the unfolded and BLM-bound unfolded GQ population. This analysis method was preferred over fitting multiple Gaussian peaks to smFRET distributions and quantifying the population of each peak as a function of effector concentration. The main reason behind this choice was the difficulty in uniquely identifying the peaks that would best fit the relatively broad FRET distributions.

Finally, Langmuir binding isotherm fit, of the form $y = \alpha x/(x + K_{eq})$, is used to analyze the results obtained from these subtractions. The independent variable x is the effector concentration (either BLM or nucleotide concentration depending on the measurement), and the dependent variable y is the percent unfolded population with respect to a reference state. In this expression, K_{eq} is the equilibrium constant and α describes the maximum unfolded population under saturating effector concentration. The error bars associated with the data were obtained from standard deviations of multiple data sets obtained for a given condition. The error values for the parameters of the Langmuir binding isotherm fits were obtained as a result of a weighted fit, i.e. the uncertainties in the individual data points were taken into account while fitting the data. Subtraction analysis and fits to data were performed using Origin Pro 8.5.

Identification of the observed FRET levels

The coiled DNA is stabilized into a GQ structure by K^+ ions, resulting in a high E_{FRET}. Interaction of BLM with these folded GQ constructs results in various states with lower E_{FRET} (Figure 1A). The observed states from highest to lowest E_{FRET} are: folded GQ, BLM-bound folded GQ (i.e. BLM bound to the overhang with GQ remaining folded), unfolded GQ (or unfolded DNA which is essentially coiled DNA that is not bound by BLM) and BLM-bound unfolded DNA. E_{FRET} for the folded GQ is determined in the presence of 150 mM K^+, the physiological concentration, before BLM is added to the sample chamber. In a few cases either 50 mM K^+ or 50 mM Na^+ was used instead, and is explicitly stated. In the case of pd-hGQ12T, which is a pdDNA GQ construct with a 12 thymine long overhang formed by hybridizing hGQ12T and RNA-Stem of Table 1, the folded state shows a broad distribution that can be fit by two Gaussian functions with $E_{FRET} = 0.64 \pm 0.07$ and $E_{FRET} = 0.78 \pm 0.05$. In human telomeric constructs with shorter overhangs, these multiple peaks were interpreted as signatures of different folding conformations, which are also observed in circular dichroism (CD) and NMR studies (61). We sought to determine the FRET efficiencies of unfolded and BLM-bound unfolded states of pd-hGQ12T by using a pdDNA construct with a polythymine tail of similar length as a reference. This approach avoids the complications that might arise due to possible secondary structure formation of pd-hGQ12T. The ssDNA part of pd-hGQ12T (GQ forming segment which is 21 nt plus an additional 2 nt on the 5′ side and a 12 nt 3′-overhang) is 35 nt long which is the same length as that of pd-polyT35. Therefore, the two constructs would result in very similar FRET efficiencies in the unfolded (coiled) and BLM-bound unfolded states. This analysis results in $E_{FRET} = 0.40 \pm 0.06$ for the unfolded state, and $E_{FRET} = 0.20 \pm 0.08$ for the BLM-bound unfolded state (Supplementary Figure S1). The BLM-bound folded state would have an E_{FRET} between the folded and unfolded states, hence $E_{FRET} \approx 0.55$, which is distinctly observed in single molecule traces (data not shown) and is also visible in the steady-state histograms in Figures 1 and 2. E_{FRET} for the unfolded states should be similar for the two main constructs of this study, pd-hGQ12T and pd-hGQ15T, as they only differ in length by 3 nt. Correspondingly, E_{FRET} for their BLM-bound unfolded states should be similar. Therefore, the E_{FRET} levels measured for pd-polyT35 for unfolded and BLM-bound unfolded states should also be similar to those of pd-hGQ15T, respectively. pd-polyT12 and pd-polyT12–5′ differ only in terms of the directionality of their overhangs but otherwise have the same separation between their donor–acceptor pairs. Therefore, the E_{FRET} values for these constructs should be the same.

Electrophoretic mobility shift assay (EMSA)

BLM binding to pd-hGQ12T construct was measured by EMSA. Native polyacrylamide gel electrophoresis (PAGE) was used for this measurement. The partial duplex construct was formed by annealing the two strands via heating/slow cooling prior to the gel binding assay. Annealed substrates were mixed with varying BLM concentrations (0–500 nM) in 50 mM K^+, 5 mM Mg^{++}, 50 mM Tris-HCl (pH 7.5) and 1 mM DTT. Binding reactions were carried out for 10 min at 22°C and then mixtures were loaded onto a 4–20% polyacrylamide TBE gel and run in 0.5× TBE at 50V for 5 h at 4°C. Gel was imaged using a Molecular Dynamics Typhoon 9400 Multilaser Scanner.

RESULTS

ATP binding or hydrolysis is not required for BLM-mediated intramolecular GQ unfolding

We employed smFRET assay to measure intramolecular GQ unfolding activity of BLM in nucleotide-free (nt-free), ATPγS and ADP states under physiological salt concentrations (150 mM K^+). In this study we used a core BLM polypeptide, $BLM^{(642–1290)}$, that exists only as a monomer both in solution and in the DNA-bound state (57). Figure 1B shows the folded GQ state before BLM is introduced to the chamber for pd-hGQ12T (see Figure 1A for a schematic). The smFRET distribution representing the folded state did not change when 1 mM ATPγS or 1 mM ADP were added to the chamber in the absence of BLM (data not shown). Therefore, the folded state in Figure 1B is used as the reference state for the subtraction analysis for all nucleotide states presented in Figure 1. Figure 1C shows

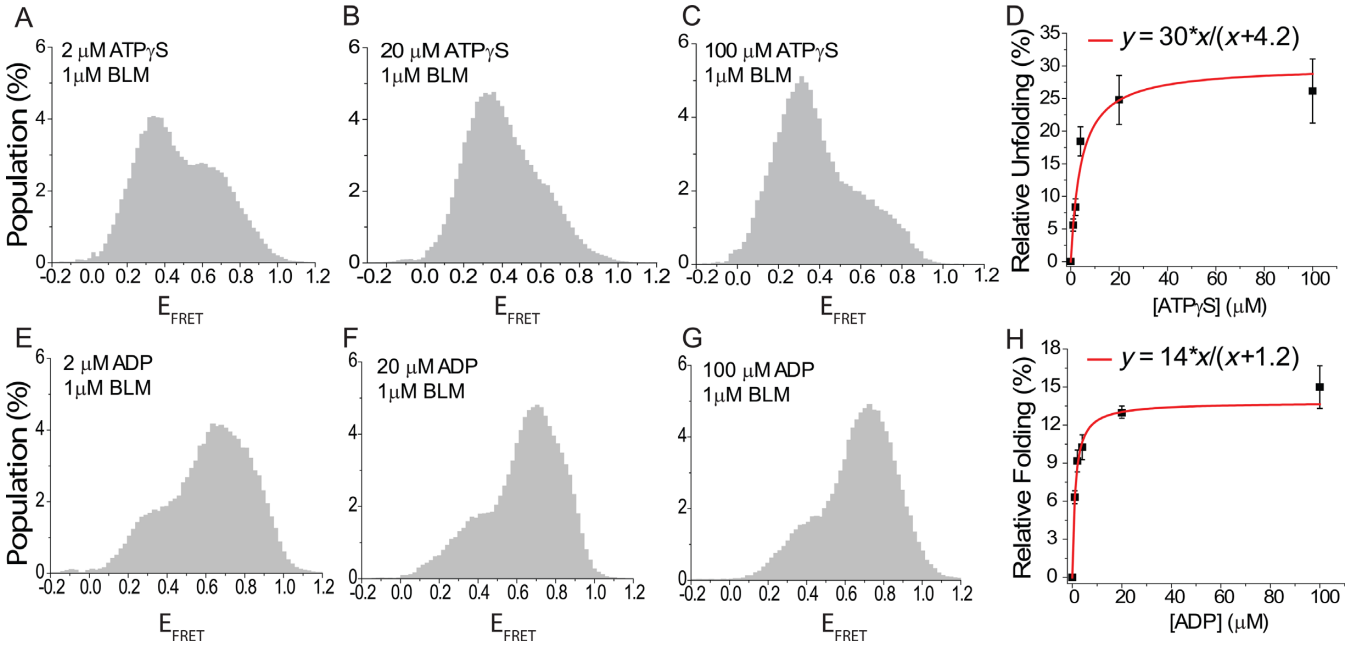

Figure 2. BLM-mediated unfolding for pd-hGQ12T in which ATPγS or ADP is titrated while BLM concentration is kept at 1 μM (150 mM K^+, pH 7.5). (A)–(D) ATPγS titration data. (A) 2 μM ATPγS; (B) 20 μM ATPγS; (C) 100 μM ATPγS. (D) Subtraction analysis as in Figure 1E. The histogram for 1 μM BLM data, before any ATPγS is introduced as shown in Figure 1D, is subtracted from the histograms for different ATPγS concentrations in the presence of 1 μM BLM. This choice ensures that the change in the unfolded population is due to the changing ATPγS concentration. As the reference state already shows some GQ unfolding, the *y*-axis of the graph represents relative unfolding with respect to this reference state. The redline is a Langmuir binding isotherm fit to the data. (E)–(H) ADP titration data. The low E_{FRET} peak decreases and the high E_{FRET} peak increases as the ADP concentration is increased, representing an increase in the folded GQ population. (E) 2 μM ADP. (F) 20 μM ADP. (G) 100 μM ADP. (H) Subtraction analysis in which the reference histogram is that for 1 μM BLM in the absence of ADP (nt-free state with 1 μM BLM shown in Figure 1D). Unlike the previous cases, the folded population increases as ADP concentration is increased, which shows that BLM is less efficient at unfolding GQ in the ADP state compared to the nt-free state. The relative folded population is thus plotted in (H) to maintain a positive population.

the smFRET distribution when 300 nM BLM is added to the chamber in the nt-free state. A low FRET population, at $E_{FRET} \approx 0.30$, representing BLM-mediated GQ unfolding accumulates as the BLM concentration is increased to 1 μM BLM (Figure 1D). As this FRET level is in between unfolded ($E_{FRET} = 0.40 \pm 0.06$) and BLM-bound unfolded ($E_{FRET} = 0.20 \pm 0.08$) states identified in Supplementary Figure S1, an equilibrium of both states is represented by the peak at $E_{FRET} = 0.30$. Figure 1E shows a summary of the subtraction analysis performed for different BLM concentrations. The reference data for the subtraction analysis were the folded state in Figure 1B. Langmuir binding isotherm fit (red curve in Figure 1E) to the data yields an equilibrium constant of $K_{eq} = 305 \pm 16$ nM and $\alpha = 49 \pm 1\%$, (i.e. at saturating BLM concentration 49% of all initially folded GQ molecules are unfolded). We have further confirmed BLM-mediated GQ unfolding in the absence of ATP with a CD assay. In this assay, we measured the CD spectrum of DNA before and after adding 1 μM BLM to the environment. The characteristic peaks indicating GQ formation are diminished after adding BLM to the environment, indicating destabilization of GQ (Supplementary Figure S2A). Finally, smFRET measurements were performed on a DNA construct in which donor–acceptor fluorophores are moved directly to the ends of the GQ. This construct eliminates any significant FRET changes that might take place due to binding of BLM to the overhang, and results in lower FRET efficiency only when GQ is unfolded. The schematic of this construct and the smFRET data are shown in Supplementary Figure S2B. Even though this construct resulted in a reduction in the amount of unfolding in 150 mM K^+, probably due to the internal fluorophore interfering with BLM-GQ interactions, a significant low FRET population, representing unfolded GQ was observed in 50 mM and 10 mM K^+ (Supplementary Figure S2C and D). As is clear from these different measurements, BLM does not need ATP or any other nucleotide to unfold an intramolecular GQ at physiological pH and ionic strength. This is a novel observation as earlier studies performed on intermolecular GQs (50,52), as well as a previous bulk study on an intramolecular GQ (56), reported BLM-mediated unfolding only in the presence of ATP.

Figure 1F–I show BLM titration experiments in the presence of 1 mM ATPγS. The folded GQ state before BLM is introduced is not shown as it is identical to that in Figure 1B. Similar to the nt-free state, a low FRET population emerges and increases as BLM concentration is increased. However, this low FRET population is clearly greater for any given BLM concentration in the ATPγS state compared to the nt-free state. This is also reflected in the Langmuir binding isotherm fit in Figure 1I which yields an equilibrium constant of $K_{eq} = 108 \pm 24$ nM, 3-fold lower than that of the nt-free state, and $\alpha = 53 \pm 3\%$, which is same as that of the nt-free state within the uncertainties of the measurements. The effect of ATPγS on GQ-unfolding by BLM is substrate-specific as we have previously shown that BLM

could not unwind traditional forked DNA substrates in the presence of ATPγS (12). This result was confirmed under our assay conditions as well.

Figure 1J–M show BLM titration measurements in the presence of 1 mM ADP. BLM-mediated GQ unfolding is less efficient in the ADP state compared to the nt-free and ATPγS states. Langmuir binding isotherm fit in Figure 1M results in $K_{eq} = 55 \pm 5$ nM and $\alpha = 32 \pm 1\%$. The lower α parameter suggests that in steady state, a lower fraction of the GQ molecules are unfolded by BLM in saturating ADP concentration compared to the nt-free and ATPγS states. Fitting parameters obtained from all Langmuir isotherm fits performed in the manuscript are summarized in Table 2. The smFRET histograms and the subtraction analysis for BLM concentrations that are not shown in the manuscript are presented in Supplementary Figures S3 and S4.

We performed several control and complementary measurements to study BLM-mediated GQ unfolding in the absence of ATP and eliminate alternative explanations. We provided an independent determination of BLM binding to GQ-forming construct using a native PAGE EMSA with pd-hGQ12T substrate. A single shifted band was observed as BLM was titrated, although the GQ folding state upon BLM binding is not discernible in this assay (Supplementary Figure S5). No GQ unfolding was observed upon addition of storage buffer without BLM or in the presence of heat-denatured BLM, confirming that activity required native BLM and was not due to GQ-destabilizing elements, such as metal chelators in the buffer (Supplementary Figure S6). We ruled out the possibility of ATP contamination in purified BLM by testing whether BLM could unwind a forked DNA substrate (12) in the absence of any additional ATP. No unwinding of this substrate was observed in the nt-free or ATPγS states but activity was measured only upon addition of ATP (Supplementary Figure S7). We eliminated the possibility that the GQ unfolding activity we observe may be due to another protein co-purifying with BLM that possesses GQ unfolding activity in the absence of ATP (e.g. a ssDNA binding protein), as sodium dodecyl sulphate-PAGE analysis of our purified BLM displayed a single band that corresponds to the expected molecular weight of BLM (Supplementary Figure S8).

Finally, to ensure BLM-mediated GQ unfolding does not require ATPase and helicase activity, we performed measurements with a mutant BLM construct that cannot hydrolyze ATP, BLM^{K695M}. This construct is the core BLM with a lysine to methionine substitution at amino acid 695, and is similar to BLM^{K695A} and BLM^{K695T} mutants studied earlier (54,62). The absence of helicase activity of BLM^{K695M} was confirmed by the absence of DNA unwinding activity with the forked DNA construct (see Supplementary Figure S7A for a schematic of the construct) at saturating BLM^{K695M} (500 nM) and ATP concentration (1 mM). Despite the lack of helicase activity, BLM^{K695M} showed significant GQ unfolding activity in the absence of ATP (Supplementary Figures S9 and S10). These measurements confirm that BLM does not require ATP hydrolysis to unfold GQ.

BLM-mediated GQ unfolding is most efficient in ATPγS state and least efficient in ADP state

Figure 2 shows data from smFRET studies on pd-hGQ12T in which the BLM concentration is kept at 1 μM while ATPγS (Figure 2A–D) or ADP (Figure 2E–H) is titrated. In Figure 2A–D, it is clear that increasing the ATPγS concentration increases the low FRET population, suggesting that BLM-mediated GQ unfolding is more efficient in the ATPγS state compared to the nt-free state. Figure 2D shows results of subtraction analysis in which the zero ATPγS, nt-free and 1 μM BLM state (Figure 1D) is used as the reference state. The Langmuir binding isotherm fit in Figure 2D results in $K_{eq} = 4.2 \pm 1.1$ μM (for ATPγS) and $\alpha = 30 \pm 4\%$. The relatively low K_{eq} obtained suggests that the system reaches saturation at very low ATPγS concentration. The α parameter of this fit is a measure of the difference in the efficiency of BLM-mediated GQ unfolding in the ATPγS state relative to the nt-free state (Figure 1D). In this case, 30% more unfolding is observed in the presence of ATPγS relative to its absence at 1 μM BLM. These results are also consistent with the data presented in Figure 1. The unfolded population for 1 μM BLM in the nt-free state is $40 \pm 6\%$ (Figure 1E), while the corresponding value for 1 μM BLM in ATPγS state is $47 \pm 3\%$ (Figure 1I). Taking the mean values in these measurements, i.e. 40% and 47%, would result in an 18% increase in the ATPγS state with respect to the nt-free state. Similar measurements were performed with another non-hydrolysable ATP analog, AMP-PNP. In agreement with the ATPγS results, BLM-mediated GQ unfolding was more efficient in the AMP-PNP state compared to the nt-free state. An analysis similar to that shown in Figure 2D resulted in $\alpha = 18 \pm 1\%$ and $K_{eq} = 2.1 \pm 0.3$ μM for AMP-PNP titration in 1 μM BLM (Supplementary Figure S11).

Figure 2E–H show an interesting trend in BLM-mediated GQ unfolding as ADP is titrated in the presence of 1 μM BLM. Increasing ADP concentration increases the folded GQ conformation as opposed to the unfolded population, suggesting that BLM is less efficient in unfolding GQ in the ADP state compared to the nt-free state. In order to quantify this, the increase in the folded population is obtained from a subtraction analysis using the nt-free state as the reference, e.g. zero ADP and 1 μM BLM concentration (Figure 1D). A Langmuir isotherm fit to the data results in $K_{eq} = 1.2 \pm 0.1$ μM (for ADP) and $\alpha = 14 \pm 1\%$. The low K_{eq} suggests that BLM-mediated GQ unfolding is very sensitive to ADP concentration and even a low micromolar concentration of ADP is adequate to reduce the unfolding activity by as much as 14%. Langmuir binding isotherm fit constants for Figure 2 are listed in Table 2. These results are also consistent with those obtained in Figure 1 within the uncertainties of the measurements. The data in Figure 1M show $30 \pm 3\%$ BLM-mediated GQ unfolding at 1 μM BLM in 1 mM ADP compared to $40 \pm 7\%$ at 1 μM BLM in nt-free state (Figure 1E). Comparing the mean values in these measurements, 30% and 40%, would result in a 25% reduction in BLM-mediated GQ unfolding in ADP state with respect to the nt-free state. The smFRET histograms and the subtraction analysis for ATPγS and ADP concentrations not

Table 2. A summary of Langmuir binding analysis performed for pd-hGQ12T

Summary of Langmuir Isotherm fits $y = \alpha x/(x + K_{eq})$						
State	K^+ Con.	Effector	Reference state	α (%)	K_{eq}	Figure
Nt-free	150 mM	BLM	Folded state	49 ± 1	305 ± 16 nM BLM	Figure 1E
1 mM ATPγS	150 mM	BLM	Folded state	53 ± 3	108 ± 24 nM BLM	Figure 1I
1 mM ADP	150 mM	BLM	Folded state	32 ± 1	55 ± 5 nM BLM	Figure 1M
1 μM BLM	150 mM	ATPγS	1 μM BLM, Nt-free	30 ± 4	4.2 ± 1.1 μM ATPγS	Figure 2D
1 μM BLM	150 mM	ADP	1 μM BLM, Nt-free	14 ± 1	1.2 ± 0.1 μM ADP	Figure 2H
1 μM BLM	150 mM	AMP-PNP	1 μM BLM, Nt-free	18 ± 1	2.1 ± 0.3 AMP-PNP	Figure S11

All assays include 5 mM Mg^{++} in addition to the indicated K^+ concentration. Folded state refers to the state in the presence of the indicated K^+ concentration but in the absence of BLM. In the titrations where ATPγS or ADP is the effector, the reference state is selected as the nt-free state in the presence of BLM (at the indicated concentration) to reflect the influence of nucleotide on BLM-mediated GQ unfolding. Note that isotherm fit parameters cannot be compared if the reference state is different. Also, note that the fit parameters for ADP titration at 1 μM BLM, last row of table, represent relative folding rather than unfolding.

shown in Figure 2, are shown in Supplementary Figures S12 and S13.

The BLM footprint on ssDNA has been reported as either 7 (63) or 14 nt (64). To ensure that our results obtained with the GQ substrate containing a 12 nt overhang are not compromised by an inefficient binding of BLM to this overhang, we measured BLM-mediated GQ unfolding in different nucleotide states on pd-hGQ15T at saturating BLM concentrations. pd-hGQ15T is a GQ construct with 15-nt long 3′ overhang which is formed by annealing hGQ15T and the RNA-Stem given in Table 1. These measurements yielded consistent results with those on pd-hGQ12T and showed that BLM-mediated GQ unfolding is most efficient in the ATPγS state, followed by the nt-free state and then the ADP state (Supplementary Figure S14).

BLM-GQ interactions with ATP

We also measured BLM-mediated GQ unfolding in the presence of ATP with pd-hGQ12T. The measurements were performed at 150 mM K^+ and pH 7.5. However, we observed that BLM not only unfolds the GQ but also unwinds the RNA-DNA heteroduplex stem at significant levels at saturating BLM and ATP concentrations (Supplementary Figure S9B). To avoid complications that would arise due to duplex unwinding, we repeated these measurements with a DNA construct in which the polarity of DNA was reversed, e.g. 5′ is the free end, and the overhang that enables BLM binding is placed between the duplex and GQ (Figure 3 and Table 1, pd-12ThGQ-5′ construct). With this construct, BLM translocates away from the duplex, therefore, unwinding of the duplex is avoided. These measurements clearly showed that BLM unfolds intramolecular GQ in an ATP-dependent manner, however, an interesting trend is observed in the steady-state histograms (Figure 3). In this figure, the unfolded GQ population is represented with the peak at $E_{FRET} \approx 0.25$, while the peak at $E_{FRET} \approx 0.50$ represents the BLM-bound folded GQ state. With increasing ATP concentration at 1 μM BLM, the unfolded GQ population systematically decreases, with maximum unfolding taking place in the absence of ATP, e.g. nucleotide-free state. This trend is similar to that observed for ADP with pd-hGQ12T, which suggests that more frequent dissociation of BLM from the DNA enables refolding of the GQ and therefore a decrease in the unfolded GQ population. However, the kinetics of BLM-GQ interactions is not captured in these steady-state histograms. It is possible that GQ repetitively unfolds and refolds at a rate that increases with ATP concentration, as recently reported for Pif1 helicase (65). The steady-state histograms do not detect these types of underlying dynamics which are crucial for attaining an accurate picture of BLM-GQ interactions in the presence of ATP. A comprehensive study of these dynamics is beyond the scope and focus of this manuscript.

BLM-mediated GQ unfolding correlates with stability of BLM binding to the ssDNA overhang

The data presented thus far show that BLM-mediated GQ unfolding is most efficient in the ATPγS state, followed by the nt-free and ADP states. Earlier bulk measurements have shown that the stability of BLM binding to ssDNA in different nucleotide states follows a similar order (63). This correlation suggests that BLM-mediated GQ unfolding strongly depends on the stability of BLM binding to the overhang ssDNA in the vicinity of GQ. In order to study binding of BLM to an overhang ssDNA in the absence of GQ, we performed smFRET measurements on pd-polyT15 which is formed by hybridizing polyT15 and the RNA-Stem (Table 1). pd-polyT15 has a 15-nt long flanking 3′-ssDNA which is same in length and sequence to the overhang of pd-hGQ15T. A scheme of the construct is given in the inset of Figure 4A. BLM binding to pd-polyT15 results in a lower E_{FRET} compared to the coiled state of DNA, and enables us to quantify BLM binding activity. For these measurements, all experimental conditions were kept identical to those used for the GQ constructs (150 mM K^+, pH 7.5). Figure 4A shows the smFRET histogram for the coiled state which shows a single peak at $E_{FRET} \approx 0.85$. Figure 4B–D show smFRET histograms when 1 μM BLM is added to the chamber in nt-free, 1 mM ATPγS and 1 mM ADP states, respectively. The new peak at $E_{FRET} \approx 0.60$ represents the DNA population that is bound by BLM. A subtraction analysis performed on these data with the coiled state in Figure 4A taken as the reference shows that 21%, 36% and 12% of DNA molecules are bound by BLM in the nt-free, ATPγS and ADP states, respectively. Thus, the efficiency of BLM binding to ssDNA in different nucleotide states and the efficiency of BLM-mediated GQ unfolding in these nucleotide states show the same trend. A quantitative

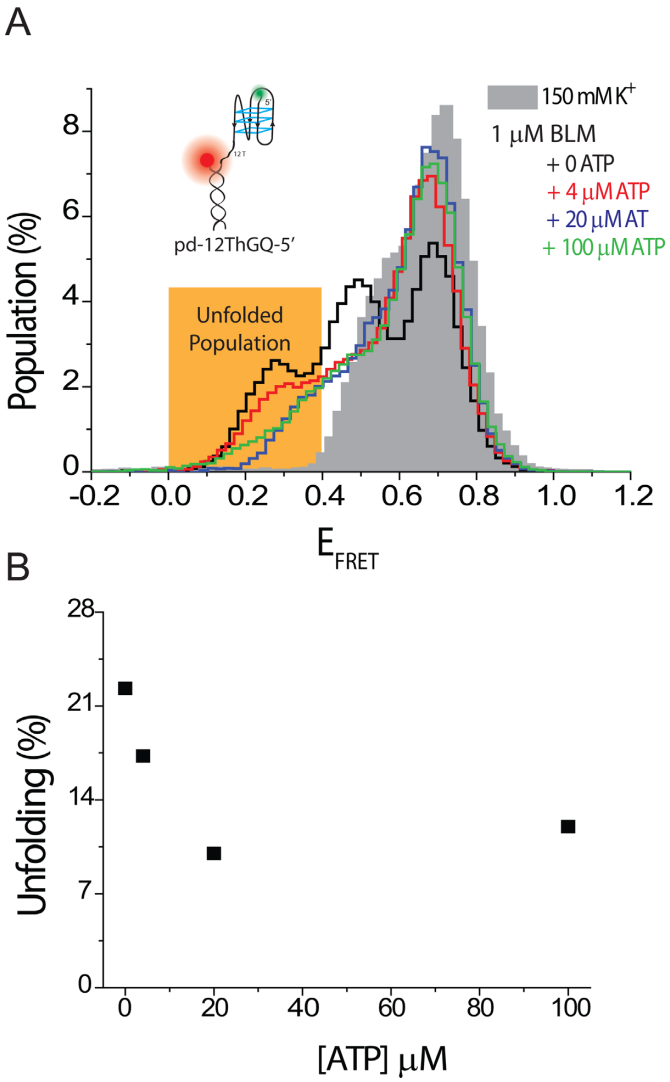

Figure 3. smFRET measurements on pd-12ThGQ-5′ construct at 150 mM K^+ and different ATP concentrations. The BLM concentration is maintained at 1 μM during ATP titration. (A) The gray shaded histogram shows the folded state, while the histogram with black, red, green and blue outlines represent 0, 4, 20 and 100 μM ATP, respectively. The unfolded GQ population is represented by $E_{FRET} \leq 0.40$, and is highlighted by the orange rectangle. The peak at $E_{FRET} \approx 0.50$ in black histogram represents the BLM-bound folded GQ state. The inset shows a schematic of the DNA construct used for these measurements. (B) The total unfolded population in these steady-state histograms, as obtained by integrating the area at $E_{FRET} \leq 0.40$, decreases as ATP concentration is increased. This decrease is attributed to more frequent dissociation of BLM from the DNA substrate.

comparison of BLM binding to pd-polyT15 and BLM unfolding of pd-hGQ15T in different nucleotide states shows significant variation: 21%, 36% and 12% for binding in nt-free, ATPγS and ADP states, respectively, for pd-polyT15, compared to 48%, 57% and 22% unfolding in the respective nucleotide-state for the GQ construct (Supplementary Figure S14). This difference suggests that once pd-hGQ15T unfolds, the unfolded conformation is maintained for extended time periods before it can refold.

BLM-mediated GQ unfolding increases with the overhang length

In order to systematically study the influence of the ssDNA overhang in GQ substrates on BLM-mediated GQ unfolding, we performed smFRET studies in which the overhang length was systematically varied. Increasing the overhang length is expected to result in higher BLM-binding stability and in turn, higher BLM-mediated GQ unfolding. Figure 5 shows results for 2, 4, 6, 8, 10, 12 and 15 nt long overhangs in nt-free and 1 mM ATPγS states. pd-hGQxT with $x = 2$, 6, 8, 10, 12 or 15 and pd-hGQ4nt DNA constructs were used for these studies (see Table 1 for sequences). The BLM concentration was kept at 1 μM and the ion concentration was 150 mM K^+ for all experiments. The bars shown in Figure 5 were obtained from subtraction analysis in which the folded state, in the absence of BLM or ATPγS, was taken as the reference. We observed a systematic increase in the unfolding activity as the overhang length increased between 6 and 15 nt. We did not observe any unfolding for 2 and 4 nt long overhangs, suggesting that a minimum overhang length of 5–6 nt is required for BLM-mediated GQ unfolding. This result is similar to that obtained for intermolecular GQs which required a 4 nt overhang for BLM-mediated GQ unfolding (52). For the constructs that showed BLM-mediated GQ unfolding, the ATPγS state consistently showed 10–60% higher activity compared to the nt-free state.

BLM-mediated GQ unfolding depends on the stability of GQ

All our work on BLM-GQ interactions reported so far was performed at 150 mM K^+ in order to mimic the physiological conditions. The K^+ concentration is an important determinant of the GQ stability and folding conformation (15), both of which could significantly influence the interactions between BLM and GQ. In order to test whether BLM-mediated GQ unfolding depends on the stability of GQ, we performed smFRET measurements at 50 mM K^+, which would reduce GQ stability (66) and increase BLM binding stability to the overhang. BLM was titrated in the nt-free state and ATPγS was titrated in the presence of 300 nM BLM at 50 mM K^+ (see Supplementary Figures S15 and S16). BLM titration in the nt-free state resulted in $\alpha = 55 \pm 4\%$ and $K_{eq} = 28 \pm 9$ nM. Note that the K_{eq} at 50 mM K^+ is 10.8-fold lower than that at 150 mM K^+ (Figure 1E and Table 2). In order to quantify the increase in BLM binding affinity to ssDNA due to reduced ion concentration, we measured the equilibrium constant in 50 and 150 mM Na^+ in the nt-free state (Supplementary Figure S17). The protein stock used for these measurements was in Na^+, therefore, the measurements were performed in Na^+ rather than K^+. As BLM binding to ssDNA should not depend on the type of monovalent ion, this change is not expected to influence the results. We used a pdDNA with a 15-nt long 3′ ssDNA tail (pd-polyT15). These measurements showed ~4.7× increase in K_{eq} in 150 mM Na^+ compared to 50 mM Na^+. As we observed a 10.8× decrease in K_{eq} in 50 mM K^+, we conclude that the decrease in GQ stability contributes ~2.3-fold to the increase in the K_{eq} in 150 mM K^+. These results demonstrate that both BLM binding affinity and GQ stability are significant contributors to the change in the equilibrium constant for BLM-mediated GQ unfolding. Finally,

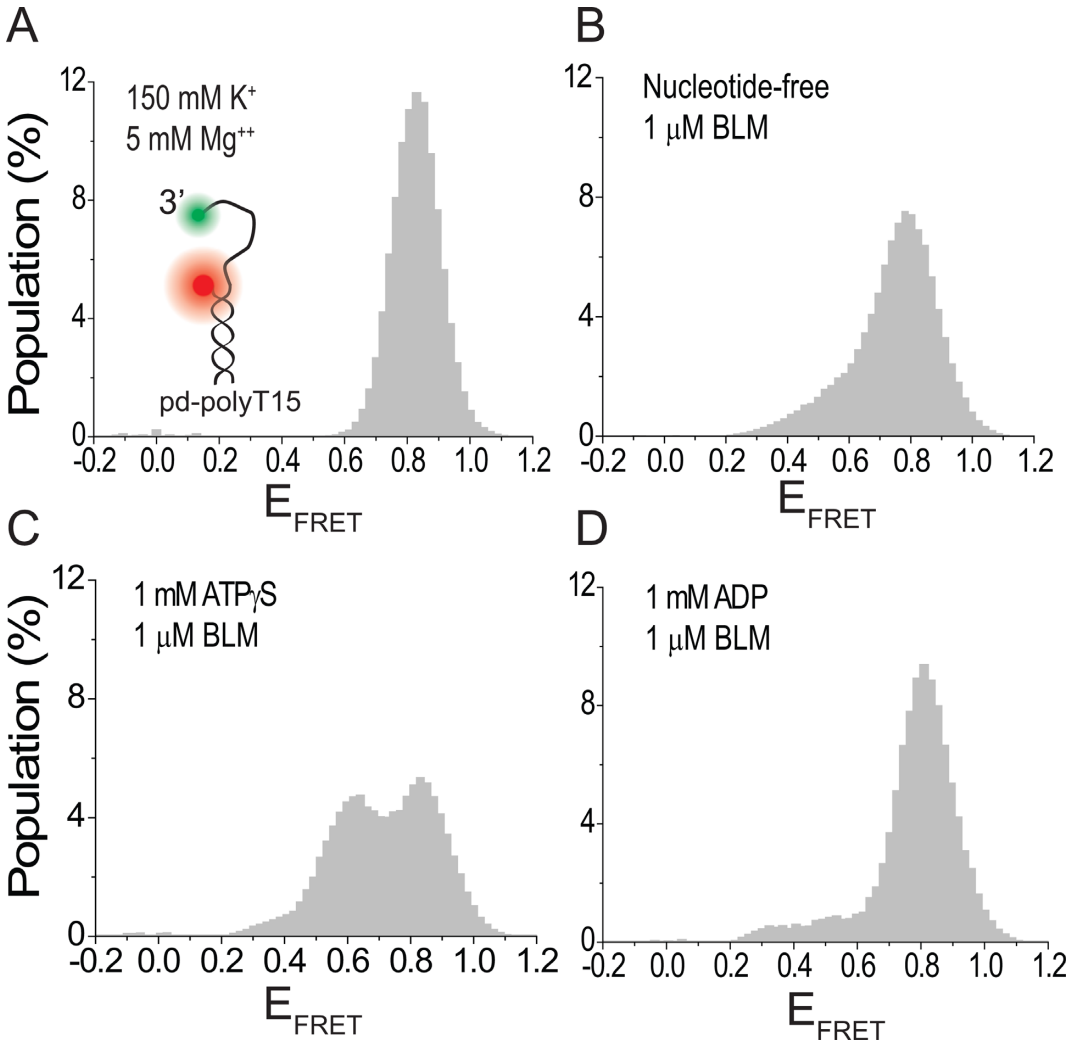

Figure 4. smFRET measurements on pd-polyT15 (pdDNA with 15 thymine long 3′ overhang) at 150 mM K^+. BLM binding to ssDNA representing the overhang in the GQ substrate depends on the nucleotide state. (A) pd-polyT15 is in coiled conformation with $E_{FRET} \approx 0.85$ before BLM is added. (B)–(D) BLM binding to the overhang in different nucleotide states at 1 μM BLM. (B) Nt-free state. (C) 1 mM ATPγS. (D) 1 mM ADP. Binding is most efficient in the ATPγS state, followed by the nt-free state and then the ADP state.

we measured BLM-mediated GQ unfolding as a function of ATPγS concentration in 300 nM BLM at 50 mM K^+. These measurements resulted in $\alpha = 23\%$ and $K_{eq} = 0.7 \pm 0.1$ μM, which is 6-fold lower compared to K_{eq} at 150 mM K^+ (Figure 2D).

Another method to modulate GQ stability is to change the length of the loops in the GQ structure. Shortening the loops is known to increase thermal stability of GQ (67) as well as increasing the stability of GQ against RPA-mediated unfolding (43). RPA is a ssDNA binding protein and does not require ATP for unfolding GQ, making it a similar system to BLM studies in the absence of ATP. In order to test BLM-mediated GQ unfolding on a GQ construct significantly more stable than the telomeric GQ structures used in this study, a three layer GQ with single nucleotide loops and an overhang of 12 thymines was used (will be referred to as pd-3Ly1Lp12T). To illustrate, this construct was shown to have two orders of magnitude higher stability against RPA-mediated unfolding compared to the human telomeric GQ with the same overhang (43). Our measurements with pd-3Ly1Lp12T at 150 mM K^+ did not show any unfolding at 1 μM BLM in either nt-free or 1 mM ATPγS states (Figure 6A), in agreement with the increased stability of this construct. However, our measurements at 50 mM K^+ showed BLM-mediated unfolding of pd-3Ly1Lp12T in both nt-free and ATPγS states. Figure 6B shows folding of pd-3Ly1Lp12T, and its BLM-mediated unfolding in the nt-free and ATPγS states at 50 mM K^+. At 1 μM BLM, we observed 46% unfolding in nt-free state, and 58% unfolding at 1 mM ATPγS, showing a similar ATPγS enhancement of BLM-mediated GQ unfolding as with the other constructs. This experiment shows that the nucleotide-independent BLM-mediated unfolding of the pd-hGQ12T intramolecular GQ at 150 mM K^+ is substrate specific. Such an activity cannot be achieved with more stable GQ, such as pd-3Ly1Lp12T, unless a significant reduction is made in the monovalent ionic strength.

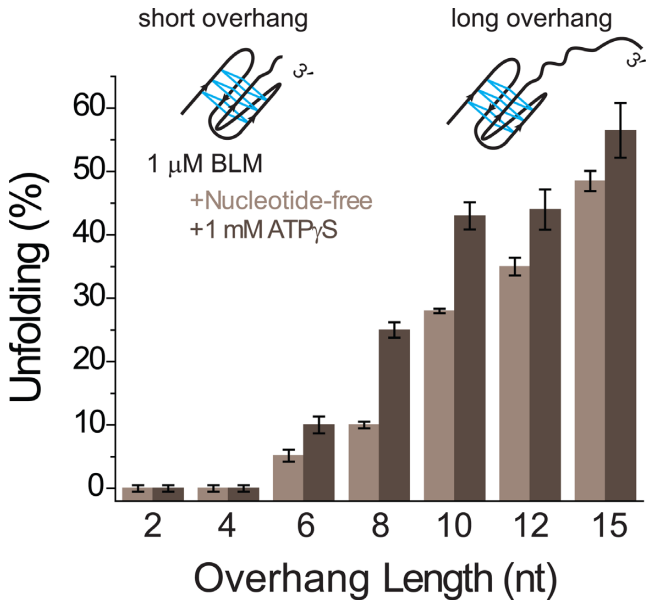

Figure 5. Bar diagrams illustrating the overhang length dependence of BLM-mediated GQ unfolding in the nt-free (light gray) and 1 mM ATPγS states (dark gray). All measurements were carried out at 150 mM K^+, and 1 μM BLM concentration. Overhangs of 2, 4, 6, 8, 10, 12 and 15 nt were studied. The unfolded populations were determined by subtracting the folded state at 150 mM K^+ for each construct from the respective nucleotide state with 1 μM BLM concentration. The error bars were obtained based on the variation in BLM-mediated GQ unfolding activity for different data sets.

Directionality of the overhang impacts BLM binding and its GQ unfolding activity

BLM translocates in the 3′ to 5′ direction and, therefore, binds to the overhang ssDNA in an orientation that accommodates this directionality. As BLM is able to unfold GQs in the absence of ATP, presumably without translocating on DNA, we sought to determine whether the polarity of the overhang is still significant for BLM-mediated GQ unfolding. For these studies, we used a construct identical to pd-hGQ12T with the exception of the overhang having a 5′-end rather than a 3′-end (will be referred to as pd-hGQ12T-5′). BLM-mediated GQ unfolding was not observed in this construct at 150 mM K^+ in either nt-free or ATPγS states even at 1 μM BLM concentration (Figure 7A). The low FRET population observed upon adding BLM to the chamber is not significantly different from the folded state at 150 mM K^+, hence, we do not consider this as BLM-mediated GQ unfolding. However, at 50 mM K^+, 21% and 30% unfolding were observed in nt-free and ATPγS states, respectively (Figure 7B), demonstrating that the ionic strength mediated effects on GQ stability and BLM binding to the 5′ overhang likely influence this outcome. To further explore these points, we studied BLM binding to a pdDNA with a 15-thymine ssDNA overhang that has a 5′ end (will be referred to as pd-polyT15–5′). pd-polyT15–5′ is formed by hybridizing polyT15–5′ and DNA-Stem strands given in Table 1. smFRET studies on pd-polyT15–5′ at 150 mM K^+ did not show any BLM binding in the nt-free state and showed very little binding in the ATPγS state (Supplementary Figure S18A) in contrast to the significant binding (36%) observed for the corresponding 3′ construct (pd-polyT15 construct in Figure 4) in the ATPγS state (Supplementary Figure S18A). Reducing the K^+ concentration to 50 mM resulted in significantly higher BLM binding to pd-polyT15–5′ in the ATPγS state (53%) even though the nt-free state still did not show significant BLM binding. Interestingly, BLM-mediated unfolding of pd-hGQ12T-5′ was observed in the nt-free state at 50 mM K^+ in the presence of 1 μM BLM (Figure 7B), even though significant BLM binding to pd-polyT15–5′ was not observed under these conditions (Supplementary Figure S18B). These two observations may be reconciled by more efficient BLM binding to the 35-nt long ssDNA that becomes available upon transient melting of the pd-hGQ12T-5′ GQ compared to the 15 nt in pd-polyT15–5′. Such transient melting events could either be induced by BLM or by thermal fluctuations. These observations are consistent with the lower GQ unfolding activity observed for 5′-end construct being influenced by the lower binding ability of BLM to this overhang.

GQ conformation dependence of BLM-mediated GQ unfolding

GQs often fold into multiple conformations in K^+. Changing the loop lengths, number of layers or the overhang sequences could result in changes in conformations (68) in addition to variations in the stability of the GQ. In particular, human telomeric sequence has been shown to fold into parallel, anti-parallel and various hybrid conformations in 150 mM K^+, while it folds into a single anti-parallel conformation in 150 mM Na^+ (61). In order to study a possible conformation dependence of BLM-mediated GQ unfolding while maintaining similar DNA binding affinities, we compared BLM-mediated GQ unfolding in 150 mM K^+ with that in 150 mM Na^+ for pd-hGQ12T. As shown in Figure 8A, pd-hGQ12T shows a single narrow smFRET peak in Na^+, which is indicative of a single conformation, unlike the broader peak in K^+, which is indicative of multiple conformations (shown with black and red dashed curves). Figure 8B and C show BLM-mediated unfolding at 300 and 1000 nM BLM, respectively, in 150 mM Na^+. Figure 8D shows a comparison of the unfolded GQ populations for 300 and 1000 nM BLM in 150 mM Na^+ and 150 mM K^+. Note that 22 ± 3% and 17 ± 2% GQ were unfolded by 300 nM BLM in 150 mM K^+ and 150 mM Na^+, respectively. Similarly, 41 ± 6% and 38 ± 2% GQ were unfolded by 1000 nM BLM in 150 mM K^+ and 150 mM Na^+, respectively. Therefore, BLM unfolds GQ at similar levels, within the uncertainties of the measurements, in Na^+ and K^+. These results suggest that BLM unfolds different conformations of GQ with similar efficiency.

Protein-mediated GQ unfolding for other RecQ family helicases

In order to determine whether BLM is an exceptional case in terms of a helicase destabilizing GQ in the absence of ATP, we sought to test whether such an activity is observed for closely related proteins from the RecQ family. *E. coli* RecQ, human RECQ5 and human WRN, all full-length constructs, were used for these studies. WRN has

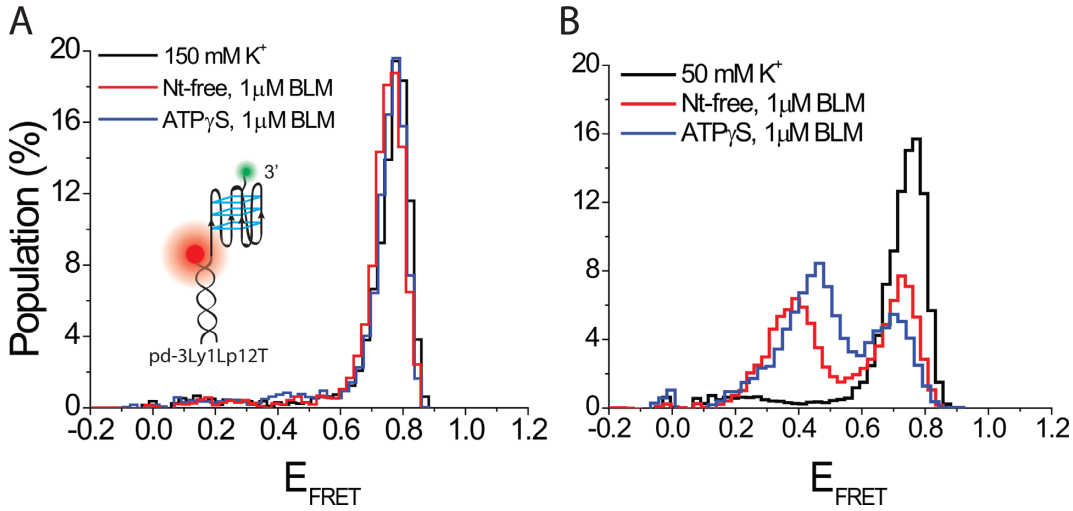

Figure 6. smFRET histograms showing BLM-mediated unfolding for pd-3Ly1Lp12T, three layer one loop GQ construct with 12 nt long 3′ overhang. (A) BLM cannot unfold this GQ at 150 mM K^+ in either nt-free or 1 mM ATPγS states. These results show that the ability of BLM to unfold intramolecular GQ in the absence of ATP under physiological ionic conditions is substrate specific. (B) Significant GQ unfolding is observed in both nt-free and ATPγS states when ion concentration is reduced to 50 mM K^+, in which GQ is less stable and BLM binding to the overhang is more efficient.

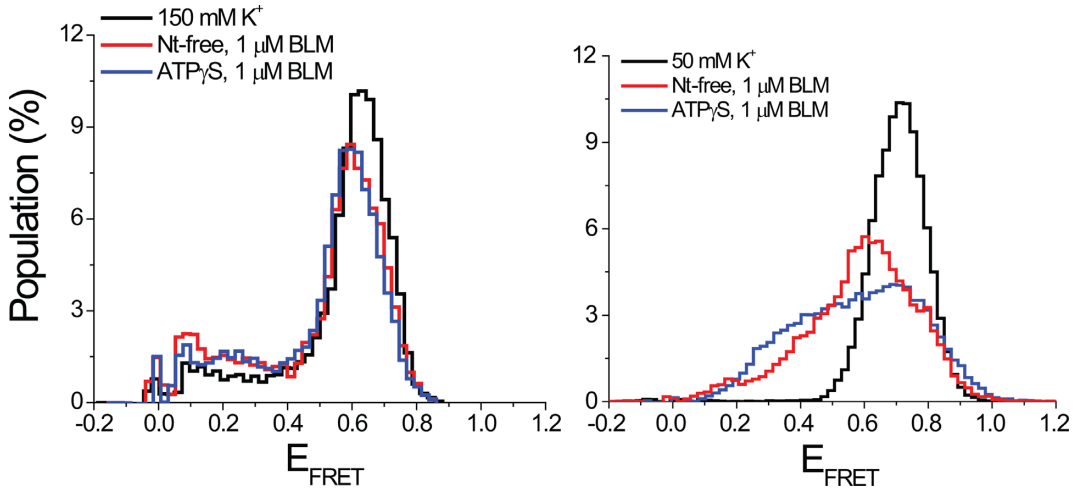

Figure 7. smFRET histograms showing BLM-mediated GQ unfolding of pd-hGQ12T-5′. This construct has a 12 thymine long 5′ overhang. (A) BLM cannot unfold this construct at 150 mM K^+ in either nt-free or ATPγS states, indicating orientation of binding on the overhang is important. (B) However, if the GQ stability is lowered at 50 mM K^+, significant BLM-mediated GQ unfolding occurs in both nt-free and ATPγS states.

been shown to unfold GQ in the presence of ATP (53). We are not aware of any studies on RecQ and RECQ5 in terms of their GQ unfolding activity. pd-hGQ12T construct was used for these studies. RecQ and WRN studies were performed at 300 and 25 nM concentrations, respectively, due to limitations in the protein stock concentrations. The RECQ5 measurements were performed at 1 μM concentration, similar to BLM. Due to these lower protein concentrations, we performed measurements under different ionic conditions that are more likely to demonstrate protein-mediated GQ unfolding. We also performed these measurements in nt-free and ATPγS states in order to check the consistency of BLM results, i.e. higher GQ unfolding in ATPγS state, with these proteins. In the case of RecQ, we performed measurements in 50 mM K^+ or 50 mM Na^+. RecQ did not show any GQ unfolding activity in 50 mM K^+ (see Supplementary Figure S19A) while signs of GQ destabilization were observed at 50 mM Na^+ in both nt-free and ATPγS states (Figure 7A). As BLM binding to ssDNA is expected to be similar for 50 mM K^+ and 50 mM Na^+, the observed difference in BLM-mediated GQ unfolding is considered to be due to the weaker GQ stability in Na^+ (69). In both 50 mM K^+ and 50 mM Na^+, the folded FRET peak shifts from $E_{FRET} \approx 0.68$ to $E_{FRET} \approx 0.52$ upon introduction of RecQ. This lower peak has very small population at $E_{FRET} < 0.40$, which is the expected range for the unfolded DNA of this length (Supplementary Figure S1). Therefore, the shift of the FRET peak position upon adding RecQ is most likely due to binding of one or more RecQ proteins to the 12-nt long overhang, rather than unfolding of the GQ. Similarly, RECQ5 did not unfold GQ at 150 mM K^+ (see Supplementary Figure S19B), but showed GQ unfold-

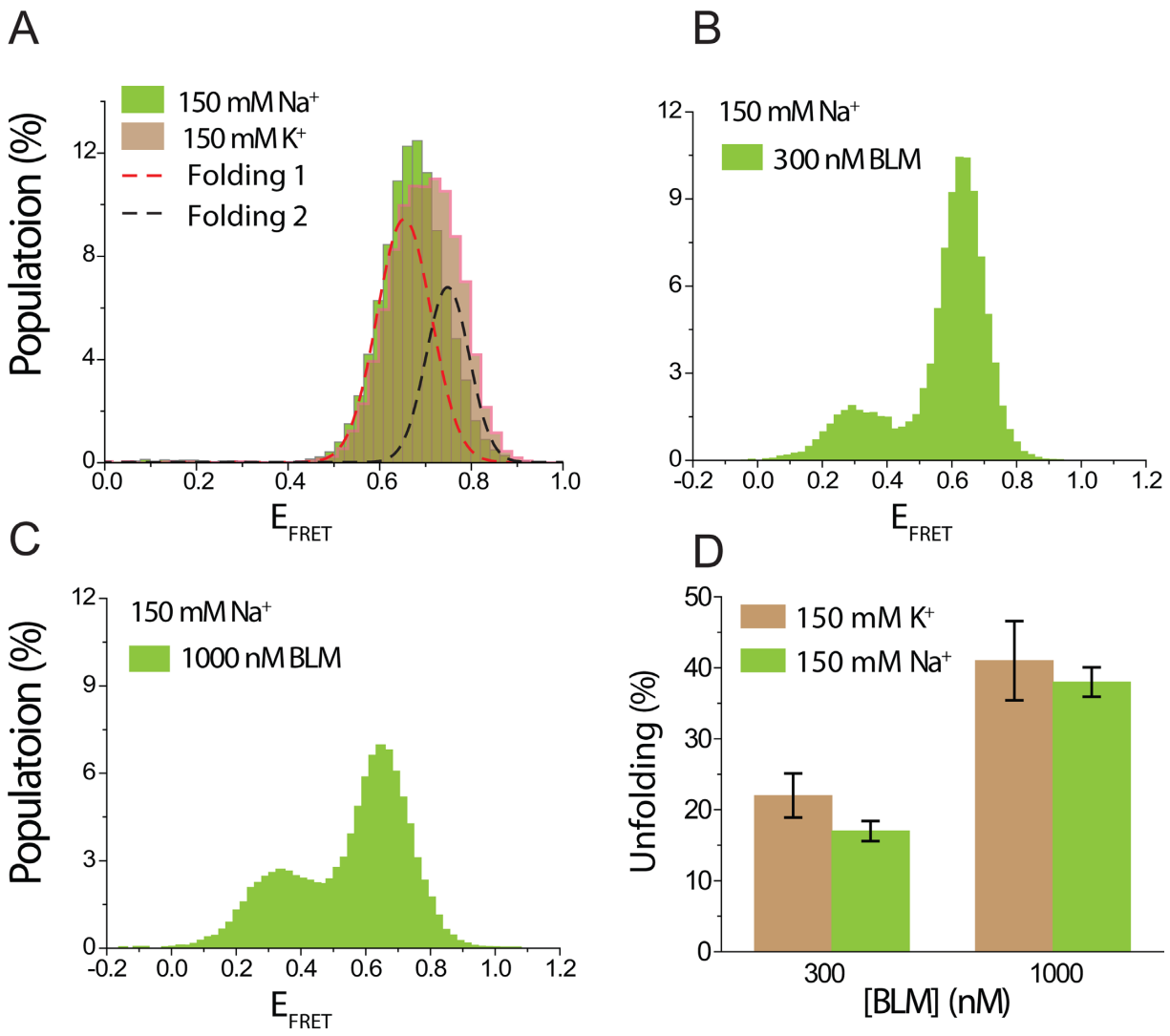

Figure 8. A comparison of BLM-mediated GQ unfolding in 150 mM K^+ and 150 mM Na^+, in which pd-hGQ12T folds into different conformations. (A) The green shaded histogram represents the folded GQ state in 150 mM Na^+, and the brown histogram represents the folded state in 150 mM K^+. The histogram in Na^+ is narrower and can be fit by a single Gaussian peak, indicative of a single conformation, while that for K^+ is broader and requires two Gaussian peaks for fitting (shown by black and red dashed curves), indicative of multiple folding conformations. (B) and (C) BLM-mediated GQ unfolding in 150 mM Na^+ in 300 and 1000 nM BLM, respectively. (D) A comparison of BLM-mediated GQ unfolding in 150 mM Na^+ and 150 mM K^+ for 300 and 1000 nM BLM. These data show that unfolded GQ population is at similar levels in both ionic conditions, suggesting that BLM unfolds different conformations at similar levels.

ing activity at 50 mM Na^+ in both nt-free and ATPγS states (Figure 9B). Due to the very low stock concentration, measurements with WRN were performed only at 50 mM Na^+. Nevertheless, significant GQ unfolding was observed even at 25 nM WRN (Figure 9C). In order to perform a quantitative comparison with BLM, similar measurements were performed with 25 nM BLM at 50 mM Na^+ (Figure 9D). At 50 mM Na^+, 25 nM WRN resulted in 8% and 25% unfolding of pd-hGQ12T in nt-free and ATPγS states, respectively. Similarly, 25 nM BLM resulted in 18% and 25% unfolding of pd-hGQ12T in nt-free and ATPγS states, respectively. Combined, our measurements on RecQ, RECQ5 and WRN show a broad range of efficiencies in GQ unfolding activity in the absence of ATP, which have implications for the role of DNA binding activity versus translocase activity of helicases in GQ destabilization.

DISCUSSION

Based on the presented data, we propose that BLM-mediated GQ unfolding strongly depends on the stability of BLM binding in the vicinity of GQ and does not require any nucleotide cofactor. The binding stability is primarily affected by the length of the 3′ overhang ssDNA and the nucleotide state. Prior bulk biochemical studies have shown that BLM binding to ssDNA, of similar length to the overhangs used in our study, is significantly more stable in the nt-free and AMP-PNP states compared to the ADP state and that BLM dissociates from ssDNA in the ADP state (63,64). These observations are also complemented by our smFRET measurements which show that binding of BLM to pd-polyT15, a pdDNA with a 15-nt long ssDNA overhang, is most stable in the ATPγS state, followed by the

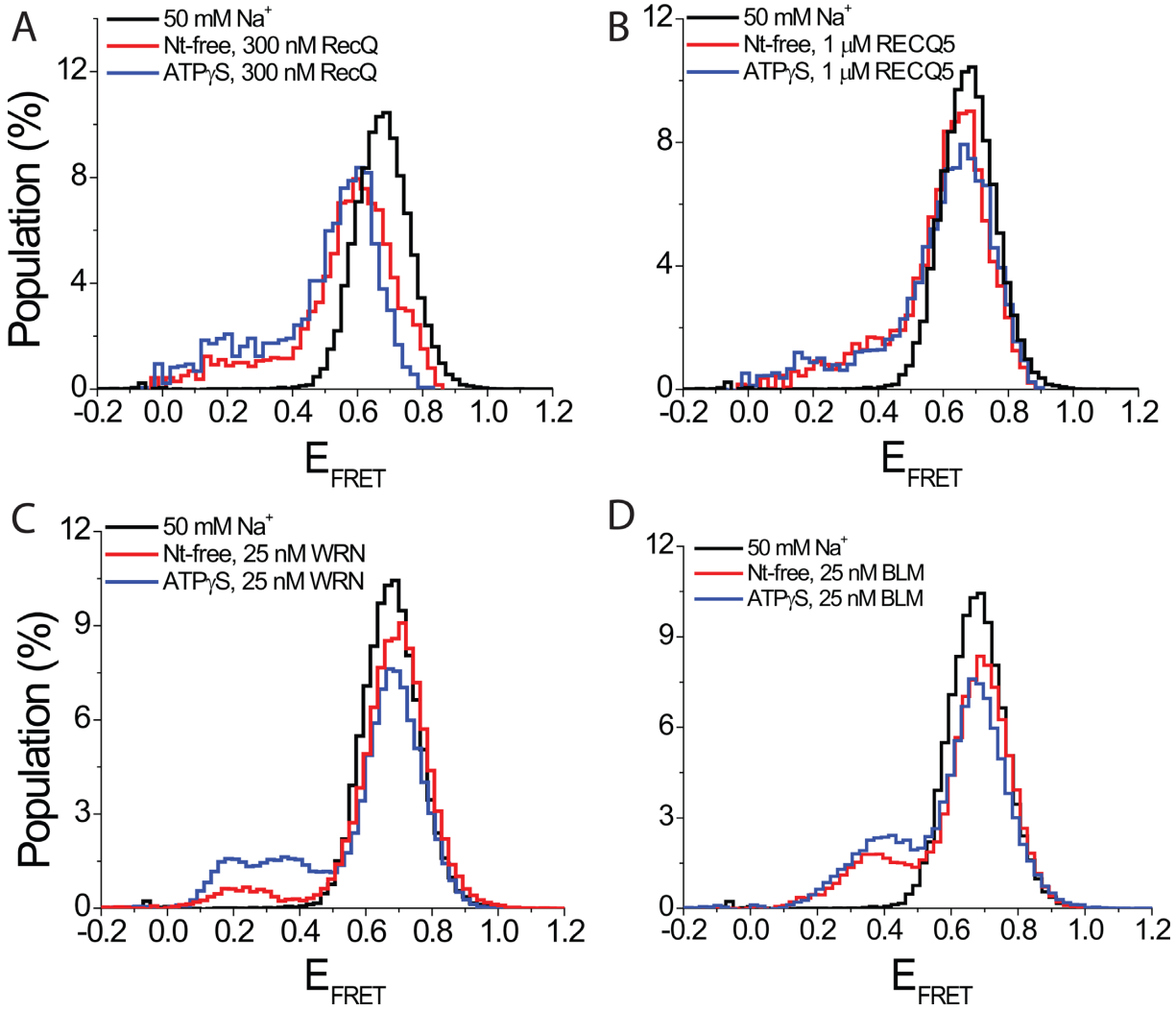

Figure 9. smFRET histograms showing interactions of *E. coli* RecQ, human RECQ5, human WRN and BLM with pd-hGQ12T at 50 mM Na^+. Note the cation was changed to Na^+ as GQ unfolding was not observed in K^+, which results in a more stable GQ, for RecQ and RECQ5. (A) Signs of GQ destabilization are observed in both the nt-free and ATPγS states in 300 nM RecQ. (B) 1 μM RECQ5 also shows weak GQ unfolding activity in both nt-free and ATPγS states. (C) WRN unfolds GQ even at 25 nM concentration in both nt-free and ATPγS states. (D) As a reference to compare with WRN-mediated GQ unfolding, BLM-mediated GQ unfolding is also measured in 25 nM BLM at 50 mM Na^+. The observed GQ unfolding activities of BLM and WRN are similar under these conditions.

nt-free state and then the ADP state. The enhanced GQ unfolding by BLM in the presence of non-hydrolysable ATP analogs ATPγS and AMP-PNP demonstrate the role of nucleotide binding in BLM-mediated GQ unfolding. This enhanced activity suggests that translocation of the helicase is not required and is certainly not the only activity that destabilizes the GQ.

Comparison of the α parameter of Langmuir binding analysis indicates that under saturating BLM and nucleotide concentrations, BLM-mediated GQ unfolding is 10–60% more efficient in the ATPγS state and 15–30% less efficient in the ADP state compared to the nt-free state (Table 2). The maximum GQ unfolding does not rise above 55% in any nucleotide state suggesting a dynamic equilibrium between BLM-mediated GQ unfolding and GQ refolding. The equilibrium constants describing BLM-mediated GQ unfolding for different nucleotide states show large variations. BLM titration in the nt-free state results in $K_{eq} = 305 \pm 16$ nM, while $K_{eq} = 108 \pm 24$ nM for the ATPγS state, and $K_{eq} = 54 \pm 5$ nM for ADP state. These concentrations are significantly higher than the dissociation constants reported for BLM (63,64) as they are a measure of not only BLM binding to the overhang ssDNA but also of unfolding of the GQ that follows this binding. On a related note, our method of probing BLM-mediated GQ unfolding has an advantage over the other published method in which GQ is essentially prevented from refolding due to an irreversible transition to a hairpin structure, unless ethylenediaminetetraacetic acid is added to the environment (56). Our data suggest that GQ can refold if not prevented by hairpin formation. This would explain why the maximum unfolding in our assay is less than that of the other study in which about 90% unfolding was observed (56). It might be argued that at high BLM concentration, multiple BLM molecules

might bind to ssDNA that becomes available after GQ is unfolded, and in that way essentially create an irreversibly unfolded state. However, smFRET time traces show that such a stable unfolded conformation is not attained even at 1 μM BLM concentration. Supplementary Figure S20 shows that the system remains dynamic with GQ unfolding and refolding multiple times within ∼2 min observation time of our traces.

The correlation between the binding stability of BLM to the overhang and the BLM-mediated GQ unfolding activity highlights the significance of the overhang region in the vicinity of GQ. The function of the overhang region was previously studied in the context of intermolecular GQs and it was shown that BLM unfolds GQ with an overhang as short as 4 nt but cannot unfold GQ that lack an overhang (52). Our results on an intramolecular GQ are similar as we observe unfolding for overhangs of 6 nt or longer. We furthermore demonstrate that the BLM-mediated GQ unfolding efficiency gradually increases as the overhang length is increased. Given the 7 or 14 nt footprint of BLM (63,64), the dramatic increase in BLM-mediated GQ unfolding observed at overhang lengths of 6 and 8 nt could provide supporting evidence for 7 nt footprint. Therefore, localization of BLM to the vicinity of GQ, even if stable binding is not established, as might be the case for 6 nt overhang, enables BLM to interact with the GQ structure and eventually destabilize it. A similar mechanism was suggested for ssDNA binding protein RPA which also unfolds GQs in the absence of ATP (43). These observations are consistent with isothermal differential hybridization (IDH) studies which showed that a protein binding to the vicinity of telomeric GQ dramatically reduces GQ stability as measured by the folding equilibrium constant (K_F) of GQ (70). These IDH studies measured the change K_F via a competition of GQ with Watson–Crick pairing with the complementary C-rich strand. The studies reported an order of magnitude reduction in K_F when a digoxigenin and antidigoxigenin antibody were attached to the vicinity of GQ. To our knowledge, these IDH studies are the first and only work that directly probed the influence of protein binding to the vicinity of GQ and GQ stability. Our studies improve on this important study in several significant ways. In our studies, the dynamic nature of the system is preserved as BLM binding dissociation or GQ folding-unfolding were not trapped in any particular state. In the IDH measurements, the antidigoxigenin antibody is permanently bound to the vicinity of GQ and dsDNA formation is essentially an irreversible step that blocks refolding of the GQ. Furthermore, our studies show that protein-mediated GQ unfolding can be altered by either (i) modulating the binding stability of the protein on the overhang, via changing the nucleotide state or the length of the overhang or (ii) changing the GQ stability, via monovalent ion concentration or changing the loop length in GQ.

Another important issue that should be addressed is whether the truncated BLM construct, RecQ-core of BLM or core-BLM, used in this study is representative of the full-length BLM (wt-BLM) construct that is physiologically relevant. Even though core-BLM has been shown to be a good model system for kinetic studies (12), its DNA binding properties, which are significant for this study, could be different from those of the wt-BLM. There are two main reasons why this study was limited to the core-BLM construct. The first one is a practical reason in that it was not possible to attain high enough wt-BLM concentrations required to observe significant GQ unfolding in the absence of ATP. The lower yield attained due to different requirements of the purification protocol limited protein concentration to ∼50 nM BLM in the sample chamber, which is not high enough to observe wt-BLM-mediated GQ unfolding in our assay conditions which require ≥300 nM core-BLM. The other aspect of this discussion, is the 'model protein' aspect of core-BLM. Our study essentially shows that many helicases that bind to the vicinity of GQ have the potential to destabilize these structures in the absence of ATP. In this respect, it is not critical to use the wt-BLM, particularly when core-BLM provides a much broader range of concentrations that enable testing a large array of different cases presented in this work. Even though a detailed kinetic study of BLM-mediated GQ unfolding in ATP and other nucleotide states is missing and would be an excellent complement to this work, the scope of such a study is beyond the current work and the focus is significantly different. Therefore, these topics will be addressed in a future study. To our knowledge, our study is the first to show that BLM-mediated GQ unfolding does not require ATP. However, previous studies were almost exclusively performed on intermolecular GQs. The contrasting results of our study and these earlier works could either arise due to inherent differences between intermolecular and intramolecular GQs or possibly due to better sensitivity of the single-molecule methods we use. In the rare case in which an intramolecular GQ was used, BLM-mediated unfolding of a human telomeric GQ with 10 nt overhang was probed via a bulk fluorescence method in the nt-free state (56). This study did not show the characteristic decrease in the fluorescence signal which was used as a signature for BLM-mediated GQ unfolding. However, we do not think our results necessarily contradict with this study. A novel DNA construct which could transition from a GQ to a hairpin, upon BLM-mediated unfolding of the GQ, was used in that assay (Figure 1A in (56)). The fluorescence intensity of the fluorophore, which is attached to the overhang of GQ, is reduced as a result of hairpin formation, due to its interactions with the complementary strand. A reduction in fluorescence intensity was not observed in the nt-free state even though BLM is shown to bind to the overhang, via polarization measurements. However, in order for a reduction to be observed in fluorescence intensity, BLM needs to unfold the GQ and dissociate from the overhang, which will then allow hairpin formation. If BLM unfolds GQ but does not dissociate from the overhang, the hairpin cannot form and fluorescence intensity would not decrease. Therefore, even if BLM-mediated GQ unfolding takes place, this assay might not be sensitive to it unless BLM dissociates from the overhang. The contrasting results for the intermolecular and intramolecular GQ constructs are significant and might be an indicator of different mechanisms being employed by BLM to interact with these different secondary structures. Therefore, it would be of interest to study whether BLM shows such an unfolding activity in the absence of ATP for other types of DNA secondary structures, such as Holliday junctions or D-loops, using similar single molecule methods. Whether other helicases are also able to unfold in-

tramolecular GQ in the nt-free, ATPγS or ADP states is another important question that is raised by our study. Our measurements on RecQ, RECQ5 and WRN show a broad range of efficiencies in GQ unfolding activity in the absence of ATP. However, recent studies on helicases FANCJ and XPD showed that these helicases can unfold intramolecular and intermolecular GQ, respectively, in the ATP state, but not in nt-free, ATPγS or ADP states (71,72). These contrasting results show the need for further systematic studies on other helicases which could identify the relevant factors that enable or prevent a helicase to unfold a GQ in the absence of ATP. The answers to these questions could potentially challenge our current understanding of the mechanism behind helicase-mediated GQ unfolding.

Another important point highlighted in this study is the influence of the overhang on BLM-mediated GQ unfolding. Various helicases have been shown to possess GQ unfolding activities and the efficiencies of these activities show large variations (41,48). Our study suggests that the observed differences in the GQ unfolding activities of various helicases may partially be due to their ssDNA binding affinities and directionality and the lengths of ssDNA segments that are available in the vicinity of GQ constructs, or other secondary structures, used in such studies.

We demonstrate that BLM-mediated intramolecular GQ unfolding does not require ATP, and can occur in any nucleotide state including the nt-free state. Hence, translocase or helicase activity of BLM is not required for unfolding intramolecular GQ that has a long enough overhang. A limited range of measurements also showed WRN to have a similar GQ unfolding activity. RecQ and RECQ5 were able to unfold GQ only when the ionic concentration was lowered significantly below the physiological conditions, which resulted in a weaker GQ structure. The GQ unfolding activity of these proteins in the absence of ATP are in contrast to prior bulk studies performed on intermolecular GQs which showed GQ unfolding only in the presence of ATP. We also observe that BLM-mediated GQ unfolding is most efficient in the ATPγS state followed by the nt-free state and least efficient in the ADP state. This order correlates with BLM binding stability to the overhang ssDNA in these nucleotide states. We also show that BLM-mediated GQ unfolding becomes more efficient as the overhang length is increased or as the GQ stability is reduced. Finally, we showed that BLM does not show a significant conformation dependence in unfolding GQ. Our study raises a number of questions that challenge our current understanding of helicase-GQ interactions and the mechanism behind the GQ unfolding that results from these interactions. In particular, binding of proteins in the vicinity of GQ, even if the protein is not a translocase or translocation does not take place for different reasons, results in significant destabilization of GQ, which could be a major mechanism for resolving these structures inside the cells.

SUPPLEMENTARY DATA

Supplementary Data are available at NAR Online.

ACKNOWLEDGEMENT

J.B.B. thanks ICAM for the travel award to UIUC for getting trained on BLM purification. At the final stages of this work, we became aware of another single molecule study, which was under peer review then, from Prof. Eli Rothenberg's group (New York University, Department of Biochemistry and Molecular Pharmacology) on the interactions of BLM with GQ.

FUNDING

Farris Family Innovation Award [to H.B.]. U.S. National Science Foundation through the Physics Frontiers Center Program [1430124 to J.G.Y.]. Funding to P.J. was provided by the Czech Science Foundation [GA204/09/0565 to P.J.]. Funding for open access charge: Internal funds of corresponding authors.
Conflict of interest statement. None declared.

REFERENCES

1. German,J. (1993) Bloom syndrome: a mendelian prototype of somatic mutational disease. *Medicine (Baltimore)*, **72**, 393–406.
2. Karow,J.K., Chakraverty,R.K. and Hickson,I.D. (1997) The Bloom's syndrome gene product is a 3′-5′ DNA helicase. *J. Biol. Chem.*, **272**, 30611–30614.
3. Chakraverty,R.K. and Hickson,I.D. (1999) Defending genome integrity during DNA replication: a proposed role for RecQ family helicases. *Bioessays*, **21**, 286–294.
4. Ellis,N.A., Groden,J., Ye,T.Z., Straughen,J., Lennon,D.J., Ciocci,S., Proytcheva,M. and German,J. (1995) The Bloom's syndrome gene product is homologous to RecQ helicases. *Cell*, **83**, 655–666.
5. Kitao,S., Ohsugi,I., Ichikawa,K., Goto,M., Furuichi,Y. and Shimamoto,A. (1998) Cloning of two new human helicase genes of the RecQ family: biological significance of multiple species in higher eukaryotes. *Genomics*, **54**, 443–452.
6. Vindigni,A. and Hickson,I.D. (2009) RecQ helicases: multiple structures for multiple functions? *HFSP J.*, **3**, 153–164.
7. Watt,P.M. and Hickson,I.D. (1996) Failure to unwind causes cancer. Genome stability. *Curr. Biol.*, **6**, 265–267.
8. Bachrati,C.Z. and Hickson,I.D. (2003) RecQ helicases: suppressors of tumorigenesis and premature aging. *Biochem. J.*, **374**, 577–606.
9. Opresko,P.L., Cheng,W.H. and Bohr,V.A. (2004) Junction of RecQ helicase biochemistry and human disease. *J. Biol. Chem.*, **279**, 18099–18102.
10. Karow,J.K., Newman,R.H., Freemont,P.S. and Hickson,I.D. (1999) Oligomeric ring structure of the Bloom's syndrome helicase. *Curr. Biol.*, **9**, 597–600.
11. Xu,Y.N., Bazeille,N., Ding,X.Y., Lu,X.M., Wang,P.Y., Bugnard,E., Grondin,V., Dou,S.X. and Xi,X.G. (2012) Multimeric BLM is dissociated upon ATP hydrolysis and functions as monomers in resolving DNA structures. *Nucleic Acids Res.*, **40**, 9802–9814.
12. Yodh,J.G., Stevens,B.C., Kanagaraj,R., Janscak,P. and Ha,T. (2009) BLM helicase measures DNA unwound before switching strands and hRPA promotes unwinding reinitiation. *EMBO J.*, **28**, 405–416.
13. Barefield,C. and Karlseder,J. (2012) The BLM helicase contributes to telomere maintenance through processing of late-replicating intermediate structures. *Nucleic Acids Res.*, **40**, 7358–7367.
14. Hoadley,K.A., Xu,D., Xue,Y., Satyshur,K.A., Wang,W. and Keck,J.L. (2010) Structure and cellular roles of the RMI core complex from the Bloom syndrome dissolvasome. *Structure*, **18**, 1149–1158.
15. Chaires,J.B. (2010) Human telomeric G-quadruplex: thermodynamic and kinetic studies of telomeric quadruplex stability. *FEBS J.*, **277**, 1098–1106.
16. Gray,R.D. and Chaires,J.B. (2008) Kinetics and mechanism of K+- and Na+-induced folding of models of human telomeric DNA into G-quadruplex structures. *Nucleic Acids Res.*, **36**, 4191–4203.
17. Lane,A.N., Chaires,J.B., Gray,R.D. and Trent,J.O. (2008) Stability and kinetics of G-quadruplex structures. *Nucleic Acids Res.*, **36**, 5482–5515.

18. Stegle,O., Payet,L., Mergny,J.L., MacKay,D.J. and Leon,J.H. (2009) Predicting and understanding the stability of G-quadruplexes. *Bioinformatics*, **25**, i374–i382.
19. Blackburn,E.H. (1991) Structure and function of telomeres. *Nature*, **350**, 569–573.
20. Sen,D. and Gilbert,W. (1988) Formation of parallel four-stranded complexes by guanine-rich motifs in DNA and its implications for meiosis. *Nature*, **334**, 364–366.
21. Sundquist,W.I. and Klug,A. (1989) Telomeric DNA dimerizes by formation of guanine tetrads between hairpin loops. *Nature*, **342**, 825–829.
22. Blackburn,E.H., Greider,C.W. and Szostak,J.W. (2006) Telomeres and telomerase: the path from maize, Tetrahymena and yeast to human cancer and aging. *Nat. Med.*, **12**, 1133–1138.
23. Fletcher,T.M., Sun,D., Salazar,M. and Hurley,L.H. (1998) Effect of DNA secondary structure on human telomerase activity. *Biochemistry*, **37**, 5536–5541.
24. Gellert,M., Lipsett,M.N. and Davies,D.R. (1962) Helix formation by guanylic acid. *Proc. Natl. Acad. Sci. U.S.A.*, **48**, 2013–2018.
25. Gilbert,D.E. and Feigon,J. (1999) Multistranded DNA structures. *Curr. Opin. Struct. Biol.*, **9**, 305–314.
26. Williamson,J.R. (1994) G-quartet structures in telomeric DNA. *Annu. Rev. Biophys. Biomol. Struct.*, **23**, 703–730.
27. Eddy,J. and Maizels,N. (2006) Gene function correlates with potential for G4 DNA formation in the human genome. *Nucleic Acids Res.*, **34**, 3887–3896.
28. Eddy,J. and Maizels,N. (2008) Conserved elements with potential to form polymorphic G-quadruplex structures in the first intron of human genes. *Nucleic Acids Res.*, **36**, 1321–1333.
29. Huppert,J.L. and Balasubramanian,S. (2005) Prevalence of quadruplexes in the human genome. *Nucleic Acids Res.*, **33**, 2908–2916.
30. Huppert,J.L. and Balasubramanian,S. (2007) G-quadruplexes in promoters throughout the human genome. *Nucleic Acids Res.*, **35**, 406–413.
31. Todd,A.K., Johnston,M. and Neidle,S. (2005) Highly prevalent putative quadruplex sequence motifs in human DNA. *Nucleic Acids Res.*, **33**, 2901–2907.
32. Du,Z., Zhao,Y. and Li,N. (2008) Genome-wide analysis reveals regulatory role of G4 DNA in gene transcription. *Genome Res.*, **18**, 233–241.
33. Qin,Y. and Hurley,L.H. (2008) Structures, folding patterns, and functions of intramolecular DNA G-quadruplexes found in eukaryotic promoter regions. *Biochimie*, **90**, 1149–1171.
34. Balasubramanian,S., Hurley,L.H. and Neidle,S. (2011) Targeting G-quadruplexes in gene promoters: a novel anticancer strategy? *Nat. Rev. Drug Discov.*, **10**, 261–275.
35. Huppert,J.L., Bugaut,A., Kumari,S. and Balasubramanian,S. (2008) G-quadruplexes: the beginning and end of UTRs. *Nucleic Acids Res.*, **36**, 6260–6268.
36. Kumari,S., Bugaut,A., Huppert,J.L. and Balasubramanian,S. (2007) An RNA G-quadruplex in the 5′ UTR of the NRAS proto-oncogene modulates translation. *Nat. Chem. Biol.*, **3**, 218–221.
37. Morris,M.J. and Basu,S. (2009) An unusually stable G-quadruplex within the 5′-UTR of the MT3 matrix metalloproteinase mRNA represses translation in eukaryotic cells. *Biochemistry*, **48**, 5313–5319.
38. Morris,M.J., Negishi,Y., Pazsint,C., Schonhoft,J.D. and Basu,S. (2010) An RNA G-quadruplex is essential for cap-independent translation initiation in human VEGF IRES. *J. Am. Chem. Soc.*, **132**, 17831–17839.
39. Biffi,G., Tannahill,D., McCafferty,J. and Balasubramanian,S. (2013) Quantitative visualization of DNA G-quadruplex structures in human cells. *Nat. Chem.*, **5**, 182–186.
40. Lipps,H.J. and Rhodes,D. (2009) G-quadruplex structures: in vivo evidence and function. *Trends Cell. Biol.*, **19**, 414–422.
41. Paeschke,K., Capra,J.A. and Zakian,V.A. (2011) DNA replication through G-quadruplex motifs is promoted by the Saccharomyces cerevisiae Pif1 DNA helicase. *Cell*, **145**, 678–691.
42. Qureshi,M.H., Ray,S., Sewell,A.L., Basu,S. and Balci,H. (2012) Replication protein A unfolds G-quadruplex structures with varying degrees of efficiency. *J. Phys. Chem. B.*, **116**, 5588–5594.
43. Ray,S., Qureshi,M.H., Malcolm,D.W., Budhathoki,J.B., Celik,U. and Balci,H. (2013) RPA-mediated unfolding of systematically varying G-quadruplex structures. *Biophys. J.*, **104**, 2235–2245.
44. Fernando,H., Sewitz,S., Darot,J., Tavare,S., Huppert,J.L. and Balasubramanian,S. (2009) Genome-wide analysis of a G-quadruplex-specific single-chain antibody that regulates gene expression. *Nucleic Acids Res.*, **37**, 6716–6722.
45. Ribeyre,C., Lopes,J., Boule,J.B., Piazza,A., Guedin,A., Zakian,V.A., Mergny,J.L. and Nicolas,A. (2009) The yeast Pif1 helicase prevents genomic instability caused by G-quadruplex-forming CEB1 sequences in vivo. *PLoS Genet.*, **5**, e1000475.
46. Sanders,C.M. (2010) Human Pif1 helicase is a G-quadruplex DNA-binding protein with G-quadruplex DNA-unwinding activity. *Biochem. J.*, **430**, 119–128.
47. Johnson,J.E., Cao,K., Ryvkin,P., Wang,L.S. and Johnson,F.B. (2010) Altered gene expression in the Werner and Bloom syndromes is associated with sequences having G-quadruplex forming potential. *Nucleic Acids Res.*, **38**, 1114–1122.
48. Paeschke,K., Bochman,M.L., Garcia,P.D., Cejka,P., Friedman,K.L., Kowalczykowski,S.C. and Zakian,V.A. (2013) Pif1 family helicases suppress genome instability at G-quadruplex motifs. *Nature*, **497**, 458–462.
49. Hershman,S.G., Chen,Q., Lee,J.Y., Kozak,M.L., Yue,P., Wang,L.S. and Johnson,F.B. (2008) Genomic distribution and functional analyses of potential G-quadruplex-forming sequences in Saccharomyces cerevisiae. *Nucleic Acids Res.*, **36**, 144–156.
50. Huber,M.D., Lee,D.C. and Maizels,N. (2002) G4 DNA unwinding by BLM and Sgs1p: substrate specificity and substrate-specific inhibition. *Nucleic Acids Res.*, **30**, 3954–3961.
51. Mohaghegh,P., Karow,J.K., Brosh,R.M. Jr, Bohr,V.A. and Hickson,I.D. (2001) The Bloom's and Werner's syndrome proteins are DNA structure-specific helicases. *Nucleic Acids Res.*, **29**, 2843–2849.
52. Sun,H., Karow,J.K., Hickson,I.D. and Maizels,N. (1998) The Bloom's syndrome helicase unwinds G4 DNA. *J. Biol. Chem.*, **273**, 27587–27592.
53. Kamath-Loeb,A., Loeb,L.A. and Fry,M. (2012) The Werner syndrome protein is distinguished from the Bloom syndrome protein by its capacity to tightly bind diverse DNA structures. *PloS ONE*, **7**, e30189.
54. Huber,M.D., Duquette,M.L., Shiels,J.C. and Maizels,N. (2006) A conserved G4 DNA binding domain in RecQ family helicases. *J. Mol. Biol.*, **358**, 1071–1080.
55. Wang,Q., Liu,J.Q., Chen,Z., Zheng,K.W., Chen,C.Y., Hao,Y.H. and Tan,Z. (2011) G-quadruplex formation at the 3′ end of telomere DNA inhibits its extension by telomerase, polymerase and unwinding by helicase. *Nucleic Acids Res.*, **39**, 6229–6237.
56. Liu,J.Q., Chen,C.Y., Xue,Y., Hao,Y.H. and Tan,Z. (2010) G-quadruplex hinders translocation of BLM helicase on DNA: a real-time fluorescence spectroscopic unwinding study and comparison with duplex substrates. *J. Am. Chem. Soc.*, **132**, 10521–10527.
57. Janscak,P., Garcia,P.L., Hamburger,F., Makuta,Y., Shiraishi,K., Imai,Y., Ikeda,H. and Bickle,T.A. (2003) Characterization and mutational analysis of the RecQ core of the Bloom syndrome protein. *J. Mol. Biol.*, **330**, 29–42.
58. Bernstein,D.A. and Keck,J.L. (2003) Domain mapping of Escherichia coli RecQ defines the roles of conserved N- and C-terminal regions in the RecQ family. *Nucleic Acids Res.*, **31**, 2778–2785.
59. Garcia,P.L., Liu,Y., Jiricny,J., West,S.C. and Janscak,P. (2004) Human RECQ5beta, a protein with DNA helicase and strand-annealing activities in a single polypeptide. *EMBO J.*, **23**, 2882–2891.
60. Orren,D.K., Brosh,R.M. Jr, Nehlin,J.O., Machwe,A., Gray,M.D. and Bohr,V.A. (1999) Enzymatic and DNA binding properties of purified WRN protein: high affinity binding to single-stranded DNA but not to DNA damage induced by 4NQO. *Nucleic Acids Res.*, **27**, 3557–3566.
61. Ambrus,A., Chen,D., Dai,J., Bialis,T., Jones,R.A. and Yang,D. (2006) Human telomeric sequence forms a hybrid-type intramolecular G-quadruplex structure with mixed parallel/antiparallel strands in potassium solution. *Nucleic Acids Res.*, **34**, 2723–2735.
62. Neff,N.F., Ellis,N.A., Ye,T.Z., Noonan,J., Huang,K., Sanz,M. and Proytcheva,M. (1999) The DNA helicase activity of BLM is necessary for the correction of the genomic instability of Bloom syndrome cells. *Mol. Biol. Cell*, **10**, 665–676.

63. Yang,Y., Dou,S.X., Xu,Y.N., Bazeille,N., Wang,P.Y., Rigolet,P., Xu,H.Q. and Xi,X.G. (2010) Kinetic mechanism of DNA unwinding by the BLM helicase core and molecular basis for its low processivity. *Biochemistry*, **49**, 656–668.
64. Gyimesi,M., Sarlos,K. and Kovacs,M. (2010) Processive translocation mechanism of the human Bloom's syndrome helicase along single-stranded DNA. *Nucleic Acids Res.*, **38**, 4404–4414.
65. Zhou,R., Zhang,J., Bochman,M.L., Zakian,V.A. and Ha,T. (2014) Periodic DNA patrolling underlies diverse functions of Pif1 on R-loops and G-rich DNA. *eLife*, **3**, e02190.
66. Wlodarczyk,A., Grzybowski,P., Patkowski,A. and Dobek,A. (2005) Effect of ions on the polymorphism, effective charge, and stability of human telomeric DNA. Photon correlation spectroscopy and circular dichroism studies. *J. Phys. Chem. B*, **109**, 3594–3605.
67. Guedin,A., Gros,J., Alberti,P. and Mergny,J.L. (2010) How long is too long? Effects of loop size on G-quadruplex stability. *Nucleic Acids Res.*, **38**, 7858–7868.
68. Tippana,R., Xiao,W. and Myong,S. (2014) G-quadruplex conformation and dynamics are determined by loop length and sequence. *Nucleic Acids Res.*, **42**, 8106–8114.
69. Tran,P.L., Mergny,J.L. and Alberti,P. (2011) Stability of telomeric G-quadruplexes. *Nucleic Acids Res.*, **39**, 3282–3294.
70. Wang,Q., Ma,L., Hao,Y.H. and Tan,Z. (2010) Folding equilibrium constants of telomere G-quadruplexes in free state or associated with proteins determined by isothermal differential hybridization. *Anal. Chem.*, **82**, 9469–9475.
71. Bharti,S.K., Sommers,J.A., George,F., Kuper,J., Hamon,F., Shin-Ya,K., Teulade-Fichou,M.P., Kisker,C. and Brosh,R.M. Jr (2013) Specialization among iron-sulfur cluster helicases to resolve G-quadruplex DNA structures that threaten genomic stability. *J. Biol. Chem.*, **288**, 28217–28229.
72. Gray,L.T., Vallur,A.C., Eddy,J. and Maizels,N. (2014) G quadruplexes are genomewide targets of transcriptional helicases XPB and XPD. *Nat. Chem. Biol.*, **10**, 313–318.

Supplementary Data

BLM-mediated Telomeric G-quadruplex Unfolding in the Absence of ATP

Jagat B. Budhathoki[1], Sujay Ray[1], Vaclav Urban[2], Pavel Janscak[2,3], Jaya G. Yodh[4,*], Hamza Balci[1,*]

[1] Department of Physics, Kent State University, Kent, OH, 44242, USA

[2] Institute of Molecular Genetics AS CR, Prague, Czech Republic

[3] Institute of Molecular Cancer Research, University of Zurich, Zurich, Switzerland;

[4] Department of Physics and Center for the Physics of Living Cells, University of Illinois at Urbana-Champaign, Urbana, IL, 61801, USA

* To whom correspondence should be addressed. Tel: +1 (330) 672 2577; Fax: +1 (330) 672 2959; Email: hbalci@kent.edu

Correspondence may also be addressed to Jaya G. Yodh. Tel: +1 (217) 244 1155; Fax: +1 (217) 244 1155; Email: jyodh@illinois.edu

Identification of the Unfolded and BLM-bound Unfolded FRET States

The telomeric sequence we studied forms a stable GQ structure at 150 mM K^+. However, various other FRET states emerge upon introduction of BLM. Identifying the DNA conformations these new FRET states represent is complicated on a GQ forming sequence as the sequence could potentially form various secondary structures. In particular, we aimed to identify the FRET states representing the unfolded and BLM-bound unfolded states as these states would be expected to form upon interaction with BLM. To avoid such complications we performed smFRET measurements on a 35 nucleotide (nt) long polythymine DNA construct (pd-polyT35, see Table 1 in manuscript for sequence), which is hybridized with the RNA-Stem to form a pdDNA construct similar to that used for GQ forming sequences. The single strand DNA (ssDNA) section of this construct has the same length as that of pd-hGQ12T, i.e. they are both 35 nt long. Therefore, it can be used as a model to represent the unfolded and BLM-bound unfolded states of pd-hGQ12T. Figure S1-A shows the smFRET distribution at 150 mM K^+ in the absence of BLM. The peak at E_{FRET} = 0.40 corresponds to the coiled DNA structure for a 35 nt long ssDNA, which is equivalent to the unfolded structure of pd-hGQ12T. Figure S1-B shows the smFRET distribution when 50 nM BLM is introduced to the sample chamber. In addition to the peak at E_{FRET} = 0.40, a new peak is observed at E_{FRET} = 0.20 which we interpret as the BLM-bound peak. Therefore, E_{FRET} =0.20 represents the BLM-bound unfolded peak of pd-hGQ12T.

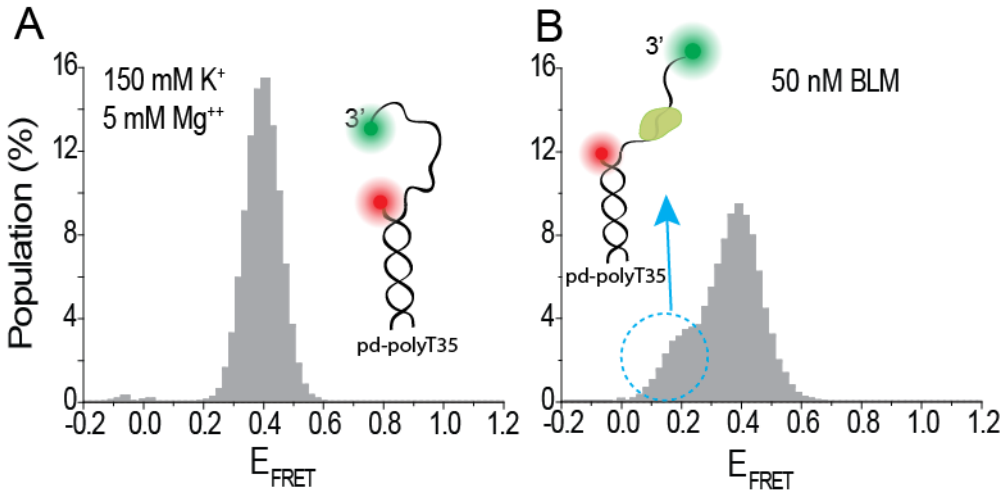

Supplementary Figure S1: smFRET measurements on pd-polyT35 construct which has a 35 nt long polythymine ssDNA tail, which is same length as the ssDNA section of pd-hGQ12T. pd-polyT35 is used to characterize the FRET levels corresponding to the unfolded and BLM-bound unfolded states of pd-hGQ12T. (A) smFRET distribution at 150 mM K^+ before BLM is added. The peak at E_{FRET} = 0.40 corresponds to the coiled DNA structure for a 35 nt long ssDNA, which is equivalent to the unfolded structure of pd-hGQ12T. The inset shows a schematic of the DNA construct. (B) smFRET distribution after adding 50 nM BLM to the chamber. The new peak at E_{FRET} = 0.20 represents the BLM-bound peak, which corresponds to the BLM-bound unfolded peak of pd-hGQ12T. The inset shows a schematic of the BLM-DNA complex represented by the peak at E_{FRET} = 0.20.

Circular Dichroism Assay and smFRET Data on Internally Labeled DNA Construct

Circular dichroism measurements were performed on pd-hGQ12T to obtain an independent confirmation of BLM-mediated GQ unfolding in the absence of ATP. The DNA concentration needs to be maintained at 1 μM to achieve a reliable CD signal. Therefore, we performed the measurements only at the highest protein concentration possible in our system -1 μM- in order to attain a significant change in the CD spectrum. Figure S2-A shows these data before and after adding 1 μM BLM to a cuvette that contains folded pd-hGQ12T in 150 mM K^+. The peak at ~290 nm is a characteristic signature of GQ structure, which diminishes upon addition of 1 μM BLM, which is consistent with GQ unfolding by BLM. Another smFRET DNA construct was designed in order to more directly probe GQ unfolding in which the donor fluorophore is moved from the 3' end to an internal site a couple nucleotides away from the GQ (inset of Figure S2-B).). This construct, pd-hGQ-2T-Cy3-10T, was formed by hybridizing the 18 nt RNA-Stem with 5'- TGG CGA CGG CAG CGA GGC TTG GGT TAG GGT TAG GGT TAG GG TT-Cy3-10T. pd-hGQ-2T-Cy3-10T eliminates any significant FRET changes that might take place due to binding of the protein to the overhang, and results in a significant FRET change only when the GQ is unfolded. The measurements on this construct resulted in considerable reduction in BLM-mediated GQ unfolding at 150 mM K^+, which is considered to be due to interference caused by the donor fluorophore on BLM-GQ interactions (data not shown). Nevertheless, a clear BLM-mediated unfolded GQ population was observed in both nt-free and 1 mM ATPγS states in 1 μM BLM. Figure S2-B and S2-C show these data in 50 mM K^+ and 10 mM K^+, respectively. Figure S2-D shows the quantification of the unfolded GQ population for the data presented in Figure S2-B and S2-C.

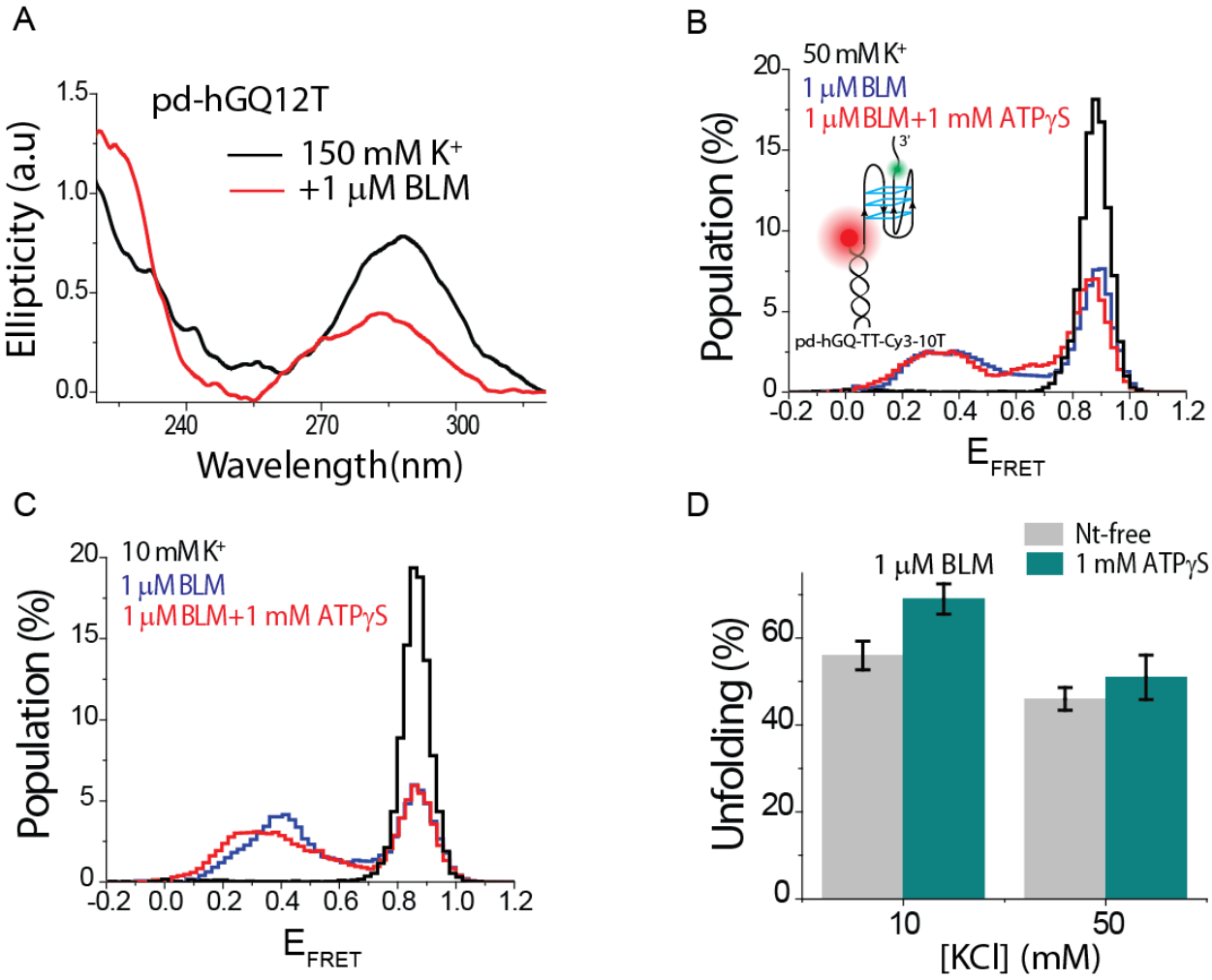

Figure S2: (A) CD data on pd-hGQ12T with and without 1 μM BLM. **(B)** and **(C)** smFRET data on pd-hGQ-TT-Cy3-10T in 50 mM and 10 mM K^+, respectively. **(D)** Quantitation of the unfolded GQ population in the histograms in (B) and (C).

FRET Histograms and Subtraction Analysis for BLM Titration on pd-hGQ12T

Figure 1 of the manuscript shows sample histograms of BLM-GQ interactions when BLM is titrated under different nucleotide conditions for the pd-hGQ12T construct. Figure S3 is an extension of this figure that shows the histograms for the BLM concentrations not shown in Figure 1. Figure S4 shows the corresponding histograms of subtraction analysis we performed to quantify BLM-mediated GQ unfolding. For all the subtraction analysis presented in Figure S4, the folded state before BLM is introduced to chamber is taken as the reference. This folded state does not vary upon introduction of ATPγS or ADP to chamber as the ionic strength - which determines GQ stability -is kept constant. In Figure S3 and S4, the nucleotide states and the BLM concentrations are written on the graphs. All experiments were performed at 150 mM K^+.

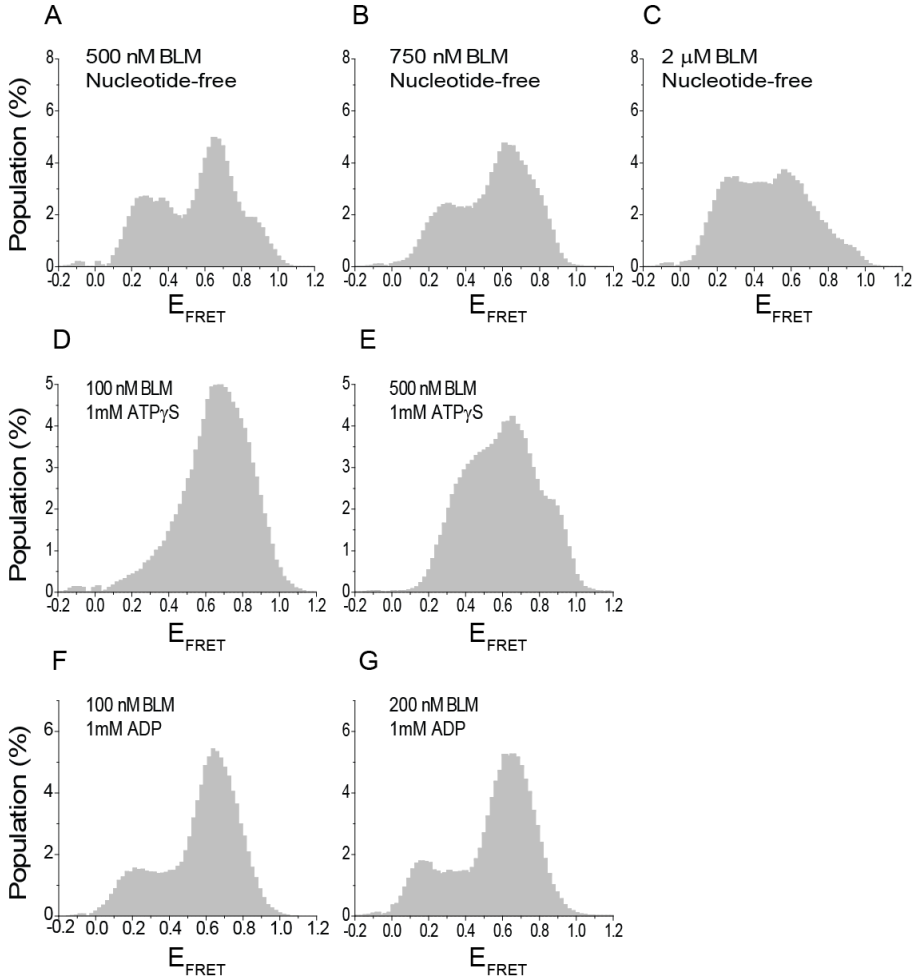

Supplementary Figure S3: smFRET histograms showing the BLM concentrations we studied, other than those shown in Figure 1 of the manuscript, in the nucleotide-free, 1 mM ATPγS, or 1 mM ADP states. The data shown in **(A)-(C)** were taken in the nucleotide-free state at 500 nM, 750 nM, and 1 μM BLM concentration, respectively. The data shown in **(D)-(E)** were taken at 1 mM ATPγS at 100 nM and 500 nM BLM concentration, respectively. The data shown in **(F)-(G)** were taken at 1 mM ADP at 100 nM and 200 nM BLM concentration, respectively. The BLM concentration and the nucleotide state for each histogram are written on the graphs.

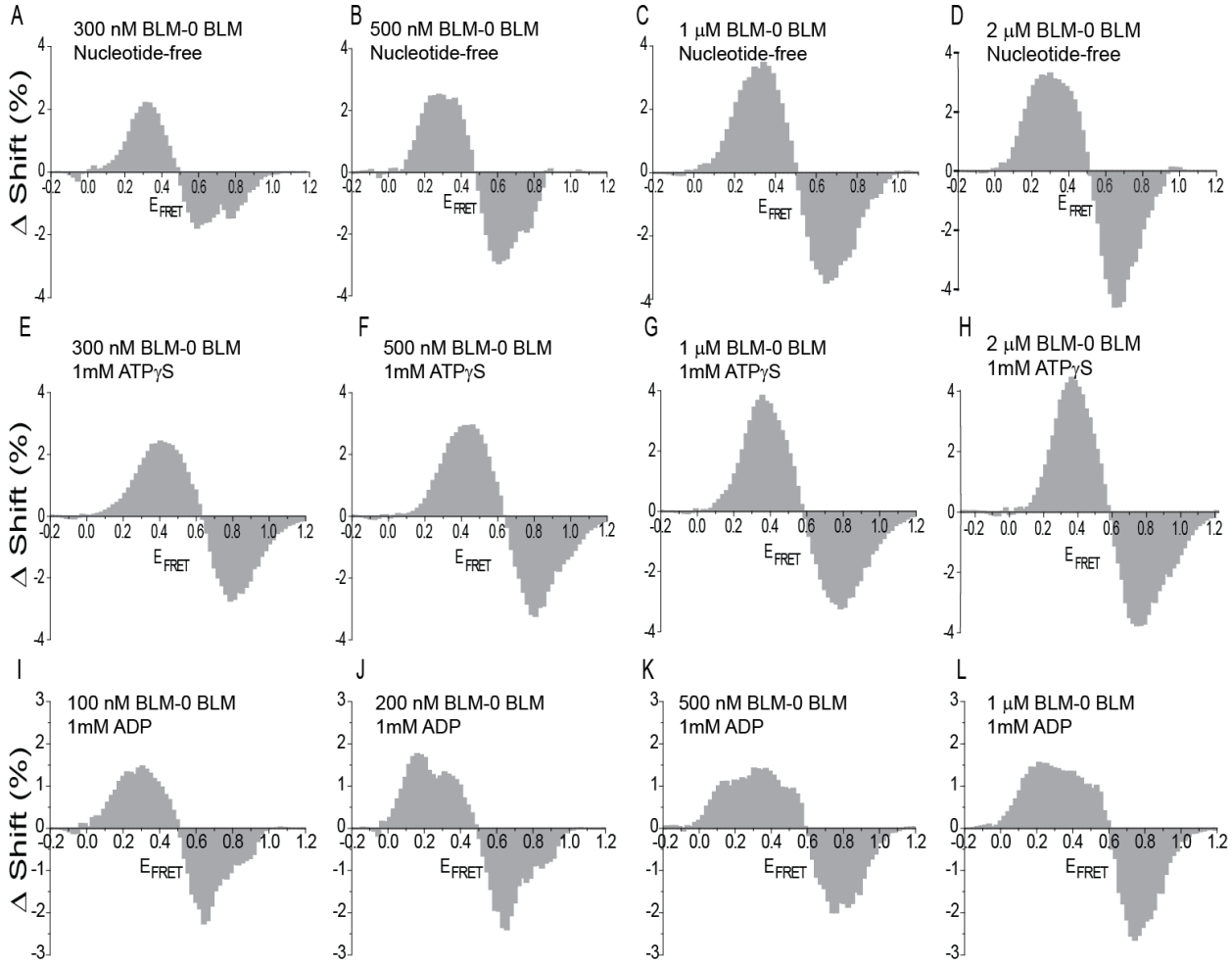

Supplementary Figure S4: Subtraction analysis performed on the data shown in Figure 1 and Figure S3 using the folded state shown in Figure 1B as the reference. This folded state is the same for all nucleotide-states in the absence of BLM, enabling its use as the reference state for all the presented data in Figure 1 and Figure S3. The subtraction analysis was performed for data taken in **(A)-(D)** Nucleotide-free state; **(E)-(H)** 1 mM ATPγS; and **(I)-(L)** 1 mM ADP. The BLM and nucleotide concentrations used for each histogram are written on the graphs. These data were included in the Langmiur isotherms shown in Figure 1.

Electrophoretic Mobility Shift Assay of BLM binding to GQ constructs

A native PAGE gel binding assay of BLM binding to pd-hGQ12T GQ construct is shown in Figure S8. This assay is not capable of distinguishing between BLM-bound folded and BLM-bound unfolded GQ as only a single shifted band is observed upon introducing BLM. Therefore, this observation only confirms binding of BLM to the DNA substrate. The measurements were performed at 0, 50, 100, 150, 200, 300, 400, 500, and 1000 nM BLM concentrations, while the DNA concentration was 5 nM. The buffer contained 50 mM K^+, 5 mM Mg^{++}, 50mM Tris-HCl (pH7.5), and 1 mM DTT. The constructs were annealed via heating/slow cooling prior to the gel binding assay. BLM-DNA binding reactions were carried out at 22 °C for 10 minutes, followed by electrophoresis through a 4-20% native PAGE gel at 4 °C. The gel was run at 50 V for 5-8 hours in 0.5xTBE buffer. Figure S5-A shows the gel image and Figure S5-B shows a quantification of the unfolded band. The data were fit by Hill equation, which results in K_A=139 nM BLM which is ~5x greater than that observed in smFRET measurements performed in 25 °C. We attribute this difference to lower temperature of the EMSA measurements in which BLM activity is lower and GQ is more stable.

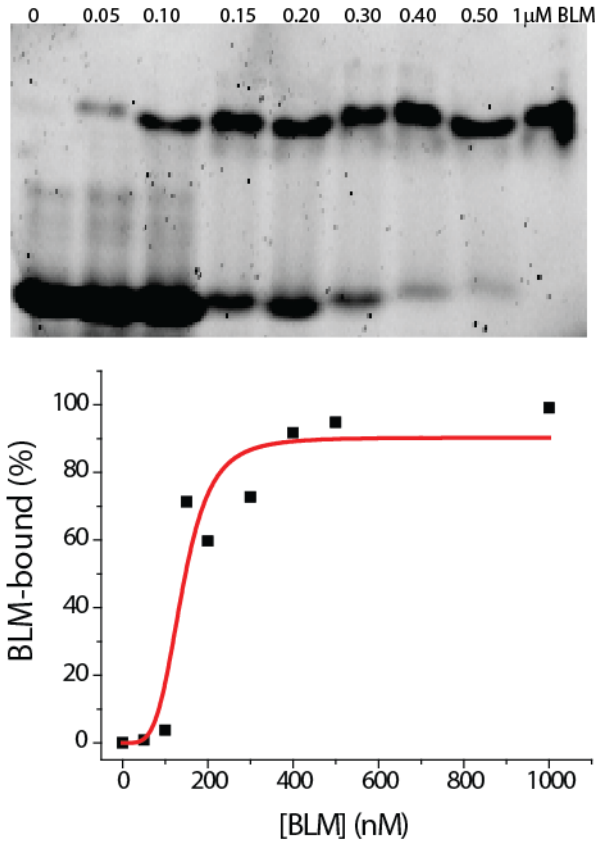

Supplementary Figure S5: Electrophoretic Mobility Shift Assay of BLM binding to pd-hGQ12T. Gels were imaged using a Molecular Dynamics Typhoon 9400 Multilaser Scanner. Cy5 image is shown. The lower panel shows quantification of the shifted band, for which we used GelQuant.NET software provided by biochemlabsolutions.com.

Measurements with Denatured Proteins and Control Measurements on Storage Buffer

Due to the unexpected nature of the observation that BLM unfolds GQ in the absence of ATP, we sought to ensure that the reason for GQ destabilization is not related to the buffer that BLM is stored in (50 mM Tris-HCl (pH=7.5), 200 mM NaCl, 50 % (v/v) glycerol and 1 mM DTT). The BLM is significantly diluted in imaging buffer, which contains 150 mM K^+ and 5 mM Mg^{++}, before it is added to the sample chamber. Therefore, any GQ destabilizing agent (such as a metal chelator) present in the storage buffer would be at a significantly less concentration. Nevertheless, we performed control measurements to study the influence of the storage buffer on the folded GQ state and did not observe any destabilization induced by this buffer in the absence of BLM. Figure S6 shows these data.

Another control measurement we performed was to denature BLM by heating it at 95 °C for 5 minutes before adding it to the sample chamber that contains folded GQ molecules. This measurement was an attempt to ensure that GQ destabilization is due to native BLM protein. We did not observe any GQ unfolding with 1 μM denatured BLM in either nt-free state or in 1 mM ATPγS state, as shown in Figure S6.

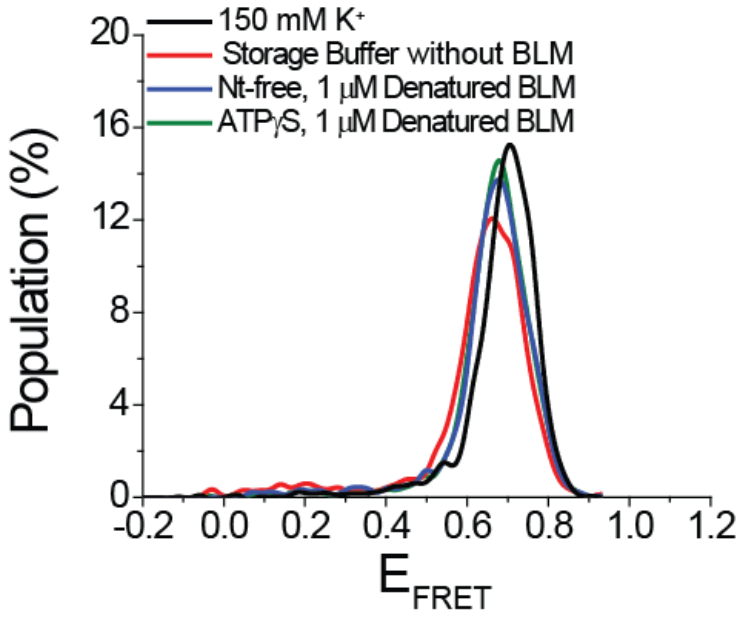

Supplementary Figure S6: Control measurements testing the storage buffer and thermally denatured BLM. GQ is not destabilized by any agent that might be in the storage buffer in the absence of BLM. Also, thermally denatured BLM does not destabilize GQ in either nt-free or ATPγS states.

Measurement to Test for Possible ATP Contamination of Purified BLM

In order to ensure that our smFRET assays probing BLM-mediated GQ unfolding do not contain ATP that is not accounted for, possibly ATP that might co-purify with BLM, we performed duplex DNA unwinding assays without adding any ATP to the medium. We used a forked DNA construct that was used by Yodh *et al.* (The EMBO Journal (2009) 28, 405–416), as shown in Figure S7-A. Unwinding of this duplex requires translocation along the ssDNA tracking strand in the 3'-5' direction. Figure S7-B shows that even saturating concentrations of BLM (1 μM) do not unwind the dsDNA in the nt-free state or in the presence of 1 μM ATPγS. On the other hand 10 nM BLM gives rise to visible dsDNA unwinding in the presence of 100 μM ATP. Figure S7-B shows an example trace showing such a repetitive unwinding event in agreement with those observed by Yodh *et al.* (The EMBO Journal (2009) 28, 405–416). The bottom panel in Figure S7-C is a zoomed in version of Figure S7-B to better show the repetitive unwinding events.

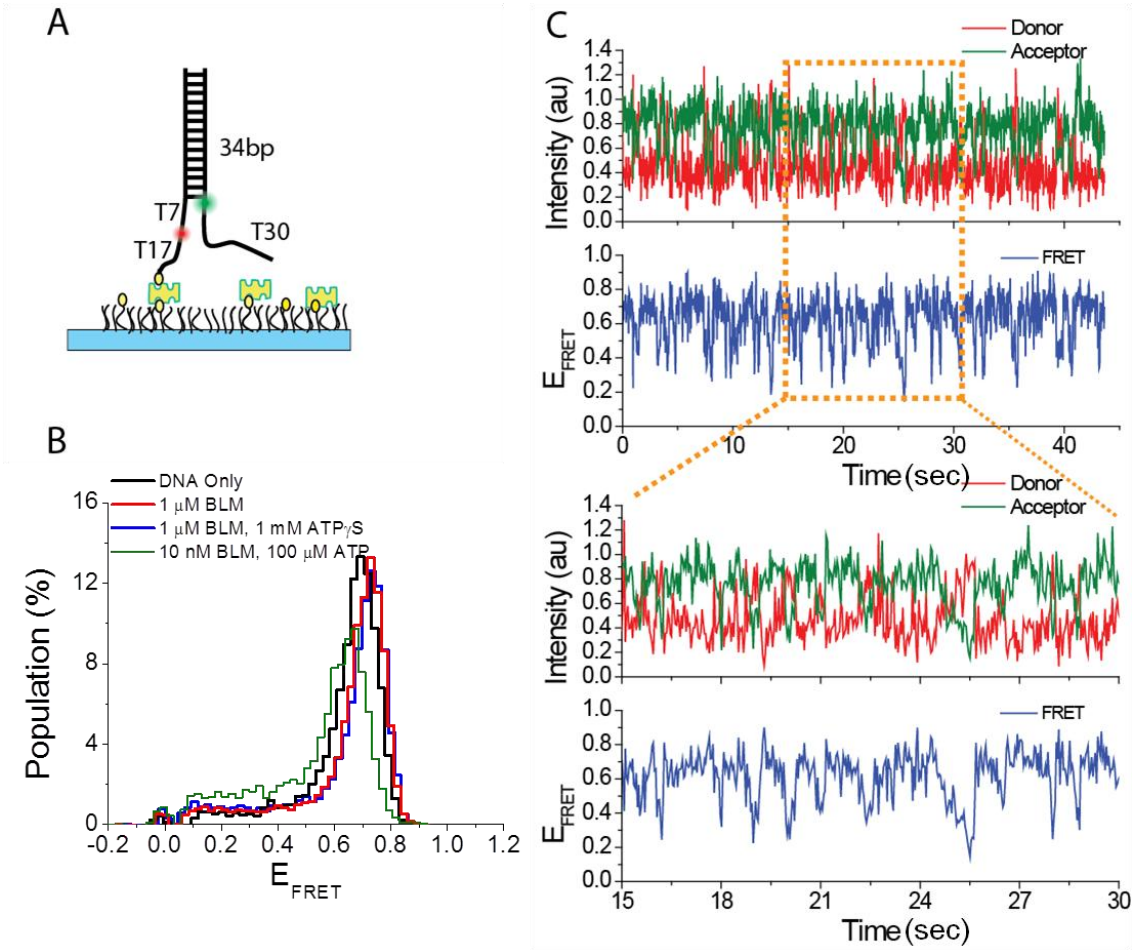

Supplementary Figure S7: Control measurements performed to ensure that our assays are not contaminated by ATP that co-purifies with BLM. **(A)** The forked DNA unwinding construct used in these studies. **(B)** BLM does not unwind dsDNA in the absence of ATP. **(C)** BLM catalyzes repetitive unwinding events only in the presence of ATP. The bottom panel is a zoomed in version of the top panel in the time interval between 15-30 seconds.

SDS-PAGE Measurements of Purified BLM

The purity of the BLM used in the single molecule FRET measurements was analyzed by 12% SDS-PAGE. Figure S8, displays a coomassie-stained 12% SDS-PAGE of core-BLM (1-5 μg) from which we estimate purity at >98%. Based on this, it is highly unlikely that BLM used in this study is contaminated with other proteins which are known to destabilize GQ in the absence of ATP, such as ssDNA binding proteins.

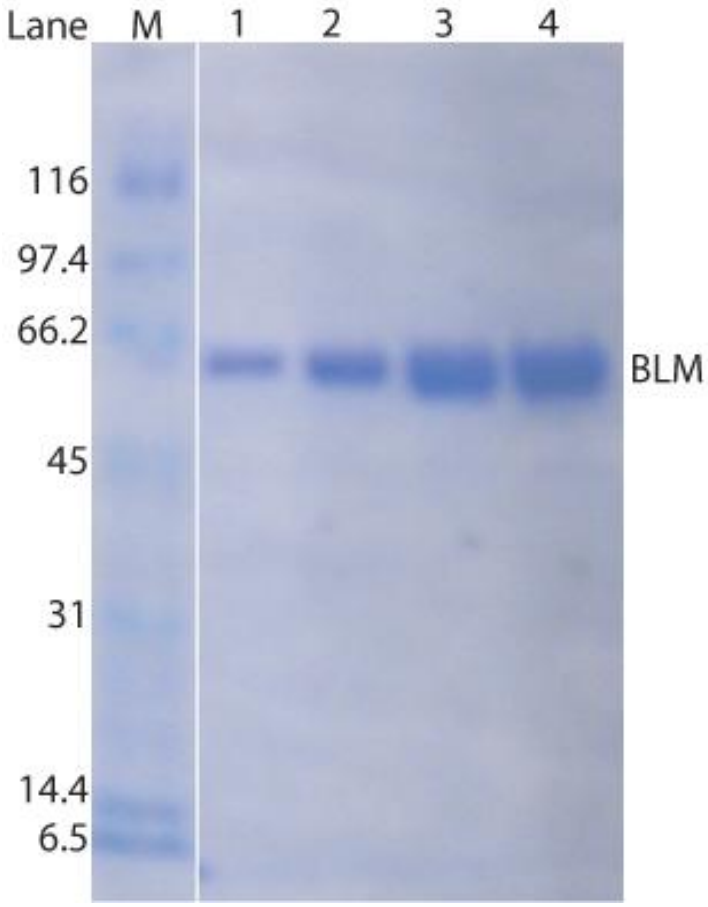

Supplementary Figure S8: Coomassie-stained 12% SDS-PAGE gel of purified Core BLM for assessment of BLM purity. Lane M includes protein size standards with the indicated molecular weight (kD). Lanes 1, 2, 3, and 4 contain 1, 2, 4, and 5 μg purified core BLM, respectively. A single band (estimate > 98% pure) is observed at the expected molecular weight for BLM. Thus , the probability is very low that another protein, such as an ssDNA binding protein that might be capable of unfolding GQ in the absence of ATP, copurifies with BLM.

GQ Unfolding by a BLM Mutant that does not Hydrolyze ATP

In order to directly demonstrate that helicase activity is not required for BLM-mediated GQ unfolding, a BLM mutant which does not hydrolyze ATP was generated by mutating the lysine at aminoacid 695 of $BLM^{(642-1290)}$ with methionine. This construct, BLM^{K695M}, was purified following a similar protocol to that of core BLM. The final BLM^{K695M} stock had a concentration of 1.78 μM and was in a buffer containing 400 mM Na^+. As the protein stock was in Na^+, we performed the smFRET measurements in 150 mM Na^+. In these measurements, the total Na^+ concentration was maintained at 150 mM by adjusting the additional Na^+ added to the sample chamber taking into account the salt that is introduced from the protein stock.

In order to ensure BLM^{K695M} does not have helicase activity, we introduced ATP and BLM^{K695M} to chamber that has surface immobilized pd-hGQ12T, which has a 3' tail. Under these circumstances, an active helicase would unfold the GQ and unwind the duplex stem, releasing the Cy3 strand. The Cy5 strand will continue to remain on the surface as it is bound via a biotin-neutravidin linker. We monitored the number of molecules that had Cy3 or Cy5 before and after adding 250 nM BLM^{K695M} and 1 mM ATP to the chamber. The Cy5 molecules were directly imaged by a red (632.8 nM) excitation laser, while green (532 nm) excitation illuminates all Cy3 and some Cy5 molecules (those that are within FRET range of an active Cy3 molecule). We did not observe any significant change in the number Cy3 molecules upon addition of BLM^{K695M} and ATP, which demonstrates that the duplex was not unwound by BLM^{K695M} (Figure S9). On the other hand, adding 250 nM core-BLM and 1 mM ATP to the same chamber nearly eliminated all Cy3 molecules while no significant change was observed in the number of Cy5 molecules, clearly demonstrating helicase activity.

Figure S10A-E show interactions of BLM^{K695M} with GQ in the nt-free state. The folded state in the absence of protein has a single high FRET peak (Figure S10-A), and introducing BLM^{K695M} at different concentrations results in a lower FRET peak representing the unfolded GQ population (Figure S10B-D). As BLM^{K695M} cannot hydrolyze ATP, even if there is ATP contamination in the protein stock it should not be hydrolyzed by BLM^{K695M}. Figure S10-E show the unfolded pd-hGQ12T population as a function of BLM^{K695M} concentration, and the red line is Langmuir isotherm fit to the data which results in α=61% and K_{eq}=133 nM. The unfolding activity of BLM^{K695M} is similar to that of the core-BLM, demonstrating that helicase activity is not required for protein-mediated GQ unfolding.

In order to ensure that this activity is also observed in the presence of K^+, we performed measurements in which the total ion concentration (Na^+ and K^+ in total) is kept at 150 mM. In these measurements, a certain concentration of Na^+ is introduced to the chamber by the protein stock, which was supplemented by the additional K^+ in the imaging buffer to reach a total monovalent ion concentration of 150 mM. For example, when 150 nM BLM^{K695M} is added to the chamber, 30 mM Na^+ is introduced from the protein stock. In order to reach 150 mM concentration, 120 mM K^+ is introduced by the imaging buffer. Similarly, in the case of 300 nM BLM^{K695M}, 60 mM Na^+ is introduced from the protein stock and 90 mM K^+ was added in the imaging buffer. Given that core-BLM shows similar GQ unfolding activity in 150 mM K^+ and 150 mM Na^+, the observed GQ unfolding in these cases should be similar to 150 mM Na^+ case. We tested 150 nM and 300 nM BLM^{K695M} in the ion concentrations stated above and obtained similar GQ unfolding to the 150 mM Na^+ case, as expected. These data are shown in Figure S10-F.

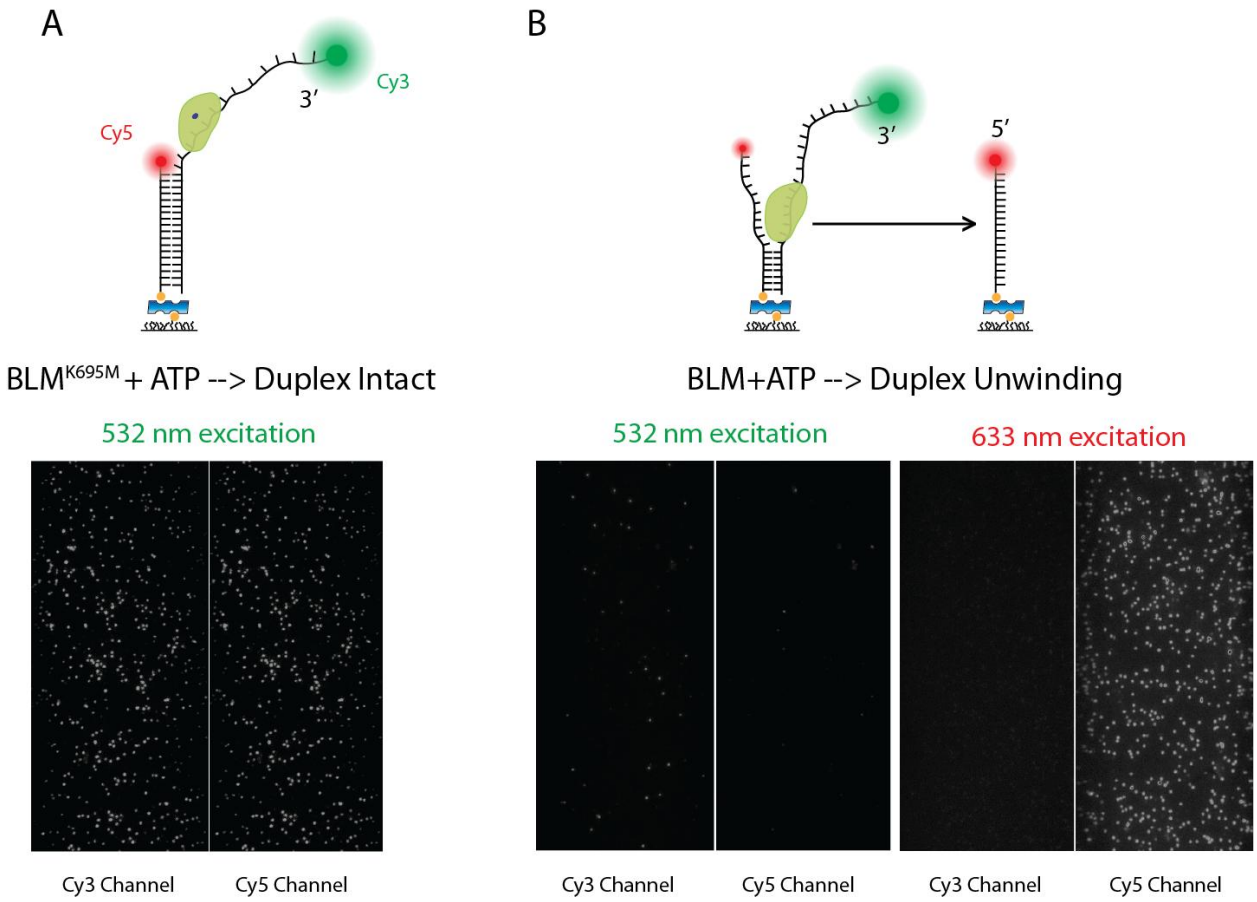

Supplementary Figure S9: smFRET measurements demonstrating that BLM^{K695M} does not unwind duplex DNA in the presence of ATP, while core-BLM unwinds the duplex DNA under the same conditions. Duplex unwinding is demonstrated by the release of the Cy3 strand from the surface, while the Cy5 strand remains bound.

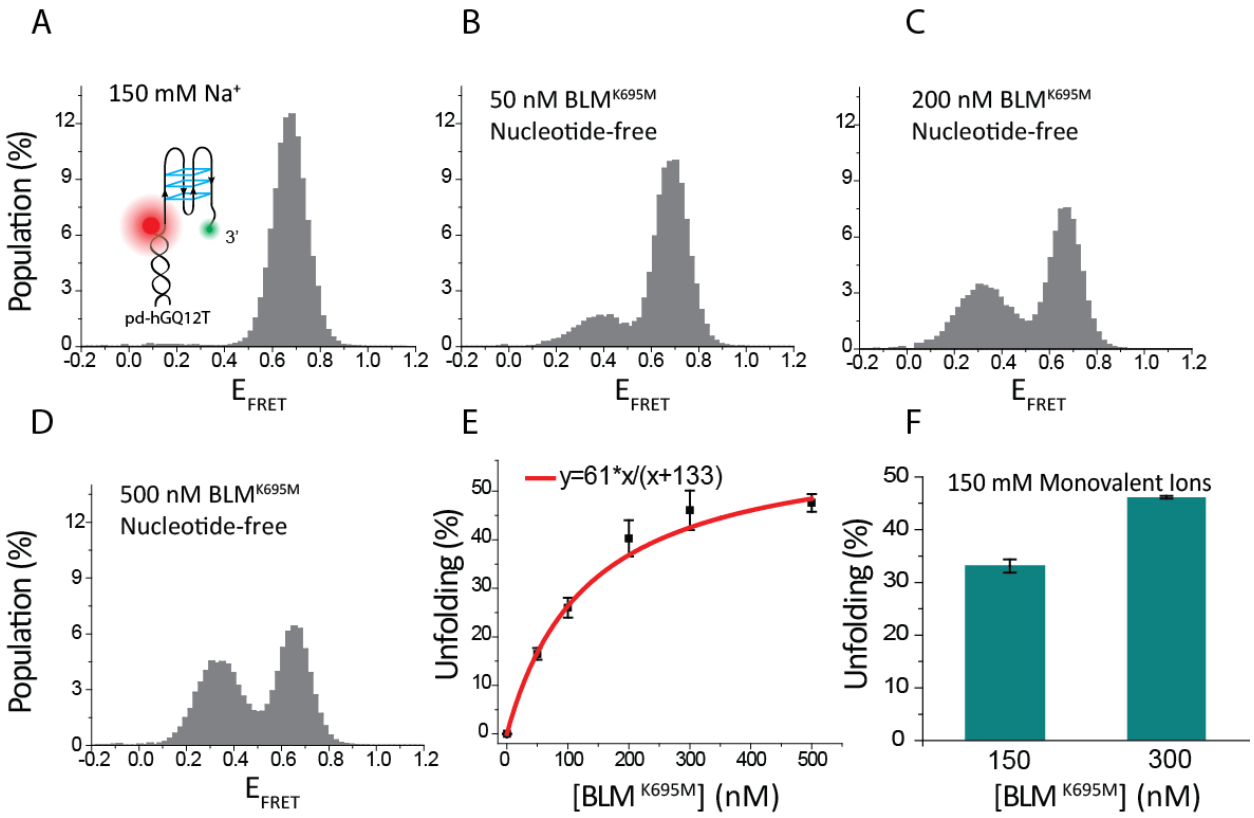

Supplementary Figure S10: smFRET measurements on pd-hGQ12T in 150 mM Na^+ at 0, 50, 200, and 500 nM BLM^{K695M} are shown in **(A)-(D)**, respectively. The data was taken in the nt-free state. **(E)** Langmuir binding isotherm fit was performed to quantify BLM^{K695M} mediated GQ unfolding activity in the nt-free state. **(F)** The unfolded pd-hGQ12T population is shown in the bar graph for 150 nM BLM^{K695M} (in 30 mM Na^+ and 120 mM K^+) and 300 nM BLM^{K695M}.

BLM-Mediated GQ Unfolding in AMP-PNP State

In order to confirm our results with another non-hydrolysable ATP analog, we performed BLM-mediated GQ interactions in the presence of AMP-PNP. We performed AMP-PNP titration measurements in the presence of 1 μM BLM and quantified the unfolded GQ population by performing subtraction analysis using the 1 μM BLM nt-free state as the reference. These data are shown in Figure S11. A Langmuir binding isotherm fit to the data results in α=18±1 % and K_{eq}=2.1±0.3 nM AMP-PNP. These results are consistent with the ATPγS, another non-hydrolysable ATP analog, measurements reported in Figure 2. Both ATPγS and AMP-PNP resulted in significantly more BLM-mediated GQ unfolding compared to the nt-free state.

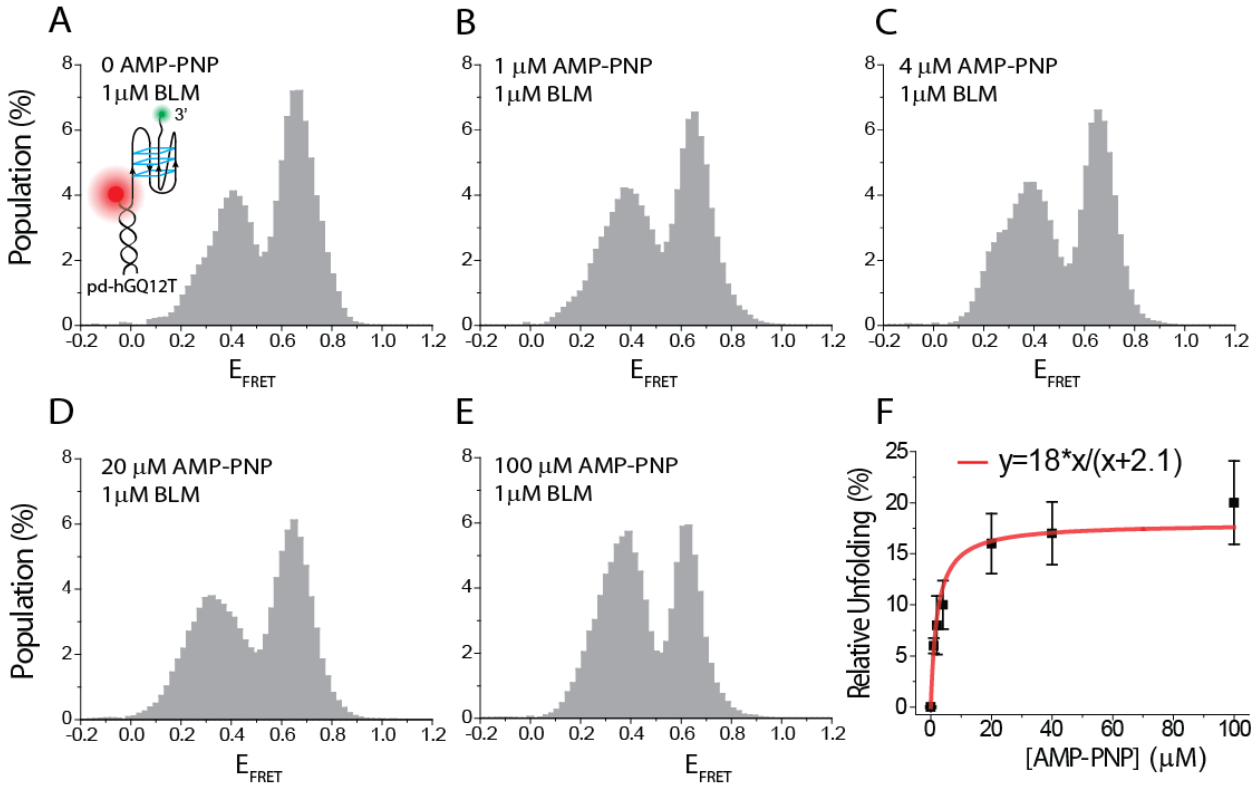

Supplementary Figure S11: smFRET measurements on pd-hGQ12T in 1 μM BLM in 0, 1 μM, 4 μM, 20 μM, and 100 μM AMP-PNP. Langmuir binding isotherm fit is shown in the bottom-right panel.

FRET Histograms and Subtraction Analysis for ATPγS and ADP Titration on pd-hGQ12T

Figure 2 of the manuscript shows sample histograms of BLM-GQ interactions when ATPγS or ADP concentration is titrated at 1 μM BLM concentration for the pd-hGQ12T construct. Figure S12 shows the histograms for the ATPγS and ADP concentrations that were not shown in Figure 2. Figure S13 shows the corresponding histograms of subtraction analysis which we used to quantify BLM-mediated GQ unfolding. The BLM and nucleotide concentration used for each histogram are written on the graph. All experiments were performed at 150 mM K^+. Data were included in the Langmuir isotherms shown in Figure 2.

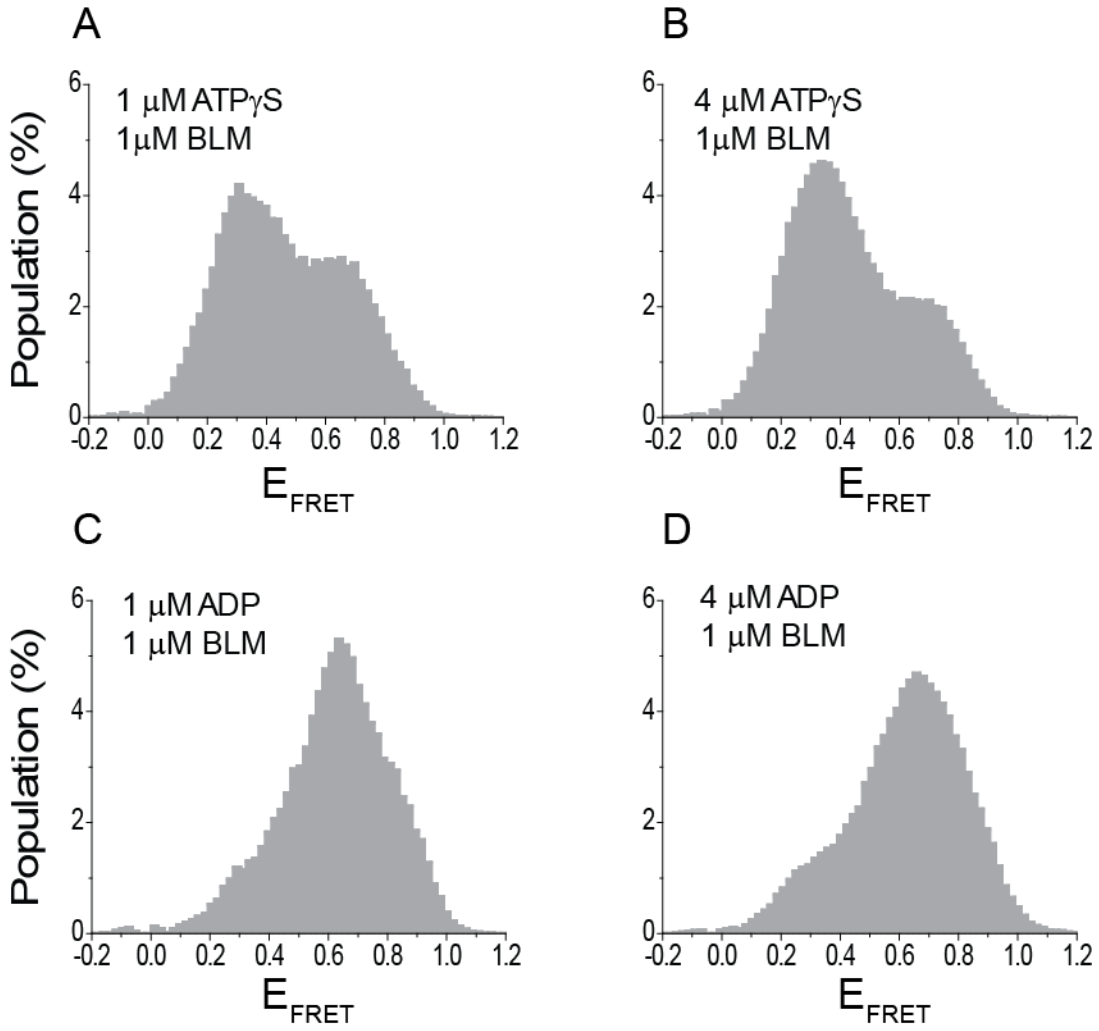

Supplementary Figure S12: smFRET histograms for ATPγS and ADP concentrations we studied, other than those shown in Figure 2 of the manuscript. All data are at 1 μM BLM concentration. **(A)** 1 μM ATPγS. **(B)** 4 μM ATPγS. **(C)** 1 μM ADP. **(D)** 4 μM ADP. The BLM and nucleotide concentrations used for each histogram is indicated on the graphs.

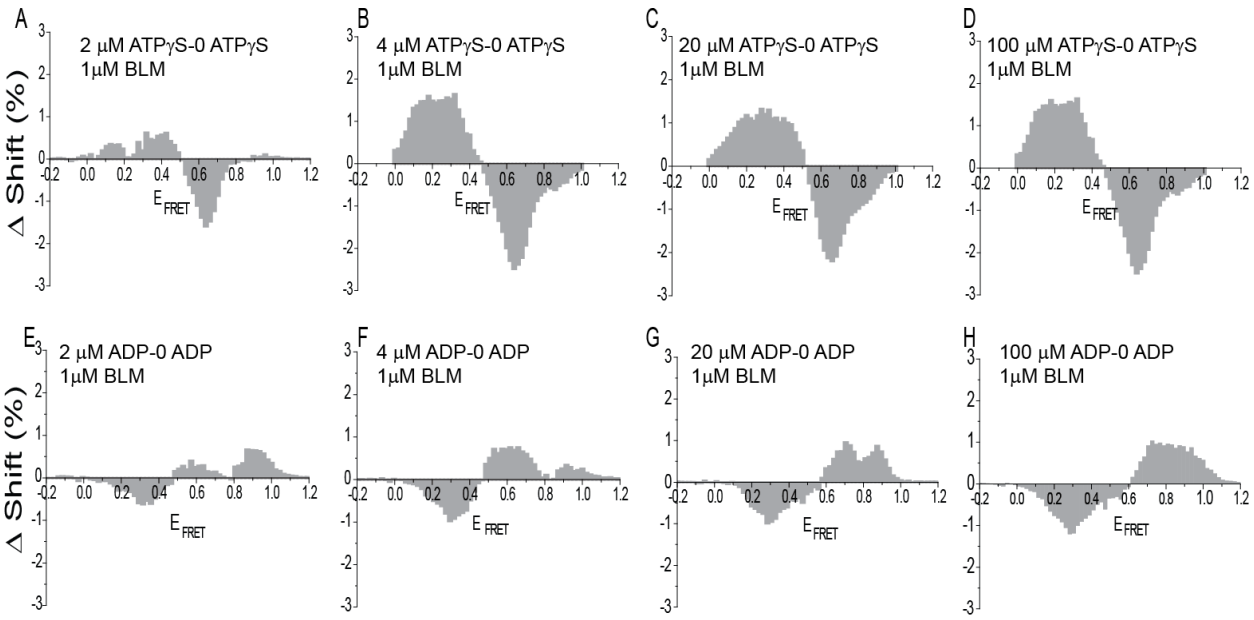

Supplementary Figure S13: Subtraction analysis performed on the data shown in Figure 2 and Figure S12 using the nt-free state at 1 μM BLM concentration as the reference state (Figure 1D of the manuscript). The subtraction analysis was performed for data taken at 2 μM, 4 μM, 20 μM, and 100 μM ATPγS concentrations as shown in **(A)-(D)**, respectively. Similarly, the subtraction analysis was performed for data taken at 2 μM, 4 μM, 20 μM, and 100 μM ADP concentration as shown in **(E)-(H)**, respectively. The BLM and nucleotide concentrations used for each histogram are indicated on the graphs.

smFRET Measurements on a GQ with a 15-nt long overhang

In order to ensure that the measurements on pd-hGQ12T are not compromised by the possibility of the ssDNA overhang being shorter than the BLM footprint, we repeated these measurements on pd-hGQ15T, which has an 15 nt long overhang. This 15 nt overhang is longer than the reported 14 nt footprint (Gyimesi *et al.* Nucleic Acids Research, 38, 4404-4414 (2010)), providing an opportunity for more stable binding of BLM to the overhang. The results of this study are shown in Figure S14. In this figure, we compared BLM-mediated GQ unfolding under different nucleotide-states, at saturating BLM and nucleotide concentrations. Figure S14A shows that the GQ stably folds at 150 mM K^+ and pH 7.5, even though GQ stability is known to decrease as the overhang gets longer (Hatzakis et al. Biochemistry, 49, 9152-9160 (2010)). Moreover, single-molecule time traces in the folding state were observed to be steady over the time of recording (~2 min.), suggesting that the folded GQ is robust even with this overhang. Figure S14B-D show the data in nt-free , 1 mM ATPγS, and 1 mM ADP states, respectively, which were all acquired at a constant BLM concentration of 1 μM. Figure S14-E shows a comparison of BLM-mediated GQ unfolding for different nucleotide states when the folded FRET distribution in Figure S14-A is subtracted from the data in these nucleotide states (similar to the analysis shown in Figure 1E). BLM-mediated GQ unfolding on pd-hGQ15T is most efficient in the ATPγS state (57% of GQ molecules unfolded), followed by nt-free state (48%), and is least efficient in the ADP state (22%), similar to the results with pd-hGQ12T.

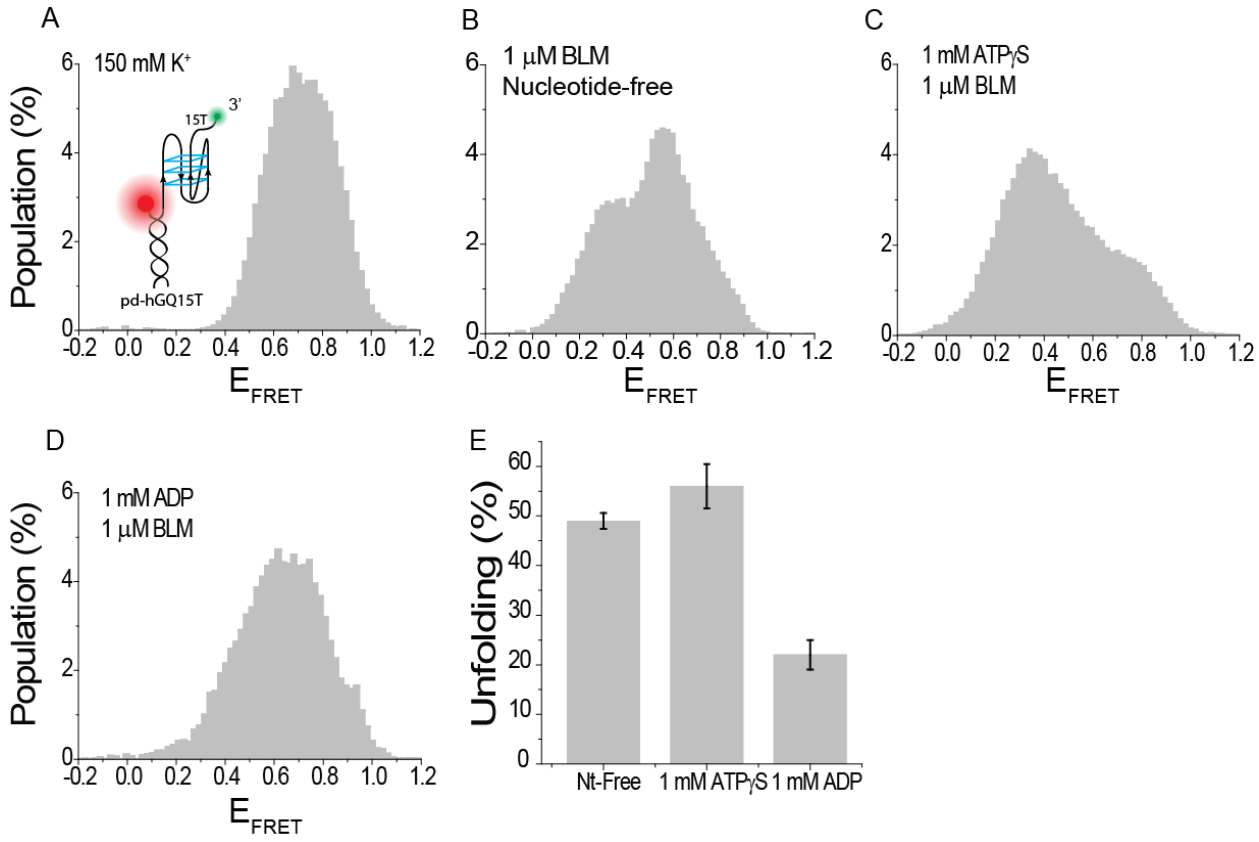

Figure S14. BLM-mediated GQ unfolding on a substrate containing a 15-nt overhang (pd-hGQ15T) at 150 mM K^+. (A) pd-hGQ15T folds into a stable GQ at 150 mM K^+, resulting in a high FRET peak. (B)-(D) smFRET data at 1 μM BLM for different nucleotide states. (B) Nt-free state. (C) 1 mM ATPγS. (D) 1 mM ADP. (E) The folded GQ data shown in (A) is subtracted from respective nucleotide states shown in (B)-(D) to obtain the unfolded populations in these nucleotide states.

FRET Histograms and Subtraction Analysis for BLM and ATPγS Titration in 50 mM K^+ for pd-hGQ12T

Figure S15 shows the histograms for ATPγS and BLM concentrations for pd-hGQ12T construct at 50 mM K^+. Figure S16 shows the corresponding histograms of subtraction analysis which we used to quantify BLM-mediated GQ unfolding. The nucleotide and BLM concentrations used for each histogram are indicated on the graphs.

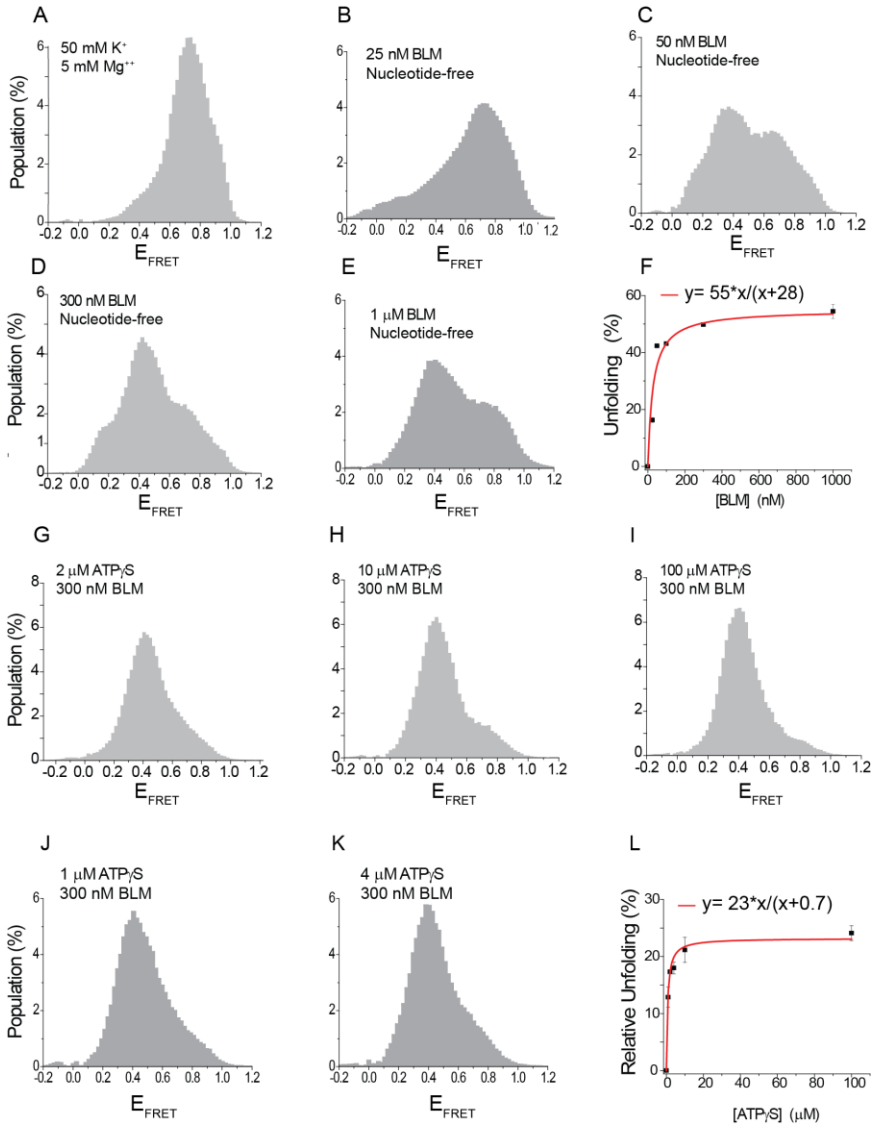

Supplementary Figure S15: smFRET histograms showing the ATPγS and BLM concentrations we studied. All data were taken at 50 mM K^+. **(A)-(E)** Data at the nt-free state where BLM is titrated at 0, 25 nM, 50 nM, 300 nM, and 1 μM concentration, respectively. **(F)** Langmuir binding isotherm fit to the data shown in (A)-(E). **(G)-(K)** Data in the presence of 300 nM BLM where ATPγS is titrated at 1 μM, 2 μM, 4 μM, 10 μM, and 100 μM, respectively. **(L)** Langmuir binding isotherm fit to the data shown in (G)-(K).The nucleotide and BLM concentration used for each histogram is indicated on the graphs.

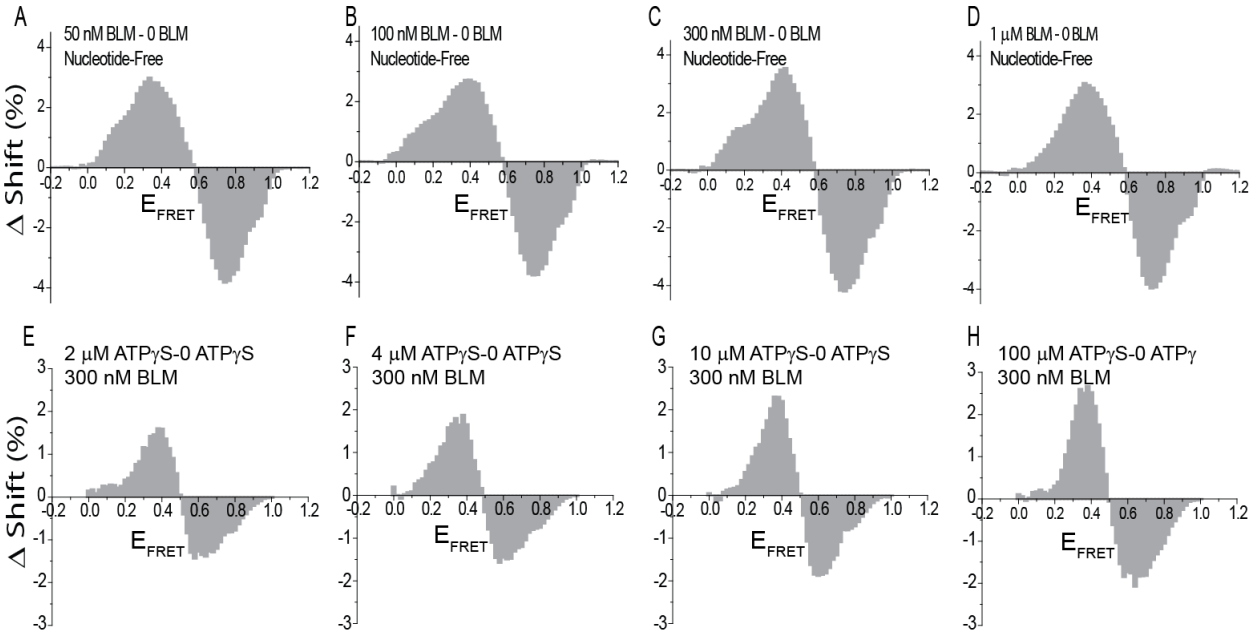

Supplementary Figure S16: Subtraction analysis performed on the data shown in Supplementary Figure S15. Four representative concentrations for BLM or ATPγS titration are shown. **(A)-(D)** Subtraction analysis for data taken at 50 nM, 100 nM, 300 nM, and 1 μM BLM concentration in the nt-free state, respectively. The reference state for this analysis was the nt-free state in the absence of BLM. **(E)-(H)** Subtraction analysis performed for data taken at 2 μM, 4 μM, 10 μM, and 100 μM ATPγS concentration, respectively, in the presence of 300 nM BLM. The nt-free state, e.g. zero ATPγS, in the presence of 300 nM BLM was used as the reference state for the subtraction analysis in (E)-(H). The BLM and ATPγS concentration used for each histogram are indicated on the graphs.

Quantifying the Change in BLM Binding Affinity to ssDNA at 150 mM K^+ *vs*. 50 mM K^+

Reducing the monovalent ion concentration from 150 mM to 50 mM does not only reduce the GQ stability but also increases the binding affinity of BLM to the overhang ssDNA. As both effects would result in increased BLM-mediated GQ unfolding in 50 mM, we sought to estimate the relative contribution of each effect. We used a partial duplex DNA with a 15 nt long unstructured polythymine ssDNA segment for these studies (pd-polyT15), and measured the equilibrium constant of BLM for 50 mM and 150 mM Na^+. Figure S17 shows these data which result in a 4.7 fold increase in K_{eq} in 150 mM Na^+ compared to 50 mM Na^+. In comparison BLM-mediated GQ unfolding increased by 10.8 fold in 50 mM K^+ compared to 150 mM K^+. Therefore, we conclude that the GQ stability contributes approximately a factor of 2.3 in this 10.8 fold increase in K_{eq}.

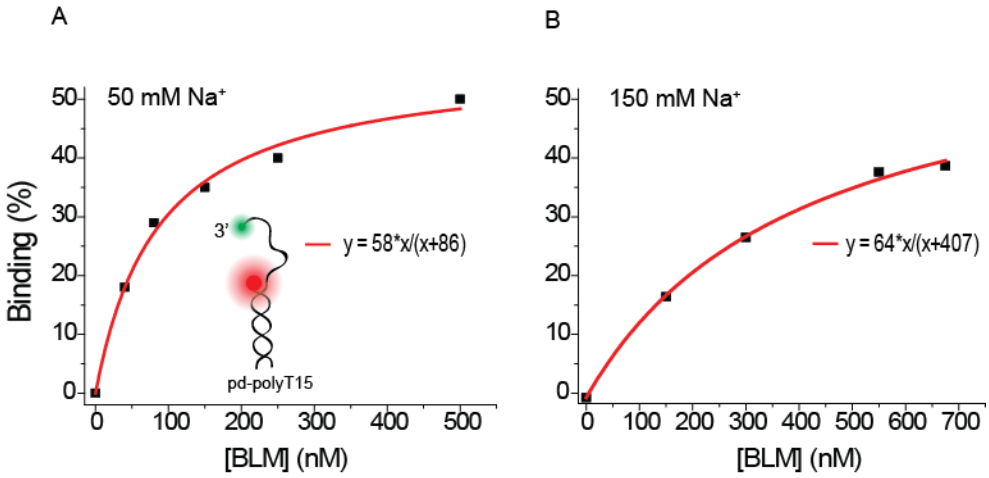

Supplementary Figure S17: The change in BLM binding affinity to ssDNA due to lower ionic strength is characterized by an smFRET assay. BLM binding to pd-polyT15 is quantified in **(A)** 50 mM Na^+ and **(B)** 150 mM Na^+. The fits are Langmuir binding isotherms.

BLM Binding to a Partial Duplex DNA with 5'-end

In order to determine whether the reduced BLM-mediated GQ unfolding observed for the GQ construct with 5' overhang is related to the ability of BLM to bind the 5'-overhang, we performed smFRET measurements similar to those presented in Figure 3 of the manuscript. Figure S18 shows these data and a schematic of the construct used in these studies, pd-polyT15-5', which is a partial duplex DNA with 15 thymine long ssDNA overhang with 5' polarity. pd-polyT15-5' is formed by hybridizing polyT15-5' and DNA-Stem strands given in Table 1. Figure S18-A shows that 1 μM BLM does not bind to pd-polyT15-5' in 150 mM K^+ in the nt-free state. The data representing these conditions are shown with dashed red curve in Figure S18-A as this curve has a nearly perfect overlap with the black solid curve representing the folded state in the absence of BLM. The solid blue curve in Figure S18-A represents the 1 mM ATPγS state which shows a small amount of BLM binding to the overhang. Reducing the K^+ concentration to 50 mM did not have a significant influence on BLM-binding to pd-polyT15-5' in the nt-free state however, significant binding (53%) is observed in the 1 mM ATPγS state (Figure S18-B).

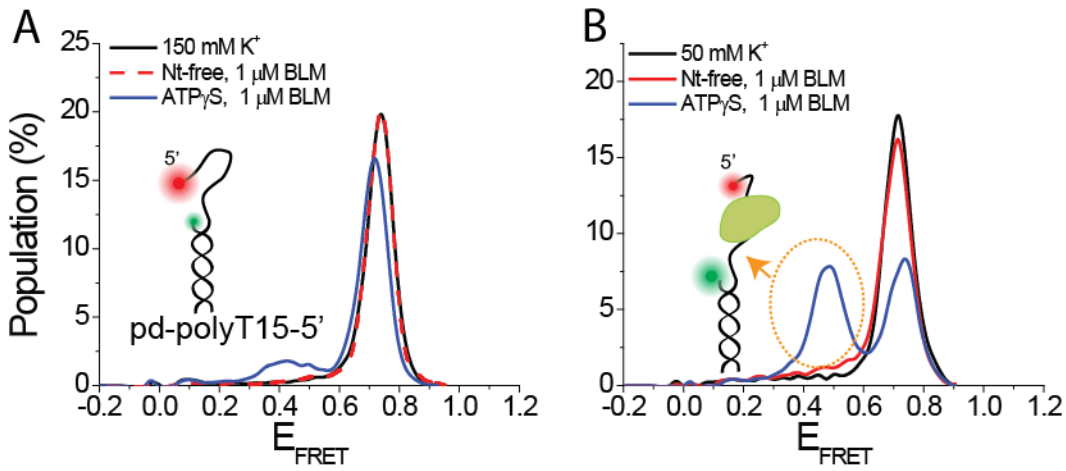

Supplementary Figure S18: BLM binding to pd-polyT15-5' in 150 mM and 50 mM K^+. **(A)** 1 μM BLM does not bind to pd-polyT15-5' in the nt-free state in 150 mM K^+, but a small amount of binding is observed in 1 mM ATPγS. (B) Reducing the ion concentration to 50 mM K^+ results in significant BLM binding in the ATPγS state (blue curve) but not in the nt-free state (red curve).

Interactions of *E. coli* RecQ and human RECQ5 with GQ

Figure 7 of the manuscript shows interactions of *E. coli* RecQ and human RECQ5 with pd-hGQ12T in 50 mM Na^+. These measurements were initially performed with 50 mM K^+ or 150 mM K^+, which resulted in no detectable GQ unfolding. Figure S19 shows these data in 50 mM K^+ for RecQ and 150 mM K^+ for RECQ5 in both nt-free and 1 mM ATPγS states. For both RecQ and RECQ5 cases, the FRET peak representing the folded state shifts towards lower FRET. However, this shift is not large enough to account for GQ unfolding and most likely represents binding of RecQ or RECQ5 to the overhang. As shown in Figure S1, the unfolded state for a DNA of this length in 50 mM K^+ should have E_{FRET}<0.40 since the unfolded state at 150 mM K^+ has E_{FRET}=0.40. The protein bound state should have $E_{FRET} \approx 0.20$. Since the shift we observe results in E_{FRET} >0.40, these shifts do not represent unfolding of the GQ.

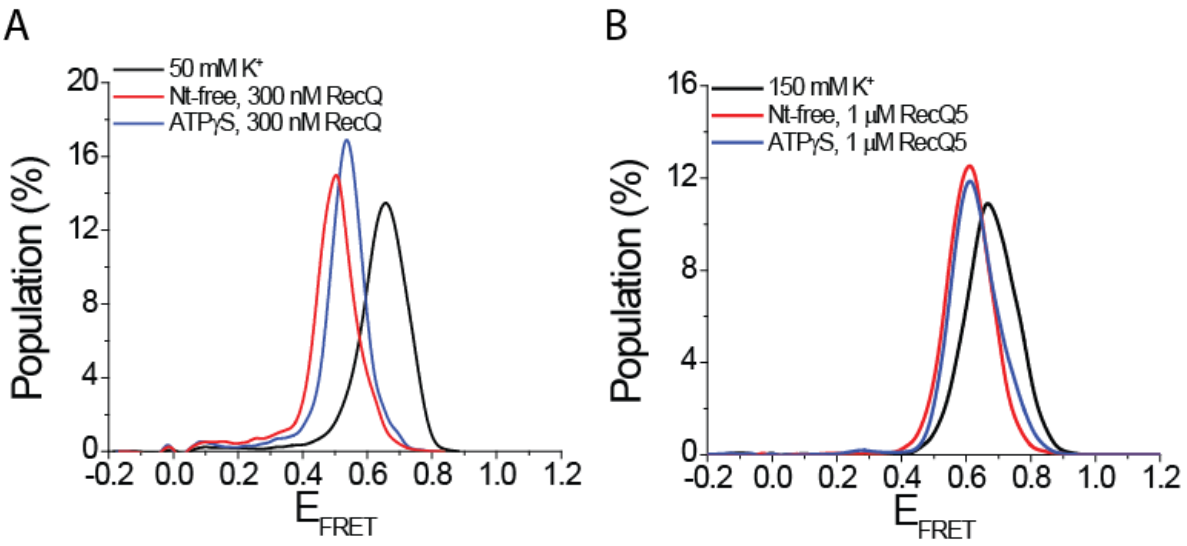

Supplementary Figure S19: smFRET histograms showing interactions of RecQ and RECQ5 with pd-hGQ12T in nt-free and ATPγS states. (A) 300 nM RecQ does not unfold this GQ in 50 mM K^+ in either nt-free or ATPγS state. The shift towards lower FRET upon adding RecQ represents binding of RecQ to the 12 nt overhang. (B) 1 μM RECQ5 does not unfold pd-hGQ12T in either nt-free or ATPγS states. The slight shift towards lower FRET upon adding RECQ5 represents binding of RECQ5 to the 12 nt overhang.

BLM-GQ Complex Remains Dynamic at All BLM Concentrations

smFRET time traces were examined to determine whether at high BLM concentrations, multiple BLM molecules bind to the ssDNA that becomes available upon GQ unfolding. This would essentially result in a permanently unfolded GQ state. However, smFRET time traces show that even at 1 μM BLM the system remains dynamic in saturating nucleotide concentrations. Figure S20 shows three example time traces that demonstrate these dynamics in the nt-free, 100 μM AMP-PNP, or 100 μM ATPγS. These data demonstrate that GQ unfolds and refolds multiple times within 1-2 minute observation time, ruling out the possibility that GQ is locked in a permanently unfolded state.

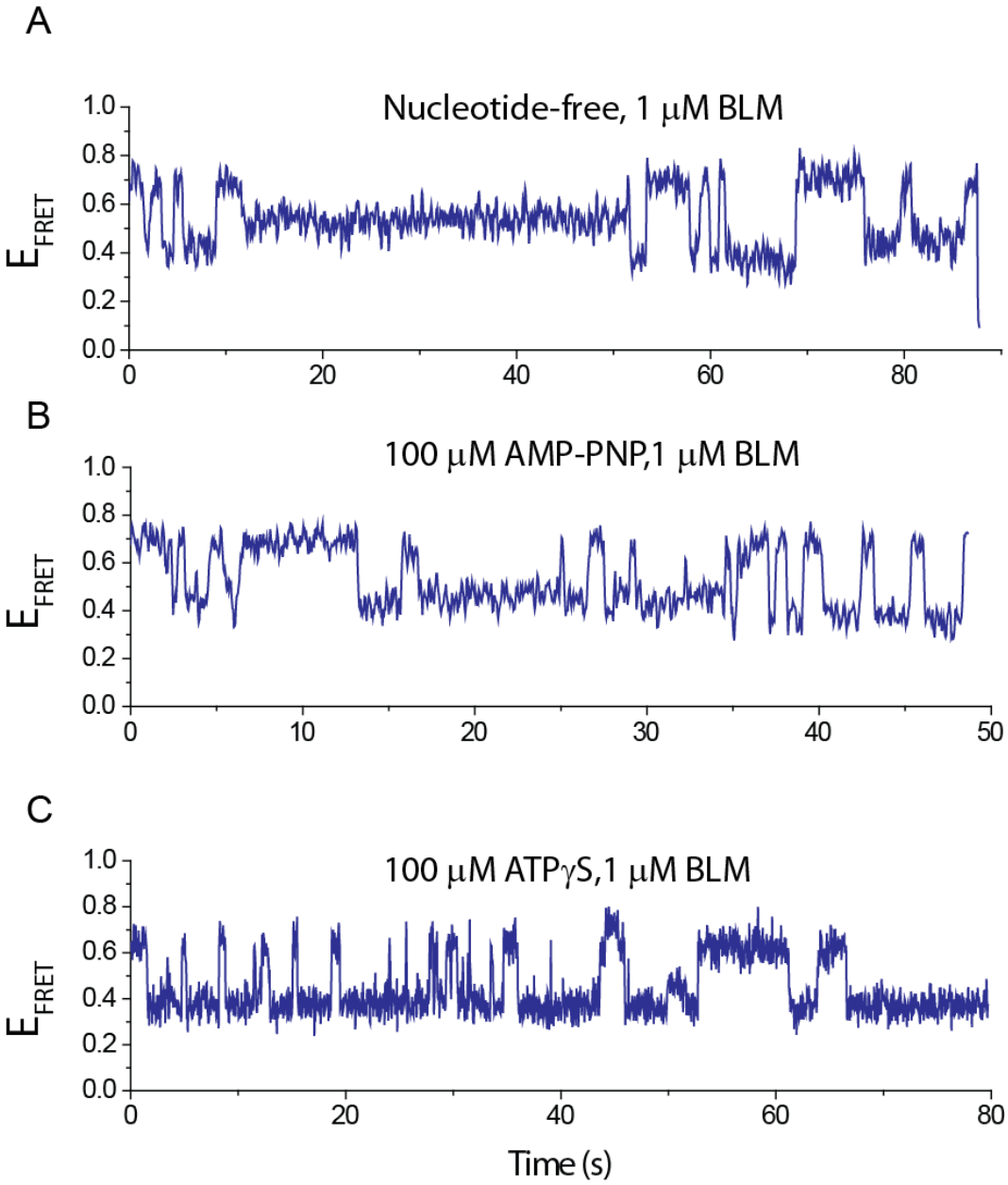

Supplementary Figure S20: Example smFRET time traces in 1 μM BLM in **(A)** Nt-free; **(B)** 100 μM AMP-PNP; and **(C)** 100 μM ATPγS. The dynamics observed in such traces demonstrate that GQ is not permanently unfolded due to binding of multiple BLM molecules.

Published online 12 August 2010 *Nucleic Acids Research, 2010, Vol. 38, No. 22* ***8131–8140***
doi:10.1093/nar/gkq697

RECQ5 helicase associates with the C-terminal repeat domain of RNA polymerase II during productive elongation phase of transcription

Radhakrishnan Kanagaraj[1], Daniela Huehn[1], April MacKellar[2], Mirco Menigatti[1], Lu Zheng[1], Vaclav Urban[3], Igor Shevelev[3], Arno L. Greenleaf[2] and Pavel Janscak[1,3,*]

[1]Institute of Molecular Cancer Research, University of Zurich, CH-8057 Zurich, Switzerland, [2]Department of Biochemistry, Duke University Medical Center, Durham, NC 27710, USA and [3]Institute of Molecular Genetics, Academy of Sciences of the Czech Republic, 143 00 Prague, Czech Republic

Received April 28, 2010; Revised July 15, 2010; Accepted July 22, 2010

ABSTRACT

It is known that transcription can induce DNA recombination, thus compromising genomic stability. RECQ5 DNA helicase promotes genomic stability by regulating homologous recombination. Recent studies have shown that RECQ5 forms a stable complex with RNA polymerase II (RNAPII) in human cells, but the cellular role of this association is not understood. Here, we provide evidence that RECQ5 specifically binds to the Ser2,5-phosphorylated C-terminal repeat domain (CTD) of the largest subunit of RNAPII, RPB1, by means of a Set2–Rpb1-interacting (SRI) motif located at the C-terminus of RECQ5. We also show that RECQ5 associates with RNAPII-transcribed genes in a manner dependent on the SRI motif. Notably, RECQ5 density on transcribed genes correlates with the density of Ser2-CTD phosphorylation, which is associated with the productive elongation phase of transcription. Furthermore, we show that RECQ5 negatively affects cell viability upon inhibition of spliceosome assembly, which can lead to the formation of mutagenic R-loop structures. These data indicate that RECQ5 binds to the elongating RNAPII complex and support the idea that RECQ5 plays a role in the maintenance of genomic stability during transcription.

INTRODUCTION

The numerous processes that occur in the nucleus during cell proliferation have to be tightly coordinated to ensure genome integrity and faithful genome propagation. Transcription is known to stimulate DNA recombination, thus affecting genome stability (1). This phenomenon, called transcription-associated recombination (TAR), has been linked to replication fork pausing that results from the convergence of transcription and replication. TAR has also been linked to the formation RNA : DNA hybrids (R-loops) between the nascent transcript and the template DNA strand, which increases the susceptibility of the non-transcribed strand to damage or to the formation of secondary structures that impair replication fork progression (1). R-loops are formed when the co-transcriptional assembly of mRNA-particle complexes is impaired (1). For example, it has been shown that inactivation of the human SR protein ASF/SF2, which is required for spliceosome assembly, results in DNA fragmentation, cell-cycle arrest and genomic instability as a consequence of R-loop formation (2). ASF/SF2 depletion also leads to accumulation of stalled replication forks, and chromosome breaks caused by ASF/SF2 deficiency occur specifically in S-phase, preferentially at gene-rich regions (3). These data suggest that TAR results as a consequence of replication fork collapse at R-loops (3).

RECQ5 belongs to the RecQ family of DNA helicases that play critical roles in the maintenance of genomic stability and cancer suppression (4). Recent studies in mammalian cells have established RECQ5 as an important anti-recombination factor that acts by controlling the assembly of the RAD51 filament on single-stranded DNA (ssDNA), which catalyses the homology search and strand invasion during homologous recombination (HR) (5,6). RECQ5 binds directly to the RAD51 recombinase and disrupts the RAD51-ssDNA filament in a reaction driven by ATP hydrolysis, thus preventing homologous duplex invasion during HR (6). In accordance with this finding, RECQ5-deficient cells versus RECQ5-proficient cells show an increased efficiency of HR-mediated DNA double-strand break (DSB) repair, an elevated frequency of sister chromatid exchange, a prolonged persistence of RAD51 foci in response to DNA damage and an increased rate of chromosomal

*To whom correspondence should be addressed. Tel: +41 (0)44 635 3470; Fax: +41 (0)44 635 3484; Email: pjanscak@imcr.uzh.ch

rearrangements (5,6). Moreover, RECQ5 has been shown to accumulate at sites of DSBs and sites of replication arrest in a manner dependent on the MRE11–RAD50–NBS1 complex, a key player in DNA damage signaling and repair (7).

A number of recent proteomic studies have revealed that RECQ5 forms a stable complex with RNA polymerase II (RNAPII) in human cells (7–9). The RECQ5–RNAPII interaction is direct and is mediated by the largest subunit of RNAPII, RPB1 (8). Knockdown of the RECQ5 transcript in human cells has been found to increase the transcription of several genes (9). Likewise, RECQ5 has been shown to inhibit RNAPII transcription in an *in vitro* system reconstituted using purified proteins (10). Despite these findings, the function of RECQ5 during the RNAPII transcription cycle remains elusive.

Here, we provide evidence that RECQ5 associates with RNAPII during the productive elongation phase of transcription through direct binding to the C-terminal repeat domain (CTD) of RPB1. Moreover, we show that depletion of RECQ5 reduces the cellular sensitivity to diospyrin, a plant-derived bisnaphthoquinonoid, which interferes with spliceosome assembly, presumably by inhibiting DNA topoisomerase I (Top1)-mediated phosphorylation of ASF/SF2, and hence is likely to promote formation of R-loops during RNAPII transcription (3,11). These findings are discussed in light of a possible role for RECQ5 in promoting genomic stability at sites of RNAPII transcription.

MATERIALS AND METHODS

Plasmids, proteins and antibodies

The vector pTXB1 (New England Biolabs) was used for bacterial expression of wild-type and mutant forms of human RECQ5 as fusions with the self-cleaving chitin-binding domain (CBD) tag. Construction of these plasmids was previously described (12). The expression vector for RECQ5 Δ908–954 (ΔSRI) was constructed in the same way as the vector for RECQ5 Δ640–653 (12). Point mutations in RECQ5 were made using QuickChange Site-Directed Mutagenesis Kit (Stratagene). The vector pLexA-Km (Dualsystems) was used for construction of the yeast two-hybrid bait plasmids carrying different parts of the human RECQ5 cDNA. RECQ5 cDNA was amplified by PCR and ligated in pLexA-Km via EcoRI and SalI sites in frame with a LexA DNA-binding domain. Internal deletions and point mutations of RECQ5 were subcloned from the pTXB1 constructs. To express RECQ5 and its mutants in human cells as N-terminal fusions with green fluorescent protein (GFP), the respective RECQ5 cDNA cloned in the pTXB1 vector was PCR amplified using Phusion high-fidelity DNA polymerase (Finnzymes) and the following set of primers: 5′-AAACTCGAGCTATGAGCA GCCACCATACC-3′ and 5′ AAAGAATTCTCTCTGG GGGCCACACAGGCCTAA-3′. The resulting amplicon was digested and cloned into pEGFP-C1 (Clontech) between the XhoI and EcoRI sites. The RECQ5 protein and its mutants were produced in bacteria as fusions with CBD and purified as described previously (13). The antibodies used in this study are listed in Supplementary Table S1.

Cell culture

HeLa, HEK293 and HEK293T cells were maintained in DMEM (Gibco) containing 5% fetal calf serum (Gibco) and 100 U/ml penicillin/streptomycin. Transfections of HEK293 cells were carried out using the TransIT®-LT1 reagent according to the manufacturer's instructions (Invitrogen). Transfection efficiency was >90% as determined by visualization of GFP expression using a fluorescence microscope 48 h post-transfection. Transfection of siRNA oligonucleotides (Microsynth) was carried out using Lipofectamine RNAiMAX (Invitrogen) according to manufacturer's instructions. The following oligonucleotides were used: siRECQ5#1 (sense strand): 5′-CA GGAGGCUGAUAAAGGGUUA-3′; siRECQ5#2 (sense strand): 5′-GGAGAGUGCGACCAUGGCU-3′; and siCtrl (sense strand): 5′-CGUACGCGGAAUACUUC GA-3′.

Yeast two-hybrid assay

The yeast two-hybrid screen for proteins that interact with RECQ5 was carried out using *Saccharomyces cerevisiae* strain L40 (*MAT*a *trp1 leu2 his3 LYS2*::*lexA-HIS3 URA3*::*lexA-lacZ*), which was sequentially transformed with the bait plasmid encoding the LexA-RECQ5 411-991 and a randomly primed human peripheral blood cDNA library cloned into the BglII sites of pACT (Clontech). Among the 1.4×10^7 transformants tested for histidine prototrophy and β-galactosidase staining, 198 positive clones were found. Clones carrying the bait and prey plasmids were tested for β-galactosidase activity using a pellet X-gal (PXG) assay as previously described (14).

Far western assay

Far western assays were performed as described previously (15). Briefly, duplicate samples of ∼1.5 μg of the purified proteins were separated on a 4–20% Criterion gel (Bio-Rad). One half of the gel was stained with Coomassie brilliant blue and the second half was transferred to nitrocellulose membrane. The membrane was incubated overnight at 4°C in blocking/renaturation buffer, containing 1× PBS, 3% non-fat dry milk, 0.2% Tween 20, 0.1% PMSF, 5 mM NaF and 2 mM dithiothreitol. The nitrocellulose was then probed with ≥300 000 cpm [^{32}P]-labeled GSTyCTD fusion protein that had been hyperphosphorylated with CTDK-I for 4 h at 4°C. After extensive washing, the nitrocellulose was air-dried and subjected to autoradiography.

Immobilized CTD peptide binding assay

Synthetic biotinylated peptides were dissolved in PBS and incubated with 300 μl of TetraLink Tetrameric Avidin Resin (Invitrogen) for 45 min at room temperature (RT). The peptide concentrations in the column onput, flow-through and wash fractions were monitored by

absorbance at 280 nm and these values were used to approximate the amount of peptide on the column. Generally, 30–50 μg of biotinylated peptide was conjugated to the 300 μl column. The peptide columns were stored in PBS at 4°C and were stable for ~2 months. Approximately 10–15 μg of purified protein and 50 mg insulin were dissolved in PBS for a final volume of 500 μl as the onput; 450 μl of the onput was applied to the peptide resin and incubated for 20 min at RT with mixing every for 5 min. The flow-through and two washes with half-column volumes of PBS were collected. The resin was then extensively washed with 5 ml of buffer containing 25 mM HEPES (pH 7.6), 8% glycerol, 150 mM NaCl and 0.1 mM EDTA (HGNE150). The bound protein was then eluted with four half-column volumes of HGNE300 and four half-column volumes of HGNE1000. The resin was regenerated with 5 ml HGNE1000 and 5 ml PBS. Samples were analyzed by SDS–PAGE followed by Coomassie blue staining.

CBD pull-down assay

CBD-tagged RECQ5 and its variants were produced in *Escherichia coli* BL21-CodonPlus(DE3)-RIL cells (Stratagene) and immobilized on chitin beads (20 μl; New England Biolabs) as previously described (7). Beads were incubated for 2 h at 4°C with a total extract from HEK293 T cells (600 μg of protein) in a volume of 500 μl of buffer TN2 [50 mM Tris–HCl (pH 8), 120 mM NaCl, 20 mM NaF, 15 mM sodium pyrophosphate and 0.5% (v/v) NP-40] supplemented with 1 mM benzamidine, 0.2 mM PMSF, 0.5 mM sodium orthovanadate and protease inhibitor cocktail (Roche) and then were washed three times with buffer TN2. Bound proteins were released from the beads by addition of 25 μl of 3× SDS-loading buffer followed by incubation at 95°C for 7 min. Eluted proteins were separated by 10% SDS–PAGE and analyzed by western blotting using the indicated antibodies. RECQ5 was detected by Ponceau S staining.

Chromatin immunoprecipitation

Chromatin immunoprecipitation (ChIP) assays were performed using the ChIP-IT Express kit from Active Motif (Carlsbad, CA, USA) according to manufacturer's instructions. Briefly, HeLa or 293 (mock or GFP-RECQ5 transfected) cells grown to 70-80% confluency were crosslinked with 1% formaldehyde (Sigma) at RT for 10 min, and glycine (0.125 M) was added to stop the reaction. Isolated nuclei were then sheared using a Bioruptor sonicator (Diagenode, Liege, Belgium) to obtain chromatin fragments between 200 and 500 bp. Ten percent of the sonicated chromatin was reserved for use as an input DNA control. For each ChIP reaction, ~6.3 μg of crosslinked chromatin were immunoprecipitated overnight at 4°C with 4 μg of a specific antibody or control IgG. After elution of immune complexes and reversion of crosslinking, DNA was recovered by using the QIAquick PCR Purification Kit (Qiagen).

Quantitative real-time PCR

The amount of immunoprecipitated DNA in each ChIP reaction was measured by quantitative real-time PCR (qPCR) using a Roche LightCycler 480 Real-Time PCR System and a Roche LightCycler 480 DNA SYBR Green I Master. Primer sequences used for the qPCR reactions are listed in Supplementary Table S2. Specificity of target amplification was confirmed by agarose gel electrophoresis and melting curve analysis. For each primer pair, a series of 5-fold dilutions of input DNA were used to generate a linear standard curve in which the crossing point was plotted versus $\log_{10}$ of template concentration. Primer pair efficiency was calculated from these data as $E = 10^{(-1/\text{slope})}$, and primer pairs with $E > 1.8$ were used for qPCR. For data analysis, Pfaffl's method was used (16). Fold enrichment of immunoprecipitated target regions was expressed as ratio of the amount of DNA estimated for a specific antibody versus the amount of DNA estimated for the control IgG antibody. All qPCR reactions were performed at least six times using DNA template obtained from two independent ChIP experiments. The data were plotted using GraphPad Prism software as mean ± SEM.

Helicase assay

PAGE-purified DNA and RNA oligonucleotides used for helicase assays were purchased from Microsynth. The sequences are: deoxy-18 (d18): 5′-tcc cag tca cga cgt tgt-3′; ribo-18 (r18): 5′-ucc cag uca cga cgu ugu-3′. The oligonucleotides were 5′-end labeled with T4 polynucleotide kinase and γ[^{32}P]ATP (GE HealthCare) and annealed to M13mp2 ssDNA at a 1 : 1 (mol/mol) ratio in the presence of 20 mM Tris–HCl (pH 7.4) and 150 mM NaCl. For helicase assays, RECQ5 at concentrations ranging from 0 to 360 nM was incubated either with 1 nM M13mp2/d18 or with 1 nM M13mp2/r18 substrate for 30 min at 37°C in 10 μl of 33 mM Tris–acetate buffer (pH 7.9) containing 10 mM Mg-acetate, 66 mM K-acetate, 0.1 mg/ml BSA and 2 mM ATP. Helicase reactions were stopped by addition of 2.5 μl of 5× stop dye (100 mM EDTA, 60% glycerol, 1.5% SDS, 0.1% bromophenol blue and 0.1% xylene cyanol). Products were separated by electrophoresis on 15% native polyacrylamide gels in TBE buffer and visualized by autoradiography.

Cell viability assay

Cell viability was measured using Resazurin Fluorimetric Cell Viability Assay Kit (Biotium, Inc.) according to the manufacturer's instructions. Briefly, HeLa cells were seeded at the confluency of 20% in 10-cm plates. After 24 h, cells were transfected with appropriate siRNA as described above. One day after transfection, siRNA-treated cells were harvested and seeded in a 96-well plate at a density of 10 000 cells/well in a volume of 100 μl of DMEM containing fetal calf serum and penicillin/streptomycin. Next day, cells were treated with different concentrations of diospyrin (compound D1; obtained from Dr Banasri Hazra of Jadavpur University, Kolkata) ranging from 0 to 100 μM. Experiments were

carried out in hexaplicates for each drug concentration. After 24 h, cells were washed gently once with pre-warmed PBS, and then a mixture of resazurin and DMEM (100 µl) in a ratio 1 : 10 was added in to each well. After 4 h of incubation at 37°C, cell viability was monitored by measuring fluorescence with excitation wavelength at 540 nm and emission wavelength at 590 nm in a SpectraMax reader M5 (Molecular Devices). The fluorescent signal generated from the assay is directly proportional to the number of living cells in the sample. The percentage of survival of diospyrin-treated cells was calculated relative to mock (DMSO)-treated cells and plotted using GraphPad Prism as mean ± SD

RESULTS

RECQ5 binds to the CTD of RNAPII through a conserved motif

In a yeast two-hybrid screen for proteins that interact with the non-conserved C-terminal region of human RECQ5 (amino acids 411–991 fused to the LexA DNA-binding domain), we isolated a clone from a human peripheral blood cell cDNA library that encoded the CTD of the largest subunit of RNAPII, RPB1 (amino acids 1266–1970). This domain consists of evolutionary conserved repeats of the heptapetide sequence YSPTSPS that serve as a binding platform for proteins involved in transcription and mRNA processing (17–19). Thus, our finding suggests that RECQ5 is a novel RNAPII CTD-binding protein.

During transcription, the CTD undergoes dynamic phosphorylation on serine residues, producing different phosphorylation patterns that predominate in individual stages of the transcription cycle and determine the recruitment of a specific set of proteins (17–19). Using the MotifScan software, we found that the extreme C-terminal region of RECQ5 (amino acids 910–950) contains a putative phospho-CTD (P-CTD)-binding motif, called a Set2–Rpb1-interacting (SRI) domain (Figure 1A). This motif was initially identified as a Ser2,5 P-CTD-binding module in the yeast methyltransferase Set2, which catalyses histone H3 lysine 36 methylation during transcription (20). NMR studies on the SRI domains of the yeast Set2 and its human homologue SETD2 have revealed a novel CTD-binding fold consisting of a left-turned three-helix bundle (21,22). RECQ5 appears to contain only helices 1 and 2 that form the CTD-binding surface.

To show that the putative SRI motif of RECQ5 is important for RECQ5 binding to the CTD of RNAPII, we deleted it (amino acids 908–954) from the bait plasmids carrying the full-length RECQ5 and RECQ5 411–991,

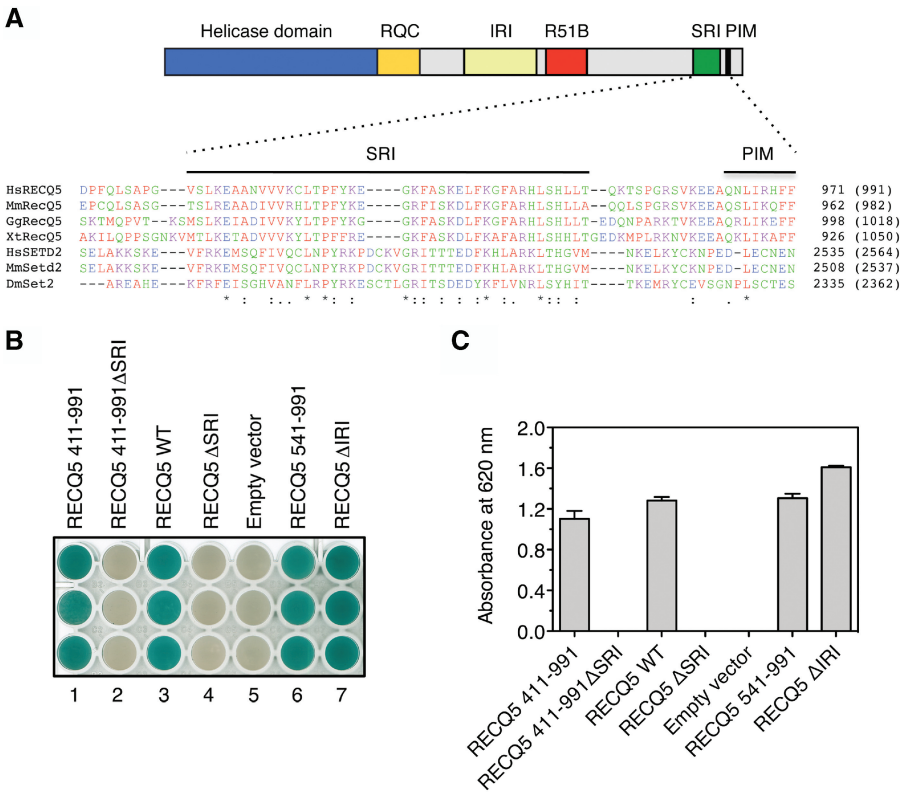

Figure 1. RECQ5 binds to the CTD of RNAPII through a SRI motif. (**A**) RECQ5 contains a CTD-binding motif. Top panel: domain organization of RECQ5. R51B, RAD51-binding domain; PIM, PCNA-interacting motif. Bottom panel: alignment of RECQ5 homologues with selected Set2 homologues carried out using ClustalX. The locations of the SRI and PIM motifs are indicated by black lines. (**B**) Interaction of RECQ5 and its mutants with the RNAPII CTD in the yeast two-hybrid system. Clones carrying the bait (RECQ5) and prey (CTD) plasmids were tested for β-galactosidase activity using the pellet X-gal assay. Blue color indicates positive interaction. (**C**) Plot of absorbance at 620 nm measured after 35 min in individual wells of the ELISA plate shown in (**B**) relative to wells with empty bait vector. The values represent the mean of three experiments.

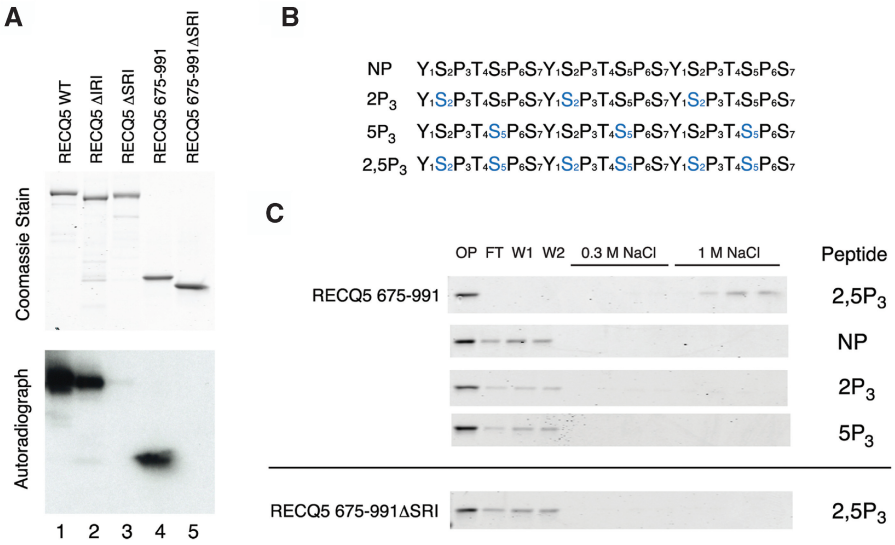

Figure 2. Effect of CTD phosphorylation status on RECQ5–CTD interaction. (**A**) Binding of RECQ5 and its mutants to *in vitro* phosphorylated CTD. Top panel: Coomassie stained gel. Bottom panel: far western blot probed with ^{32}P-labeled GSTyCTD fusion protein hyperphosphorylated with CTDK-I. (**B**) Depiction of synthetic three-repeat CTD peptides used for the binding assay. The serines in blue are phospho-serines. (**C**) Immobilized peptide-binding assay of RECQ5 675-991 on the four synthetic peptides. Fractions were analyzed by SDS–PAGE with Coomassie blue staining. OP, onput; FT, flow-through; W1 and W2, washes.

respectively. The resulting constructs were tested for yeast two-hybrid interaction with the CTD prey plasmid isolated in our yeast two-hybrid screen. We found that neither of these mutants interacted with RNAPII CTD (Figure 1B and C). In contrast, the full-length RECQ5 as well as RECQ5 411-991 showed positive yeast two-hybrid interaction with CTD (Figure 1B and C). A previous study demonstrated that human CTD was phosphorylated when expressed in yeast (23). Thus, our data suggest that RECQ5 binds to the P-CTD of RNAPII by means of the SRI domain.

It has been shown that RECQ5 binds to RNAPII through a region including amino acids 396–617 (9). Using a series of internal deletion variants of RECQ5, we mapped more precisely the boundaries of this domain to amino acids 515 and 640, respectively (Supplementary Figure S1). Hereafter, this domain is referred to as the Internal RNAPII-interacting (IRI) domain. A deletion of the proximal part of the IRI domain of RECQ5 that spans amino acids 515–568 (ΔIRI) completely abolished binding of RECQ5 to the hypophosphorylated form of RNAPII (RNAPIIA) (Supplementary Figure S1C, Lane 4). In contrast, yeast two-hybrid analysis indicated that the RECQ5 ΔIRI mutant bound to the RNAPII CTD to a similar extent as wild-type RECQ5 (Figure 1B and C). Likewise, an N-terminally truncated variant of RECQ5 of amino acids 541–991 was found to interact with the RNAPII CTD in the yeast two-hybrid system, although it was defective in interacting with RNAPIIA (Figure 1B and C, and data not shown).

RECQ5 specifically binds to Ser2,5-phosphorylated CTD heptapeptide repeats

As an initial test of P-CTD binding, purified recombinant versions of RECQ5 were subjected to SDS–PAGE and far western analysis using a ^{32}P-labeled GSTyCTD fusion protein phosphorylated on Ser2 and Ser5 by yeast CTDK-I (binding probe is expected to carry ~25 doubly phosphorylated repeats). The full-length RECQ5 bound very well to the P-CTD fusion protein (Figure 2A, Lane 1), whereas RECQ5 deleted for the SRI domain did not bind appreciably (Figure 2A, Lane 3). Likewise, a C-terminal fragment containing the SRI domain (residues 675–991) bound to P-CTD-like full-length RECQ5, but a similar fragment lacking the SRI domain did not show any binding (Figure 2A, Lanes 4 and 5). Notably, RECQ5 missing only the IRI domain bound P-CTD almost as well as the wild-type protein (Figure 2A, Lane 2 versus 1). These data indicate that RECQ5 binding to the P-CTD requires the SRI domain.

To check whether the SRI domain of RECQ5 has the same binding specificity as the SRI domain of Set2 (22), synthetic biotinylated peptides with three consensus CTD heptapeptide repeats were immobilized on avidin-coated beads to create affinity resins. Because the full-length RECQ5 showed significant background interaction with the TetraLink resin, we used the C-terminal fragment of RECQ5 with and without the SRI domain for the peptide-binding experiments. Binding was evaluated with four different phosphorylated peptides: (i) a non-phosphorylated peptide (NP); (ii) a peptide with phospho-serines at position 2 of each repeat ($2P_3$); (iii) a peptide with phospho-serines at position 5 of each repeat ($5P_3$); and (iv) a peptide with phospho-serines at positions 2 and 5 of each repeat ($2,5P_3$) (Figure 2B). The RECQ5 675-991 protein bound well to the resin with the $2,5P_3$ peptide: the protein was depleted from the column flow-through fraction and was only eluted from the resin by 1 M NaCl (Figure 2C, top panel). In contrast, RECQ5 675–991 did not bind detectably to resins with the NP, $2P_3$ or $5P_3$ peptides (Figure 2C, top panel). Moreover,

RECQ5 675-991ΔSRI was unable to bind to the 2,5P$_3$ column, confirming that the SRI domain of RECQ5 is required for interaction with the phosphorylated CTD (Figure 2C, bottom panel). These results substantiate that the SRI domain of RECQ5, like the SRI domain of Set2, binds directly and specifically to CTD repeats with phospho-serines at positions 2 and 5.

The SRI, but not IRI, domain of RECQ5 mediates its binding to the hyperphoshorylated form of RNAPII

Next we compared the binding capabilities of wild-type and mutant forms of RECQ5 to RNAPII holoenzyme from human cells. To do so, RECQ5 proteins were produced in bacteria as fusions with a CBD, bound to chitin beads and incubated with a total extract of HEK293T cells. RNAPII binding was analyzed by western blotting using two different mouse monoclonal antibodies against the RNAPII CTD: (i) H5 that recognizes CTD repeats containing phospho-Ser2 and hence selectively detects the hyperphosphorylated form of RNAPII (IIO); and (ii) 7C2 that recognizes CTD repeats irrespective of their phosphorylation status and, therefore, can detect both RNAPIIO and RNAPIIA. As expected, wild-type RECQ5 was found to bind both forms of RNAPII (Figure 3, Lane 3). RECQ5 ΔIRI was impaired in binding to RNAPIIA but exhibited binding to RNAPIIO with an extent similar to that of wild-type RECQ5 (Figure 3, Lane 4). On the contrary, RECQ5 ΔSRI showed binding to RNAPIIA but was impaired in interacting with RNAPIIO (Figure 3, Lane 5). These data indicate that the binding of RECQ5 to the hyperphosphorylated form of RNAPII is mediated by the SRI domain of RECQ5.

RECQ5 associates with RNAPII-transcribed genes within the region of productive elongation

RNAPII binds to the promoter with a CTD in the non-phosphorylated state. CTD phosphorylation on Ser5 is one of the first steps in transcription initiation and leads to the movement of the transcription complex to a promoter-proximal pausing site. The escape of RNAPII from the pausing site and subsequent productive elongation of the transcript is associated with Ser2 phosphorylation of the CTD repeats (19). To investigate the interaction between RECQ5 and RNAPII during the transcription cycle, we used ChIP to characterize the distribution of RECQ5 along constitutively expressed genes. We chose two genes, the ACTG1 gene encoding γ-actin (3.1 kb) and the DHFR gene encoding dihydrofolate reductase (30 kb) (Figure 4A and B, top panels), which were used previously to dissect the distribution of RNAPII and its phosphorylated isoforms along the transcriptional unit (24). Exponentially growing HeLa cells were crosslinked with formaldehyde. Isolated chromatin fraction was sonicated to shear the genomic DNA into small fragments ranging from 200 to 500 bp and subjected to immunoprecipitation using the following antibodies: (i) 8WG16 that specifically recognizes non-phosphorylated CTD repeats; (ii) ab5095 that specifically binds to phospho-Ser2 in CTD; and (iii) anti-RECQ5 antibody raised against the

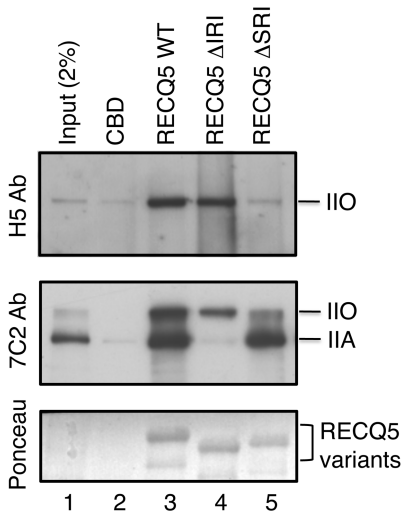

Figure 3. Binding of RECQ5 and its mutants to RNAPIIA and RNAPIIO. Chitin beads coated with either wild-type (WT) or mutant forms (ΔIRI or ΔSRI) of RECQ5 produced in bacteria as fusions with the CBD were incubated with HEK293T cell extract. RNAPII binding was analyzed by western blotting using the H5 antibody that recognizes RNAPIIO (top panel) and 7C2 antibody that recognizes both RNAPIIA and RNAPIIO (middle panel). RECQ5 proteins were visualized by Ponceau S staining (bottom panel). Lane 1, 2% of input material.

C-terminal fragment of RECQ5 spanning amino acids 675–991. After reversing the crosslinks, ChIP-enriched DNA fragments were subjected to qPCR analysis using primers amplifying the core promoter, different regions within the transcriptional unit and an intergenic region located downstream of each gene (Figure 4A and B, top panels). Amplicon sizes ranged between 109 and 174 bp. In agreement with the published data (24), we found that the non-phosphorylated RNAPII was bound exclusively to the core promoter of the tested genes (Figure 4). Ser2-phosphorylation of RNAPII was nearly absent at the core promoter and accumulated in the body of each gene (Figure 4). On both genes, the phospho-Ser2 signal dramatically dropped in the 3′-untranslated region (3′-UTR) and reached intergenic background levels (Figure 4). Although RECQ5 could bind to the hypophosphorylated form of RNAPII, it showed a relatively low occupancy at the promoter region (Figure 4). Notably, the RECQ5 distribution pattern was almost identical to that of phospho-Ser2-CTD (Figure 4). Thus, our data suggest that, during the RNAPII transcription cycle, RECQ5 associates with the productive elongation complex most likely through binding to Ser2,5 P-CTD.

The SRI, but not IRI, domain of RECQ5 mediates its association with RNAPII-transcribed genes

To investigate which of the two RNAPII-binding domains of RECQ5 is responsible for the observed accumulation of RECQ5 at the coding regions of the ACTG1 and DHFR genes, the full-length RECQ5, RECQ5 ΔIRI, RECQ5 ΔSRI and RECQ5 ΔIRIΔSRI, respectively, were ectopically expressed in HEK293 cells as fusions with GFP (Supplementary Figure S2) and subjected to

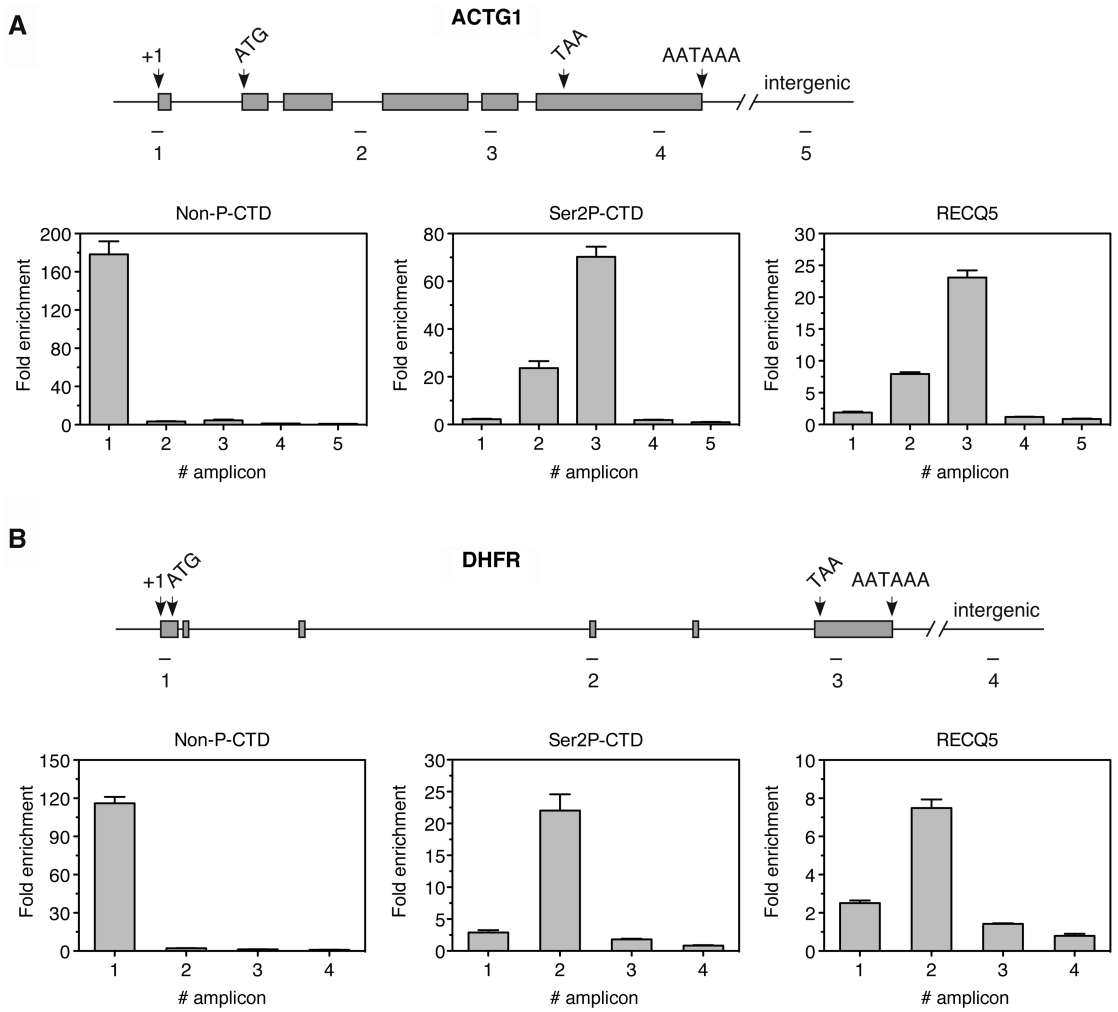

Figure 4. Distribution of RECQ5 and RNAPII along the ACTG1 and DHFR genes. (**A**) and (**B**) Top panels: schematic depiction of the ACTG1 and DHFR genes showing the locations of the transcription start site (+1), exons (grey boxes) and introns (lines connecting the grey boxes), the start codon (ATG), the stop codon (TAA) and the polyadenylation signal (AATAAA). The location of the amplicons used in qPCR analysis is also shown. The positions of the central base pair of each amplicon relative to the transcription start site are given in Supplementary Table S2. (**A**) and (**B**) Bottom panels: plots of data from qPCR analysis. ChIPs of HeLa cells were performed with the 8WG16 antibody that specifically recognizes the non-phosphorylated CTD (non-P-CTD) of RNAPII, the ab5095 antibody that specifically recognizes the Ser2 phosphorylated CTD (Ser2P-CTD) of RNAPII and anti-RECQ5 antibody. Fold enrichment was calculated as a ratio of the amount of DNA estimated for a specific antibody versus the amount of DNA estimated for the control IgG. The amplification of an intergenic region served as an internal background control.

ChIP analysis using an anti-GFP antibody. In control ChIP experiments, cells were transfected with empty vector expressing GFP only. The results obtained from the qPCR analysis clearly indicated that the SRI domain of RECQ5 was essential for the binding of RECQ5 to the coding regions of the ACTG1 and DHFR genes (Figure 5). In contrast, the IRI domain of RECQ5 was found to be dispensable for its association with these genes (Figure 5). To confirm our finding, we also examined the binding of RECQ5 and its mutants to the coding regions of two other genes, namely CDKN1A (encoding p21) and HSP70-2. As expected, GFP-tagged wild-type RECQ5 was largely enriched at the coding region of these two genes (Figure 5). The mutants lacking the SRI domain, RECQ5 ΔSRI and RECQ5 ΔIRIΔSRI, failed to accumulate at these regions, while the RECQ5 ΔIRI mutant showed similar fold of enrichment as wild-type RECQ5 (Figure 5).

Point mutagenesis studies on the SRI domain of human SETD2 identified several residues as critical for P-CTD binding (22). We generated mutations in equivalent residues of RECQ5 (F938L, K939A and R943A). Out of these, the R943A mutation completely abolished the interaction of RECQ5 411–991 with the CTD in the yeast two-hybrid system (Supplementary Figure S3A). Likewise, the R943A mutation abolished the association of RECQ5 with the coding region of the ACTG1 gene (Supplementary Figure S3B).

Taken together, our results indicate that out of the two RNAPII-interacting domains of RECQ5, the SRI domain is necessary and sufficient to mediate the association of RECQ5 with the coding regions of RNAPII-transcribed

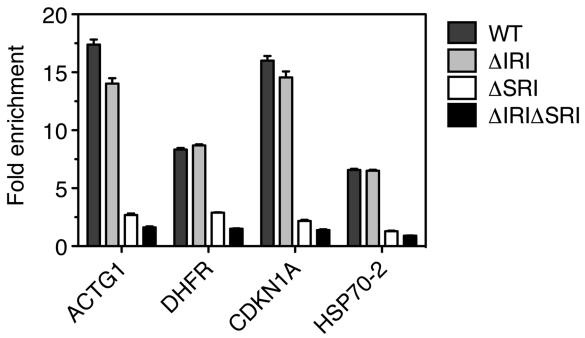

Figure 5. The SRI domain of RECQ5 mediates its association with RNAPII-transcribed genes. HEK293 cells were transfected either with empty vector (mock) or with vectors expressing wild-type (WT) or mutant (ΔIRI, ΔSRI or ΔIRIΔSRI) forms of RECQ5 as fusions with GFP. Forty-eight hours post-transfection, chromatin was immunoprecipitated by anti-GFP antibody and subjected to qPCR analysis using primer pairs complementary to the coding regions of the ACTG1, DHFR, CDKN1A and HSP70-2 genes (Supplementary Table S2). Fold enrichment was calculated as a ratio of the qPCR values obtained with RECQ5-transfected cells versus mock-transfected cells.

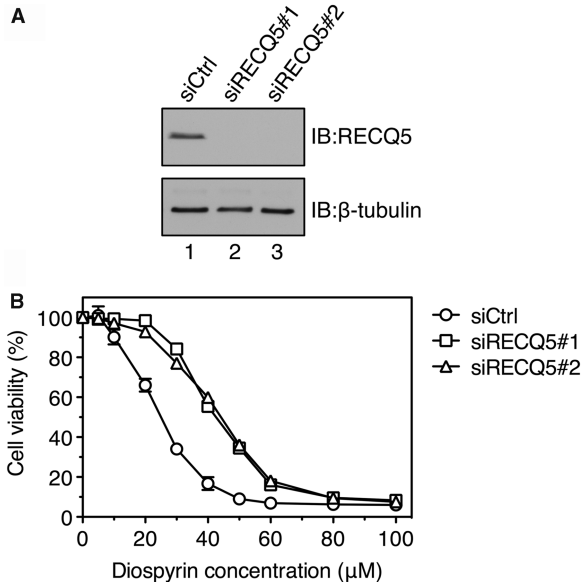

Figure 6. RECQ5 depletion alleviates sensitivity of human cells to diospyrin. (**A**) Western blot analysis of extracts of HeLa cells transfected with RECQ5 siRNA (siRECQ5 #1 and 2) and control siRNA (siCtrl), respectively. Cells were harvested 72 h post-transfection. Blots were probed with antibodies against RECQ5 and β-tubulin (loading control). (**B**) Graph showing the percentage survival of RECQ5-proficient and RECQ5-deficient cells after treatment with different concentrations of diospyrin. Cell viability assays were performed as described in 'Materials and Methods' section. Each data point represents mean ± SD ($n = 6$). IB, immunoblotting.

genes. Moreover, these data imply that the recruitment of RECQ5 to the sites of transcription is dependent on Ser2,5 phosphorylation of the RNAPII CTD.

RECQ5 negatively affects cell viability upon inhibition of spliceosome assembly

To understand the functional role of RECQ5 during RNAPII transcription, we explored the possibility that RECQ5 is involved in the cellular response to co-transcriptionally formed R-loops. To this end, we first examined whether RECQ5 could unwind an RNA : DNA hybrid duplex prepared by annealing of a synthetic 18-mer RNA oligonucleotide to M13mp2 ssDNA. We found that RECQ5 failed to unwind this structure although it could unwind the corresponding DNA : DNA duplex (Supplementary Figure S4). This finding suggests that RECQ5 does not disrupt R-loops *in vivo*.

Next, we evaluated the effect of RECQ5 depletion on cell survival upon inhibition of spliceosome assembly, which leads to the formation of R-loops. To do so, RECQ5 was down-regulated in HeLa cells by RNA interference using two different siRNAs (Figure 6A). RECQ5-proficient and RECQ5-deficient cells were treated with diospyrin that blocks spliceosome assembly. It was shown that this Top1 kinase inhibitor caused the same phenotypic defects as ASF/SF2 depletion (3). Surprisingly, we found that RECQ5-proficient cells displayed a much higher sensitivity to diospyrin than RECQ5-deficient cells (Figure 6B). These data suggest that RECQ5 negatively affects cell viability in conditions leading to the formation of R-loops.

DISCUSSION

Genetic ablation of RECQ5 helicase in mice results in genomic instability and cancer susceptibility (6). Studies in mouse and human cells have suggested that RECQ5 regulates HR by promoting disassembly of the RAD51 presynaptic filament (6). However, RECQ5 was also found to interact with RNAPII in human cells, suggesting a role in transcription (7–9). In this work, we provide evidence that RECQ5 associates with RNAPII during the productive elongation phase of transcription through direct binding to the Ser2,5 P-CTD of RPB1 by means of a SRI motif located at the C-terminus of RECQ5. Although RECQ5 could also bind to hypophosphorylated form of RNAPII through an additional domain, herein referred as IRI domain, it showed relatively low occupancy at the promoter regions of RNAPII-transcribed genes, excluding a role for RECQ5 during transcription initiation. In addition, we show that RECQ5 negatively affects cell viability upon inhibition of spliceosome assembly, which can induce the formation of mutagenic R-loop structures. Moreover, we demonstrate that RECQ5 cannot unwind RNA : DNA duplexes *in vitro*, which excludes the possibility the RECQ5 directly disrupts R-loops. Together, these findings suggest that RECQ5 might play a role in the maintenance of genomic stability during RNAPII transcription.

Recently, Islam *et al.* (25) have also reported that the SRI domain of RECQ5 mediates its binding to the hyperphosphorylated form of RNAPII in human cells. In addition, these authors have found that the IRI domain of RECQ5 shares extensive homology with the so-called KIX domain identified as a protein interaction module in several RNAPII transcription regulators. In agreement with our results, they demonstrated that

mutations at conserved residues in the IRI/KIX domain of RECQ5 abolished the interaction of RECQ5 with RNAPIIA, but not with RNAPIIO (25). However, in contrast to our observations, Islam *et al*. (25) found that the IRI/KIX domain of RECQ5 could bind to both RNAPIIA and RNAPIIO. This discrepancy may arise from the use of different experimental approaches. Whereas we analyzed binding of RNAPII from a cell extract to beads coated with recombinant RECQ5 protein produced in bacteria, Islam *et al*. (25) monitored RECQ5–RNAPII complex formation *in vivo* by immunoprecipitation. Thus, it is possible that efficient binding of the IRI/KIX domain of RECQ5 to RNAPIIO is dependent on a post-translational modification of RECQ5, which is absent if the protein is produced in bacteria. Nevertheless, our ChIP experiments clearly show that the IRI/KIX domain of RECQ5 does not play a role in the association of RECQ5 with the coding regions of RNAPII-transcribed genes, where the RNAPII CTD exists in the hyperphosphorylated state. Further studies are needed to elucidate the complex mode of the RECQ5–RNAPII interaction. In particular, the site of interaction for the IRI/KIX domain of RECQ5 on RNAPII needs to be determined.

What is the exact role of RECQ5 during the elongation phase of RNAPII transcription? Our experiments with diospyrin suggest that RECQ5 might be involved in the suppression of the DNA-damaging effects of RNAPII transcription rather than in the repair of transcription-induced DNA damage. Interestingly, a recent study by Aygun *et al*. (10) showed that RECQ5 could directly inhibit RNAPII transcription *in vitro* in a manner dependent on its IRI/KIX domain, which led the authors to propose a model in which RECQ5 promotes genome stability by regulating RNAPII transcription itself. In line with this hypothesis, Islam *et al*. (25) demonstrated that the IRI/KIX, but not the SRI, domain of RECQ5 was required for suppression of sister chromatid exchange and resistance to camptothecin-induced DNA damage. However, it should be noted that the *in vitro* transcription system used by Aygun *et al*. (10) lacked CTD kinase activity responsible for CTD phosphorylation on Ser2 during transcription. Our experiments with the RECQ5 ΔSRI mutant have indicated that hyperphosphorylation of RNAPII prevents binding of RECQ5 to RNAPII via the IRI/KIX domain, suggesting that Ser2 CTD phosphorylation may alleviate the inhibitory effect of RECQ5 on RNAPII transcription so that RECQ5 could not affect RNAPII transcription during productive elongation *in vivo*. However, it is possible that a formation of an R-loop during transcription could trigger a domain interaction switch in the RECQ5–RNAPII complex to adopt the inhibitory arrangement, which would prevent further extension of the R-loop structure and hence diminish its DNA-damaging effect. Our finding of negative effect of RECQ5 on cell viability under conditions that favor R-loop formation is consistent with this hypothesis. Future work will clarify the molecular mechanism of this phenomenon to shed light on the biological processes that enforce genomic stability during transcription.

SUPPLEMENTARY DATA

Supplementary Data are available at NAR Online.

ACKNOWLEDGEMENTS

We thank Dr Jean Marc Egly for the RNAPII 7C2 antibody, Dr Banasri Hazra (Jadavpur University, Kolkata, India) for diospyrin, Stefano di Marco for help with cell culture and Christiane Koenig for excellent technical assistance.

FUNDING

Swiss National Science Foundation (3100A0-116008); UBS AG; Indo-Swiss Research Programme; Sassella-Stiftung; Czech Science Foundation (GA204/09/0565); National Institutes of Health (USA) (GM040505). Funding for open access charge: UBS AG.

Conflict of interest statement. None declared.

REFERENCES

1. Aguilera,A. and Gomez-Gonzalez,B. (2008) Genome instability: a mechanistic view of its causes and consequences. *Nat. Rev. Genet*., **9**, 204–217.
2. Li,X. and Manley,J.L. (2005) Inactivation of the SR protein splicing factor ASF/SF2 results in genomic instability. *Cell*, **122**, 365–378.
3. Tuduri,S., Crabbe,L., Conti,C., Tourriere,H., Holtgreve-Grez,H., Jauch,A., Pantesco,V., De Vos,J., Thomas,A., Theillet,C. *et al*. (2009) Topoisomerase I suppresses genomic instability by preventing interference between replication and transcription. *Nat. Cell Biol*., **11**, 1315–1324.
4. Chu,W.K. and Hickson,I.D. (2009) RecQ helicases: multifunctional genome caretakers. *Nat. Rev. Cancer*, **9**, 644–654.
5. Hu,Y., Lu,X., Barnes,E., Yan,M., Lou,H. and Luo,G. (2005) Recql5 and Blm RecQ DNA helicases have nonredundant roles in suppressing crossovers. *Mol. Cell. Biol*., **25**, 3431–3442.
6. Hu,Y., Raynard,S., Sehorn,M.G., Lu,X., Bussen,W., Zheng,L., Stark,J.M., Barnes,E.L., Chi,P., Janscak,P. *et al*. (2007) RECQL5/Recql5 helicase regulates homologous recombination and suppresses tumor formation via disruption of Rad51 presynaptic filaments. *Genes Dev*., **21**, 3073–3084.
7. Zheng,L., Kanagaraj,R., Mihaljevic,B., Schwendener,S., Sartori,A.A., Gerrits,B., Shevelev,I. and Janscak,P. (2009) MRE11 complex links RECQ5 helicase to sites of DNA damage. *Nucleic Acids Res*., **37**, 2645–2657.
8. Aygun,O., Svejstrup,J. and Liu,Y. (2008) A RECQ5-RNA polymerase II association identified by targeted proteomic analysis of human chromatin. *Proc. Natl Acad. Sci. USA*, **105**, 8580–8584.
9. Izumikawa,K., Yanagida,M., Hayano,T., Tachikawa,H., Komatsu,W., Shimamoto,A., Futami,K., Furuichi,Y., Shinkawa,T., Yamauchi,Y. *et al*. (2008) Association of human DNA helicase RecQ5beta with RNA polymerase II and its possible role in transcription. *Biochem. J*., **413**, 505–516.
10. Aygun,O., Xu,X., Liu,Y., Takahashi,H., Kong,S.E., Conaway,R.C., Conaway,J.W. and Svejstrup,J.Q. (2009) Direct inhibition of RNA polymerase II transcription by RECQL5. *J. Biol. Chem*., **284**, 23197–23203.
11. Tazi,J., Bakkour,N., Soret,J., Zekri,L., Hazra,B., Laine,W., Baldeyrou,B., Lansiaux,A. and Bailly,C. (2005) Selective inhibition of topoisomerase I and various steps of spliceosome assembly by diospyrin derivatives. *Mol. Pharmacol*., **67**, 1186–1194.
12. Schwendener,S., Raynard,S., Paliwal,S., Cheng,A., Kanagaraj,R., Shevelev,I., Stark,J.M., Sung,P. and Janscak,P. (2010) Physical

interaction of RECQ5 helicase with RAD51 facilitates its anti-recombinase activity. *J. Biol. Chem.*, **285**, 15739–15745.
13. Kanagaraj,R., Saydam,N., Garcia,P.L., Zheng,L. and Janscak,P. (2006) Human RECQ5beta helicase promotes strand exchange on synthetic DNA structures resembling a stalled replication fork. *Nucleic Acids Res.*, **34**, 5217–5231.
14. Mockli,N. and Auerbach,D. (2004) Quantitative beta-galactosidase assay suitable for high-throughput applications in the yeast two-hybrid system. *Biotechniques*, **36**, 872–876.
15. Phatnani,H.P. and Greenleaf,A.L. (2004) Identifying phosphoCTD-associating proteins. *Meth. Mol. Biol.*, **257**, 17–28.
16. Pfaffl,M.W. (2001) A new mathematical model for relative quantification in real-time RT-PCR. *Nucleic Acids Res.*, **29**, e45.
17. Phatnani,H.P. and Greenleaf,A.L. (2006) Phosphorylation and functions of the RNA polymerase II CTD. *Genes Dev.*, **20**, 2922–2936.
18. Egloff,S. and Murphy,S. (2008) Cracking the RNA polymerase II CTD code. *Trends Genet.*, **24**, 280–288.
19. Venters,B.J. and Pugh,B.F. (2009) How eukaryotic genes are transcribed. *Crit. Rev. Biochem. Mol. Biol.*, **44**, 117–141.
20. Kizer,K.O., Phatnani,H.P., Shibata,Y., Hall,H., Greenleaf,A.L. and Strahl,B.D. (2005) A novel domain in Set2 mediates RNA polymerase II interaction and couples histone H3 K36 methylation with transcript elongation. *Mol. Cell. Biol.*, **25**, 3305–3316.
21. Vojnic,E., Simon,B., Strahl,B.D., Sattler,M. and Cramer,P. (2006) Structure and carboxyl-terminal domain (CTD) binding of the Set2 SRI domain that couples histone H3 Lys36 methylation to transcription. *J. Biol. Chem.*, **281**, 13–15.
22. Li,M., Phatnani,H.P., Guan,Z., Sage,H., Greenleaf,A.L. and Zhou,P. (2005) Solution structure of the Set2-Rpb1 interacting domain of human Set2 and its interaction with the hyperphosphorylated C-terminal domain of Rpb1. *Proc.Natl Acad. Sci. USA*, **102**, 17636–17641.
23. Bourquin,J.P., Stagljar,I., Meier,P., Moosmann,P., Silke,J., Baechi,T., Georgiev,O. and Schaffner,W. (1997) A serine/arginine-rich nuclear matrix cyclophilin interacts with the C-terminal domain of RNA polymerase II. *Nucleic Acids Res.*, **25**, 2055–2061.
24. Cheng,C. and Sharp,P.A. (2003) RNA polymerase II accumulation in the promoter-proximal region of the dihydrofolate reductase and gamma-actin genes. *Mol. Cell. Biol.*, **23**, 1961–1967.
25. Islam,M.N., Fox,D. 3rd, Guo,R., Enomoto,T. and Wang,W. (2010) RecQL5 promotes genome stabilization through two parallel mechanisms—interacting with RNA polymerase II and Acting as a helicase. *Mol. Cell Biol.*, **30**, 2460–2472.

Supplementary Table 1. Antibodies used in this study.

Name	Description	Source/Reference	Catalogue number
RNA Polymerase II 8WG16 antibody	Mouse monoclonal IgG2a antibody recognizing the non-phosphorylated form of RNAPII CTD repeat YSPTSPS (used for ChIP)	Covance	MMS-126R
RNA Polymerase II H5 antibody	Mouse monoclonal IgM antibody recognizing the phosphoserine 2 version of RNAPII CTD repeat YSPTSPS (used for Western blot)	Covance	MMS-129R
RNA Polymerase II CTD repeat YSPTSPS (phospho S2) antibody	Rabbit polyclonal antibody recognizing the phosphoserine 2 version of RNAPII CTD repeat YSPTSPS (used for ChIP)	Abcam	ab5095
RNA polymerase II 7C2 antibody	Mouse monoclonal antibody that recognizes CTD irrespective of its phosphorylation status (used for Western blot)	A kind gift from Prof. Jean Marc Egly	
RECQ5 antibody	Rabbit polyclonal antibody raised against C-terminal fragment of RECQ5 (amino acids 675-991)	Kanagaraj et al (2006)	
GFP antibody	Rabbit polyclonal antibody against GFP (used for ChIP)	Abcam	ab290
β Tubulin (D-10) antibody	Mouse monoclonal antibody raised against a recombinant protein corresponding to amino acids 210-444 of human β-tubulin	Santa Cruz	sc-5274
Sheep anti-mouse IgG HRP	Secondary antibody used for Western blot	GE Healthcare	NA931V
Goat anti-mouse IgM HRP	Secondary antibody used for Western blot	Southern Biotech	1021-05

Supplementary Table 2. Sequences of primers and parameters of amplicons used for quantitative real time PCR analysis.

Amplicon	Sequences of primers	Annealing temperature (°C)	Length of amplicon (bp)	Central bp position relative to TSS
ACTG1				
1	FOR: 5′-ggaaagatcgccatatatggac-3′ REV: 5′-tcaccggcagagaaacgcgac-3′	57	174	-15
2	FOR: 5′-gctgttccaggctctgttcc-3′ REV: 5′-atgctcacacgccacaacatgc-3	57	134	+1055
3	FOR: 5′-gtgacacagcatcactaagg-3′ REV: 5′-acagcaccgtgttggcgt-3	57	134	+1722
4	FOR: 5′-tctgtcagggttggaaagtc-3′ REV: 5′-aaatgcaaaccgcttccaac-3	57	114	+2605
5	FOR: 5′-gtgacacagtgagaccctat-3′ REV: 5′-gatttgtaggcgttctttac-3	57	110	+4837
DHFR				
1	FOR: 5′-ctgcacctgtggaggagga-3′ REV: 5′-tccttgccctgccatgtctc-3′	50	143	+196
2	FOR: 5′-gttctatagtcactgcatcttagtc-3 REV: 5′-tgctaattctggttgttcagtaag-3	50	168	+16967
3	FOR: 5′-gagtatgtttctgtcttagattgg-3 REV: 5′-atgagaacctgctcgctgac-3	50	168	+26533
4	FOR: 5′-ttgtttcagggacagggtctt-3 REV: 5′-ctgtggtgggaagatggct-3	50	109	+46523
CDKN1A	FOR: 5′-ccagctgggctctgcaatt-3′ REV: 5′-ccttccagtccattgactg-3′	54	129	+7907
HSP70-2	FOR: 5′-cgtgctcatctttgacctgg-3′ REV: 5′-ggtggctcaccatgcggttg-3′	54	140	+1042

Note that ACTG1-3 and DHFR-2 amplicons were used for qPCR analysis shown in Figure 5. TSS, transcription start site; FOR, forward primer; REV, reverse primer; bp, base pair.

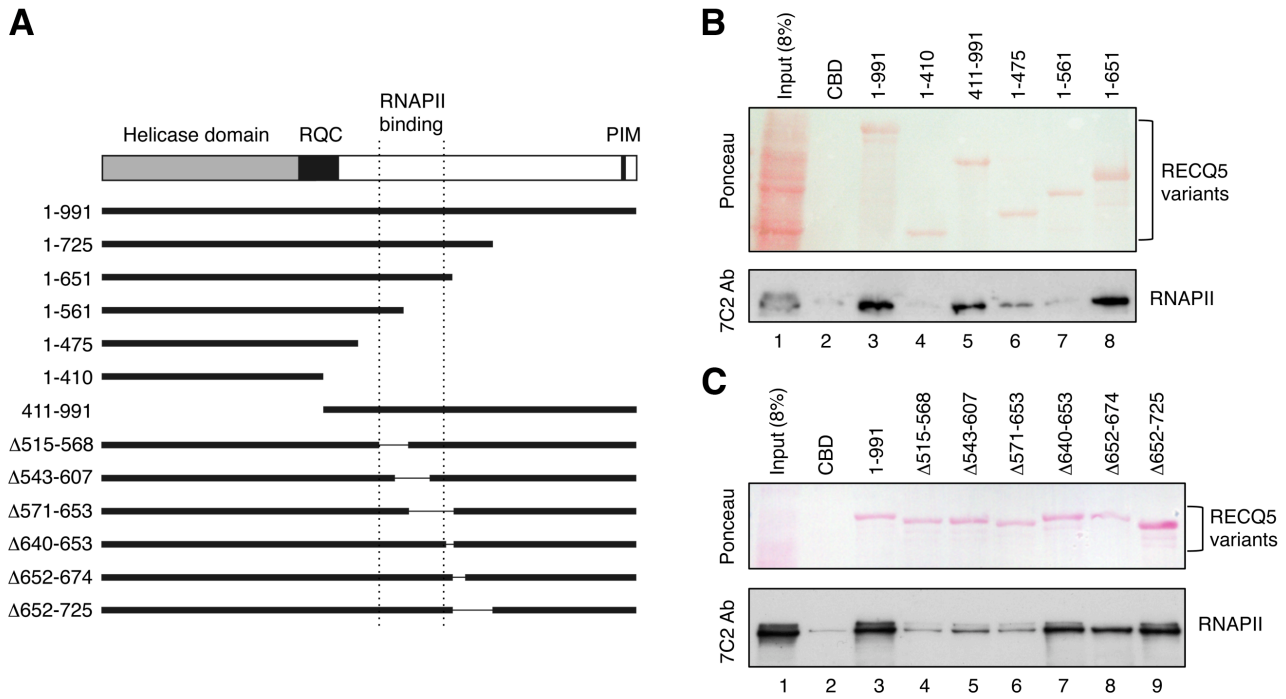

Figure S1. Mapping the RNAPII-interacting domain in RECQ5. **(A)** Domain organization of human RECQ5 and schemes of RECQ5 deletion variants used in this study. RQC, RecQ C-terminal domain, which contains a Zn^{2+}-binding motif that is essential for the helicase activity of RECQ5; PIM, PCNA-interacting motif. The dashed lines indicate the location of the RNAPII-interacting domain. **(B,C)** CBD pull-down assay. The indicated RECQ5 variants were produced in *E. coli* as fusions with the chitin-binding domain (CBD) and bound to chitin beads. Beads were incubated with a 293T cell extract and RNAPII binding was analyzed by Western blotting using the 7C2 antibody that binds to RNAPII CTD repeats irrespective of the phosphorylation status. Blots were also stained with Ponceau S to visualize RECQ5 and its variants. Note that phosphatase inhibitors were not included in these assays so that RNAPII is predominantly in the hypophosphorylated state.

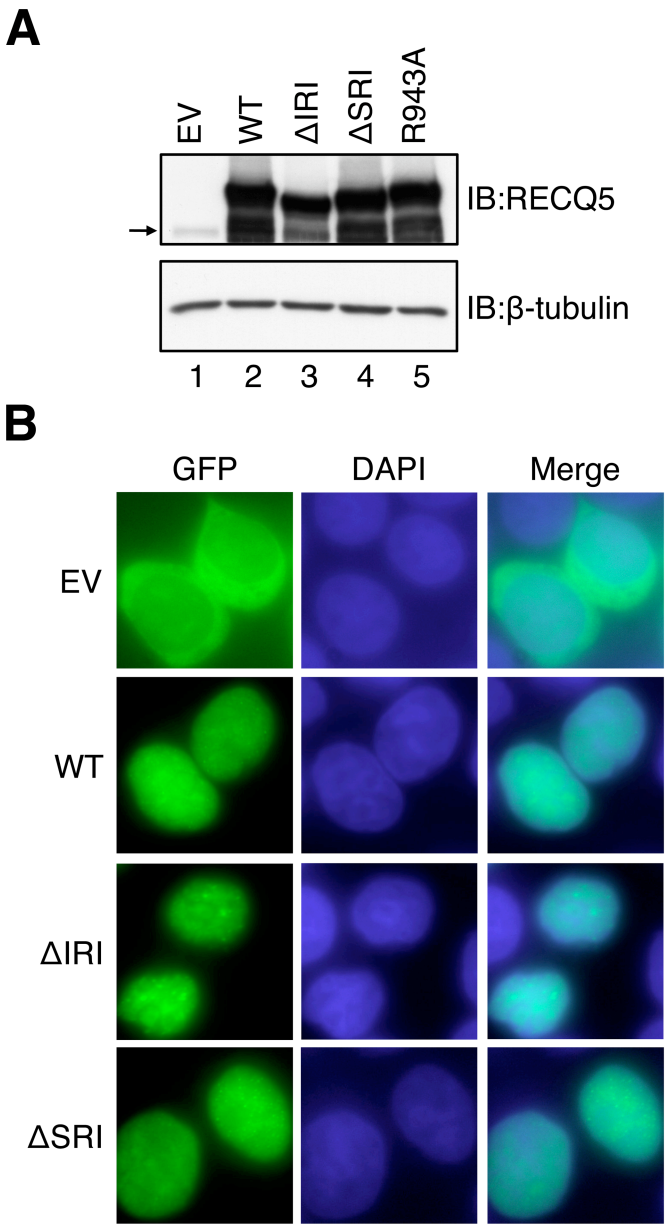

Figure S2. Expression of recombinant GFP-RECQ5 protein and its mutants in HEK293 cells. **(A)** Western blot analysis of extracts of HEK293 cells transiently transfected with constructs expressing GFP-tagged wild-type (WT) RECQ5 or its mutants (as indicated) or empty vector (EV). Transient transfection of expression vectors was performed as described in Materials and Methods. 48 hours post-transfection, whole-cell extracts (20 μg of total protein) were analyzed by Western blotting using antibodies against RECQ5 and β-tubulin (loading control). The arrow indicates the position of endogenous RECQ5 protein. Note that the endogenous RECQ5 in lanes 2-5 is masked by degradation products of recombinant RECQ5 proteins **(B)** Subcellular localization of GFP-RECQ5 and its mutants over-expressed in HEK293 cells. 48 hours post-transfection, cells were fixed with ice-cold methanol at -20 °C for 30 minutes. Fixed cells were washed thrice with PBS and mounted on slides using Vectashield mounting medium containing DAPI (Vector Laboratories, Inc.). Images were captured on an Olympus IX81 fluorescence microscope with a CCD camera (Orca AG, Hamamatsu) using cellR software (Olympus). IB: immunoblot.

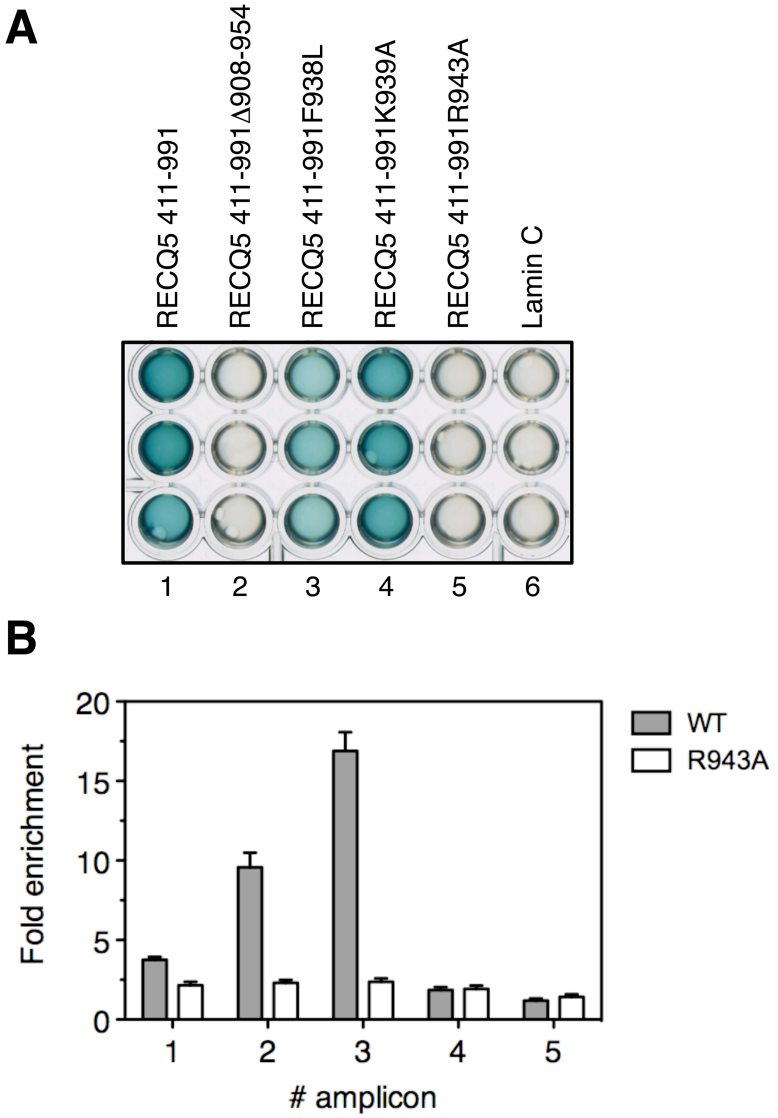

Figure S3. Mutational analysis of the conserved residues in the SRI domain of RECQ5. **(A)** Interaction of RECQ5 mutants with the CTD in the yeast two-hybrid system. Clones carrying the bait (RECQ5) and prey (CTD) plasmids were tested for β-galactosidase activity using the pellet X-gal assay. Blue color indicates a positive interaction. **(B)** Effect of the R943A substitution in the SRI domain of RECQ5 on its association with the ACTG1 gene. HEK293 cells were transfected either with empty vector (mock) or with vectors expressing wild-type (WT) or mutant (R943A) forms of RECQ5 as fusions with GFP. Forty-eight hours post-transfection, chromatin was immunoprecipitated using an anti-GFP antibody and subjected to qPCR analysis with the same amplicons as in Figure 4A (*top panel*). Fold enrichment was calculated as described in the legend of Figure 5.

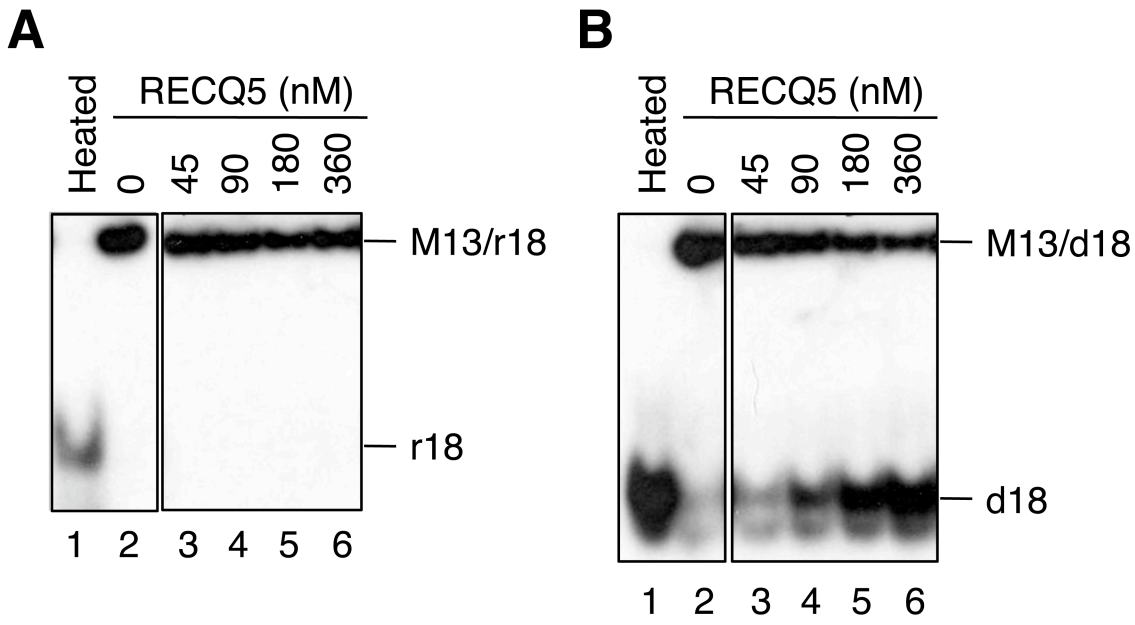

Figure S4. RECQ5 can not unwind RNA:DNA hybrid duplexes. Helicase activity of RECQ5, at indicated concentration, was measured on 1 nM M13mp2/r18 (DNA:RNA; panel A) and 1 nM M13/d18 (DNA:DNA; panel B) partial duplexes, respectively, as described in Materials and Methods. Lane 1, heat-denatured substrate.

Manuscript Details

Manuscript number	BIOPHYSCHEM_2016_258
Title	Distinct functions of human RecQ helicases during DNA replication
Article type	Research Paper

Abstract

DNA replication is the most vulnerable process of DNA metabolism in proliferating cells and therefore it is tightly controlled and coordinated with processes that maintain genomic stability. Human RecQ helicases are among the most important factors involved in the maintenance of replication fork integrity, especially under conditions of replication stress. RecQ helicases promote recovery of replication forks being stalled due to different replication roadblocks of either exogenous or endogenous source. They prevent generation of aberrant replication fork structures and replication fork collapse, and are involved in proper checkpoint signaling. The essential role of human RecQ helicases in the genome maintenance during DNA replication is underlined by association of defects in their function with cancer predisposition.

Keywords	DNA replication; Replication stress; RecQ helicases; Genomic instability; Cancer

Corresponding Author	Pavel Janscak
Corresponding Author's Institution	Institute of Molecular Cancer Research, University of Zurich
Order of Authors	Vaclav Urban, Jana Dobrovolna, Pavel Janscak

Submission Files Included in this PDF

File Name [File Type]

CoverLetter.pdf [Cover Letter]

Manuscript.pdf [Manuscript File]

To view all the submission files, including those not included in the PDF, click on the manuscript title on your EVISE Homepage, then click 'Download zip file'.

University of Zurich[UZH]

Institute of Molecular Cancer Research

University of Zurich
Institute of Molecular Cancer Research
Winterthurerstrasse 190
CH-8057 Zurich
Phone +41 44 635 34 51
Fax +41 44 635 34 84
www.imcr.uzh.ch

The Editorial Board
of Biophysical Chemistry

PD Dr. Pavel Janscak
Group Leader
Phone +41 44 635 34 70
Fax +41 44 635 34 84
pjanscak@imcr.uzh.ch

Zurich, September 28, 2016

Dear Editor

I would like you to consider our manuscript entitled "Distinct functions of human RecQ helicases during DNA replication" for publication in the special issue of *Biophysical Chemistry* organized by Professor Alessandro Vindigni to review recent advances in the field of DNA replication/repair.

Thank you for receiving our manuscript and considering it for peer review. We appreciate your time and look forward to your response.

Yours sincerely,

Pavel Janscak

Distinct functions of human RecQ helicases during DNA replication

Vaclav Urban[1], Jana Dobrovolna[1], and Pavel Janscak[1,2,*]

[1]*Institute of Molecular Genetics, Academy of Sciences of the Czech Republic, 142 20 Prague 4, Czech Republic,* [2]*Institute of Molecular Cancer Research, University of Zurich, 8057 Zurich, Switzerland*

*Correspondence: pjanscak@imcr.uzh.ch

Abstract

DNA replication is the most vulnerable process of DNA metabolism in proliferating cells and therefore it is tightly controlled and coordinated with processes that maintain genomic stability. Human RecQ helicases are among the most important factors involved in the maintenance of replication fork integrity, especially under conditions of replication stress. RecQ helicases promote recovery of replication forks being stalled due to different replication roadblocks of either exogenous or endogenous source. They prevent generation of aberrant replication fork structures and replication fork collapse, and are involved in proper checkpoint signaling. The essential role of human RecQ helicases in the genome maintenance during DNA replication is underlined by association of defects in their function with cancer predisposition.

Key words:

DNA replication; Replication stress; RecQ helicases; Genomic instability; Cancer

Introduction

Mammalian DNA replication is a well-orchestrated and tightly regulated cellular process that requires enzymatic activities of many factors involved not only in DNA synthesis but also in checkpoint signaling, DNA repair, chromatin remodeling, sister chromatid cohesion and cell cycle control. Defects in any of these activities can cause replication fork slowing or stalling, a condition referred to as replication stress, which leads to genomic instability manifested by birth defects, developmental abnormalities, neurodegeneration, premature aging and cancer predisposition [1-5]. Evidence suggests that members of the RecQ helicase family are among the most important factors that maintain genomic stability during DNA replication, especially under conditions of replication stress. The importance of RecQ helicases is underlined by the presence of at least one RecQ family member in all organisms with some exceptions for bacteria and archaea that mostly possess small genomes [6]. Bacteria and yeasts usually contain a single representative of the RecQ family, namely RecQ in *E. coli*, Sgs1p in *S. cerevisiae* and Rqh1p in *S. pombe*. Intriguingly, the number of RecQ family members expressed in particular organism increases with the size of its genome [6]. Non-redundant functions of multiple RecQ homologues in an organism are apparent from their structure. Eukaryotic RecQ helicases share an evolutionary conserved helicase domain flanked by unique N- and C-terminal regions containing

interaction sites for other proteins that determine specific functions [7]. In humans, five RecQ homologues have been identified thus far and named RECQ1, BLM, WRN, RECQ4 and RECQ5 (encoded by *RECQL*, *BLM*, *WRN*, *RECQL4* and *RECQL5* genes, respectively). The significance of these RecQ helicases is highlighted by the association of mutations in the genes encoding for BLM, WRN and RECQ4 with severe hereditary disorders named Bloom, Werner and Rothmund-Thompson syndrome, respectively [7]. These rare recessive disorders are characterized by genomic instability and predisposition to cancer (clinical features reviewed in [8-11]). Recently, defects in RECQ1 and RECQ5 have been also connected to cancer development [12-16]. Moreover, the *RECQL* gene has been added on the list of breast cancer susceptibility genes that mostly contains genes involved in the maintenance of the integrity of replication forks like *BRCA1/2* [17, 18].

Despite the accumulating evidence for the role of human RecQ helicases in the maintenance of genome stability, the underlying molecular mechanisms remain elusive. Human RecQ helicases have been associated with DNA repair by homologous recombination, base excision repair and non-homologous end joining (reviewed in [7]). However, recent studies have particularly demonstrated the involvement of human RecQ helicases in different aspects of DNA replication. In this article, recent contributions to this topic are reviewed with emphasis on the role of human RecQ helicases in the processing of stalled replication forks.

Role of RECQ4 in the initiation of DNA replication

The initial step of DNA replication is the assembly of origin recognition complex (ORC1 to ORC6 subunits) in late mitosis or early G1 phase [19]. Next, CDC6 (cell-division cycle 6) and CDT1 (cdc10-dependent transcript 1) assist to load an inactive double hexamer of minichromosome maintenance proteins 2–7 (MCM helicase) to complete the formation of pre-replication complex required for the establishment of bidirectional replication forks [19]. At the G1/S boundary, S-phase specific DDK (DBF4-dependent kinase) and CDK (CDK2/cyclin A/E) kinases activate MCM helicase, which requires the recruitment of CDC45 and the GINS complex to form the so-called CMG complex (CDC45-MCM-GINS) [19]. Activation of the CMG complex at origins of replication is achieved by recruitment of additional initiation factors including TOBP1, Treslin/TICRR and MCM10, and the loading of DNA polymerase α/ε permit DNA synthesis [19]. Evidence suggests that RECQ4 is among these essential initiation factors

[20-22]. The N-terminus of RECQ4 shares a weak but significant homology to the yeast Sld2 that assists in the recruitment of GINS to replication origins during S phase in a manner dependent on CDK activity [20, 23-25]. Indeed, the N-terminal region of RECQ4 was shown to be essential for cell viability [20, 26, 27]. RECQ4 associates with several proteins involved in replication initiation like the MCM complex, MCM10, GINS, CDC45 [28, 29]. The absence of RECQ4 was shown to significantly affect the formation of CMG complex [28, 29]. Moreover, other replication factors including RPA, PCNA and particularly DNA polymerase α display reduced binding to chromatin in the absence of RECQ4 [21, 23]. RECQ4 is recruited to replication origins at G1/S boundary upon ORC and MCM complex assembly, and forms a complex with CTF4 and MCM10 in a process dependent on the CDK and DDK kinase activities [21, 28, 30]. The efficient binding of RECQ4 to replication origins followed by their firing may be controlled by the interaction between RECQ4 and MCM10 [21, 29-31]. However, the interaction between RECQ4 and MCM10 is not required for cell viability [31]. Interestingly, newly characterized Zn-knuckle motif in the N-terminal region of RECQ4 binds nucleic acids with a preference for RNA substrates over DNA, suggesting a connection between RECQ4 and non-coding RNAs that play an important role in the initiation of DNA replication [32].

RecQ helicases associate with replisome components

Slow replication fork movement has been observed in cells depleted for BLM, WRN, RECQ1, but not for RECQ4 and RECQ5 [21, 33-37]. However, a decreased proliferation of mouse embryonic fibroblasts lacking RECQ4 was observed [23]. Interaction partners of RecQ helicases indicate their participation in processes associated with replication fork progression. RECQ5 and WRN possess the so-called PIP (PCNA-interacting peptide) motif that mediates interaction with PCNA, one of the key replisome components, and both helicases localize to replication factories in unperturbed cells [38, 39]. WRN, RECQ5, BLM and RECQ1 interact with FEN1 flap endonuclease that participates in Okazaki fragment maturation, and all stimulate 5'-flap DNA cleavage by FEN1 *in vitro*, in a manner independent of their helicase activity [40, 41]. Moreover, RECQ1 was shown to facilitate efficient binding of FEN1 to telomeres [40]. WRN interacts with DNA polymerase δ and facilitates copying tetraplex and hairpin structures [42]. Moreover, WRN exonuclease is involved in proofreading during DNA synthesis by DNA Pol δ [43]. WRN can also help overcome DNA lesions during replication by interacting with translesion polymerases

and stimulating their action [44, 45] and by serving as their proofreader [46]. However, recent studies have shown that rather than forming a stable part of replisome, human RecQ helicases remove replication roadblocks and act to promote replication resumption.

BLM promotes resolution of aberrant DNA structures at stalled replication forks

Common feature of cells deficient in BLM is increased frequency of sister chromatid exchanges (SCEs) that are thought to arise from aberrant repair of damaged replication forks [47]. To suppress excessive homologous recombination, BLM is recruited to sites of replication fork stalling in a manner dependent on RNF8/RNF168-mediated ubiquitination of the N-terminal region of BLM and subsequent BLM binding to the ubiquitin-interacting motifs of RAP80 [48]. BLM is required for efficient replication fork restart and suppression of dormant origin firing after replication blockage, which is dependent on its helicase activity and phosphorylation (at Thr99) via the ATR/Chk1 pathway [35, 49]. Cells derived from Bloom syndrome patients accumulate abnormal replication intermediates and display increased levels of single-stranded DNA and RAD51-containing foci, which is pronounced after replication blockage by hydroxyurea (HU) or aphidicolin (Aph) [50, 51]. RAD51 is a central homologous recombination factor that plays an important role in the resumption of stalled and collapsed replication forks [52]. BLM and RAD51 act together during fork recovery [35]. Sumoylation of BLM increases the *in vitro* interaction between RAD51 and BLM, and may regulate the recovery of stalled forks by facilitating RAD51 recruitment or stabilization of its binding to stalled forks, and preventing the accumulation of single-stranded DNA coated by RPA. Accordingly, impaired BLM sumoylation (at lysine K317 and K331) increases fork collapse and cell death [53, 54].

Four-way DNA structures called Holliday junctions (HJs) can arise during the recovery of stalled replication forks [55]. BLM forms a complex with topoisomerase IIIα (TOPOIIIα) and RMI1/2 to dissolve double-HJs, which arise during homologous recombination, via a strand passage mechanism preventing crossover outcomes [56]. The TOPOIIIα-interacting domain of BLM is required for the suppression of SCEs in BS cells [57]. RMI1 also suppress SCEs and the interaction between BLM and RMI1 promotes proper fork progression and recovery from replication stress [58, 59]. The BLM-TOPOIIIα-RMI1/2 complex localizes to subnuclear foci, which is pronounced after replication blockage by HU or Aph [59]. Thus, the excess of nuclear foci containing single-stranded DNA in the absence of BLM can arise due to the impaired

localization of TOPOIIIα [60]. Recently, FANCD2 was shown to be involved in the efficient assembly of the BLM-TOPOIIIα-RMI1/2 complex at sites of stalled replication forks and to act with BLM in a common pathway to promote replication fork restart and suppression of new origin firing [61]. The dissolution reaction catalyzed by the BLM-TOPOIIIα-RMI1/2 complex appears to be a unique function of BLM among human RecQ helicases [62]. This activity is also important at sites of termination of DNA replication, because BLM accumulates on late replication intermediates to assist in duplex separation so that DNA replication can be efficiently completed [63-66].

In addition to double-HJs dissolution, BLM is able to unwind G-quadruplexes formed at guanine rich sequences [67]. In mammals, telomeres consisting of long TTAGGG tandem repeats are regions with the highest concentration of G-quadruplexes [68]. Indeed, BLM was shown to maintain stability of telomeres [66, 69]. BLM can suppress G-quadruplex formation both genome-wide and, specifically, at telomeres [70]. BLM binds to the telomere-specific shelterin proteins TRF1, TRF2 and POT1, which are essential for telomere capping and repression of DNA damage signaling [69, 71, 72]. BLM-deficient mouse cells show a high frequency of spontaneous telomere fragility visible as a separation of telomeric signals from chromatid ends [73, 74]. Moreover, it was shown that TRF1 binding to BLM prevented telomere fragility, with most of the fragile telomeres resulting from lagging strand DNA synthesis [74]. The majority of telomeres are replicated by forks moving toward the telomere end using the TTAGGG repeat strand as the template for lagging strand DNA synthesis [73]. However, compared to BLM-proficient cells, BLM-deficient cells also show a slower rate of leading strand synthesis that initiates within the telomere and higher frequency of replication initiation originating closer to the telomere [70]. Further, slowdown of telomeric replication fork movement was observed upon treatment of BLM-deficient cells with G-quadruplex stabilizer PhenDC3, suggesting that BLM facilitates telomere replication by resolving G-quadrulexes [70]. However, the G-quadruplex-stabilizing compound pyridostatin increases telomeric-SCEs in cells lacking homologous recombination factors such as BRCA1, BRCA2 or RAD51 and reduces the viability of these cells [75]. Thus, the above mention activities of BLM (in homologous recombination or double-HJs dissolution) may be utilized to promote restart of stalled forks at G-quadruplexes.

BLM is also implicated in recombination-mediated mechanism of telomere maintenance, referred to as alternative lengthening of telomeres (ALT) [76]. Overexpression of BLM in cells using ALT increases telomeric signals, suggesting that BLM promotes ALT [77]. Depletion of BLM in cells using ALT leads to increased levels of telomere length attrition and telomeric SCEs [78-80]. In the absence of functional BLM, the SLX4-nuclease complex resolves persistent HR intermediates to yield crossover products, resulting in increased SCEs [79, 81]. Recently, it has been shown that BLM function is modulated by BRCA1 and FANCD2 during ALT [82, 83].

WRN promotes restart of stalled replication forks

Cells derived from Werner syndrome patients display a high frequency of chromosomal translocations, deletions and telomere loss, but not SCEs [84-86]. Further, fibroblasts isolated from Werner syndrome patients show chromosome and chromatid fusions that result from repair attempts of dysfunctional telomeres [87]. Werner syndrome cells are also highly sensitive to replication-perturbing agents [88-91]. Similarly, WRN-deficient cells exposed to various types of replication stress accumulate DNA double-stranded breaks and show increased expression of CFSs as compared to WRN-proficient cells [92-96]. Replication stress triggers extensive co-localization of WRN with RPA at nuclear foci in a manner dependent on WRN phosphorylation by ATR [97-99]. Consistently, WRN possesses two RPA binding sites [100]. Moreover, WRN was shown to promote ATR-dependent checkpoint activation upon replication fork stalling [96, 101, 102]. The effect of WRN on the ATR-signaling pathway as well as WRN phosphorylation by ATR may result from its interaction with the checkpoint sliding clamp RAD9-RAD1-HUS1 that upon fork arrest recruits the ATR activator TOPBP1 [103]. The significance of WRN phosphorylation is underlined by the fact that stalled forks undergo collapse followed by DNA double-stranded break formation in cells expressing ATR-unphosphorylable mutant of WRN, like in WRN-deficient cells [92, 94, 98]. The accumulation of DNA double-stranded breaks in WRN-deficient cells is dependent on MUS81 nuclease activity [92, 94]. However, a co-depletion of MUS81 and WRN has more severe effect on cell viability than depletion of either protein, even without induction of replication stress, suggesting existence of alternative mechanisms for response to replication fork stalling [92, 94].

Decreased rate of replication fork progression in the absence of functional WRN is accompanied by a significant asymmetry of bidirectional forks [104]. The recovery of stalled

forks is impaired in WRN-deficient cells, which is consistent with proposed function of WRN in sustaining replication [36, 92, 98, 105]. Importantly, WRN-depleted cells accumulate reversed forks, which is more prominent after HU treatment [105]. Moreover, the human DNA2 and WRN form complex to promote replication restart that is dependent on degradation of nascent DNA by nuclease activity of DNA2 and helicase activity of WRN [105].

While the processing of replication intermediates by WRN/DNA2 is independent of other nucleases that are typically involved in DNA resection like EXO1, MRE11 or CTIP, recent evidence implicated exonuclease activity of WRN in protection of nascent DNA strands against unscheduled degradation by combined action of MRE11 and EXO1 after low dose of camptothecin (CPT) [106]. Moreover, WRN protein independently of its enzymatic activities is required to prevent degradation of nascent DNA at replication-dependent double-stranded breaks induced by high doses of CPT [107]. In this case, NBS1 recruits WRN to replication-associated DNA breaks to stabilize RAD51 binding and limit activity of MRE11 [107].

The characteristic features of cells derived from Werner syndrome patients is premature senescence and accelerated telomere shortening, suggesting that WRN has a critical function in telomere maintenance [86, 108, 109]. Similar to BLM, WRN associates with telomeres during S-phase and binds to the telomere-specific shelterin proteins TRF2 and POT1, which are essential for telomere capping and repression of DNA damage signaling [71, 72, 109]. WRN has been shown to suppress defects in telomere lagging strand synthesis [109]. Mutational inactivation of WRN helicase domain results in loss of telomeric signal only from the chromatid that uses G-rich strand as template for lagging strand synthesis, while leading strand telomere is not lost [109]. Consistently, WRN deficiency results in increased frequency of G-quadruplex formation genome-wide and, specifically, at telomeres [70]. Although BLM helicase is also contributing to chromosome-end maintenance, WRN has distinct role in this process. This is supported by observation that simultaneous loss of both helicases substantially exacerbates the telomere dysfunction in comparison to loss of individual helicase [66, 70, 73].

RECQ5 promotes resolution of replication-transcription collisions

Subunits of RNA polymerase (RNAP) II are the most prominent proteins that co-immunoprecipitate with RECQ5 from human cell extracts [110, 111]. RECQ5 interacts directly with the largest catalytic subunit of RNAPII, termed RPB1 [39, 111], and this interaction is

enhanced during S-phase [112]. Two regions of RECQ5 polypeptide were identified to mediate the interaction with RPB1: (i) the internal RNAPII-interacting (IRI) domain including the KIX motif, which binds to RPB1 jaw domain; and (ii) the Set2-Rpb1-interacting (SRI) domain, which binds to the hyperphosphorylated C-terminal repeat domain (CTD) of RPB1 [39, 113, 114]. Recently, interaction of RECQ5 with the catalytic subunit of RNAPI (RPA194) was also described [115]. RECQ5 associates with chromatin particularly at transcribed regions and prevents RNAP pausing or arrest [39, 110, 115, 116]. Importantly, RECQ5 associates with transcription in replication factories [115]. Depletion of RECQ5 results in transcription-dependent chromosome fragmentation during S phase and accumulation of chromosomal rearrangements with the breakpoints located in the pre-rRNA coding region, genes and common fragile sites (CFSs) [112, 115, 116]. In recent years, it has become increasingly clear that replication-transcription collisions cause DNA breakage and chromosomal rearrangements, particularly in cells subjected to replication stress [117-120]. In mammals, the fragility of CFSs and early replicating fragile sites (ERFSs) is associated with active transcription of very long genes or regions that contain clusters of highly transcribed genes, respectively [117, 121]. Several lines of evidence suggest that RECQ5 counteracts replication fork stalling in RNAPI- and RNAPII-transcribed genes [115]. Consistently, elongating forms of RNAPI and RNAPII accumulate on chromatin in the absence of RECQ5 [112, 115]. RECQ5-deficient cells accumulate RAD18 foci and BRCA1-dependent RAD51 foci that are both formed at sites of interference between replication and transcription and likely represent unresolved replication intermediates [115]. Further studies have shown that RECQ5 promotes RAD18-dependent ubiquitination of PCNA at sites of replication-transcription interference by directly interacting with PCNA. Moreover, the helicase activity of RECQ5 is required for the resolution of replication intermediates stabilized by RAD51 filaments upon replication-transcription encounters [115]. Together, these findings suggest that RECQ5 promotes the resolution of replication-transcription collisions. This conclusion is also supported by observation that RECQ5 counteracts thymidine-induced replication stress [122].

RECQ1 unwinds reversed replication forks

Cells lacking RECQ1 display an elevated number of genomic and telomeric SCEs [123-125]. RECQ1 deficiency results in sensitivity to various DNA damaging agents that directly or

indirectly block replication fork progression [126]. RECQ1 associates with replication origins in unperturbed cells and shows an increased binding to the lamin B2 origin and CFSs under conditions of replication stress [21]. RECQ1-depleted cells or cells expressing RECQ1 mutants that lack helicase or branch migration activity display reduced replication fork rates and defects in checkpoint activation under conditions of replication stress [21, 127]. RECQ1-defficiency also leads to nascent strand degradation at stalled replication forks, which is dependent on DNA2 and WRN [105]. A recent study revealed a role for RECQ1 in restarting stalled replication forks caused by DNA topoisomerase I inhibition with camptothecin (CPT) [128]. The ATPase activity of RECQ1 is essential for replication fork progression in cells exposed to CPT [128]. In the presence of CPT, replication forks stall and undergo fork reversal, which prevents replication fork run-off and formation of DNA double-stranded breaks [129]. The poly(ADP-ribosyl)ation activity of PARP1 is necessary for stabilization of regressed forks upon CPT treatment until the lesion is repaired [129]. PARP1 was shown to interact with RECQ1 and to regulate the restart of stabilized forks in the regressed state by RECQ1-mediated unwinding of the regressed arm [128, 130]. *In vitro* experiments indicated that PARylated PARP1 inhibits fork restoration activity of RECQ1 [128]. Reversed forks accumulate in RECQ1-depleted cells [128]. Inhibition of PARP1 activity causes an untimely restart of reversed forks in a manner dependent on RECQ1, which results in DSB formation [128]. Moreover, the restart of reversed forks by RECQ1-mediated mechanism can be a more general response to a wide variety of replication blocking agents [131].

Concluding remarks

The roles of human RecQ helicases during DNA replication are unwavering. Their common feature is to promote recovery of forks being stalled due to different replication roadblocks of either exogenous or endogenous source. Human RecQ helicases participate particularly in replication fork progression through genomic loci that represent natural impediment for replication like CFSs, repetitive sequences, telomeres and actively transcribed regions. Their activity leads to a proper checkpoint response to replication fork stalling. The absence of RecQ helicases leads to accumulation of unresolved replication intermediates, which was well described for BLM, WRN, RECQ1 and RECQ5 [50, 51, 105, 115, 128]. In the absence of WRN, the presence of HJs is expected, because expression of bacterial RusA HJ-resolvase in Werner

syndrome cells can restore DNA replication capacity [132]. The conversion of stalled forks to the HJ structure by fork reversal may be a global response to replication stress [131]. The formation of regressed arm may stabilize stalled fork for repair or removal of the roadblock, and the regressed arm also represents a suitable substrate for replication fork recovery, avoiding DNA double-stranded break formation [133]. RecQ helicases are involved in individual steps of the replication resumption process (Figure 1). Specifically, RECQ5 promotes resolution of replication-transcription collisions through its helicase activity that facilitates restart of stalled forks stabilized by RAD51 filaments [115]. RECQ1 acts to promote recovery of reversed forks by unwinding of the regressed arm [128]. WRN probably acts during nucleolytic processing of regressed arm to promote replication resumption [105]. BLM as part of the complex with TOPOIIIα and RMI1/2 dissolves double-HJs arising during replication fork recovery by homology-directed restart via the regressed arm. Only RECQ4 seems to be involved in the DNA replication process *per se*, specifically in replication origin activation. However, MCM10, the prominent interactor of RECQ4, was recently shown to promote replication fork progression under conditions of replication stress [134]. Depletion of both, MCM10 and RECQ4, results in reduced binding of DNA polymerase α and PCNA on chromatin [21, 23, 134]. Thus, MCM10 and RECQ4 may act together to keep or recover DNA polymerase α, PCNA, CDC45 and GINS at lagging strand during replication fork stalling. Consistently, the essential role of both proteins in initiation of replication is in conflict with proficient bulk DNA synthesis after their depletion [21, 135]. Interestingly, studies in budding yeast revealed that PCNA is unloaded only from the lagging strand arm of forks stalled by HU treatment [136]. Thus, RECQ4 and MCM10 may be involved in the recovery of replisome at stalled forks (Figure 1).

In conclusion, the process of replication fork stalling and recovery may be a very tangled mechanism that includes complex remodeling of both DNA and protein moieties of replication fork. The study of RecQ helicases can uncover individual steps of this process that prevents genomic instability. Understanding the mechanisms that maintain replication fork stability may be crucial for diagnosis and therapy of human diseases caused by defects in response to replication stress.

Acknowledgements

This work was supported by the Czech Science Foundation (14-05743S), the Swiss National Science Foundation (31003A-166451), the Ministry of Education, Youth and Sports of the Czech Republic (KONTAKT II LH14037), and the Neuron Fund for Support of Science.

References

1. Macheret, M. and T.D. Halazonetis, *DNA replication stress as a hallmark of cancer.* Annu Rev Pathol, 2015. **10**: p. 425-48.
2. Zeman, M.K. and K.A. Cimprich, *Causes and consequences of replication stress.* Nat Cell Biol, 2014. **16**(1): p. 2-9.
3. Boyer, A.S., D. Walter, and C.S. Sorensen, *DNA replication and cancer: From dysfunctional replication origin activities to therapeutic opportunities.* Semin Cancer Biol, 2016. **37-38**: p. 16-25.
4. Zhang, C., J. Lu, and P. Zhang, *The Roles of Chromatin Remodeling Proteins in Cancer.* Curr Protein Pept Sci, 2016. **17**(5): p. 446-54.
5. Losada, A., *Cohesin in cancer: chromosome segregation and beyond.* Nat Rev Cancer, 2014. **14**(6): p. 389-93.
6. Nakayama, H., *RecQ family helicases: roles as tumor suppressor proteins.* Oncogene, 2002. **21**(58): p. 9008-21.
7. Croteau, D.L., et al., *Human RecQ helicases in DNA repair, recombination, and replication.* Annu Rev Biochem, 2014. **83**: p. 519-52.
8. Oshima, J., J.M. Sidorova, and R.J. Monnat, Jr., *Werner syndrome: Clinical features, pathogenesis and potential therapeutic interventions.* Ageing Res Rev, 2016.
9. Sanz, M.M., J. German, and C. Cunniff, *Bloom's Syndrome*, in *GeneReviews(R)*, R.A. Pagon, et al., Editors. 1993: Seattle (WA).
10. Wang, L.L. and S.E. Plon, *Rothmund-Thomson Syndrome*, in *GeneReviews(R)*, R.A. Pagon, et al., Editors. 1993: Seattle (WA).
11. Oshima, J., G.M. Martin, and F.M. Hisama, *Werner Syndrome*, in *GeneReviews(R)*, R.A. Pagon, et al., Editors. 1993: Seattle (WA).
12. Cybulski, C., et al., *Germline RECQL mutations are associated with breast cancer susceptibility.* Nat Genet, 2015. **47**(6): p. 643-6.
13. Sun, J., et al., *Mutations in RECQL Gene Are Associated with Predisposition to Breast Cancer.* PLoS Genet, 2015. **11**(5): p. e1005228.
14. Zhi, L.Q., et al., *Association of RECQL5 gene polymorphisms and osteosarcoma in a Chinese Han population.* Tumour Biol, 2014. **35**(4): p. 3255-9.
15. Qi, Y. and X. Zhou, *Haplotype analysis of RECQL5 gene and laryngeal cancer.* Tumour Biol, 2014. **35**(3): p. 2669-73.
16. He, Y.J., et al., *Association between RECQL5 genetic polymorphisms and susceptibility to breast cancer.* Tumor Biology, 2014. **35**(12): p. 12201-12204.
17. Venkitaraman, A.R., *Cancer suppression by the chromosome custodians, BRCA1 and BRCA2.* Science, 2014. **343**(6178): p. 1470-5.
18. Banerjee, T. and R.M. Brosh, Jr., *RECQL: a new breast cancer susceptibility gene.* Cell Cycle, 2015. **14**(22): p. 3540-3.
19. Fragkos, M., et al., *DNA replication origin activation in space and time.* Nat Rev Mol Cell Biol, 2015. **16**(6): p. 360-74.
20. Matsuno, K., et al., *The N-terminal noncatalytic region of Xenopus RecQ4 is required for chromatin binding of DNA polymerase alpha in the initiation of DNA replication.* Mol Cell Biol, 2006. **26**(13): p. 4843-52.
21. Thangavel, S., et al., *Human RECQ1 and RECQ4 helicases play distinct roles in DNA replication initiation.* Mol Cell Biol, 2010. **30**(6): p. 1382-96.

22. Collart, C., et al., *Titration of four replication factors is essential for the Xenopus laevis midblastula transition.* Science, 2013. **341**(6148): p. 893-6.
23. Sangrithi, M.N., et al., *Initiation of DNA replication requires the RECQL4 protein mutated in Rothmund-Thomson syndrome.* Cell, 2005. **121**(6): p. 887-98.
24. Tanaka, S., et al., *CDK-dependent phosphorylation of Sld2 and Sld3 initiates DNA replication in budding yeast.* Nature, 2007. **445**(7125): p. 328-32.
25. Zegerman, P. and J.F. Diffley, *Phosphorylation of Sld2 and Sld3 by cyclin-dependent kinases promotes DNA replication in budding yeast.* Nature, 2007. **445**(7125): p. 281-5.
26. Ichikawa, K., T. Noda, and Y. Furuichi, *[Preparation of the gene targeted knockout mice for human premature aging diseases, Werner syndrome, and Rothmund-Thomson syndrome caused by the mutation of DNA helicases].* Nihon Yakurigaku Zasshi, 2002. **119**(4): p. 219-26.
27. Abe, T., et al., *The N-terminal region of RECQL4 lacking the helicase domain is both essential and sufficient for the viability of vertebrate cells Role of the N-terminal region of RECQL4 in cells.* Biochimica Et Biophysica Acta-Molecular Cell Research, 2011. **1813**(3): p. 473-479.
28. Xu, X., et al., *MCM10 mediates RECQ4 association with MCM2-7 helicase complex during DNA replication.* EMBO J, 2009. **28**(19): p. 3005-14.
29. Im, J.S., et al., *Assembly of the Cdc45-Mcm2-7-GINS complex in human cells requires the Ctf4/And-1, RecQL4, and Mcm10 proteins.* Proc Natl Acad Sci U S A, 2009. **106**(37): p. 15628-32.
30. Im, J.S., et al., *RecQL4 is required for the association of Mcm10 and Ctf4 with replication origins in human cells.* Cell Cycle, 2015. **14**(7): p. 1001-1009.
31. Kliszczak, M., et al., *Interaction of RECQ4 and MCM10 is important for efficient DNA replication origin firing in human cells.* Oncotarget, 2015. **6**(38): p. 40464-40479.
32. Marino, F., et al., *Structural and biochemical characterization of an RNA/DNA binding motif in the N-terminal domain of RecQ4 helicases.* Scientific Reports, 2016. **6**.
33. Park, S.J., et al., *A positive involvement of RecQL4 in UV-induced S-phase arrest.* DNA Cell Biol, 2006. **25**(12): p. 696-703.
34. Hand, R. and J. German, *A retarded rate of DNA chain growth in Bloom's syndrome.* Proc Natl Acad Sci U S A, 1975. **72**(2): p. 758-62.
35. Sidorova, J.M., et al., *Distinct functions of human RECQ helicases WRN and BLM in replication fork recovery and progression after hydroxyurea-induced stalling.* DNA Repair (Amst), 2013. **12**(2): p. 128-39.
36. Sidorova, J.M., et al., *The RecQ helicase WRN is required for normal replication fork progression after DNA damage or replication fork arrest.* Cell Cycle, 2008. **7**(6): p. 796-807.
37. Kim, T.M., et al., *RECQL5 and BLM exhibit divergent functions in cells defective for the Fanconi anemia pathway.* Nucleic Acids Res, 2015. **43**(2): p. 893-903.
38. Rodriguez-Lopez, A.M., et al., *Characterisation of the interaction between WRN, the helicase/exonuclease defective in progeroid Werner's syndrome, and an essential replication factor, PCNA.* Mech Ageing Dev, 2003. **124**(2): p. 167-74.
39. Kanagaraj, R., et al., *RECQ5 helicase associates with the C-terminal repeat domain of RNA polymerase II during productive elongation phase of transcription.* Nucleic Acids Res, 2010. **38**(22): p. 8131-40.

40. Sami, F., et al., *RECQ1 interacts with FEN-1 and promotes binding of FEN-1 to telomeric chromatin.* Biochem J, 2015. **468**(2): p. 227-44.
41. Bachrati, C.Z. and I.D. Hickson, *RecQ helicases: guardian angels of the DNA replication fork.* Chromosoma, 2008. **117**(3): p. 219-33.
42. Kamath-Loeb, A.S., et al., *Interactions between the Werner syndrome helicase and DNA polymerase delta specifically facilitate copying of tetraplex and hairpin structures of the d(CGG)n trinucleotide repeat sequence.* J Biol Chem, 2001. **276**(19): p. 16439-46.
43. Kamath-Loeb, A.S., et al., *The Werner syndrome exonuclease facilitates DNA degradation and high fidelity DNA polymerization by human DNA polymerase delta.* J Biol Chem, 2012. **287**(15): p. 12480-90.
44. Kamath-Loeb, A.S., et al., *Werner syndrome protein interacts functionally with translesion DNA polymerases.* Proc Natl Acad Sci U S A, 2007. **104**(25): p. 10394-9.
45. Phillips, L.G. and J.E. Sale, *The Werner's Syndrome protein collaborates with REV1 to promote replication fork progression on damaged DNA.* DNA Repair (Amst), 2010. **9**(10): p. 1064-72.
46. Maddukuri, L., et al., *Enhancement of human DNA polymerase eta activity and fidelity is dependent upon a bipartite interaction with the Werner syndrome protein.* J Biol Chem, 2012. **287**(50): p. 42312-23.
47. Hickson, I.D., *RecQ helicases: caretakers of the genome.* Nat Rev Cancer, 2003. **3**(3): p. 169-78.
48. Tikoo, S., et al., *Ubiquitin-dependent recruitment of the Bloom syndrome helicase upon replication stress is required to suppress homologous recombination.* EMBO J, 2013. **32**(12): p. 1778-92.
49. Davies, S.L., P.S. North, and I.D. Hickson, *Role for BLM in replication-fork restart and suppression of origin firing after replicative stress.* Nat Struct Mol Biol, 2007. **14**(7): p. 677-9.
50. Rassool, F.V., et al., *Constitutive DNA damage is linked to DNA replication abnormalities in Bloom's syndrome cells.* Oncogene, 2003. **22**(54): p. 8749-8757.
51. Lonn, U., et al., *An Abnormal Profile of DNA-Replication Intermediates in Blooms Syndrome.* Cancer Research, 1990. **50**(11): p. 3141-3145.
52. Petermann, E., et al., *Hydroxyurea-stalled replication forks become progressively inactivated and require two different RAD51-mediated pathways for restart and repair.* Mol Cell, 2010. **37**(4): p. 492-502.
53. Ouyang, K.J., et al., *BLM SUMOylation regulates ssDNA accumulation at stalled replication forks.* Front Genet, 2013. **4**: p. 167.
54. Ouyang, K.J., et al., *SUMO modification regulates BLM and RAD51 interaction at damaged replication forks.* PLoS Biol, 2009. **7**(12): p. e1000252.
55. Petermann, E. and T. Helleday, *Pathways of mammalian replication fork restart.* Nat Rev Mol Cell Biol, 2010. **11**(10): p. 683-7.
56. Wu, L. and I.D. Hickson, *The Bloom's syndrome helicase suppresses crossing over during homologous recombination.* Nature, 2003. **426**(6968): p. 870-4.
57. Hu, P., et al., *Evidence for BLM and Topoisomerase IIIalpha interaction in genomic stability.* Hum Mol Genet, 2001. **10**(12): p. 1287-98.
58. Yin, J., et al., *BLAP75, an essential component of Bloom's syndrome protein complexes that maintain genome integrity.* EMBO J, 2005. **24**(7): p. 1465-76.

59. Yang, J., et al., *RMI1 promotes DNA replication fork progression and recovery from replication fork stress.* Mol Cell Biol, 2012. **32**(15): p. 3054-64.
60. Yang, J., et al., *Human topoisomerase IIIalpha is a single-stranded DNA decatenase that is stimulated by BLM and RMI1.* J Biol Chem, 2010. **285**(28): p. 21426-36.
61. Chaudhury, I., et al., *FANCD2 regulates BLM complex functions independently of FANCI to promote replication fork recovery.* Nucleic Acids Res, 2013. **41**(13): p. 6444-59.
62. Wu, L., et al., *The HRDC domain of BLM is required for the dissolution of double Holliday junctions.* EMBO J, 2005. **24**(14): p. 2679-87.
63. Chan, K.L., P.S. North, and I.D. Hickson, *BLM is required for faithful chromosome segregation and its localization defines a class of ultrafine anaphase bridges.* EMBO J, 2007. **26**(14): p. 3397-409.
64. Chen, C.F. and S.J. Brill, *An essential DNA strand-exchange activity is conserved in the divergent N-termini of BLM orthologs.* EMBO J, 2010. **29**(10): p. 1713-25.
65. Lukas, C., et al., *53BP1 nuclear bodies form around DNA lesions generated by mitotic transmission of chromosomes under replication stress.* Nat Cell Biol, 2011. **13**(3): p. 243-53.
66. Barefield, C. and J. Karlseder, *The BLM helicase contributes to telomere maintenance through processing of late-replicating intermediate structures.* Nucleic Acids Res, 2012. **40**(15): p. 7358-67.
67. Sun, H., et al., *The Bloom's syndrome helicase unwinds G4 DNA.* J Biol Chem, 1998. **273**(42): p. 27587-92.
68. Lipps, H.J. and D. Rhodes, *G-quadruplex structures: in vivo evidence and function.* Trends Cell Biol, 2009. **19**(8): p. 414-22.
69. Lillard-Wetherell, K., et al., *Association and regulation of the BLM helicase by the telomere proteins TRF1 and TRF2.* Hum Mol Genet, 2004. **13**(17): p. 1919-32.
70. Drosopoulos, W.C., S.T. Kosiyatrakul, and C.L. Schildkraut, *BLM helicase facilitates telomere replication during leading strand synthesis of telomeres.* J Cell Biol, 2015. **210**(2): p. 191-208.
71. Opresko, P.L., et al., *Telomere-binding protein TRF2 binds to and stimulates the Werner and Bloom syndrome helicases.* J Biol Chem, 2002. **277**(43): p. 41110-9.
72. Opresko, P.L., et al., *POT1 stimulates RecQ helicases WRN and BLM to unwind telomeric DNA substrates.* J Biol Chem, 2005. **280**(37): p. 32069-80.
73. Sfeir, A., et al., *Mammalian telomeres resemble fragile sites and require TRF1 for efficient replication.* Cell, 2009. **138**(1): p. 90-103.
74. Zimmermann, M., et al., *TRF1 negotiates TTAGGG repeat-associated replication problems by recruiting the BLM helicase and the TPP1/POT1 repressor of ATR signaling.* Genes Dev, 2014. **28**(22): p. 2477-91.
75. Zimmer, J., et al., *Targeting BRCA1 and BRCA2 Deficiencies with G-Quadruplex-Interacting Compounds.* Mol Cell, 2016. **61**(3): p. 449-60.
76. Rezazadeh, S., *On BLM helicase in recombination-mediated telomere maintenance.* Mol Biol Rep, 2013. **40**(4): p. 3049-64.
77. Stavropoulos, D.J., et al., *The Bloom syndrome helicase BLM interacts with TRF2 in ALT cells and promotes telomeric DNA synthesis.* Hum Mol Genet, 2002. **11**(25): p. 3135-44.
78. Hagelstrom, R.T., et al., *Hyper telomere recombination accelerates replicative senescence and may promote premature aging.* Proc Natl Acad Sci U S A, 2010. **107**(36): p. 15768-73.

79. Sarkar, J., et al., *SLX4 contributes to telomere preservation and regulated processing of telomeric joint molecule intermediates.* Nucleic Acids Res, 2015. **43**(12): p. 5912-23.
80. Bhattacharyya, S., et al., *Telomerase-associated protein 1, HSP90, and topoisomerase IIalpha associate directly with the BLM helicase in immortalized cells using ALT and modulate its helicase activity using telomeric DNA substrates.* J Biol Chem, 2009. **284**(22): p. 14966-77.
81. Wechsler, T., S. Newman, and S.C. West, *Aberrant chromosome morphology in human cells defective for Holliday junction resolution.* Nature, 2011. **471**(7340): p. 642-6.
82. Acharya, S., et al., *Association of BLM and BRCA1 during Telomere Maintenance in ALT Cells.* PLoS One, 2014. **9**(8): p. e103819.
83. Root, H., et al., *FANCD2 limits BLM-dependent telomere instability in the alternative lengthening of telomeres pathway.* Hum Mol Genet, 2016.
84. Gebhart, E., et al., *Spontaneous and induced chromosomal instability in Werner syndrome.* Hum Genet, 1988. **80**(2): p. 135-9.
85. Fukuchi, K., G.M. Martin, and R.J. Monnat, Jr., *Mutator phenotype of Werner syndrome is characterized by extensive deletions.* Proc Natl Acad Sci U S A, 1989. **86**(15): p. 5893-7.
86. Schulz, V.P., et al., *Accelerated loss of telomeric repeats may not explain accelerated replicative decline of Werner syndrome cells.* Hum Genet, 1996. **97**(6): p. 750-4.
87. Crabbe, L., et al., *Telomere dysfunction as a cause of genomic instability in Werner syndrome.* Proc Natl Acad Sci U S A, 2007. **104**(7): p. 2205-10.
88. Pichierri, P., et al., *Werner's syndrome protein is required for correct recovery after replication arrest and DNA damage induced in S-phase of cell cycle.* Mol Biol Cell, 2001. **12**(8): p. 2412-21.
89. Poot, M., et al., *Werner syndrome diploid fibroblasts are sensitive to 4-nitroquinoline-N-oxide and 8-methoxypsoralen: implications for the disease phenotype.* FASEB J, 2002. **16**(7): p. 757-8.
90. Poot, M., K.A. Gollahon, and P.S. Rabinovitch, *Werner syndrome lymphoblastoid cells are sensitive to camptothecin-induced apoptosis in S-phase.* Hum Genet, 1999. **104**(1): p. 10-4.
91. Poot, M., et al., *Werner syndrome cells are sensitive to DNA cross-linking drugs.* FASEB J, 2001. **15**(7): p. 1224-6.
92. Franchitto, A., et al., *Replication fork stalling in WRN-deficient cells is overcome by prompt activation of a MUS81-dependent pathway.* J Cell Biol, 2008. **183**(2): p. 241-52.
93. Murfuni, I., et al., *Perturbed replication induced genome wide or at common fragile sites is differently managed in the absence of WRN.* Carcinogenesis, 2012. **33**(9): p. 1655-63.
94. Murfuni, I., et al., *The WRN and MUS81 proteins limit cell death and genome instability following oncogene activation.* Oncogene, 2013. **32**(5): p. 610-20.
95. Pirzio, L.M., et al., *Werner syndrome helicase activity is essential in maintaining fragile site stability.* J Cell Biol, 2008. **180**(2): p. 305-14.
96. Basile, G., et al., *Checkpoint-dependent and independent roles of the Werner syndrome protein in preserving genome integrity in response to mild replication stress.* Nucleic Acids Res, 2014. **42**(20): p. 12628-39.
97. Constantinou, A., et al., *Werner's syndrome protein (WRN) migrates Holliday junctions and co-localizes with RPA upon replication arrest.* EMBO Rep, 2000. **1**(1): p. 80-4.

98. Ammazzalorso, F., et al., *ATR and ATM differently regulate WRN to prevent DSBs at stalled replication forks and promote replication fork recovery.* EMBO J, 2010. **29**(18): p. 3156-69.
99. Franchitto, A. and P. Pichierri, *Werner syndrome protein and the MRE11 complex are involved in a common pathway of replication fork recovery.* Cell Cycle, 2004. **3**(10): p. 1331-9.
100. Doherty, K.M., et al., *Physical and functional mapping of the replication protein a interaction domain of the werner and bloom syndrome helicases.* J Biol Chem, 2005. **280**(33): p. 29494-505.
101. Hyun, M., et al., *The Caenorhabditis elegans Werner syndrome protein participates in DNA damage checkpoint and DNA repair in response to CPT-induced double-strand breaks.* Cell Signal, 2016. **28**(3): p. 214-23.
102. Patro, B.S., et al., *WRN helicase regulates the ATR-CHK1-induced S-phase checkpoint pathway in response to topoisomerase-I-DNA covalent complexes.* J Cell Sci, 2011. **124**(Pt 23): p. 3967-79.
103. Pichierri, P., et al., *The RAD9-RAD1-HUS1 (9.1.1) complex interacts with WRN and is crucial to regulate its response to replication fork stalling.* Oncogene, 2012. **31**(23): p. 2809-23.
104. Rodriguez-Lopez, A.M., et al., *Asymmetry of DNA replication fork progression in Werner's syndrome.* Aging Cell, 2002. **1**(1): p. 30-9.
105. Thangavel, S., et al., *DNA2 drives processing and restart of reversed replication forks in human cells.* J Cell Biol, 2015. **208**(5): p. 545-62.
106. Iannascoli, C., et al., *The WRN exonuclease domain protects nascent strands from pathological MRE11/EXO1-dependent degradation.* Nucleic Acids Res, 2015. **43**(20): p. 9788-803.
107. Su, F., et al., *Nonenzymatic role for WRN in preserving nascent DNA strands after replication stress.* Cell Rep, 2014. **9**(4): p. 1387-401.
108. Opresko, P.L., et al., *Werner syndrome and the function of the Werner protein; what they can teach us about the molecular aging process.* Carcinogenesis, 2003. **24**(5): p. 791-802.
109. Crabbe, L., et al., *Defective telomere lagging strand synthesis in cells lacking WRN helicase activity.* Science, 2004. **306**(5703): p. 1951-3.
110. Izumikawa, K., et al., *Association of human DNA helicase RecQ5beta with RNA polymerase II and its possible role in transcription.* Biochem J, 2008. **413**(3): p. 505-16.
111. Aygun, O., J. Svejstrup, and Y. Liu, *A RECQ5-RNA polymerase II association identified by targeted proteomic analysis of human chromatin.* Proc Natl Acad Sci U S A, 2008. **105**(25): p. 8580-4.
112. Li, M., X. Xu, and Y. Liu, *The SET2-RPB1 interaction domain of human RECQ5 is important for transcription-associated genome stability.* Mol Cell Biol, 2011. **31**(10): p. 2090-9.
113. Islam, M.N., et al., *RecQL5 promotes genome stabilization through two parallel mechanisms--interacting with RNA polymerase II and acting as a helicase.* Mol Cell Biol, 2010. **30**(10): p. 2460-72.
114. Kassube, S.A., et al., *Structural mimicry in transcription regulation of human RNA polymerase II by the DNA helicase RECQL5.* Nat Struct Mol Biol, 2013. **20**(7): p. 892-9.

115. Urban, V., et al., *RECQ5 helicase promotes resolution of conflicts between replication and transcription in human cells.* J Cell Biol, 2016. **214**(4): p. 401-15.
116. Saponaro, M., et al., *RECQL5 Controls Transcript Elongation and Suppresses Genome Instability Associated with Transcription Stress.* Cell, 2014. **157**(5): p. 1037-49.
117. Barlow, J.H., et al., *Identification of early replicating fragile sites that contribute to genome instability.* Cell, 2013. **152**(3): p. 620-32.
118. Helmrich, A., et al., *Transcription-replication encounters, consequences and genomic instability.* Nat Struct Mol Biol, 2013. **20**(4): p. 412-8.
119. Jones, R.M., et al., *Increased replication initiation and conflicts with transcription underlie Cyclin E-induced replication stress.* Oncogene, 2013. **32**(32): p. 3744-53.
120. Wilson, T.E., et al., *Large transcription units unify copy number variants and common fragile sites arising under replication stress.* Genome Res, 2015. **25**(2): p. 189-200.
121. Helmrich, A., M. Ballarino, and L. Tora, *Collisions between replication and transcription complexes cause common fragile site instability at the longest human genes.* Mol Cell, 2011. **44**(6): p. 966-77.
122. Blundred, R., et al., *Human RECQL5 overcomes thymidine-induced replication stress.* DNA Repair (Amst), 2010. **9**(9): p. 964-75.
123. Sharma, S., et al., *RECQL, a member of the RecQ family of DNA helicases, suppresses chromosomal instability.* Mol Cell Biol, 2007. **27**(5): p. 1784-94.
124. Sharma, S. and R.M. Brosh, Jr., *Human RECQ1 is a DNA damage responsive protein required for genotoxic stress resistance and suppression of sister chromatid exchanges.* PLoS One, 2007. **2**(12): p. e1297.
125. Popuri, V., et al., *Human RECQL1 participates in telomere maintenance.* Nucleic Acids Res, 2014. **42**(9): p. 5671-88.
126. Popuri, V., et al., *RECQ1 is required for cellular resistance to replication stress and catalyzes strand exchange on stalled replication fork structures.* Cell Cycle, 2012. **11**(22): p. 4252-65.
127. Banerjee, T., et al., *Catalytic strand separation by RECQ1 is required for RPA-mediated response to replication stress.* Curr Biol, 2015. **25**(21): p. 2830-8.
128. Berti, M., et al., *Human RECQ1 promotes restart of replication forks reversed by DNA topoisomerase I inhibition.* Nat Struct Mol Biol, 2013. **20**(3): p. 347-54.
129. Ray Chaudhuri, A., et al., *Topoisomerase I poisoning results in PARP-mediated replication fork reversal.* Nat Struct Mol Biol, 2012. **19**(4): p. 417-23.
130. Sharma, S., et al., *RECQ1 plays a distinct role in cellular response to oxidative DNA damage.* DNA Repair (Amst), 2012. **11**(6): p. 537-49.
131. Zellweger, R., et al., *Rad51-mediated replication fork reversal is a global response to genotoxic treatments in human cells.* J Cell Biol, 2015. **208**(5): p. 563-79.
132. Rodriguez-Lopez, A.M., et al., *Correction of proliferation and drug sensitivity defects in the progeroid Werner's Syndrome by Holliday junction resolution.* Rejuvenation Res, 2007. **10**(1): p. 27-40.
133. Neelsen, K.J. and M. Lopes, *Replication fork reversal in eukaryotes: from dead end to dynamic response.* Nat Rev Mol Cell Biol, 2015. **16**(4): p. 207-20.
134. Chadha, G.S., et al., *Xenopus Mcm10 is a CDK-substrate required for replication fork stability.* Cell Cycle, 2016: p. 1-13.
135. Park, J.H., et al., *Knockdown of human MCM10 exhibits delayed and incomplete chromosome replication.* Biochem Biophys Res Commun, 2008. **365**(3): p. 575-82.

136. Yu, C., et al., *Strand-specific analysis shows protein binding at replication forks and PCNA unloading from lagging strands when forks stall.* Mol Cell, 2014. **56**(4): p. 551-63.

Figure legends

Figure 1. Overview of the functions of human RecQ helicases in genome maintenance during DNA replication. Replication intermediates or obstacles proposed to be resolved by the individual RecQ helicases are shown (right). Interaction partners of human RecQ helicases involved in their actions at replication forks are also listed along with phenotypic consequences of deficiency in individual RecQ helicases (left). Upwards arrows indicate increase; downwards arrows indicate decrease.

Urban et al., Figure 1